

UNCLASSIFIED

---

AD 282 003

*Reproduced  
by the*

ARMED SERVICES TECHNICAL INFORMATION AGENCY  
ARLINGTON HALL STATION  
ARLINGTON 12, VIRGINIA



---

UNCLASSIFIED

NOTICE: When government or other drawings, specifications or other data are used for any purpose other than in connection with a definitely related government procurement operation, the U. S. Government thereby incurs no responsibility, nor any obligation whatsoever; and the fact that the Government may have formulated, furnished, or in any way supplied the said drawings, specifications, or other data is not to be regarded by implication or otherwise as in any manner licensing the holder or any other person or corporation, or conveying any rights or permission to manufacture, use or sell any patented invention that may in any way be related thereto.

62-4-5

ASD-TR-61-706  
Volume I

28 20 03

BERYLLIUM COMPOSITE STRUCTURES  
Volume I - Design and Application

TECHNICAL REPORT NO. ASD-TR-61-706 Volume I

May 1962

Flight Dynamics Laboratory  
Aeronautical Systems Division  
Air Force Systems Command  
Wright-Patterson Air Force Base, Ohio

Project No. 1368, Task No. 136806



(Prepared under Contract No. AF 33(616)-7050  
by Aeronca Manufacturing Corporation, Middletown, Ohio  
Authors: J. N. Krusos, A. S. Kjelly, J. Borosic, T. T. Byrne, F. B. Eck,  
R. E. Wiegert and V. Rosa)

282 003  
AS AD No. \_\_\_\_\_  
CHALLENGED BY ASTIA

## NOTICES

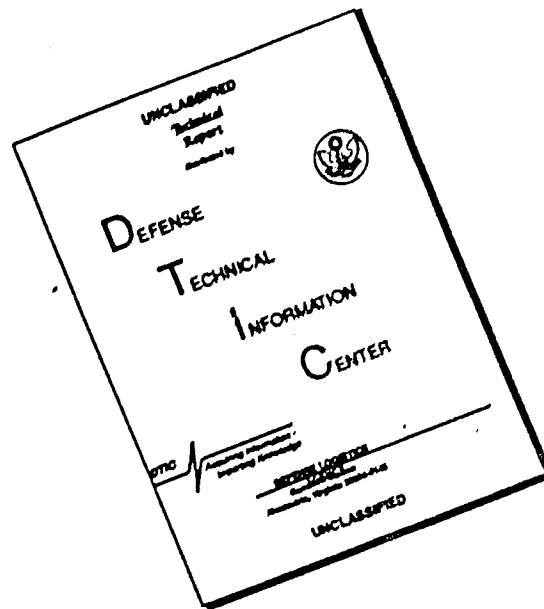
When Government drawings, specifications, or other data are used for any purpose other than in connection with a definitely related Government procurement operation, the United States Government thereby incurs no responsibility nor any obligation whatsoever; and the fact that the Government may have formulated, furnished, or in any way supplied the said drawings, specifications, or other data, is not to be regarded by implication or otherwise as in any manner licensing the holder or any other person or corporation, or conveying any rights or permission to manufacture, use, or sell any patented invention that may in any way be related thereto.

Qualified requesters may obtain copies of this report from the Armed Services Technical Information Agency, (ASTIA), Arlington Hall Station, Arlington 12, Virginia.

This report has been released to the Office of Technical Services, U.S. Department of Commerce, Washington 25, D.C., in stock quantities for sale to the general public.

Copies of this report should not be returned to the Aeronautical Systems Division unless return is required by security considerations, contractual obligations, or notice on a specific document.

# DISCLAIMER NOTICE



THIS DOCUMENT IS BEST QUALITY AVAILABLE. THE COPY FURNISHED TO DTIC CONTAINED A SIGNIFICANT NUMBER OF PAGES WHICH DO NOT REPRODUCE LEGIBLY.

## FOREWORD

This Final Technical Engineering Report covers the design and application portion of the Contract AF33(616)-7050 during the period 4 February 1960 to 31 August 1961. The materials and processes aspects of the work performed are covered in Volume II of this report.

This contract with the Defense Products Middletown Division of Aeronca Manufacturing Division, was administered by Mr. Frank E. Barnett (ASRMDS-21) of the Flight Dynamics Laboratory, Aeronautical Systems Division, Wright-Patterson Air Force Base, Ohio, under Project 1368, "Design Technologies and Structural Configuration Concepts for Aerospace Vehicles", Task 136806, "Beryllium Structural Development". This Task and Project are part of the Air Force System Command's Applied Research Program 750A, "Mechanics of Flight."

J. N. Krusos was in charge of the technical effort at Aeronca, and primary contributors included A. S. Kjølby in metallurgy and testing, T. J. Byrne and R. Wiegert in ceramics development, J. Borosic, F. Robbins and A. DeFord in process development, Frank Eck in stress analysis, and V. Rosa in thermal and dynamics analysis.

Appreciation is also expressed for the assistance provided by Dr. J. L. Pentecost (Mississippi State University) in the field of ceramics.

Acknowledgment is made and appreciation expressed for the technical assistance of Mr. Robert D. Guyton, Flight Dynamics Laboratory, ASD, throughout the life of this program.

The contractor's report number is ER-532.

### ABSTRACT

Design information is presented for beryllium and ceramic composite structures for re-entry vehicle applications.

The volume includes a summary of materials and process developments for beryllium panels and heat shield ceramics, analytical evaluations, and discussion of application of insulated structural concepts to re-entry vehicle systems. Also included are the results of panel tests in the severe environments of turbojet and ramjet exhausts.

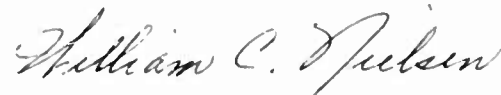
Data suitable for preliminary design considerations are presented for three reinforced heat shield ceramic foams: alumina, silica, and zirconia.

Beryllium sandwich panels constructed in the course of the program are described with regard to fabrication potential and performance in aerospace structures.

### PUBLICATION REVIEW

THIS REPORT HAS BEEN REVIEWED AND IS APPROVED

FOR THE COMMANDER:



WILLIAM C. NIELSEN  
COLONEL, USAF  
CHIEF, FLIGHT DYNAMICS LABORATORY

## TABLE OF CONTENTS

<u>SECTION</u>		<u>PAGE</u>
I	INTRODUCTION	I-1
II	CONCEPT APPLICATIONS	II-1
	A. Introduction	II-1
	B. Applications	II-4
	1. Lifting Body Re-Entry Vehicles	II-4
	2. Recoverable Booster Leading Edges	II-19
	3. Leading Edges and Nose Caps of Glider Re-Entry Vehicles	II-19
	4. Low Altitude Missiles	II-22
III	ANALYSIS AND STRUCTURAL EVALUATION OF BERYLLIUM COMPOSITE STRUCTURES	III-1
	A. Introduction	III-1
	B. Beryllium Panels	III-1
	1. General Considerations	III-1
	2. Analysis of Beryllium Panels For Re-entry Vehicles	III-3
	3. Thermoelastic Analysis	III-31
	C. Composite Panels	III-42
	1. Thermal Analysis	III-42
	2. Vibration Analysis	III-46
IV	PROPERTIES AND TEST DATA	IV-1
	A. Introduction	IV-1
	B. Ceramic Property Tests	IV-1
	1. Mechanical Properties	IV-1
	2. Thermal Conductivity	IV-1
	3. Emissivity	IV-8
	4. Thermal Expansion	IV-10
	5. Durability of Heat Shield Materials	IV-10
	C. Composite Panel Tests	IV-16
	1. Turbojet and Ramjet Tests	IV-16
	2. Mechanical and Thermal Tests	IV-27
	D. Beryllium Test Data	IV-40
	1. Mechanical Properties of Beryllium Sheet	IV-40
	a. Tensile Properties	IV-40
	b. Compressive Properties	IV-42
	c. Flexural Properties	IV-42
	d. Lap Shear Properties	IV-52

# TABLE OF CONTENTS -Continued-

<u>SECTION</u>	<u>PAGE</u>
IV -cont'd-	
2. Mechanical Properties of Beryllium-Faced Sandwich Structures	IV-52
a. Compatibility of Materials	IV-52
b. Flatwise Tensile Properties	IV-52
c. Edgewise Compressive Properties	IV-55
d. Core Shear Properties	IV-55
e. Sandwich Flexure Properties	IV-55
V BERYLLIUM FABRICATION DEVELOPMENT	V-1
A. Introduction	V-1
B. Machining	V-1
1. Sawing	V-2
2. Routing	V-2
3. Chemical Milling	V-3
4. Other Machining Operations	V-3
C. Forming	V-4
D. Brazing	V-5
1. Quartz-Lamp Brazing	V-5
2. Electric-Blanket Brazing	V-11
3. Furnace Brazing	V-18
E. Joining	V-18
1. Welding of Beryllium	V-18
2. Mechanical Joining	V-21
3. Welding of Dissimilar Metal Edge Members	V-21
REFERENCES	V-22
BIBLIOGRAPHY	V-23

## LIST OF FIGURES

<u>SECTION</u>		<u>PAGE</u>
SECTION II		
II-1	Thermantic Construction	II-2
II-2	Thermantic Construction	II-3
II-3	Views of Lifting Body Vehicle	II-5
II-4	Structural Arrangement--Lifting Body Vehicle	II-6
II-5	Cooling System--Honeycomb Structural Panel	II-10
II-6	Cooling System--Corrugated Structural Panel	II-11
II-7	Weights Distribution--Flight Vehicle	II-12
II-8	Thermal Characteristics of Lifting Body Configurations	II-13
II-9	RBS Wing Leading Edge--Cold Wall Heating	II-20
II-10	Leading Edge Segment	II-21
II-11	Maximum Temperatures for Thermantic Leading Edge	II-23
II-12	Curved Panel Design for 160 BTU/ft <sup>2</sup> --Sec. Incident Heat Flux	II-24
SECTION III		
III-1	Panel Configuration	III-5
III-2	Leading Edge Concept	III-6
III-3	Ultimate Tensile Strength vs. Temperature	III-7
III-4	Tensile Yield Strength vs. Temperature	III-8
III-5	Young's Modules vs. Temperature	III-9
III-6	Typical Tensile Stress-Strain Curves	III-10
III-7	Critical Buckling Stress (Fcr) vs. (Le/P)	III-11
III-8	Typical Tensile Stress-Strain Curves	III-12
III-9	Critical Buckling Stress (Fcr vs. (Le/P)	III-13
III-10	Typical Tensile Stress-Strain Curves	III-14
III-11	Critical Buckling Stress (Fcr) vs. (Le/P)	III-15
III-12	Typical Tensile Stress-Strain Curves	III-16
III-13	Critical Buckling Stress (Fcr) vs. (Le/P)	III-17
III-14	Shear, Moment, and Axial Load Diagram	III-18
III-15	Panel Sections	III-21
III-16	Assumptions for Flat Panel Analysis	III-24
III-17	Thermal Stress vs. Hot Skin Temperature for Varying Thermal Gradients ( $\Delta T$ ) thru Beryllium Faced Panels.	III-25
III-18	Sheet Beryllium Leading Edge	III-26
III-19	Thermal Stresses vs. Hot Skin Temperatures for Varying Thermal Gradients ( $\Delta T$ ) thru Inconel X Faced Panels	III-27
III-20	Thermal Stress vs. Hot Skin Temperature for Varying Thermal Gradients ( $\Delta T$ ) thru Inconel X Outer Face and Beryllium Inner Face	III-28
III-21	Thermal Stress vs. Hot Skin Temperatures for Varying Thermal Gradients ( $\Delta T$ ) thru Inconel Outer Face and Beryllium Inner Face	III-29
III-22	Geometry for General Analysis	III-35
III-23	Deflection vs. Edge Load for Various Temperature Gradients on a Beryllium Sandwich Panel.	III-41

# LIST OF FIGURES -continued-

<u>SECTION</u>		<u>PAGE</u>
SECTION III-cont'd		
III-24	Compressive Stress at Center of Hot Face of Beryllium Sandwich Panel vs. Compressive Edge Load for Various Temperature Gradient	III-43
III-25	Isotherm and Adiabatic Line Patterns	III-47
III-26	Thermantic Heat Flow Analysis Lumped Parameter Mathematical Model	III-48
III-27	Thermantic Heat Flow Analysis	III-49
III-28	Lumped Thermal Conductivities	III-51
III-29	Vibration--Schematic View of the Thermantic Concept	III-52
III-30	Vibration Environment for 3" x 3" Test Specimen	III-53
III-31	Resonant Frequency vs. Plate Dimensions	III-56
SECTION IV		
IV-1	Results of Emissivity Tests of Various Oxides	IV-9
IV-2	Thermal Expansion of Silica Foam	IV-11
IV-3	Thermal Expansion of Alumina Foam	IV-12
IV-4	Thermal Expansion of Zirconia Foam	IV-13
IV-5	Typical Foam Ceramic Panel before Exposure to Exhaust of J75 Turbojet	IV-21
IV-6	Foamed Ceramic Panel after Exposure to Exhaust of Turbojet	IV-22
IV-7	Schematic--Overall Test Setup	IV-23
IV-8	Results of Ramjet Exposure Test	IV-24
IV-9	Silica Panel before Exposure to Ramjet Exhaust	IV-25
IV-10	Silica Panel after Exposure to Ramjet Exhaust	IV-26
IV-11	Schematic of Panel Configuration	IV-28
IV-12	Schematic of Compression Test Fixture	IV-29
IV-13	X-ray View of a Section of the Test Panel	IV-30
IV-14	Schematic of Thermocouple and Dial Indicator Locations	IV-31
IV-15	Panel Deflections--Room Temperature Compression Test	IV-32
IV-16	Panel Deflections--Thermal Gradient Test	IV-35
IV-17	Panel Deflections--Compressive Test at 200°F (100°FΔT)	IV-36
IV-18	Panel Deflections--Compressive Test at 250°F (100°FΔT)	IV-37
IV-19	Panel Deflections--Compressive Test at 350°F (150°FΔT)	IV-38
IV-20	18" x 18" Flat Beryllium-Faced Honeycomb Panel after Testing at 350°F (150°FΔT)	IV-39
IV-21	Beryllium Sheet Compression Test--Sample #1	IV-43
IV-22	Beryllium Sheet Compression Test--Sample #2	IV-44
IV-23	Beryllium Sheet Compression Test--Sample #6	IV-45
IV-24	Beryllium Sheet Compression Test--Sample #7	IV-46
IV-25	Beryllium Sheet Compression Test--Sample #8	IV-47
IV-26	Beryllium Sheet Compression Test--Sample #9	IV-48
IV-27	Beryllium Sheet Compression Test--Sample #10	IV-49
IV-28	Cantilever Bend Test of Beryllium Sheet	IV-51

LIST OF FIGURES -continued-

<u>SECTION</u>		<u>PAGE</u>
SECTION IV -cont'd-		
IV-29	Braze Area of Honeycomb Panel--Beryllium Faces, 321	IV-54
	Stainless Steel Core and Silver-Copper--Lithium Braze Alloy	
IV-30	Failed Flatwise Tensile Specimens	IV-57
IV-31	Core Shear Specimen Under Test	IV-59
SECTION V		
V-1	Formed Beryllium Channels	V-6
V-2	Single and Double Curved Beryllium Skins	V-7
V-3	Single Curved Beryllium Leading Edge Skins	V-8
V-4	Quartz Lamp Brazing System	V-9
V-5	Typical Beryllium-Faced Brazed Honeycomb Sandwich Panels	V-12
V-6	Large Glasrock Die	V-13
V-7	18" x 18" Flat Beryllium Faced Panel	V-14
V-8	18" x 18" Flat Composite Panel	V-15
V-9	Single Curvature Beryllium Faced Panels	V-16
V-10	18" x 18" Double Curved Composite Panel	V-17
V-11	Small Leading Edge Panels with Brazing Retort	V-19
V-12	Typical Leading Edge Panels	V-20

# LIST OF TABLES

<u>SECTION</u>		<u>PAGE</u>
Section III		
III-1	Results of Thermantic Heat Flow Analysis (Microscopic Study)	III-50
Section IV		
IV-1	Results of Block Compression Tests on Foamed Ceramics	IV-2
IV-2	Results of Flexure Tests on Foamed Ceramics	IV-3
IV-3	Thermal Conductivity of Foamed Ceramics	IV-4
IV-4	Thermal Conductivity of Composite Structures	IV-5
IV-5	Thermal Expansion Rates of the Foamed Ceramics	IV-14
IV-6	Thermal Exposure Tests	IV-15
IV-7	Test Results from Afterburner and Ramjet Exposures on Thermantic Construction	IV-17
IV-8	Temperature Levels Measured in the Test Panel during Thermal Gradient Test	IV-34
IV-9	Tensile Tests of Beryllium	IV-41
IV-10	Compressive Modulus of Elasticity and 0.02% Yield Point for Sheet Beryllium at Room Temperature	IV-50
IV-11	Composition of Brazing Alloys	IV-53
IV-12	Flatwise Tensile Tests Results - Honeycomb Structure	IV-56
IV-13	Edgewise Compressive Tests of Beryllium Honeycomb Panels	IV-58
IV-14	Core Shear Test Results	IV-60
IV-15	Flexure Tests of Beryllium-faced Honeycomb Structures	IV-61
Section V		
V-1	Typical Sequence of Manufacture of Brazed Sandwich Panels	V-10

## SECTION I

### INTRODUCTION

This volume selects information from Volume II, "Materials and Process," and presents it in a form suitable for preliminary design considerations. Supplementary information is added to bring out the potential application of the thermantic\* structural concept to re-entry vehicles.

It is emphasized, however, that the prime effort of the program was to develop concepts and fabrication processes for beryllium structures and for ceramic heat shield materials for re-entry flight. Development of design information represented a relatively small portion of the work. There was no intent to compile sufficient analysis and test information to satisfy a designer; the objective was to show basic feasibility of the concepts proposed. At the time of the contract start in early 1960, the outlook for practical beryllium panels appeared discouraging. Also, the concept of radiation cooled re-entry had received little serious attention because of the unavailability of promising insulating refractory materials.

Nevertheless, in the course of developing radiation cooled concepts and structures utilizing beryllium and ceramics, enough information relevant to design, and particularly preliminary design, was obtained to make desirable the separation of this design information from the basic materials and process information covered in Volume II.

The desirability of an insulating heat shield to resist temperatures in excess of 3000°F appeared obvious with respect to (a) minimizing internal structural problems and permitting use of conventional metals, (b) avoiding oxidation problems associated with refractory metal heat shields, and (c) enabling considerable growth potential towards super-orbital flight requirements in view of the high temperature resistance of the ceramics.

However, the limitations of brittle materials were not minimized. It was decided at the outset to make maximum use of the insulating properties and temperature resistance of the oxide ceramics but to limit their structural function. Consequently, the thermantic construction distributes structural loads to the metal components. The function of the ceramic is to protect the load bearing components from the severe thermal environment. In this capacity the ceramic must exhibit high durability under extreme thermal shock, high temperature levels, and high acoustic levels.

---

\*For the purposes of this report, thermantic structures shall be defined as those structures which are capable of maintaining structural integrity when exposed to external surface temperatures in the 1800° - 3000°F range during flight operations, and thermantic flight conditions shall be described as those conditions which expose the external surface of the flight vehicle to temperatures in the 1800° - 3000°F range due to aerodynamic heating.

Manuscript released by the authors January 1962 for publication as an ASD Technical Report.

With these requirements in mind, and also the perennial necessity for minimizing weight, reinforced porous lightweight ceramics were an obvious promising approach. Early success in durability tests in turbojet and ramjet engine exhausts confirmed the concept and the potential. The development work progressed rapidly and three basic ceramic systems (zirconia, alumina, silica) were found to offer sufficient durability to merit prime consideration for re-entry vehicle systems.

The beryllium development work performed resulted in the first large brazed sandwich panels. Here again, extensive detailed design information was not derived though fabrication feasibility was demonstrated and good panel properties were obtained. The potential of beryllium panels for aerospace structures was clearly indicated. This volume summarizes the beryllium work performed, indicates a number of promising applications, and it is hoped will stimulate designers to visualize additional ways to take advantage of the unusual low weight and high stiffness of beryllium.

## SECTION II

### CONCEPT APPLICATIONS

#### A. INTRODUCTION

The composite construction (typical designs shown in Figures II-1 and II-2) is a method of combining ceramic insulation material with more conventional airframe construction. This construction provides inherent reliability in the ceramic-metal joining system. Catastrophic failure, which characterizes monolithic ceramics under thermal stresses, is eliminated by the individual ceramic cell arrangement. The airframe structure is protected from severe environments by the ceramic and consequently can consist of high temperature alloy metals rather than the more difficult to handle refractory metals. The thermantic structure is compatible with lifting body vehicle systems in that it offers very favorable weight characteristics. Panels constructed under this contract showed a weight of 3.85 lbs/ft<sup>2</sup> in heat shield and backup sandwiches. From this value, considering heat shield, load bearing structure, joints, internal structure, coolant and heat exchanger, a theoretical total weight of 4.5 lbs/ft<sup>2</sup> appears feasible. Moreover, even more favorable weight characteristics can be expected in the normal course of materials improvement. In addition, the thermantic concept has inherent reliability features which can be summarized as follows:

##### 1. Maximum Use of Available Materials

The relatively cold load bearing structure, to a large degree, is designed and constructed according to well developed aircraft techniques.

The radiation cooled insulated heat shield enables low temperature internal environments, thus permitting increased use of presently available equipment, instrumentation, and mechanisms.

##### 2. Durability and Chemical Stability

The structure utilizes components which are chemically stable in their operating environments. Ceramics are used where highest temperatures occur, and structural metal components are operated in temperature ranges in which they have good structural and chemical properties. Also, the relatively thick ceramic insulation minimizes erosion risks from meteoroids and space radiation particles, so that repeated use can be contemplated.

##### 3. Fail Safe Features

Because the load bearing structure is relatively cold, a time interval will be required in the event of heat shield failure to seriously overheat the support structure. The time interval will enable preparation for ejection or for change in re-entry path. The increase in heat transfer resulting from small local failures may be distributed by the cooling system so that a long time interval may be available for emergency action.

##### 4. Capacity for Growth

The thermantic construction utilizes the favorable thermal properties of ceramics, and by use of sufficient reinforcement avoids the mechanical limitations of ceramic materials. However, ceramic technology is in its

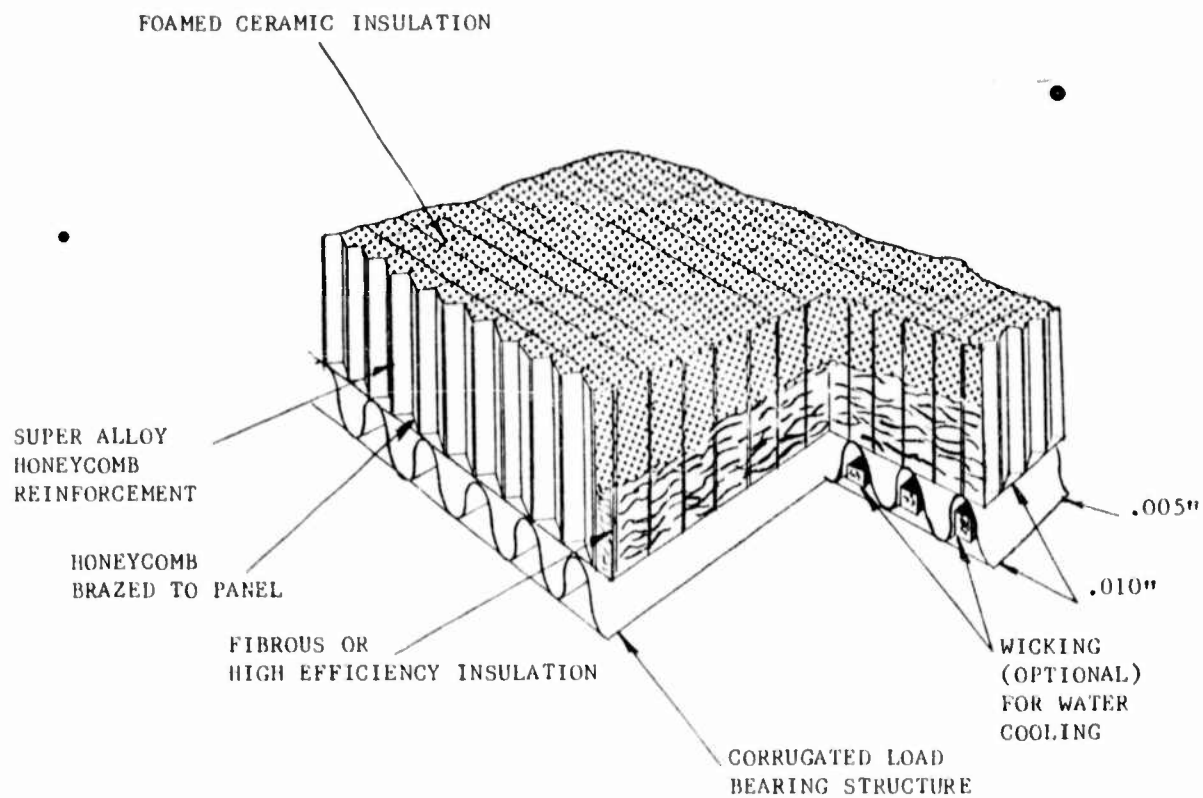


Figure II-1 Thermantic Construction

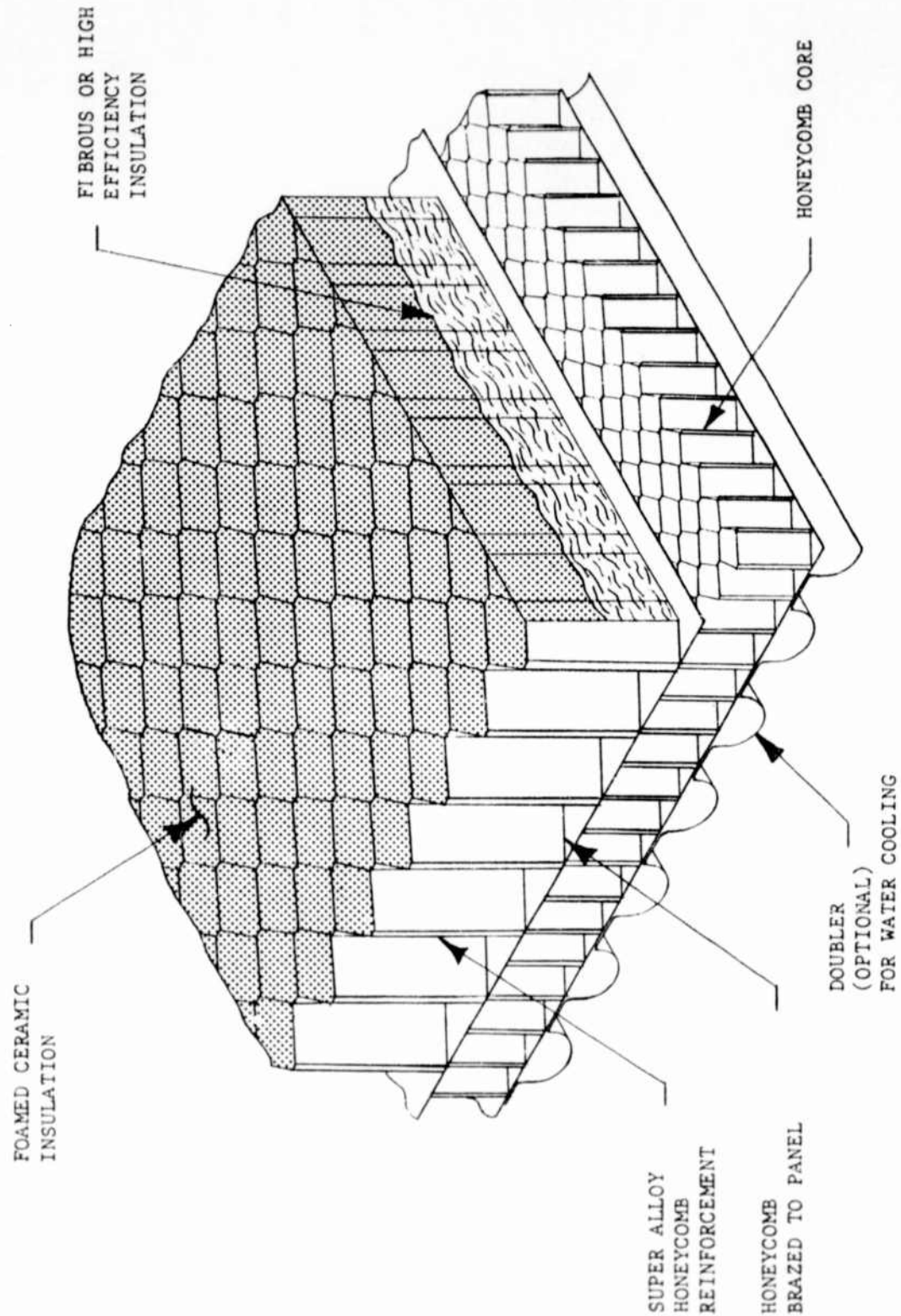


Figure II-2 Thermantic Construction

infancy and rapid progress is being made to reduce reinforcement requirements. For example, reinforcement honeycomb cell diameter has been successfully increased from  $\frac{1}{4}$ " to  $\frac{1}{2}$ ". Still larger cells are a likely future development.

Possibilities for extending the functions of this construction include the utilization of the ablative properties of ceramics or plastics. For example, for supercircular re-entry a portion of a ceramic or a plastic component may ablate, and when speeds are reduced, the remaining ceramic would act as a radiation cooled structure. Transpiration cooling during superorbital velocities is also compatible with porous ceramic heat shields. In a transpiration system, the fluid may be ejected through ports which are connected to an internal compartment cooling system.

## B. APPLICATIONS

### 1. Lifting Body Re-entry Vehicles

The ceramic composite construction shows excellent potential as the prime structure for re-entry vehicles. In the case of lifting body vehicle shapes, such as depicted in Figure II-3, the composite construction shows advantageous application on almost all of the vehicle's surfaces. Major vehicle sections which require a high temperature resistant structure include the nose cap, forward fuselage, cabin, and control surfaces. The ceramic composite offers maximum utilization of internal volume by enabling low temperatures throughout the interior. Since most of the incident heat flux is radiated away at the ceramic surface, relatively simple and small cooling systems are needed to maintain environments compatible with personnel and equipment needs.

In the following discussion, a study is presented showing the structural and thermal features of a lifting body vehicle section with ceramic composite skin construction. The vehicle portion selected is the forward fuselage section, which for a typical re-entry trajectory would be generally subjected to intense heating in the 2500° F. to 3000° F. temperature range. Temperatures in excess of 3000° F. may be experienced at local forward areas, and more widely under off-design flight conditions.

#### a. Description of Typical Fuselage Construction

The forward section of a re-entry lifting body is shown in Figure II-4. It is basically a semi-monocoque structure consisting of a thermally protected brazed sandwich shell stabilized by conventional inertia bulkheads.

The thermal protection is afforded primarily by foamed ceramic and fibrous insulation. An open face honeycomb core is brazed to the outer face of the basic sandwich panel. This open face honeycomb is partially filled with fibrous insulation and capped with foamed ceramic. The depth of the fibrous insulation and the foamed ceramic is selected, according to the expected thermal environment, to maintain an optimum weight and thermal insulation relationship. Though a one inch thick heat shield appears optimum on the basis of preliminary studies, it is possible that a thorough thermal analysis over a complete re-entry trajectory may enable reduction of heat shield

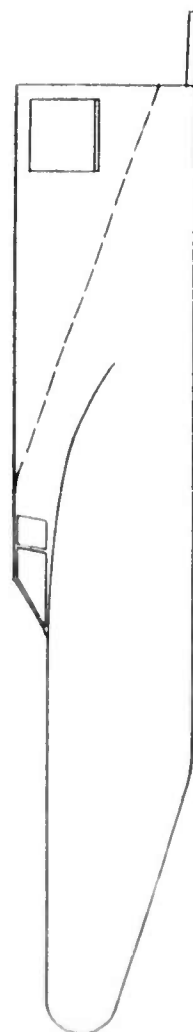
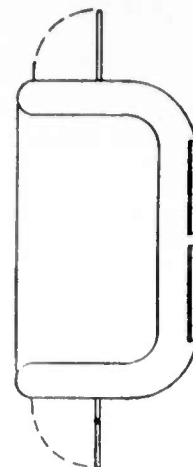
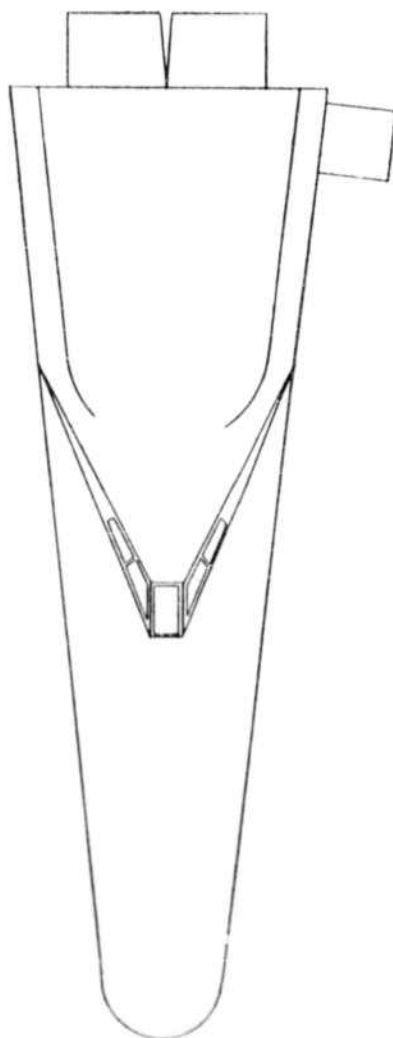


Figure II-3 Views of Lifting Body Vehicle

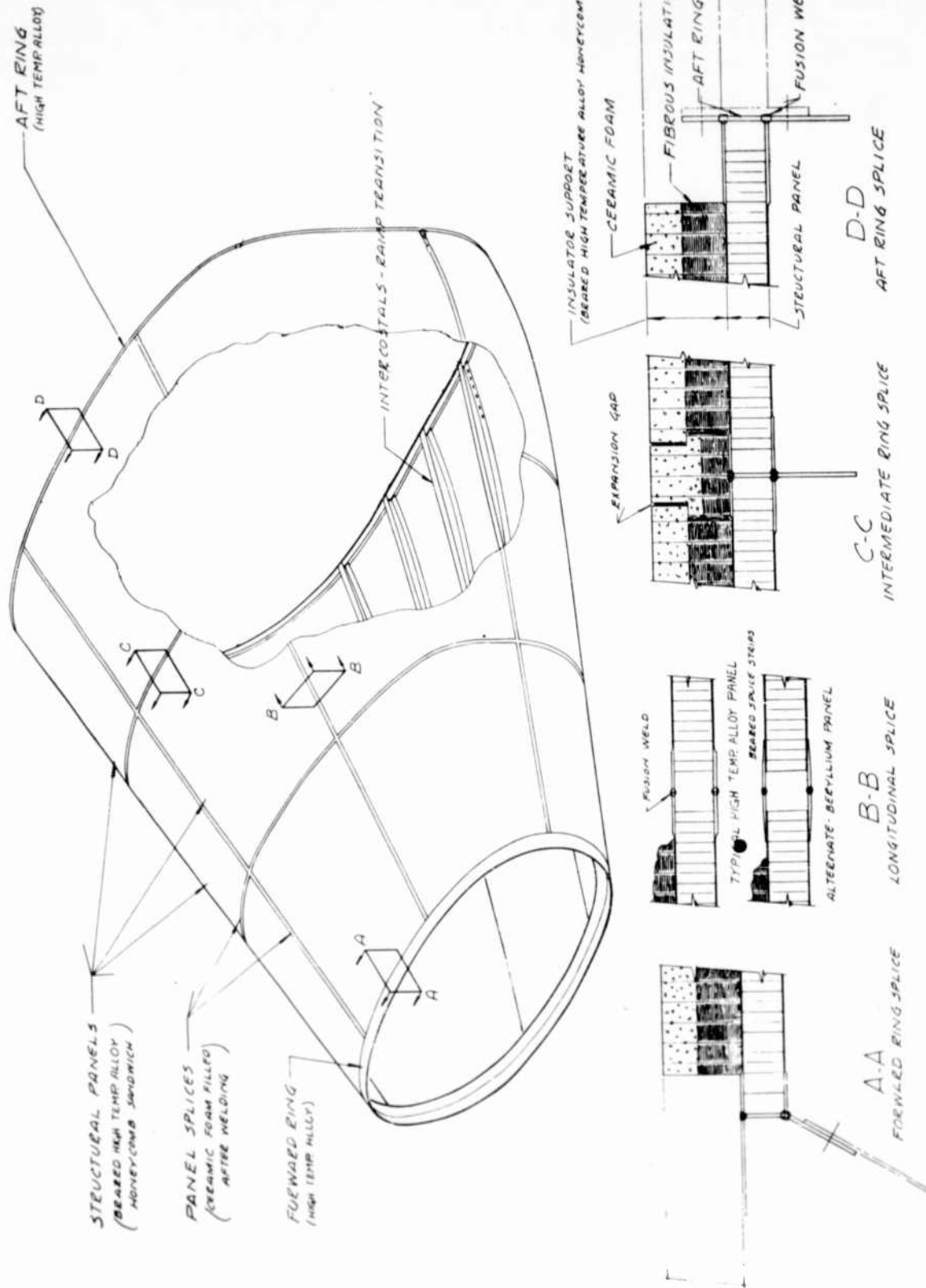


Figure II-4 Structural Arrangement-Lifting Body Vehicle

thickness in local regions. Ceramic surface treatments are provided to produce high emissivity and increased erosion resistance.

(1) Structural Panels

Several load bearing panel designs are possible: the design most readily available utilizes superalloy (such as Inconel "X") or stainless steel faces. However, beryllium faces and combinations of beryllium and superalloy faces offer weight advantages at the expense of greater fabrication costs.

The preliminary selection for the core within the panel faces is 3/16" cell diameter honeycomb, .001" thickness 17-7 PH stainless steel. Corrugated core should be given further consideration, but initial studies indicate that corrugated core designs generally require heavier faces to avoid buckling between convolutions. Beryllium faces present an exception, however, because of the high stiffness of the metal.

(2) Support Structure

It is expected that two shear distribution bulkheads are needed to transmit the shear component into the skins. The bulkheads may be located at each end of the fuselage section, or at two intermediate locations, depending on payload configuration. The bulkheads also serve as stabilizing members for the shear panels.

A vertical shear web connects the bulkheads and distributes the longitudinal load component to the bulkhead frames and the skins, thereby eliminating local introduction of loads with accompanying high moments.

Channel stiffeners are provided in the transition area between the ramp and the cabin to react to local bending moments. The moments arise because of the change in direction of the axial load path in this region.

Bulkheads and stiffeners may be constructed of 15-7 PH or 17-7 PH stainless steel.

Satisfactory thickness of bulkhead frames is approximately .020". Panel stiffener channels are expected to be .010" thick with .020" thick caps.

(3) Joints

Joint configurations for the sandwich panels are shown in Figure II-4. These designs evolved from considerations of (a) efficiency of transferring panel facing stresses, (b) attachment of any required structure, such as rings or longerons, (c) pressurization requirements, (d) dynamic loads, (e) cooling manifold requirements, (f) thermal relief, if required, and (g) manufacturing producibility consistent with the state-of-the-art of large welded aircraft steel structure.

Considerable weight saving and higher integrity can be obtained by proper treatment, or in most cases elimination of panel edge members. Solid or channel type edge members are relatively less efficient in weight and performance than splice straps or direct connections. This conclusion is also derived from analyses of B-70 structure, which utilizes direct panel connection. For lifting body panels with steel face sheets, recommended joining method is fusion welding of the adjoining skins. An additional thickness of steel is provided in the area of the weld to compensate for reduced allowables and for reaction to local differential loads.

For beryllium faced panels, for which welding is not recommended because of the low strength of beryllium welds, a tapered steel splice plate is brazed to the faces of the panels. These straps are in turn fusion welded to provide the connection.

#### (4) Cooling System

To hold the water in position during flight, two materials were considered: "Thermosorb" and wicking. The highly insulative structure results in a warm surface (approximately 400° F.) facing the sun and a cold surface away from the sun. For long orbiting flight, a completely passive coolant system would gradually exhaust the coolant attached to the warm walls. Circulation of a small amount of fluid to the warm and cold walls would provide a thermal balance and prevent consumption of the coolant during the orbiting phase. Also, the evaporation pressure would be controlled below the relief value setting. Consequently, a solid coolant system with provisions for some circulation during orbit would satisfy mission requirements.

A wicking system, again with some fluid circulation during orbit, is also feasible, though boost accelerations complicate the problem of assuring proper water distribution and avoiding weight shifts in the vehicle.

A prime consideration in the installation of the water coolant is the possibility of recharging for more than one mission. Configuration studies indicate that the lightest method of recharging the cooling system is to provide an access slot covered with a thin cover strip adhesive bonded to this manifold. Although the bond line is non-structural, the adhesive must be capable of withstanding temperatures up to 800° F. without failure.

For reliability of the cooling system, a general inter-connection is maintained between panel vents. Therefore, a failure of any one pressure relief valve will result in merely diverting exhaust vapor to a valve in another area with only a slight increase in pressure and boil-off temperature. A fail safe feature is thus

provided; in the event of local structural failure, a finite time interval would elapse before the coolant is exhausted. The time interval may be a definite design requirement to suit ejection requirements for the pilot under certain failure conditions.

Cooling systems are shown in Figures II-5 and II-6 for each of the two basic structural panels considered. Manifolding and a distributed relief valve arrangement is indicated. A central relief system is also possible though the tubing required is likely to show a weight disadvantage. A distributed relief system has potential for providing transpiration cooling over critical areas during superorbital re-entry velocities.

Relief valves, shown in Figure II-6, show relief through a porous ceramic fill. The ceramic is intended to protect metal components and prevent hot gas flow to the interior.

#### (5) Weight Analysis

The various structural configurations indicated in Figure II-7 are defined in Figure II-8. For purposes of weight analysis the structure is divided into the following major sections:

1. Heat Shield
2. Basic Panel
3. Support Structure
4. Interior Insulation
5. Miscellaneous hardware, shock mounts, bolting for equipment, etc.

It can be seen that items 1, 3, 4 and 5 are independent of the method of construction of the basic panel and are constant for a particular insulating configuration. Inspection of the component weights of the basic panel shows that all weights are constant except for skins and edge members. Consequently the differences in total weights shown in Figure II-7, for a particular insulating configuration, can be contributed to the face materials and the panel edge treatment.

Minimum weight is offered by Configuration II which, including .71 pounds  $H_2O/ft.^2$ , yields a theoretical total weight of 4.29 pounds per square foot using beryllium face sheets. (Refer to Figure II-8 for further comparison of structure and coolant weights.)

#### b. Thermal Characteristics of Structure

##### (1) Performance during Re-entry

##### (a) Performance as Lifting Re-entry Structure

The thermal performance of the ceramic surfaces proposed is based on radiation rejection of a large portion of the thermal energy received during re-entry. Ceramic surfaces

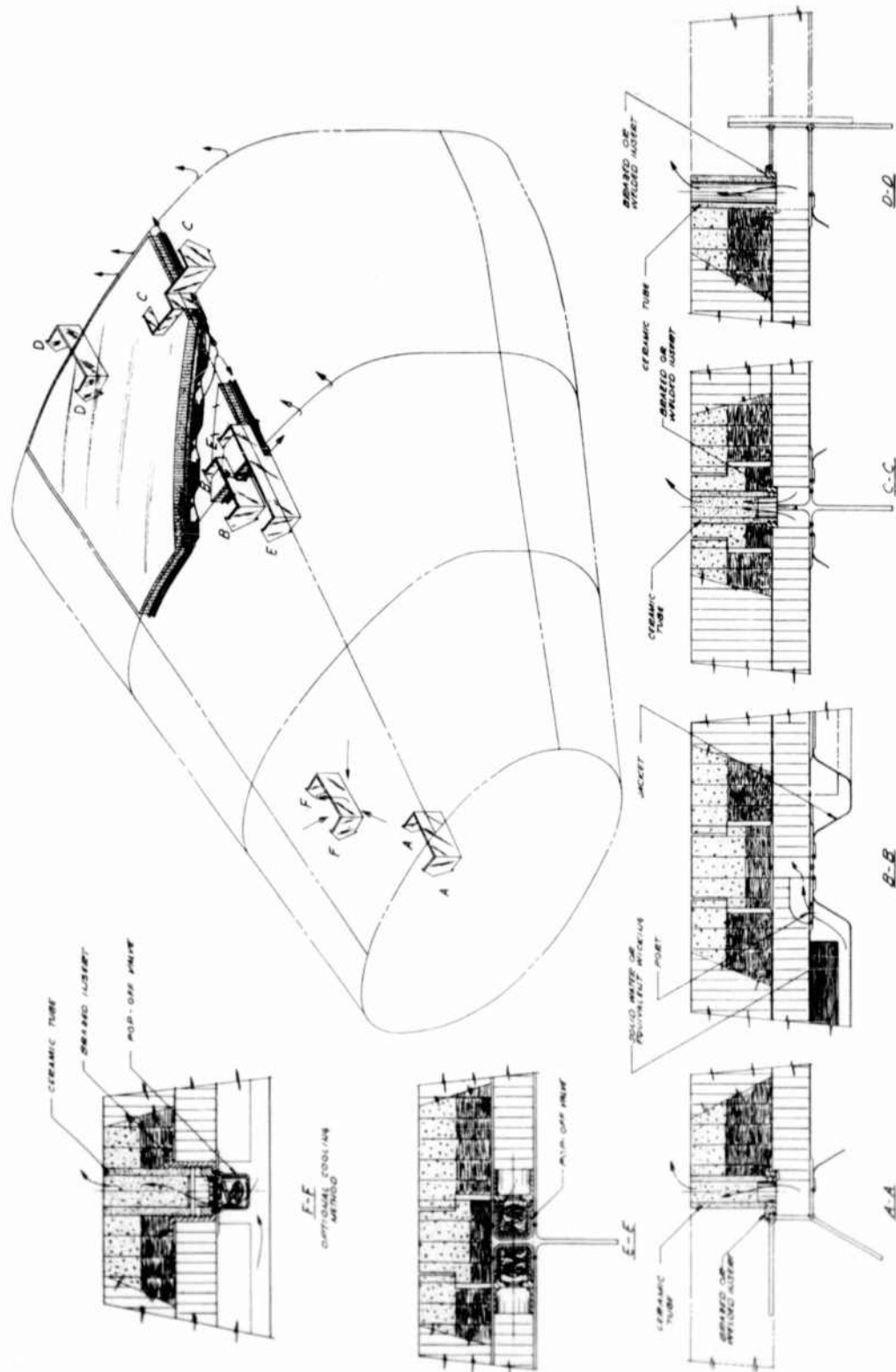


Figure II-5 Cooling System-Honeycomb Structural Panel

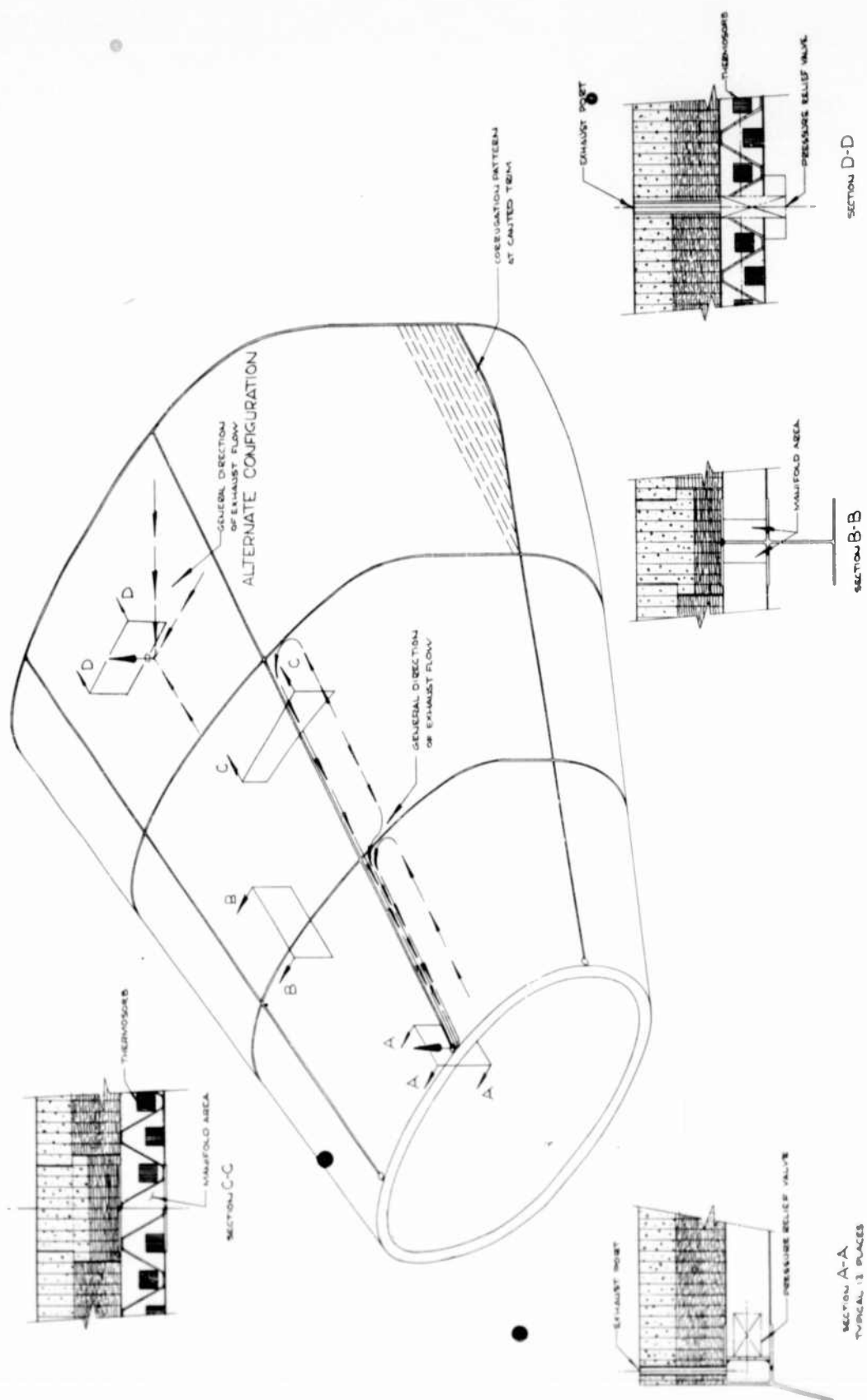


Figure II-6 Cooling System - Corrugated Structural Panel

SANDWICH FACE MATERIAL △ CONFIGURATION	BERYLLIUM						1 BERYLLIUM: 1 INCONEL X						INCONEL X					
	II	III	V	VI	II	III	V	VI	II	III	V	VI	II	III	V	VI	II	III
HEAT SHIELD (TOTAL)	1.742	1.742	2.030	2.030	1.742	1.742	2.030	2.030	1.742	1.742	2.030	2.030	1.742	1.742	2.030	2.030	1.742	1.742
CERAMIC	1.050	1.050	1.400	1.400	1.050	1.050	1.400	1.400	1.050	1.050	1.400	1.400	1.050	1.050	1.400	1.400	1.050	1.050
FLAME SPRAY	.200	.200	.200	.210	.200	.200	.200	.210	.200	.200	.200	.210	.200	.200	.200	.210	.200	.200
FIBEROUS INSULATION	.312	.312	.250	.250	.250	.250	.250	.250	.250	.250	.250	.250	.250	.250	.250	.250	.250	.250
OUTER HONEYCOMB CORE	.080	.080	.080	.080	.080	.080	.080	.080	.080	.080	.080	.080	.080	.080	.080	.080	.080	.080
BRAZE FOIL	.100	.100	.100	.100	.100	.100	.100	.100	.100	.100	.100	.100	.100	.100	.100	.100	.100	.100
BASIC PANEL (TOTAL)	1.009	1.009	1.009	1.009	1.009	1.009	1.009	1.009	1.009	1.009	1.009	1.009	1.009	1.009	1.009	1.009	1.009	1.009
OUTER SKIN	.178	.178	.178	.178	.178	.178	.178	.178	.178	.178	.178	.178	.178	.178	.178	.178	.178	.178
CORE	.249	.249	.249	.249	.249	.249	.249	.249	.249	.249	.249	.249	.249	.249	.249	.249	.249	.249
BRAZE FOIL	.200	.200	.200	.200	.200	.200	.200	.200	.200	.200	.200	.200	.200	.200	.200	.200	.200	.200
INNER SKIN	.178	.178	.178	.178	.178	.178	.178	.178	.178	.178	.178	.178	.178	.178	.178	.178	.178	.178
PANEL EDGE MEMBERS	.204	.204	.204	.204	.204	.204	.204	.204	.204	.204	.204	.204	.204	.204	.204	.204	.204	.204
SUPPORT STRUCTURE (TOTAL)	.503	.503	.503	.503	.503	.503	.503	.503	.503	.503	.503	.503	.503	.503	.503	.503	.503	.503
FRAMES	.212	.212	.212	.212	.212	.212	.212	.212	.212	.212	.212	.212	.212	.212	.212	.212	.212	.212
WEBS	.239	.239	.239	.239	.239	.239	.239	.239	.239	.239	.239	.239	.239	.239	.239	.239	.239	.239
STIFFENERS	.046	.046	.046	.046	.046	.046	.046	.046	.046	.046	.046	.046	.046	.046	.046	.046	.046	.046
INTERIOR INSULATION (TOTAL)	.225	.433	.225	.433	.225	.433	.225	.433	.225	.433	.225	.433	.225	.433	.225	.433	.225	.433
FIBEROUS INSULATION	—	.008	—	.008	—	.008	—	.008	—	.008	—	.008	—	.008	—	.008	—	.008
COOLANT SUPPORT STRUCTURE	.225	.425	.225	.425	.225	.425	.225	.425	.225	.425	.225	.425	.225	.425	.225	.425	.225	.425
MISC. HARDWARE	.100	.100	.100	.100	.100	.100	.100	.100	.100	.100	.100	.100	.100	.100	.100	.100	.100	.100
TOTAL Weight (Lbs/Ft <sup>2</sup> )	3.50	3.787	3.867	4.075	3.74	3.948	4.028	4.236	3.901	4.103	4.183	4.337	3.901	4.103	4.183	4.337	3.901	4.103
△ FOR DEFINITION OF CONFIGURATIONS SEE FIG II-8																		

Figure II-7 Weight Distribution - Flight Vehicle

		CONFIGURATION I.				CONFIGURATION II.				CONFIGURATION III.			
		AVERAGE HEATING CONDITION		TYPICAL MAXIMUM LOCAL HEATING		AVERAGE HEATING CONDITION		TYPICAL MAXIMUM LOCAL HEATING		AVERAGE HEATING CONDITION		TYPICAL MAXIMUM LOCAL HEATING	
		30	30	90	90	30	30	90	90	30	30	90	90
A	TEMP. 1 PLANE A	.8	.8	.9	.9	.8	.8	.9	.9	.8	.8	.9	.9
B	TEMP. 2 PLANE B	2500	2500	3400	3400	2500	2500	3400	3400	2500	2500	3400	3400
C	TEMP. 3 PLANE C	2320	2285	2955	3070	2210	2290	3015	3075	2265	2325	3070	3130
D	TEMP. 4 PLANE D	100	895	100	950	430	940	530	1005	745	1210	950	1405
	TEMP. 5 PLANE E	100	800	100	800	100	800	100	800	545	1130	720	1305
	TEMP. 6 PLANE F	--	--	--	--	--	--	--	--	100	800	100	800
	TEMP. 7 TO HEAT EXCHANGER	.846	--	1.3	--	.817	--	1.13	--	.692	--	.965	--
	TEMP. 8 TO HEAT EXCHANGER	--	.634	--	1.23	--	.615	--	.945	--	.504	--	.785
	TEMP. 9 TO HEAT EXCHANGER	.822	--	1.13	--	.71	--	.98	--	.601	--	.532	--
	TEMP. 10 TO HEAT EXCHANGER	1.42	1.34	1.42	1.34	1.23	1.30	1.23	1.31	1.04	1.08	1.05	1.09
	TEMP. 11 TO HEAT EXCHANGER	1.40	--	1.71	--	1.29	--	1.56	--	1.39	--	1.63	--
	TEMP. 12 TO HEAT EXCHANGER	--	--	--	--	1.45	--	1.72	--	1.55	--	1.79	--
	TEMP. 13 TO HEAT EXCHANGER	--	--	--	--	1.61	--	1.88	--	1.71	--	1.95	--

NOTE: TEMPERATURES ARE BASED ON AVERAGE HEATING AREA AND VEHICLE INTERNAL STRUCTURE.

Figure II-8 Thermal Characteristics of Lifting Body Configuration

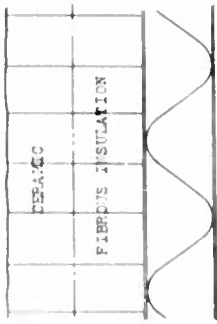
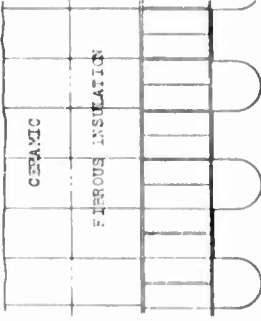
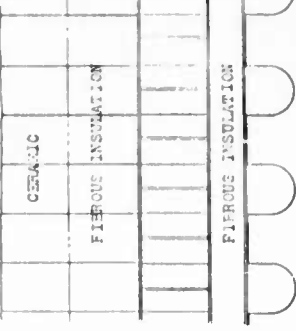
A 1 5" B 1 5" C 1 5" D 1 5"				CONFIGURATION IV.						CONFIGURATION V.						CONFIGURATION VI.					
				AVERAGE HEATING CONDITION			TYPICAL MAXIMUM LOCAL HEATING			AVERAGE HEATING CONDITION			TYPICAL MAXIMUM LOCAL HEATING			AVERAGE HEATING CONDITION			TYPICAL MAXIMUM LOCAL HEATING		
				30	30	90	30	90	90	30	30	90	30	90	90	30	30	90	30	90	90
CONVECTED	BTU/FT <sup>2</sup> -SEC			.8	.8	.9	.8	.9	.9	.8	.8	.8	.8	.9	.9	.8	.8	.8	.8	.9	.9
TEMP. OF PLATE A	OP			2500	2500	3400	2500	2500	3400	2500	2500	2500	2500	3400	3400	2500	2500	3400	2500	3400	3400
TEMP. OF PLATE B	OP			2010	2175	2725	2084	2176	2610	2084	2176	2610	2084	2176	2610	2155	2245	2915	2155	2245	3000
TEMP. OF PLATE C	OP			100	905	100	463	928	524	100	463	928	524	100	960	810	1250	1040	810	1250	1470
TEMP. OF PLATE D	OP			100	800	100	100	800	100	100	100	800	100	800	800	590	1165	785	590	1165	1360
TEMP. OF PLATE E	OP			--	--	--	--	--	--	--	--	--	--	--	--	100	800	100	100	800	800
NET Q TO HEAT EXCHANGER	BTU/FT <sup>2</sup> -SEC			1.08	--	1.49	.918	--	1.27	--	.918	--	1.27	--	1.10	.761	--	1.062	--	--	--
NET Q TO INTERIOR	BTU/FT <sup>2</sup> -SEC			--	.72	--	--	1.10	--	--	--	.715	--	--	--	--	.564	--	--	.971	--
WATER EVAPORATED IN 15 MINUTES	LB/FT <sup>2</sup>			.94	--	1.253	.80	--	1.106	--	.80	--	1.106	--	--	.661	--	.924	--	--	--
SQUARE HEAT PULSE	BTU/HR-FT <sup>2</sup>			1.624	1.52	1.624	1.38	1.521	1.389	1.515	1.38	1.515	1.389	1.521	1.521	1.14	1.19	1.16	1.14	1.16	1.21
OVER-ALL CONDUCTANCE	BTU/HR-FT <sup>2</sup>			4.81	--	5.17	1.67	--	4.97	--	1.67	--	4.97	--	--	4.74	--	5.00	--	--	--
WEIGHT OF ONE RECYCLING, ONE INTERIOR "X" FACE	LB/FT <sup>2</sup>			--	--	--	4.83	--	5.13	--	4.83	--	5.13	--	--	4.90	--	5.16	--	--	--
WEIGHT OF ONE RECYCLING, ONE INTERIOR "Y" FACE	LB/FT <sup>2</sup>			--	--	--	4.99	--	5.30	--	4.99	--	5.30	--	--	5.06	--	5.32	--	--	--
WEIGHT PER SQUARE FOOT OF SURFACE AREA INCLUDES WATER AND VEHICLES INTERNAL STRUCTURE				--	--	--	--	--	--	--	--	--	--	--	--	--	--	--	--	--	--

Figure II-8 (Cont.) Thermal Characteristics of Lifting Body Configuration

capable of withstanding temperatures in excess of 3000° F. are thermally suitable for a wide range of re-entry conditions.

(a-1) Error Conditions

A lifting re-entry vehicle flying at a constant angle of attack during initial re-entry will experience a skipping trajectory. Because of the non-zero re-entry angle, the vehicle will descend to some initial minimum altitude where the lift-force plus centrifugal force exceeds the vehicle weight. The flight path angle then increases until the resultant force is again downward. The vehicle follows this oscillatory flight path with each successive minimum altitude occurring at a lower level. Eventually the path oscillations damp out to the equilibrium glide condition. The rate at which these motions are damped out is an inverse function of vehicle L/D ratio.

The vehicle may experience the highest heat rates in the skipping phase of the trajectory. The severity of the heating will depend on the initial re-entry angle and angle of attack changes.

An entry error causing an increased entry angle will result in large increases in heat rate. A change in angle of attack at the wrong time can also cause large increases in heating rate.

The thermantic structure offers the possibility of surviving large, off-design heat rates. For extreme heat pulses, the melting point of the ceramic may be reached. Ablation of the outer surfaces will protect the structure for a certain interval. An extra thickness of ceramic may be designed into the structure to meet such conditions.

(a-2) Super-Orbital Flight and Re-entry

The thermantic structural concept is adaptable to the thermal environment associated with flight at super-orbital velocities or re-entry from lunar flights. Initially, such a vehicle will enter the atmosphere in an inverted position and develop lift in the negative direction to counteract centrifugal force. As the vehicle decelerates to orbital or sub-orbital velocity, it is rolled to the positive lift attitude and a normal re-entry is executed.

(a-3) Fail Safe Features

The construction is an inherently fail-safe design concept. In the event of skin penetration as the result of meteorite impact the water coolant will

prevent rapid local temperature rise and a catastrophic structural failure. Though the damage may be such as to ultimately render the vehicle untenable, a delay sufficient for initiation of escape procedures would most probably be available.

If the penetration should occur after the coolant supply is exhausted and is located in a non-critical area, the local interior temperature may be allowed to rise without suffering excessive damage.

(a-4) Extensions to Thermantic Concept

The thermantic structure concept is readily adaptable to modifications which will extend its mission capabilities.

In order to accommodate severe off-design heating conditions, an additional layer of ceramic may be applied to the surface and be utilized as an ablative heat shield. Plastic ablators may also be considered for short duration with large heat pulses.

Transpiration cooling may be employed for less severe applications. The porous nature of the ceramic structure is readily adaptable to this system.

In a structure where a coolant is used on the inner surface, the coolant vapors may be vented directly into the boundary layer through the coolant pressure control parts.

(2) Thermal Performance of Sandwich Design

A large number of composite sandwich configurations have been studied in the quest for an optimum design. Six of these designs were selected as being near optimum for application to lifting body re-entry vehicles. These designs are illustrated in Figure II-8 along with their respective thermal characteristics and temperature gradients. All designs can be used with or without water cooling of the inside surface depending upon internal temperature requirements. Two heating conditions were considered: (1) an average heating condition defined as that which would be experienced over large areas of the vehicle aft of the nose region; (2) the maximum local heating condition as representative of temperatures just aft of the stagnation region.

All composite structural sandwich designs are built up in the same manner. The open face honeycomb depth is one inch and is brazed to one face of a structural sandwich. Configurations I

through III utilize a 0.375 inch ceramic thickness and 0.625 inch insulation thickness. Configurations IV through VI utilize a 0.5 inch ceramic and insulation thickness.

Configurations I and IV, II and V, III and VI are similar to each other except for the ceramic-insulation proportion.

The corrugated structural sandwich utilized in Configurations I and IV also serves as a heat exchanger since the coolant is within the corrugation. Control of coolant pressure offers the means of controlling coolant temperature and, therefore, the inner compartment temperature.

Configurations II and V differ from the foregoing by replacing the corrugated sandwich with a honeycomb sandwich to overcome directional structural weakness. Coolant passages are brazed to the inside of the honeycomb sandwich.

Configurations III and VI are similar to II and V with the exception of a layer of insulation being added between the honeycomb sandwich and the coolant passages.

Additional variations to these designs can take the form of perforations in the ceramic supporting honeycomb to reduce its thermal conductance; also, various thicknesses of an oxidation resistant coating can be applied over the outer areas of the honeycomb to provide desired protection from the highly oxidizing environment.

(a) Thermal Comparison of Sandwich Designs

Thermal evaluation of the various designs are based on an exposure to heating rates of 30 BTU/ft<sup>2</sup>/sec., representative of average heating rates on the fuselage section surface. Also heating rates of 90 BTU/ft<sup>2</sup>/sec. are used in the analysis to indicate thermal condition at forward fuselage locations during maximum heating. Maximum heating may occur at Mach 18-20 during an equilibrium glide, but larger heating rates may occur during early re-entry if flight errors create excessive skip.

Emissivity values of 0.8 and 0.9 were used as being reasonable for surface temperatures of 2500° F. and 3400° F. respectively. An inner surface temperature of 100° F. was allowed for the case with a heat exchanger. For the case without a heat exchanger, inner surface temperature was allowed to increase to 800° F. with the attendant heat transfer to the interior.

The following thermal conductivity values were used in the analysis:

<u>Material</u>	<u>k - BTU/ft<sup>2</sup>-Hr-°F/in.</u>
Ceramics	2.5
Fibrous Insulation	0.7
Outer Honeycomb	270 (Inconel "X" @ 1600°F)
Inner Sandwich Core	180

The ceramic and insulation conductivity values were not decreased for the effect of reduced pressure at altitude.

Total heat transmission to the water was calculated on the basis of 15-minute exposure at equilibrium conditions. For a 15-minute flight through the maximum heating zone, the net heat transfer would actually be lower than the value presented since several minutes would be required to establish equilibrium conditions.

(b) Temperature Distributions

Temperature distributions through the composite walls are important to both structural design and heat sink provisions. Expected temperatures are briefly discussed below for the four configurations by approximate calculations.

(b-1) Surface Temperatures

Outside temperature is primarily dependent upon the convected heat flux and surface emissivity. For vehicles with maximum design heat flux values of 65-70 BTU/ft<sup>2</sup>/sec. and a surface emissivity of 0.9, the equilibrium surface temperature will be about 3100° F. A ceramic material capable of withstanding 3400° F. can tolerate heat flux values of the order of 90 BTU/ft<sup>2</sup>/sec., which provides a considerable margin for non-design flight conditions.

(b-2) Internal Temperatures

Figure II-8 shows temperature gradients through the sandwiches for equilibrium conditions of  $Q_{conv}$  of 30 and 90 BTU/ft<sup>2</sup>/sec. Several significant aspects of the temperature distributions are discussed below:

In all of the designs, the insulation is arranged to limit temperatures of brazed surfaces (particularly the outer honeycomb-to-metal face contact) within the working temperature of the braze.

Temperature gradients across the structural honeycomb in configurations II, III, V and VI must be limited to a value such that thermal stresses are below material allowables. The limiting gradient will vary with each design.

Configurations I, II, IV and V offer a safety advantage due to structural sandwich being somewhat better protected in case of damage to the ceramic. The increase in local heat flow resulting from exterior damage would be better distributed as a result of the close contact of the heat exchange system and the structure. Consequently, local structure temperatures may not become excessive in a limited damaged area which may develop, for example, from meteor impact.

(c) Water Requirements

Figure II-8 shows the net heat rate penetrating the six sandwich designs under exposure to heat rates of 30 and 90 BTU/sec-ft<sup>2</sup>. Corresponding water requirements are also presented and are based on evaporation of water at 100° F.

Note that net heat rate varies from 0.9-2.3% of incident heat for design III and from 1.2-3.6% for design I. The percentage values apply for the tabulated  $Q_{conv}$  values. For increased  $Q_{conv}$  rates, the percent transmitted through the sandwich would be reduced, and conversely at reduced  $Q_{conv}$  rates the percent transmitted would be higher.

Determination of total water needed for the lifting body requires integration of heat rates over the entire surface for the total re-entry period. However, to indicate relative performance of the six designs, water evaporation rates in Figure II-8 are based on the constant heat rates shown. The water requirements for the designs differ significantly: 0.7-1.5 pounds for Configuration IV and 0.5-1.0 pounds for Configuration III.

2. RECOVERABLE BOOSTER LEADING EDGES

The leading edge concepts in this section are necessarily preliminary, and intended to indicate a design which offers a high degree of reliability and temperature resistance. For illustration purposes, the flight conditions correspond to a possible recoverable booster system. Figure II-9 briefly describes the aerodynamic heating environment of a typical mission profile. It is interesting to note that experimental panels have survived tests more severe in temperature, sonic level, dynamic pressure, and time duration than would be required by a leading edge of a typical recoverable booster system.

a. Design Description

A typical wing leading edge segment is shown in Figure II-10. The leading edge section utilizes 3/4 inch of insulation on a 1/2 inch sandwich panel. The amount of insulation on the flat extensions is reduced due to the lower temperatures encountered.

3. LEADING EDGES AND NOSE CAPS OF GLIDER RE-ENTRY VEHICLES

Ceramic-metal composite structures are well suited for leading edges and

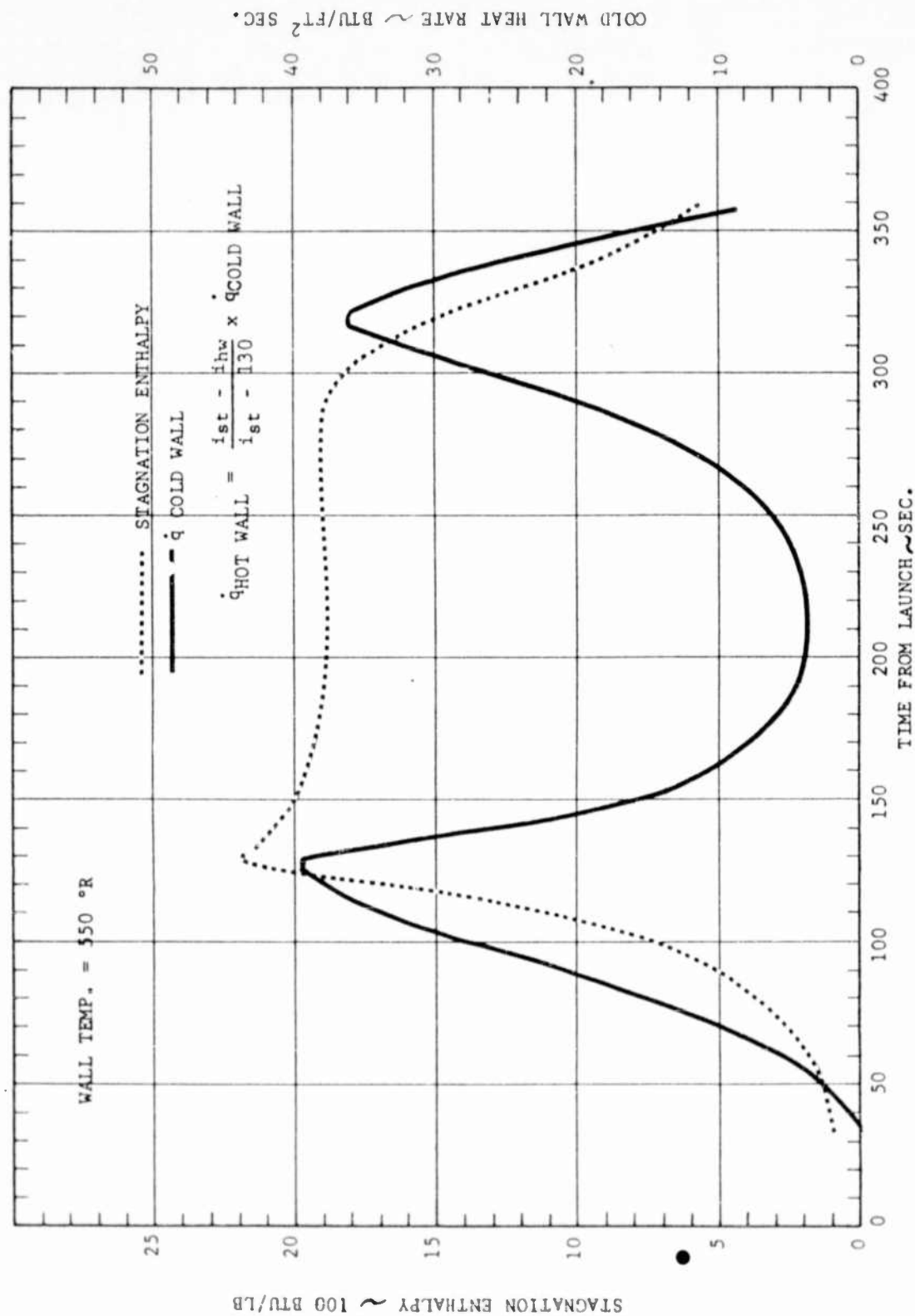


Figure II-9 RBS Wing Leading Edge Cold Wall Heating

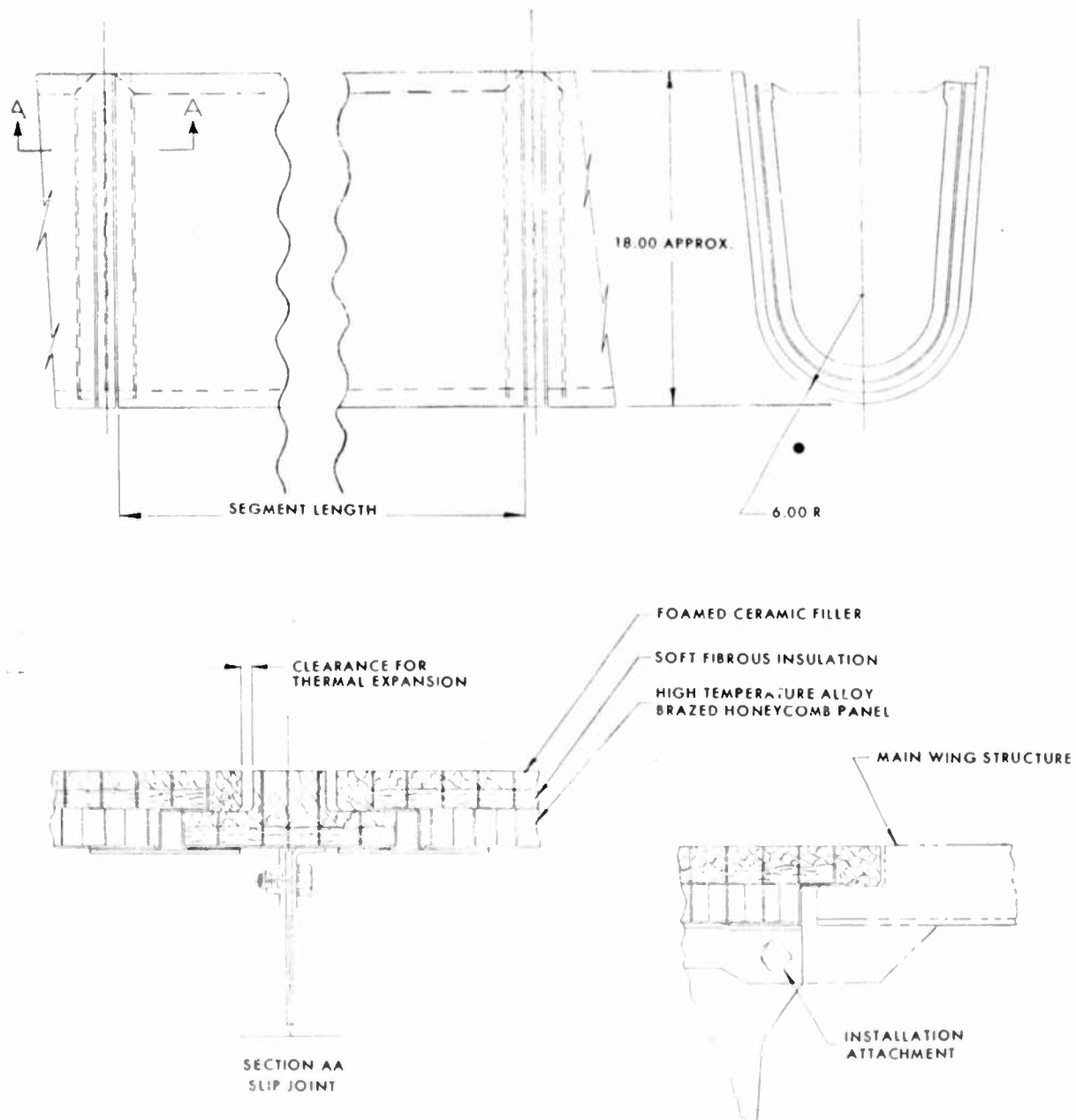


Figure II-10 Leading Edge Segment

nose caps of glide re-entry vehicles, because of good durability, high temperature resistance, good insulation and reasonable weight.

Figure II-11 is a parametric study of leading edge stagnation point temperatures for typical winged glider conditions. Note that maximum leading edge temperatures (2600° to 3200°F) are well within the capability of ceramic materials, whereas metals would present serious oxidation difficulties even at the lower range of temperatures.

Figure II-12 shows a cross section of a nose cap for operation at 4400°F. surface temperature. For an incident heat flux of 160 BTU/ft<sup>2</sup>/sec., the heat transmitted to the interior is only 0.59 BTU/ft<sup>2</sup>/sec. The low heat transmission is compatible with an insulated fuselage design. If a hot structure fuselage design is used, the nose cap section can be readily adapted into a relatively cool flight instrumentation compartment. The resultant internal temperatures 500° - 1000°F., or lower if active cooling is used, would simplify instrumentation problems and substantially reduce development costs.

The honeycomb reinforcing the ceramic (Figure II-12) may well be subject to some oxidation under certain conditions. However, with proper selection of foil thickness, the foil temperature is substantially below the temperature of the adjacent ceramic (refer to Figure III-25). Thus, oxidation problems are minimized so that the super alloys are generally adequate. In the event that refractory honeycomb becomes necessary for extreme operational temperatures, the oxidation problem is much less critical than in the case of designs using refractory metal outer shields which would be subjected to full environment temperatures as well as environmental mechanical and chemical attack.

#### 4. LOW ALTITUDE VEHICLES

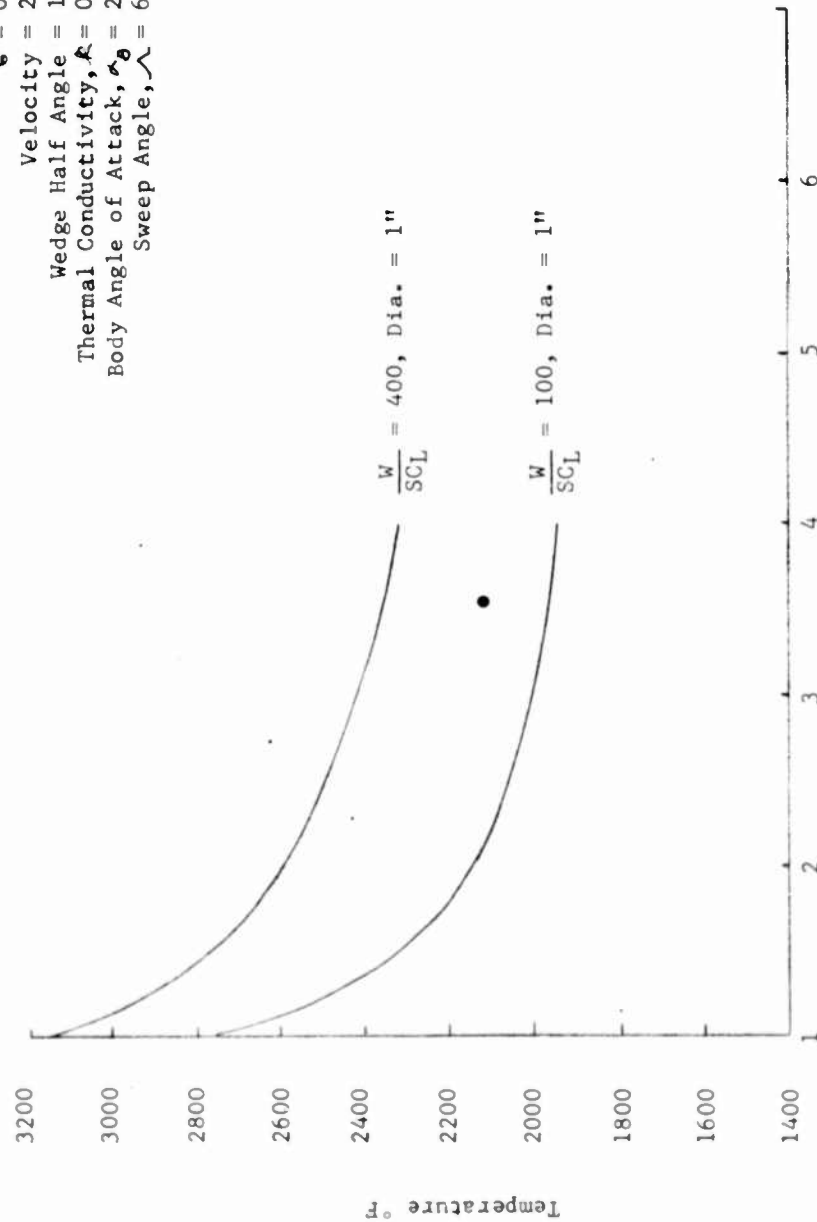
Low altitude vehicles with velocities of Mach 4 or 5 would develop severe temperature environments and create difficult materials problems. The problems are intensified if the time of flight is prolonged. This would prohibit the use of ablative materials because of excessive weight. The use of radiation cooling, however, presents advantages similar to those discussed for re-entry vehicles, greatly reducing heat sink requirements.

At Mach 5, for example, outside surface temperatures would be nearly 2800°F. near the nose stagnation point, and would average about 2100°F. in the fuselage section. With a ceramic structure, heat transfer through the walls would be comparable to internal heat loads from electrical equipment. For example, for a 30 inch diameter missile fuselage, the net heat entering the compartment through the wall would be less than  $2 \frac{\text{BTU}}{\text{sec}}$

If electrical loads are taken at  $1 \frac{\text{BTU}}{\text{sec}}$  for the same body length, or nearly 1 KW power output, it can be seen that with about 200 pounds of equipment and structure within the volume of the fuselage section, the temperature rise for a 1000 second flight time would be in the order of only 100°F. or less. Such temperature increases would likely be within equipment capabilities. Of course, specific electrical power outputs and equipment arrangements would have to be considered for any missile design. However, the above values indicate that except for possible localized areas, water cooling may be avoided or held to very minor proportions.

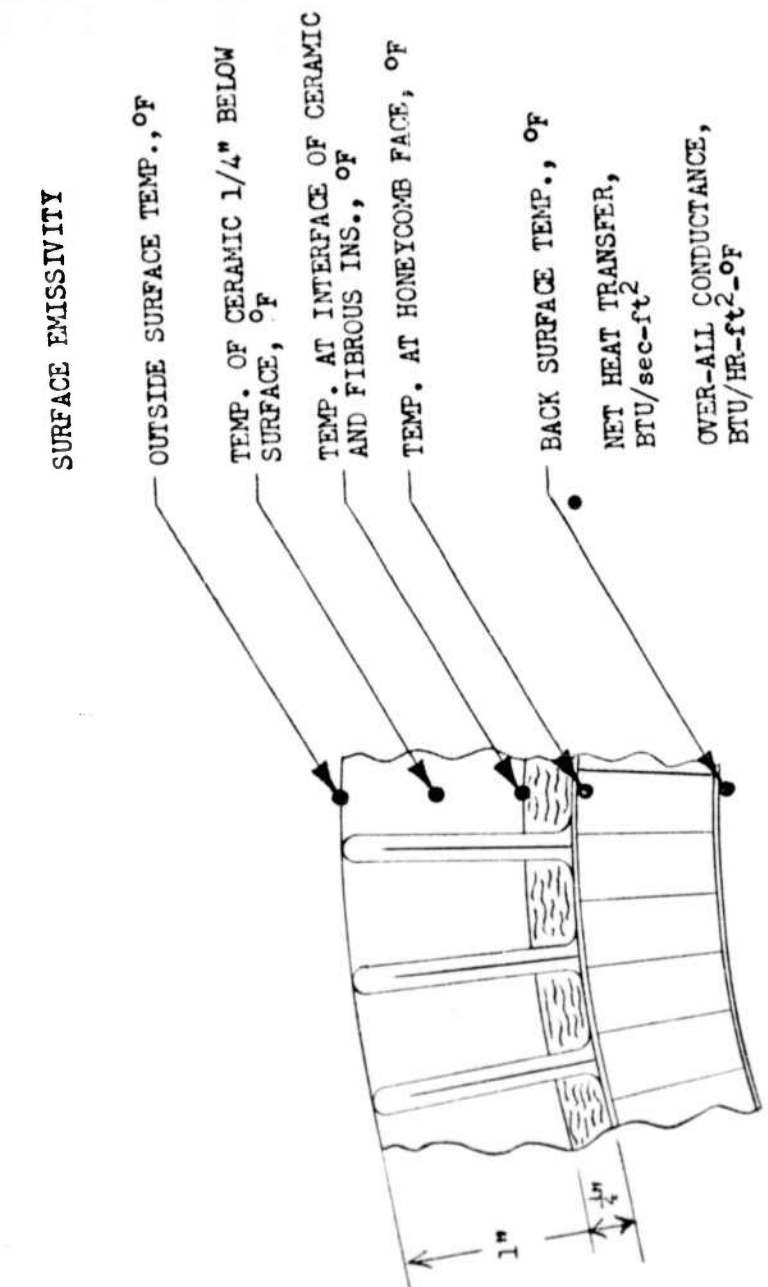
CONDITIONS

$C = 0.9$   
 Velocity = 22,000 FPS  
 Wedge Half Angle =  $10^\circ$   
 Thermal Conductivity,  $k = 0$   
 Body Angle of Attack,  $\alpha_b = 20^\circ$   
 Sweep Angle,  $\Lambda = 60^\circ$



S/R, RATIO OF DISTANCE FROM STAGNATION POINT TO RADIUS OF  
 CYLINDRICAL LEADING EDGE

Figure II-11 Maximum Temperatures for Thermantic Leading Edges



0.6
4400
3630
2230
1330
800
0.59
0.59

Figure II-12 Curved Panel Design  
for  
160 BTU/ft<sup>2</sup> - sec. Incident Heat Flux

### SECTION III

#### ANALYSIS AND STRUCTURAL EVALUATION OF BERYLLIUM COMPOSITE STRUCTURES

##### A. Introduction

Beryllium panels are discussed from a general standpoint and analyzed with respect to re-entry vehicles. A thermoelastic panel analysis is also presented in this section. The beryllium panels are evaluated for structural use under representative aerospace vehicle design conditions and in general by non-dimensional curves for use in parametric studies. The thermoelastic analysis is applicable for computer use.

Ceramic composite panel analysis are also presented, and include a thermal analysis and a vibration analysis. In the thermal work a steady state heat flow solution is given, and a general method applicable for computer solution of complex heat flow problems is described. The vibration analysis is a general solution with particular solutions presented.

##### B. Beryllium Panels

###### 1. General Considerations

The use of beryllium in composite structures as a load carrying member appears feasible when used in honeycomb panels. The honeycomb core stabilizes the beryllium faces when subjected to normal pressures and out-of-plane loads. Sheet beryllium is very susceptible to brittle failure because of out-of-plane loads. In honeycomb panels this type of failure is somewhat reduced. The use of beryllium, where buckling is the criteria and compression is the primary method of loading, is efficient because of the high value of Young's modulus of elasticity. The tests performed show that beryllium develops the full theoretical buckling stress in honeycomb panels prior to buckling and brittle failure of the beryllium face sheets.

###### a. Typical Operating Conditions for Beryllium Panels

Beryllium is usable at temperatures environments up to 1000°F for structural members in honeycomb panels. However, the temperature gradient across the panel must be controlled or maintained at a reasonable level. Thermal stresses in honeycomb panels are produced by the restraint conditions present and the thermal gradient or temperature difference ( $\Delta T$ ) between the outer and inner faces. Let us consider a couple of hypothetical conditions which indicate a typical value anticipated:

- (1) A honeycomb panel with two beryllium faces .020" thick and .5 inch A-286 4-20P core,  $\Delta T$  in the order of 100°F, normal pressures of 1.3 psi, and in a temperature environment of 1000°F.

- (2) The same honeycomb panel as (1) above except a  $\Delta T$  of 200°F and normal pressures of 0.5 psi.

These are the type of conditions under which beryllium panels would perform satisfactorily. The temperature environment can exceed 1000°F, if the outer beryllium face does not exceed 1000°F when insulated by a thermal shielding material. The thermal gradient across a restrained panel has the most significant effect on stress levels experienced in the honeycomb panels.

Composite honeycomb panels with stainless steel or superalloy outer faces, stainless steel core, and beryllium inner faces are capable of resisting higher thermal gradients with associated normal pressures and temperature environments.

Beryllium faced honeycomb panels can be joined by brazing stainless steel or superalloy edge members onto the panels and then welding the edge-members. The slenderness ratio of the edge members will determine their buckling strength. Edge-members must not be allowed to operate at stress levels which permit them to buckle. These edge-members would separate at the braze-line or cause the panel faces to fail if allowed to buckle.

b. Weight versus Strength Characteristics

The density of beryllium is almost the same as magnesium and the strength of beryllium is several times that of magnesium. The mechanical properties of beryllium remain structurally acceptable under load up to 1000°F while those of magnesium are acceptable under load up to 400°F.

The stiffness of beryllium is about 1.5 times that of superalloys based on a comparison of Young's Modulus at room temperature. At 1000°F the stiffness of beryllium based on Young's Modulus is about the same as that of superalloys.

The weight of beryllium panels to that of superalloy panels is compared as follows:

Note, this comparison is based on comparable material thickness and not on comparable material strength. The panels each consist of two .020 face sheets, 2 sheets of .002" brazing foils, and .50 inch thick 4-15P superalloy core.

<u>Beryllium Panel</u>	<u>Superalloy Panel</u>
.863 #/ft <sup>2</sup>	2.147 #/ft <sup>2</sup>

As shown, the weight per square foot of superalloy panels is nearly 2.5 times that of beryllium faced panels with superalloy core.

The weight and strength characteristics discussed above show that not only are beryllium panels much lighter but also are structurally acceptable in a temperature environment up to 1000°F. The significance of the use of beryllium may best be compared by both weight and strength parametric studies in the realm of loading and thermal environment anticipated.

c. Limitation in Present Use of Beryllium Panels

The use of beryllium in panels has not to date been tested sufficiently to produce parametric and optimization studies under the loading and thermal environment required for a vehicle design. Complex stresses are produced in structures under the loading and thermal conditions anticipated for which no estimates are available. Beryllium panels by themselves should not create extensive problems but when joint designs are incorporated to retain the panels several additional complications exist which must be analyzed in detail and tested in greater quantities to establish statistical records for use in future designs. Out of plane loads and warping conditions are critical design problems when beryllium is used.

d. Potential Applications

Applications for beryllium panels are many, although to date their use has been almost negligible. Applications that require high buckling strength, moderately high temperature environment, and low thermal gradients are structurally acceptable for beryllium panels. The preceding is only one combination of loading and thermal conditions that are structurally acceptable for beryllium panels. The principle advantages of beryllium panels are buckling strength, being structurally useful at moderately high temperature environment, and light weight.

2. Analysis of Beryllium Panels for Re-entry Vehicles

a. Introduction

The following discussion analyzes beryllium panel configurations under typical re-entry vehicle loads and thermal environment. The purpose of this analysis is to show analytically the design and structural considerations required to use beryllium as a vehicle structural material. The material allowable data was collected under this and similar programs.

The materials data is presented in a form of use to a structural designer concerned with the analysis of beryllium panels. The analysis is developed by conventional techniques in order not to obscure the fundamental problems: performance of panel faces, panel core, and edge members under a typical set of thermal, aerodynamic, and inertia loads.

b. Basic Data

The structural concept geometry, section properties, and material allowables are described in this section.

(1) Geometry

The geometry used simulates a typical lifting body re-entry vehicle fuselage nose section and a wing leading edge section. See Figures III-1 and III-2.

(2) Section Properties

The typical overall vehicle section properties are not determined. The section properties of the detailed sections are determined and included in the analysis as required.

(3) Material Allowables

The purpose of this section of the report is to establish preliminary allowables for use in design and analysis. The results of the test program covered in Section V of Volume II will be used as a guide in the determination of the allowables.

Due to the low pressure and high temperature environment in which a re-entry type vehicle operates, the criteria on which structural allowables are based are different from that of conventional aircraft. The allowables for a re-entry vehicle are based on the buckling stress rather than the ultimate and yield stress of the materials at the environmental temperatures.

The mechanical properties of beryllium versus temperature are shown in Figures III-3, 4, and 5. The beryllium tensile test data in Reference 2 and in Section V, Volume II were used to construct Figure III-6. Section V, Volume II test data was used to evaluate braze alloy effects. In Figure III-7 the critical buckling stress was determined and plotted versus  $(L_e/\rho$  or  $\pi b/\sqrt{K} t)$  for beryllium at R.T., 500, 750, and 1000°F based on Figure III-6. A comparison of Figure III-7 with the edge-wise compression data on Table IV-13 indicates that the panel test stress levels are just slightly higher than those determined for buckling of beryllium sheet. Therefore, allowing that the braze alloy effects are offset by the stability from the honeycomb core, the allowable used for beryllium panels will be based on Figure III-7.

Since the panel face edge-members will act as splice plates and be used in the "as-welded" condition in final assembly of the structure, buckling allowables for various material in this condition were determined.

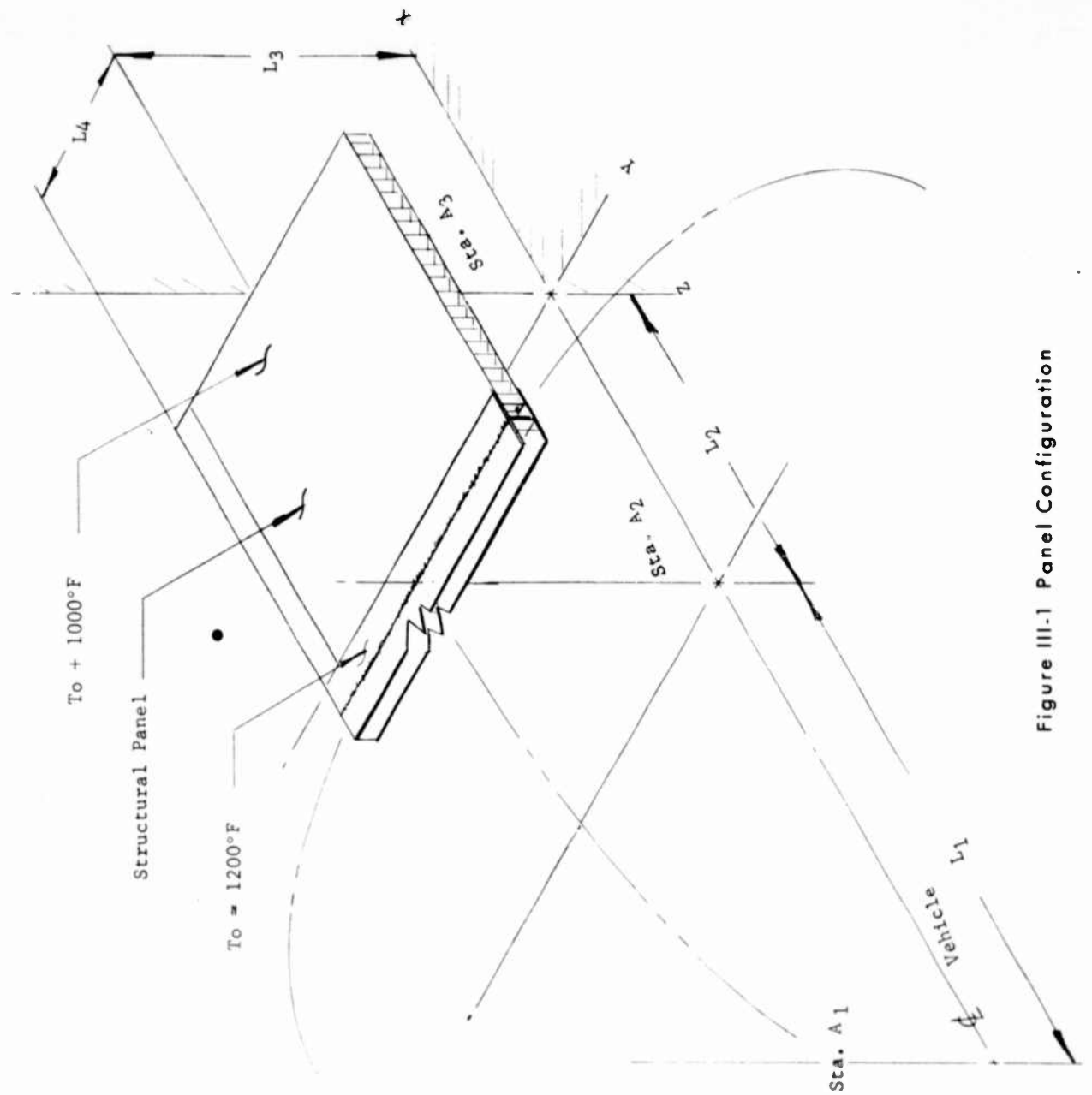


Figure III-1 Panel Configuration

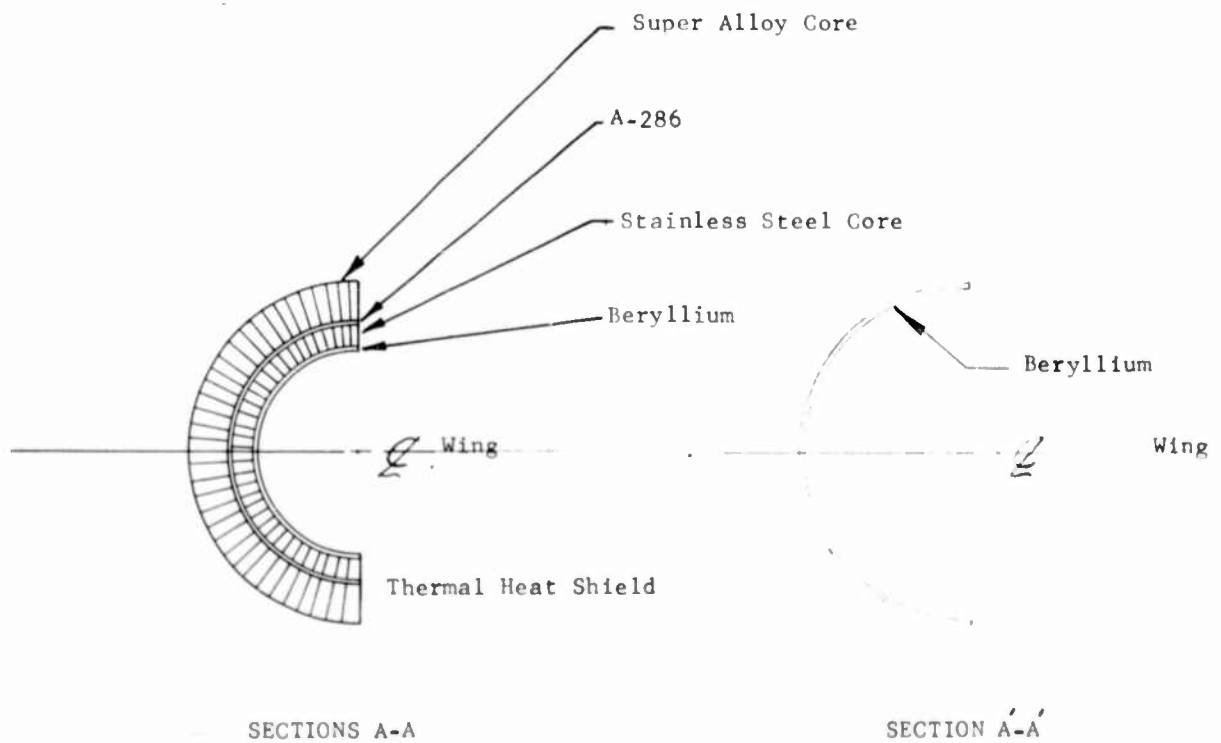
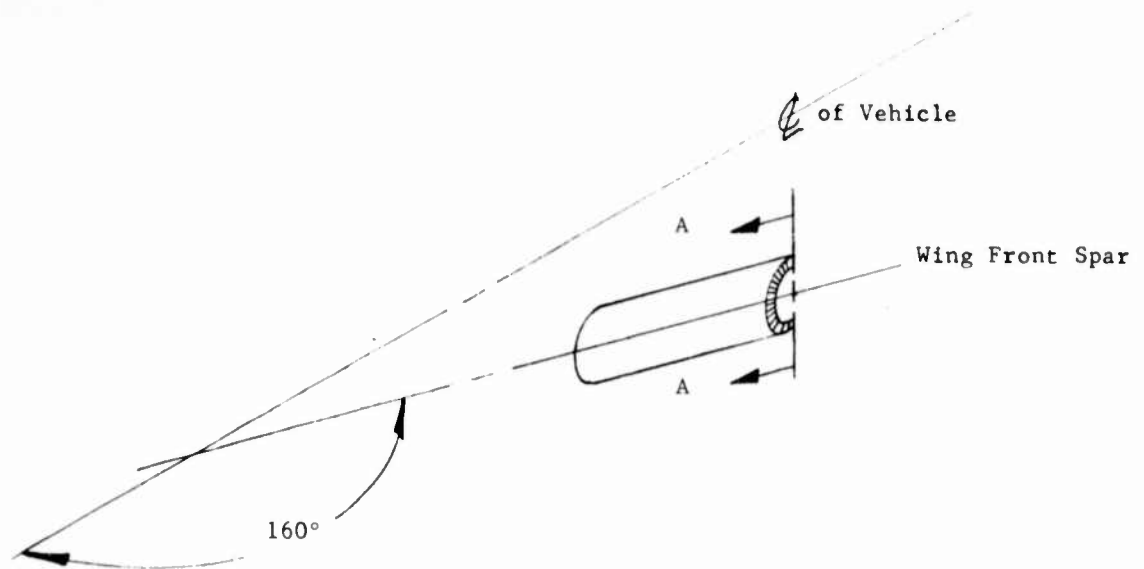
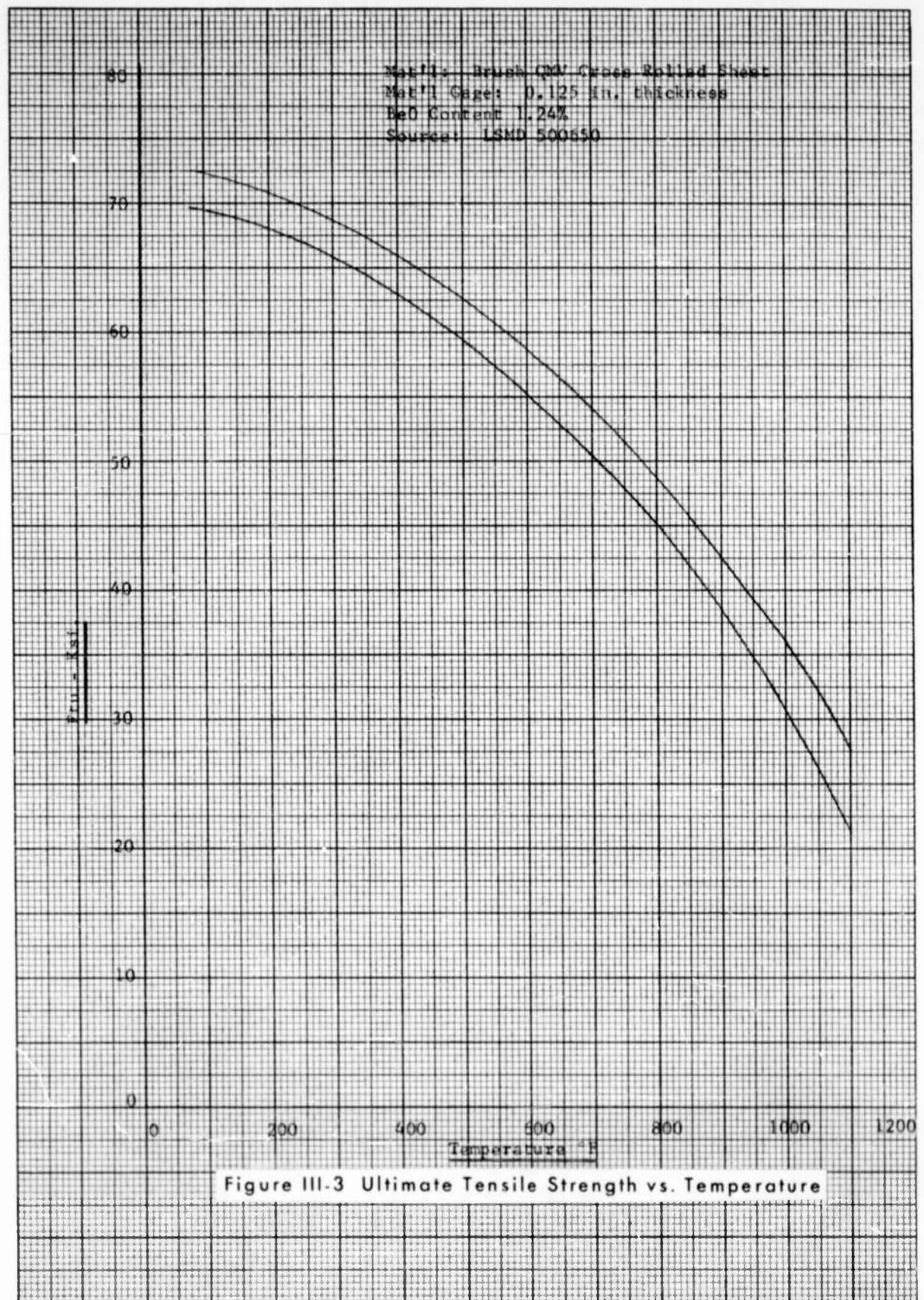
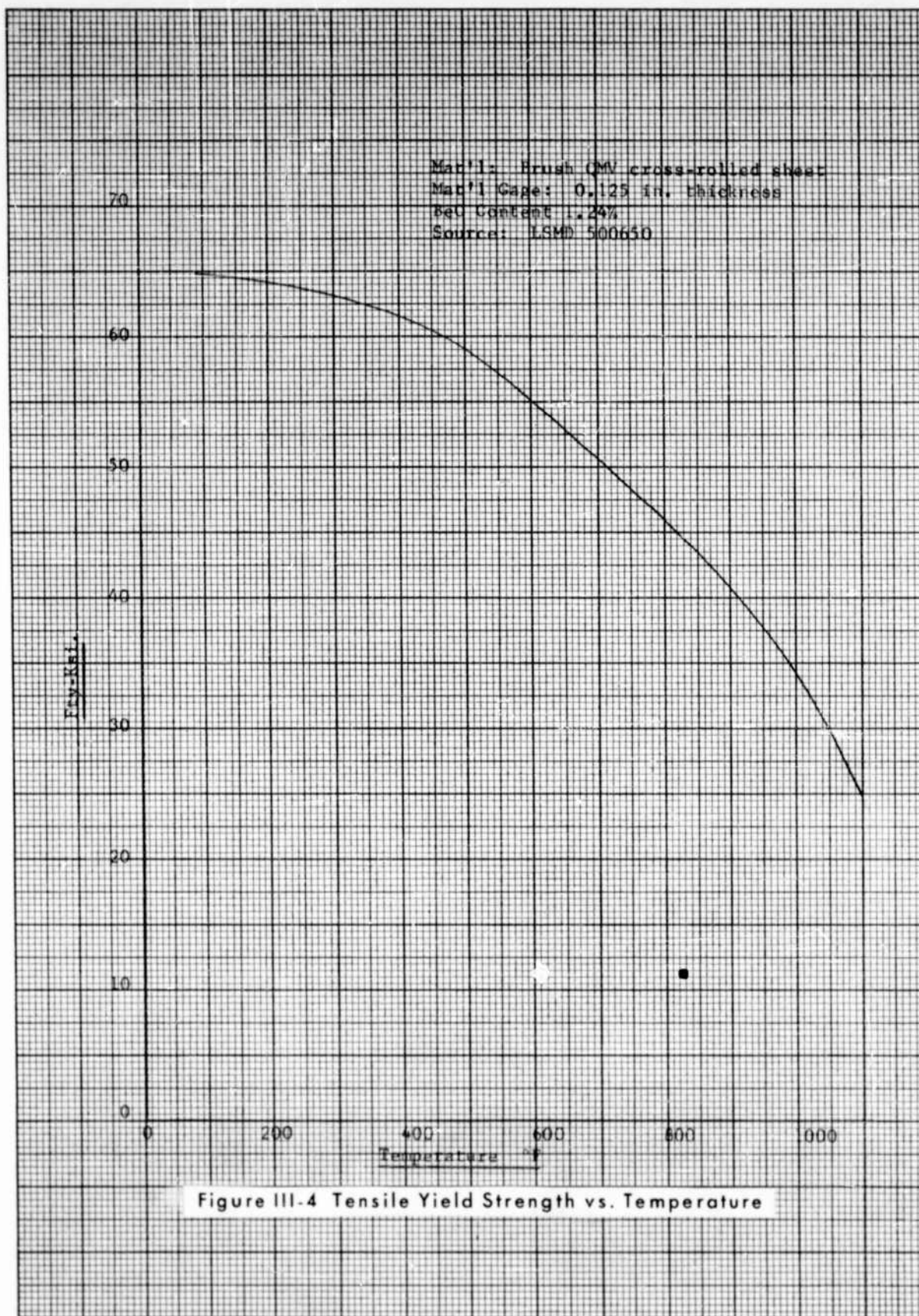


Figure III-2 Leading Edge Concept





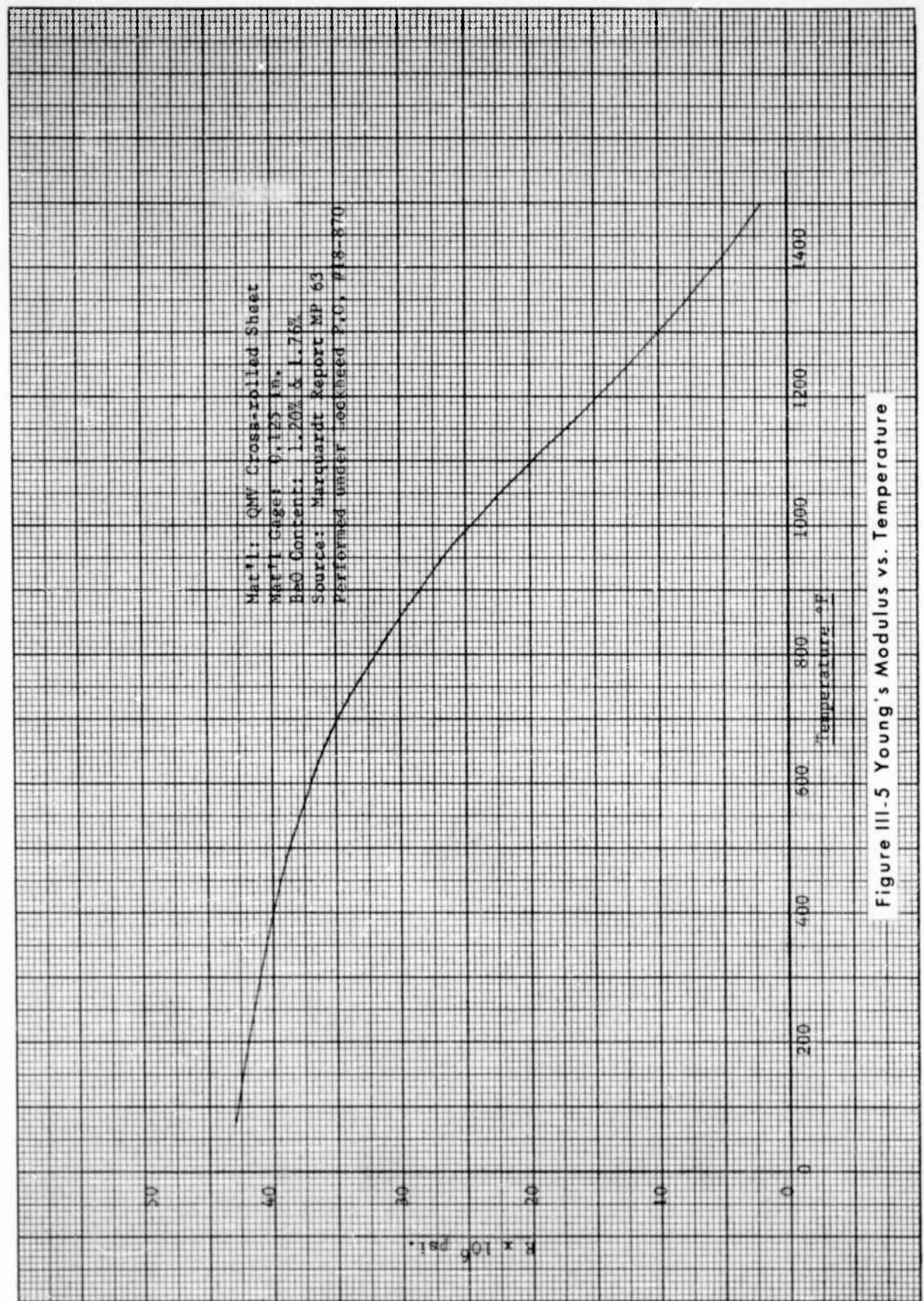


Figure III-5 Young's Modulus vs. Temperature

Mat'l: Cross-rolled beryllium sheet

Mat'l gage: 0.250 in.

Average values of specimen with BeO content of 1.20% and 1.26%

\* Strain-rate in in./in./sec. indicated by bracketed numbers

Performed under Lockheed P.O. #18-870

Note: Specimens were not etched.

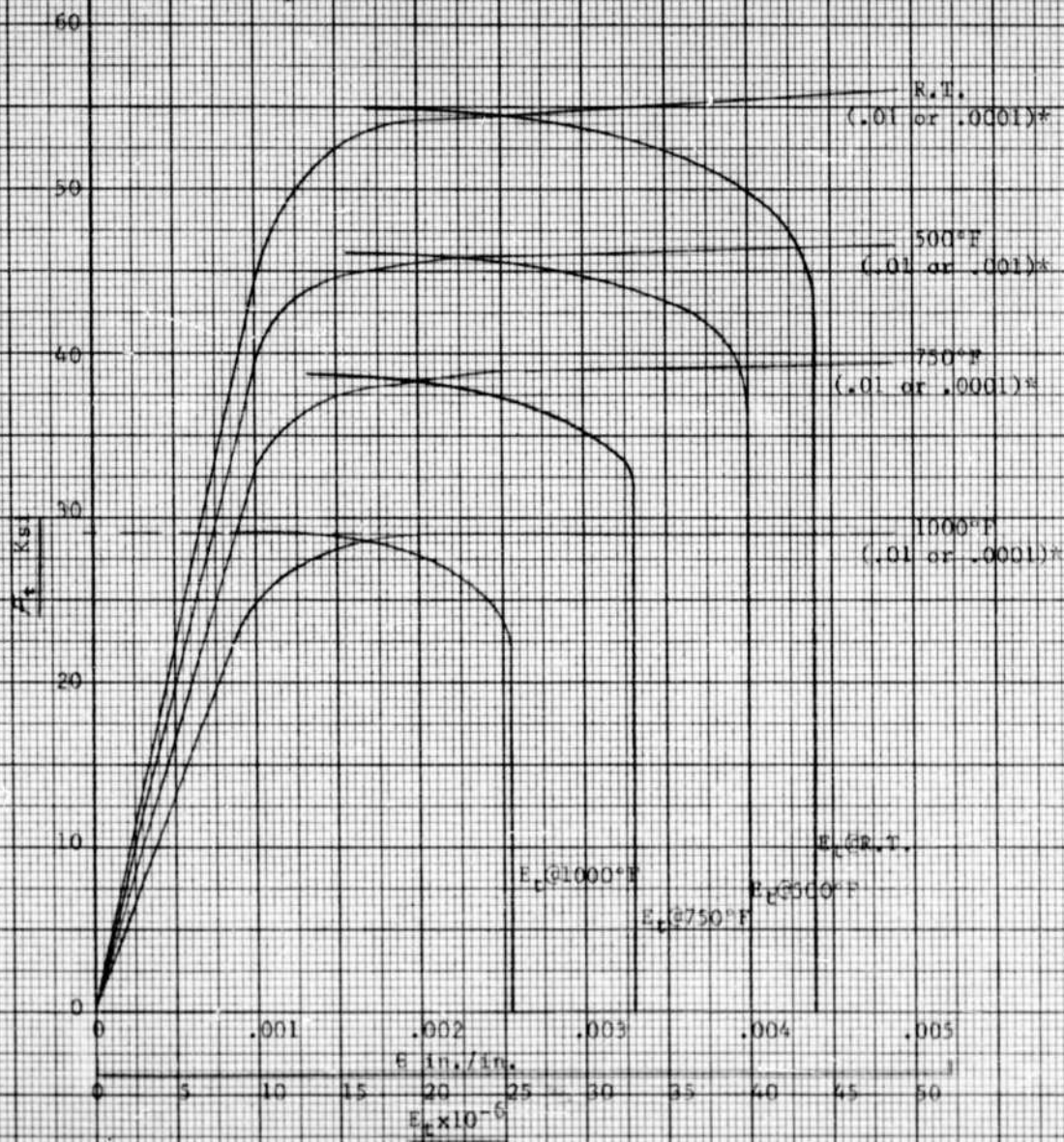


Figure III-6 Typical Tensile Stress-Strain Curves

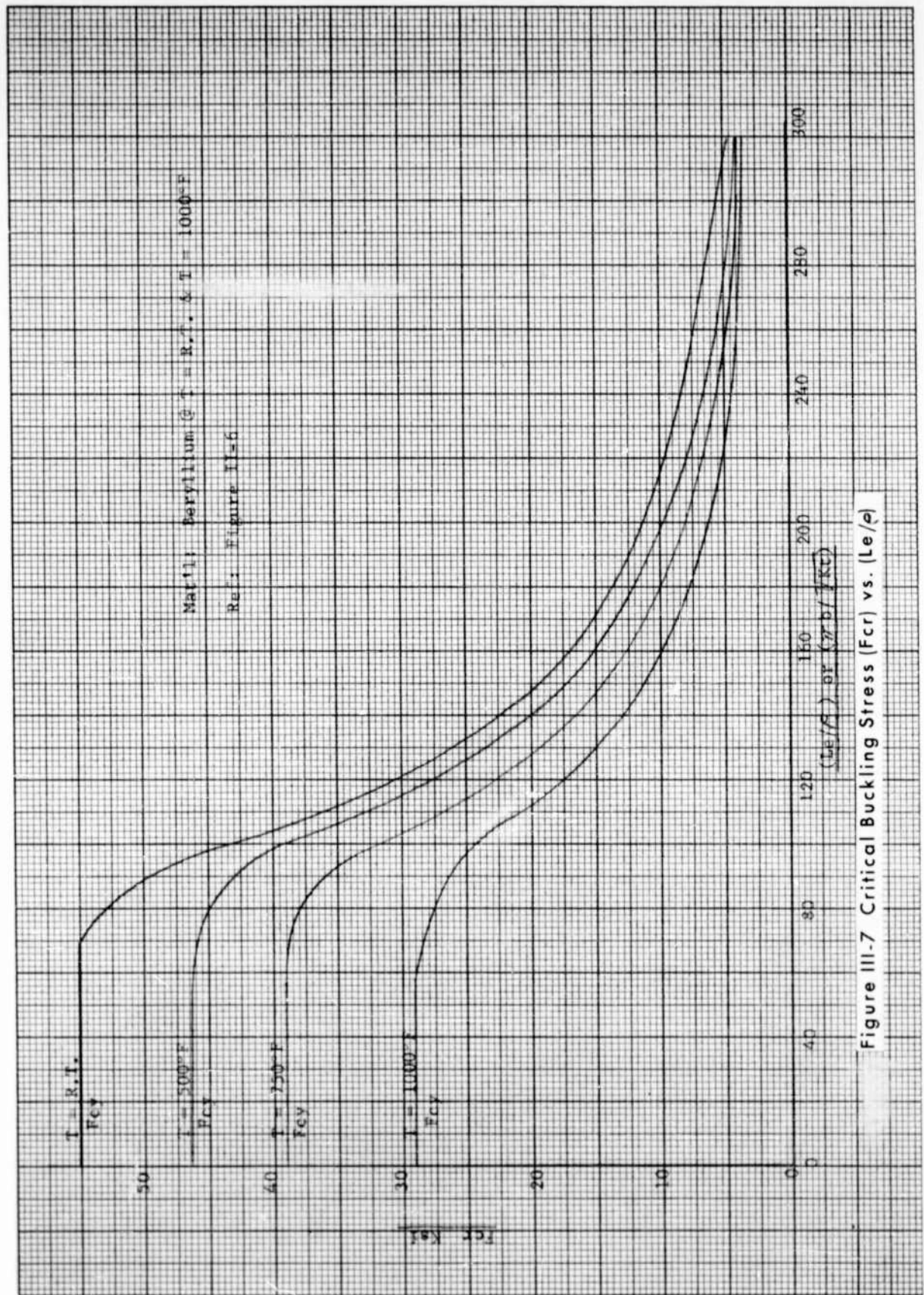


Figure III-7 Critical Buckling Stress ( $F_{cr}$ ) vs.  $(Le/\rho)$

Mat'l: Inconel X Annealed (No Aging) @ R.T.

Ref: Inco Bulletin T-16

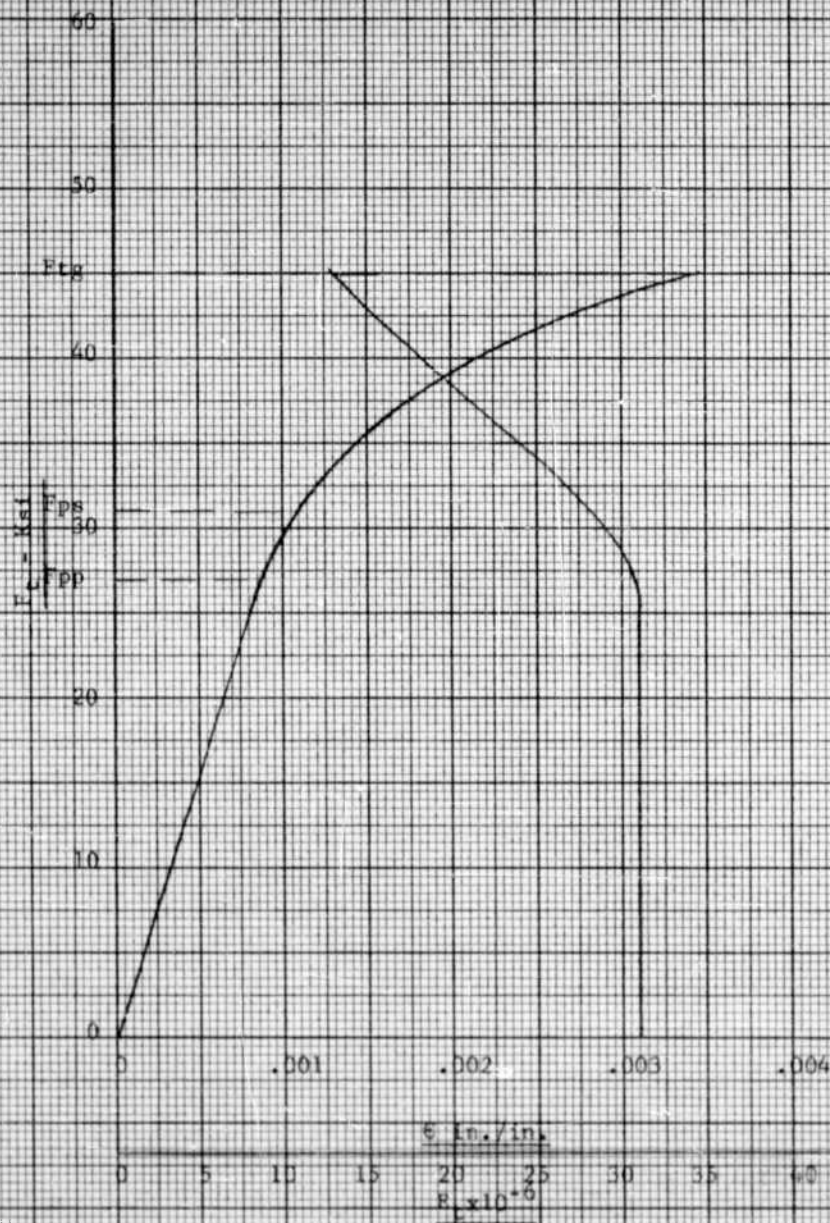


Figure III-8 Typical Tensile Stress-Strain Curves

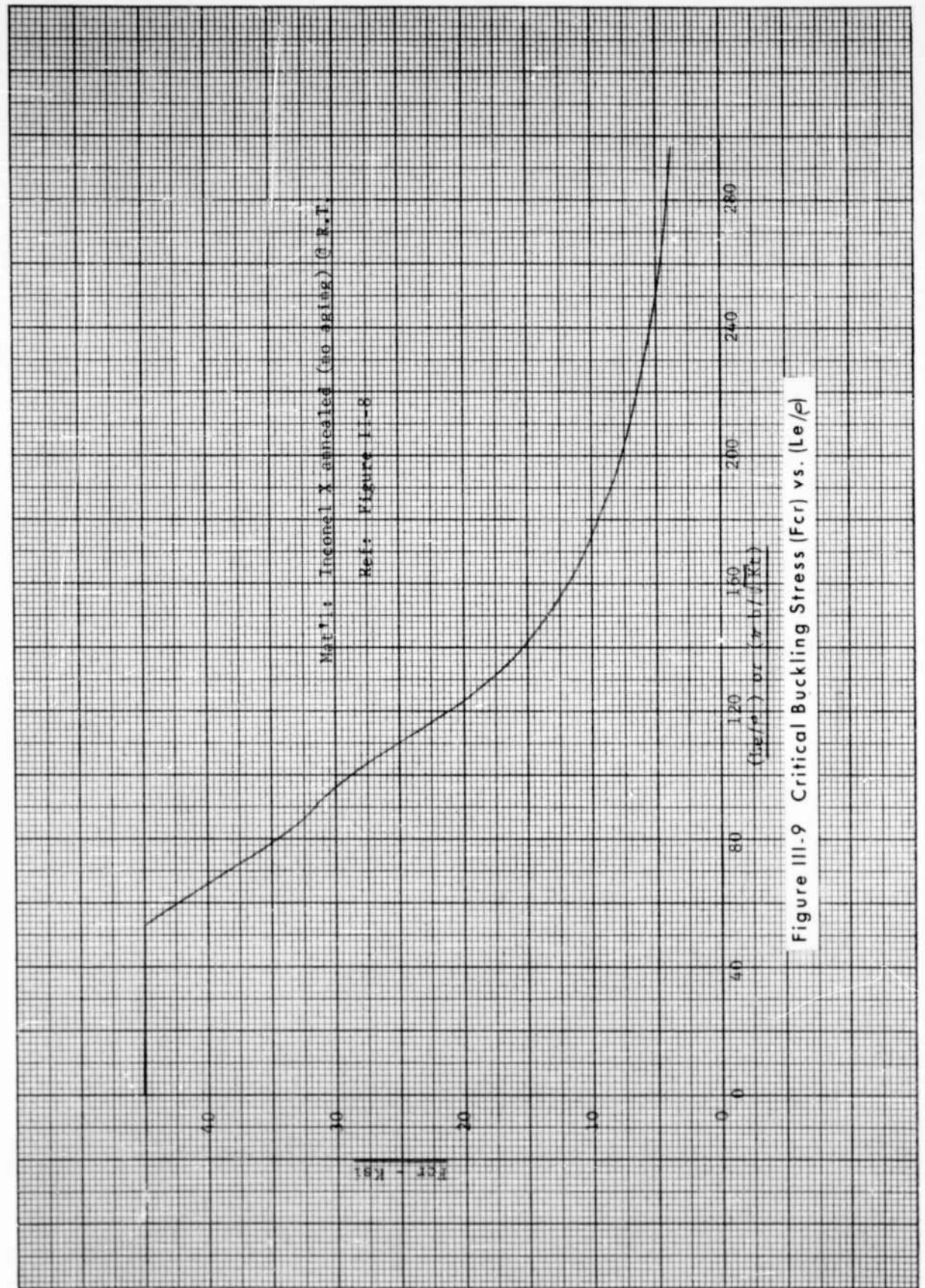


Figure III-9 Critical Buckling Stress (Fcr) vs. (Le/ρ)

Mat'l: A-286 Solution Treated Ref: Allegheny-Ludlum Blue Sheet

Data based on points and  $E = 29.1 \times 10^6$  @ R.T.

$F_{tu} = 91,000 \text{ psi}$

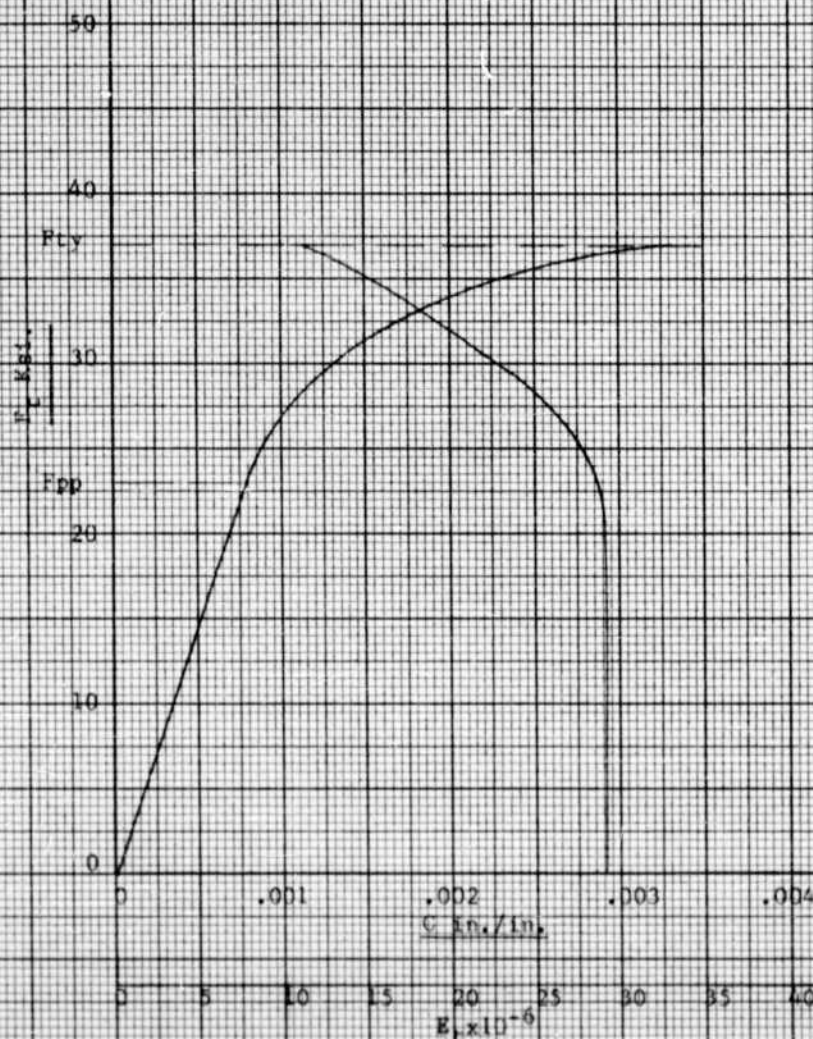
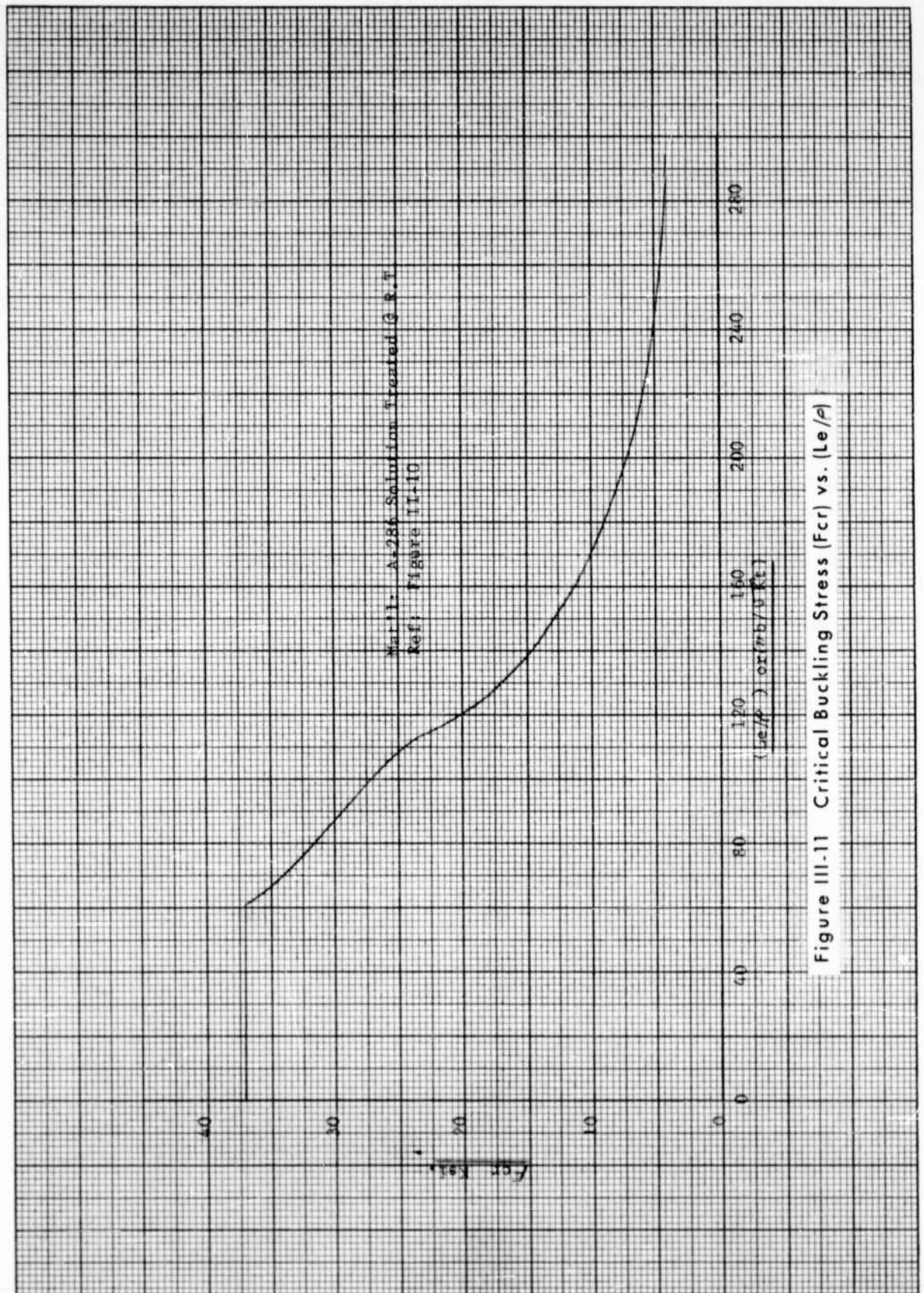
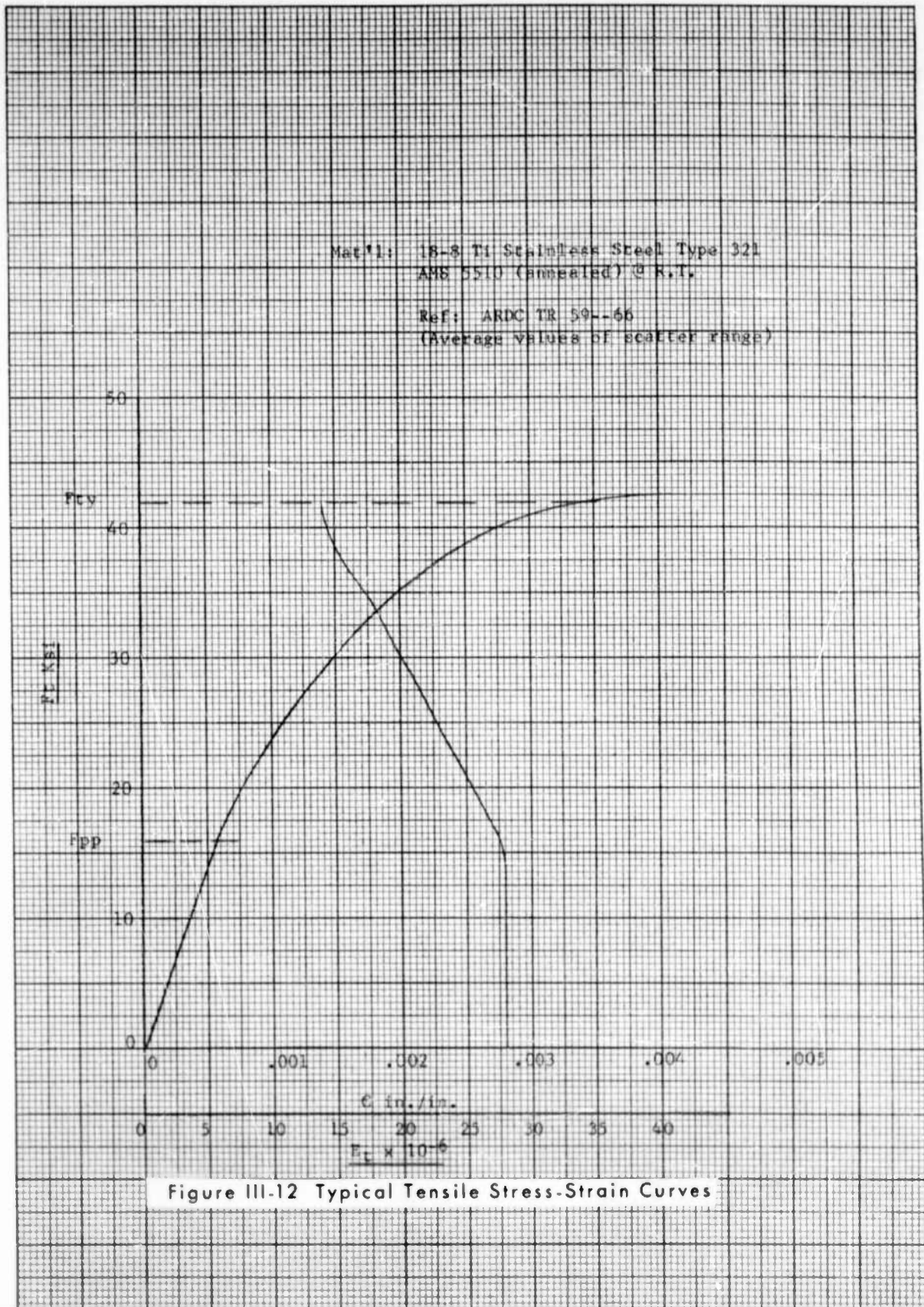


Figure III-10 Typical Tensile Stress-Strain Curves





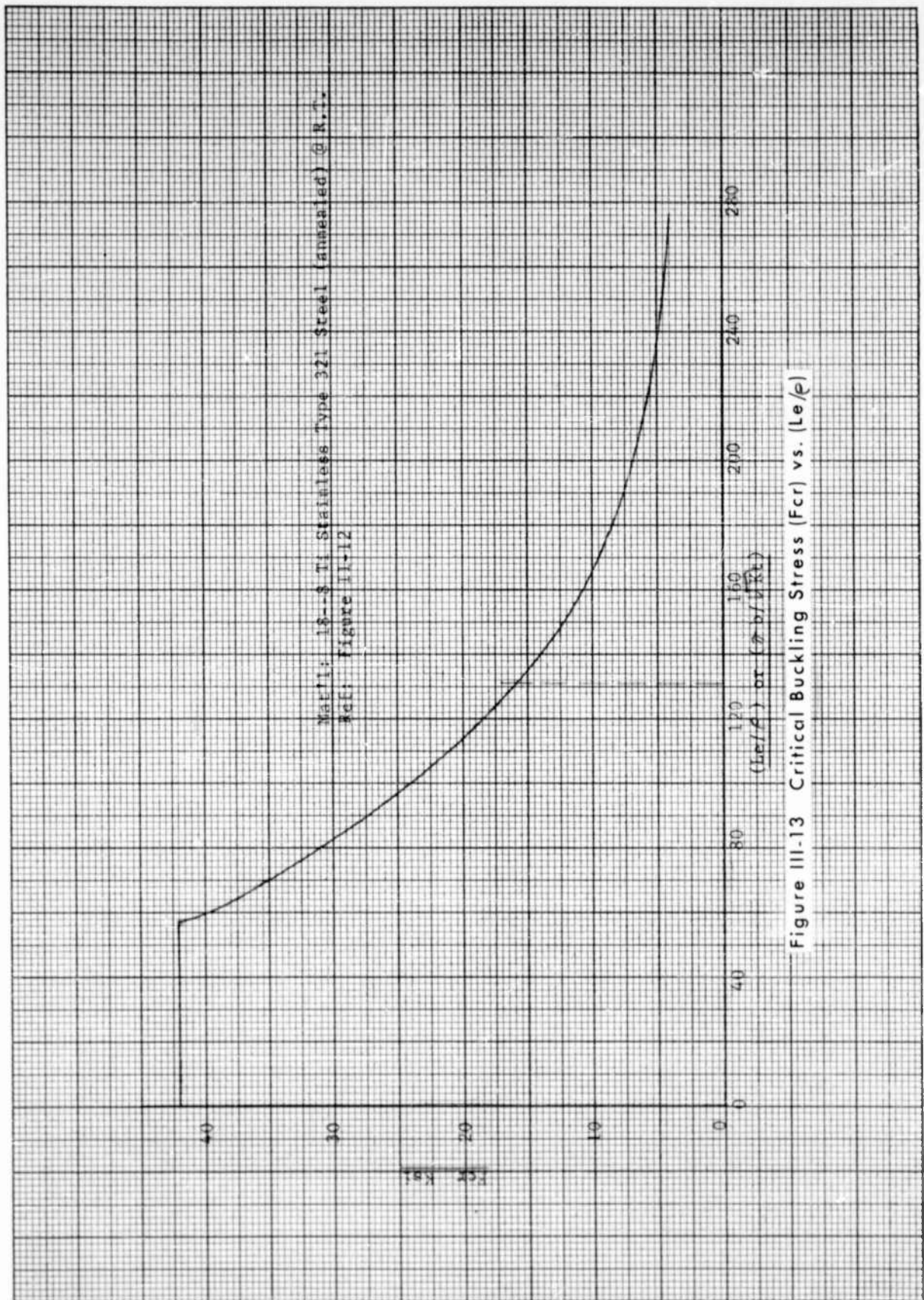


Figure III-13 Critical Buckling Stress ( $F_{cr}$ ) vs.  $(L_e/r)$

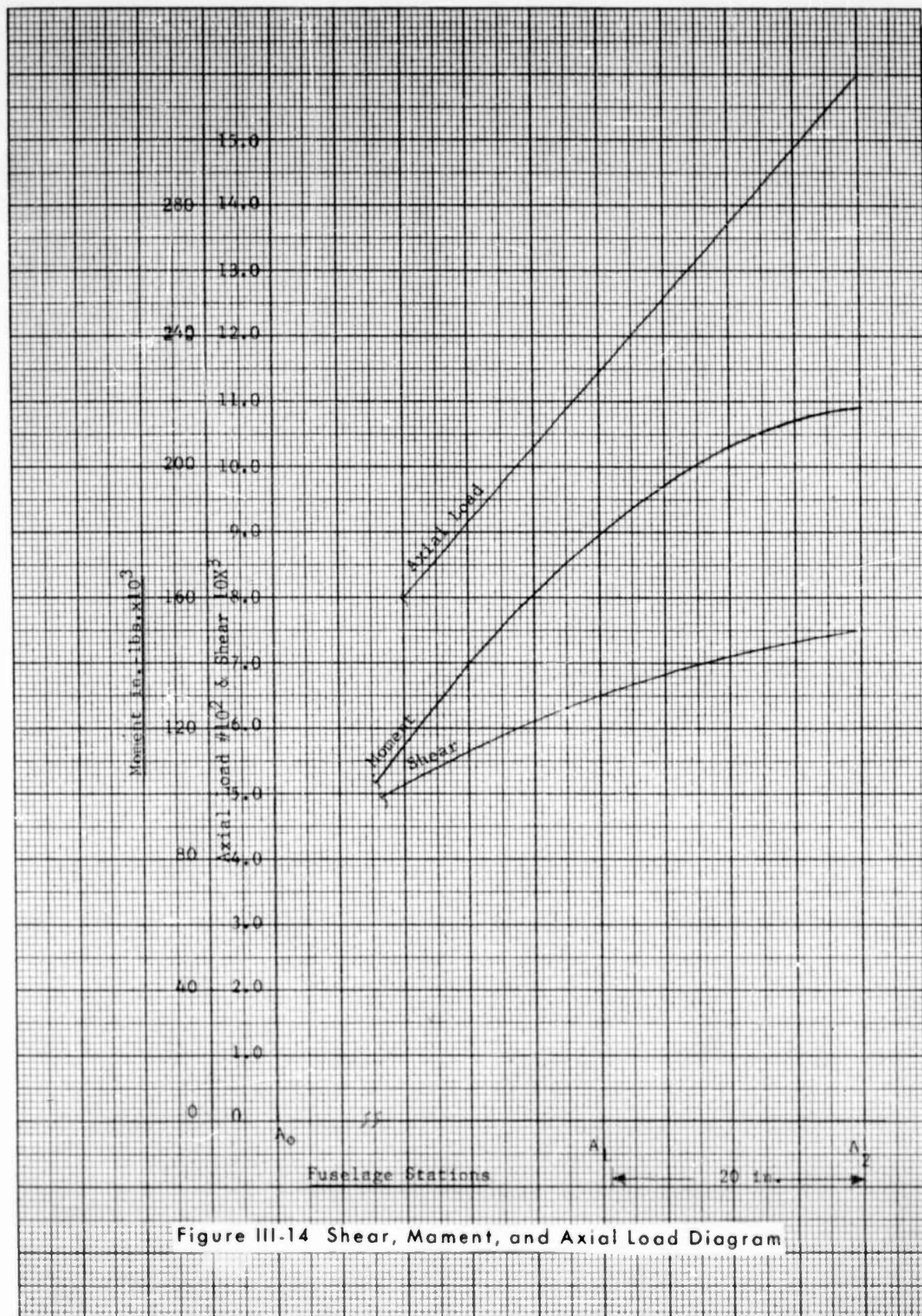


Figure III-14 Shear, Moment, and Axial Load Diagram

The data for these curves were obtained as referenced on Figures III-8 through III-13 for Inconel X, A-286 and AISI type 321 stainless steel. Although AISI type 321 stainless steel curves are shown, the material is not necessarily recommended for use in aircraft structures design except under rigid quality control procedures because of the wide scatter of properties. However, AISI type 321 stainless steel offers fabrication advantages because of its ease of welding. The first choice of these two materials for face edge-members would be Inconel X. A-286 would be a second choice.

The face edge-members would tend to negate slight edge defects in the beryllium faces which precipitate out-of-plane load failures.

No edge-wise compression data were obtained on honeycomb panels with different face materials which could be used for comparison. Therefore, allowable buckling stress curves for composite honeycomb panels will not be presented.

c. Stress Analysis

(1) Loads

The external loads will be assumed for the structure at Sta. A<sub>2</sub> in Figure III-1 and then distributed on the basis of the assumed dimensions.

Assumptions for Figure III-1:

1. Let Sta. A<sub>3</sub> be the bulkhead that joins the nose section to the cockpit section of the re-entry vehicle.
2. L<sub>2</sub> = 20 in., L<sub>3</sub> = 16 in., and L<sub>4</sub> = 15 in.
3. a. Shear @ Sta. A<sub>2</sub> = 6500#  
b. Moment @ Sta. A<sub>2</sub> = 217,500 in-#  
c. Axial Load @ Sta. A<sub>2</sub> = 1600#
4. Re-entry assumed the critical flight condition  $p \cong 1$  psi.
5. The temperature of the outer face of the structural panel (T<sub>0</sub> = 1000°F) with outer thermal insulation. Max.  $\Delta T$  across honeycomb panel is 400°F. ( $\Delta T = T_1 - T_2$ )

The shear, moment, and axial load diagram based on the above assumptions is shown in Figure III-14.

Since leading-edge sections will be made in small segmented sections and not permitted to accept spar bending induced loads, the highest stresses present will be due to thermal stresses. Airload is practically negligible at the time of highest thermal environment. Therefore, only the thermal stresses developed due to attachment restraint will be considered.

Assumptions for Figure III-2.

1.  $L_A = 2.25$ ,  $L_B = 12$  in.,  $L_C = 4.5$  in.
2. Re-entry is the critical condition  $p = .55$  psi
3.  $T_o = 1000^\circ\text{F}$  with outer thermal insulation.

(2) Panel Analysis @ Critical Temperatures (Ref.: Figure III-15)

(a) Faces: (Face Buckling)

$$V_{\max.} = 6500\#; \quad M_{\max.} = 217,500 \text{ in-lbs.}$$

$$P_a = 1600\# \quad T_o = 1000^\circ\text{F.}$$

$$Z = 16.0 \text{ in.} \quad \Delta T_{\max.} = 400^\circ\text{F.} \quad \Delta T = 100^\circ\text{F.}$$

$$t_c = .50 \text{ in.} \quad t_f = .020 \text{ if Be} \quad t_f = .010 \text{ if Inconel X}$$

Core Mat'l: A-286 (4-20P)

$$P_T = P_b + P_a/2 = 217,500/32 + 1600/2 = 7596\#$$

$$q_x = P_T/W = 7596/15 = 506 \text{ \#/in.}$$

$$f_{cf} = q_x/2t_f = 506/2(.020) = 12,650 \text{ psi}$$

$$q_y = \frac{VQ}{I} \text{ where: } Q \cong 2R^2t \sqrt{1-(Z_1/R)^2}$$

$$I \cong \pi R^3 t$$

$$(b) \quad q_y = \frac{2V}{\pi R} \sqrt{1-(Z_1/R)^2}$$

$$\text{Let } Z_1 = 15.5 \quad R = 16.0$$

$$\text{then } q_y = 65.2\#/\text{in.}$$

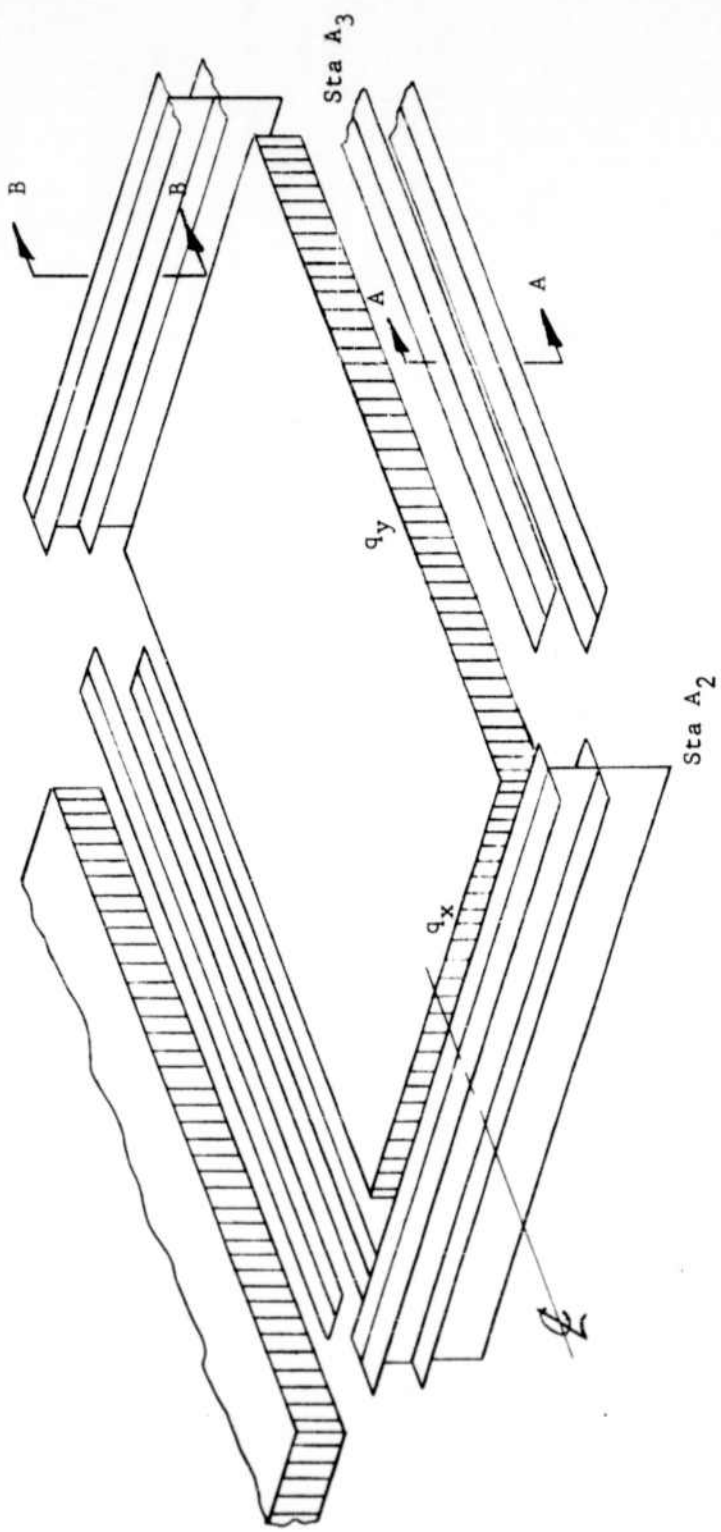
$$f_{cf} = q_y/2t = 65.2/2(.020) = 1630 \text{ psi}$$

$$Le/\rho = \frac{\pi}{(\sqrt{K})t} = 72.75$$

$$F_{ccr} @ 1000^\circ\text{F} = 28,000 \text{ psi} \quad \text{Ref. Figure III-7}$$

$$*M.S. = (F_{ccr}/f_{ccr}) - 1 = (28,000/14,280) - 1 = 0.89$$

\*Less thermal stresses



Ref: Figure III-1

Figure III-15 Panel Sections

(b) Core :

Core Shear:

$$\tau_{\max.} = q/t_c = 65.2/.5 = 130.4 \text{ psi.}$$

Although test results are not available for A-286 4-20P core, the result on a few samples of each A-286 4-15P and 4-30P are given in the test section of this report. By interpolation between the averages of these test results an acceptable core shear allowable ( $F_{CC}$ ) may be determined.

$$F_{CC} = 336 \text{ psi @ R.T.}$$

$$F_{CC} = .86 (336) = 299 \text{ psi @ } 1000^\circ\text{F.} \quad \text{Ref. 1}$$

$$*M.S. = (299/130.4) - 1 = 1.21$$

\*less thermal stresses.

(c) Joint Analysis @ Critical Temperature

Longitudinal

These members will be brazed on the honeycomb panel longitudinal edges and shall serve as splice plates between honeycomb panels. Therefore, these plates must carry axial, transverse, and normal loads without buckling. Axial internal loads will design the splice plates. Two trial cases for different thicknesses of splice plates will be analyzed.

Section A-A:

$$L_e/\rho = \pi b / \sqrt{K} \quad t(\text{assumed simple support})$$

$$\sqrt{k} = \sqrt{3.62} = 1.9 \quad b = .75 \text{ in.} \quad T = 1200^\circ\text{F.}$$

(Trial 1)

$$L_e/\rho_1 = 62.0 \quad t = .020 \text{ in.}$$

$$F_{CCr1} = .74 (42,000) = 31,100 \text{ psi Inconel X (Annealed)}$$

Ref: 1 & Figure III-9

$$f_{c1} = P_x/2bt = 571/2(.75)(.020) = 19,000 \text{ psi}$$

$$*M.S._1 = \frac{31,000}{19,000} - 1 = 0.63$$

(Trial 2)

$$L_e/\rho_2 = 82.7 \quad t = .015 \text{ in.}$$

$$F_{CCr2} = .74 (33,750) = 25,000 \text{ psi}$$

$$f_{c2} = P_x/2bt = 571/2(.75)(.015) = 25,350 \text{ psi}$$

$$*M.S._2 = \frac{25,000}{25,350} - 1 = \text{Not acceptable} \\ \text{(Negative)}$$

\*less thermal stresses

### Transverse

These members will be brazed on the honeycomb panel transverse edges and shall serve as a splice to bulkheads. Therefore, these plates must carry transverse, axial, and normal loads without buckling. Transverse internal load designs these joints. The shear redistribution will be carried by the bulkheads.

### Section B-B:

Although these splice plates could carry the loads with thinner gages of material than those of the longitudinal splice plates, ease of manufacturing and method of joining would require that the same gages of material be used in the production of a nose section. Therefore, an analysis of these members will not be shown.

## d. Thermal Stress

### (1) Introduction

The thermal stress for flat panels and a leading edge section is determined by the analysis presented in this section.

The flat panel analysis is a general solution for which the results are plotted based on the mechanical and physical properties of the materials considered. The results are plotted for various face sheet and combinations of face sheet materials. Yield strength was used as the materials allowable cut-off point and buckling was not considered in this analysis. Therefore, the maximum materials allowable cut-off point is only true as long as the geometrical parameters ( $L_e/\rho$  or  $\pi b/\sqrt{K}$ ) are such that the critical buckling stress is not exceeded.

The buckling stress could be considered in the plot of the thermal stress results by plotting a family of curves for the various geometric parameters. However, by checking to see if the thermal stress does not exceed the critical buckling stress as shown by shown by Figure III-7 the same information is obtainable.

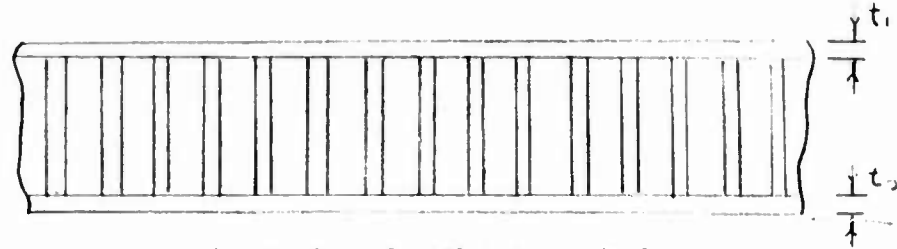
The leading edge section for which the concept is shown in Section A-A, Figure III-2, is analyzed to determine the thermal stress. The solution is general and the analysis is for a particular geometry and environment.

### (2) Flat Panel Analysis

In order to simplify the analysis, items that do not contribute substantially to the overall stress level are neglected. This is effected by making the following assumptions:

1. Constant temperatures over planes parallel to the neutral surface.
2. Constant temperature across the thickness of the face sheets.

3. The plate has complete angular restraint at the edges but is free to expand laterally.
4. The flexural rigidities of the faces are neglected.



Assumptions for Flat Panel Analysis

Figure III-16

where  $t_1$  = outer skin thickness (hot skin)

and  $t_2$  = inner skin thickness

$$\epsilon_1 = \sigma_1 \frac{(1 - \mu_1)}{E_1} + \alpha_1 \Delta T_1$$

$$\epsilon_2 = \sigma_2 \frac{(1 - \mu_2)}{E_2} + \alpha_2 \Delta T_2$$

$\epsilon$  = strain

$\sigma$  = stress

$\mu$  = Poissons ratio

$\alpha$  = linear coeff. of expansion

$E$  = Young's Modulus

$T$  = Temperature

$$\text{but } t_1 \sigma_1 + t_2 \sigma_2 = 0$$

$$\text{and } \epsilon_1 = \epsilon_2$$

$$\text{therefore } \sigma_2 = \frac{E_2 (\alpha_1 \Delta T_1 - \alpha_2 \Delta T_2)}{\left[ \frac{t_2 E_2}{t_1 E_1} (1 - \mu_1) + (1 - \mu_2) \right]}$$

$$\text{or finally } \sigma_2 = \frac{\left[ \frac{E_2}{(1 - \mu_1)} \right] (\alpha_1 \Delta T_1 - \alpha_2 \Delta T_2)}{\left[ \frac{(t_2 E_2)}{(t_1 E_1)} + \frac{(1 - \mu_2)}{(1 - \mu_1)} \right]}$$

for 0.02 Beryllium faces  $\mu_1 \approx \mu_2 = \mu$  constant

$$\text{and } \sigma_2 = \frac{\left[ \frac{E_2}{(1 - \mu)} \right] (\alpha_1 \Delta T_1 - \alpha_2 \Delta T_2)}{(E_2/E_1 + 1)} = -\sigma_1$$

For any hot skin temperature ( $T_1$ ) thermal stresses can be calculated for varying thermal gradients through the panel. This was done and is shown in Figure III-17.

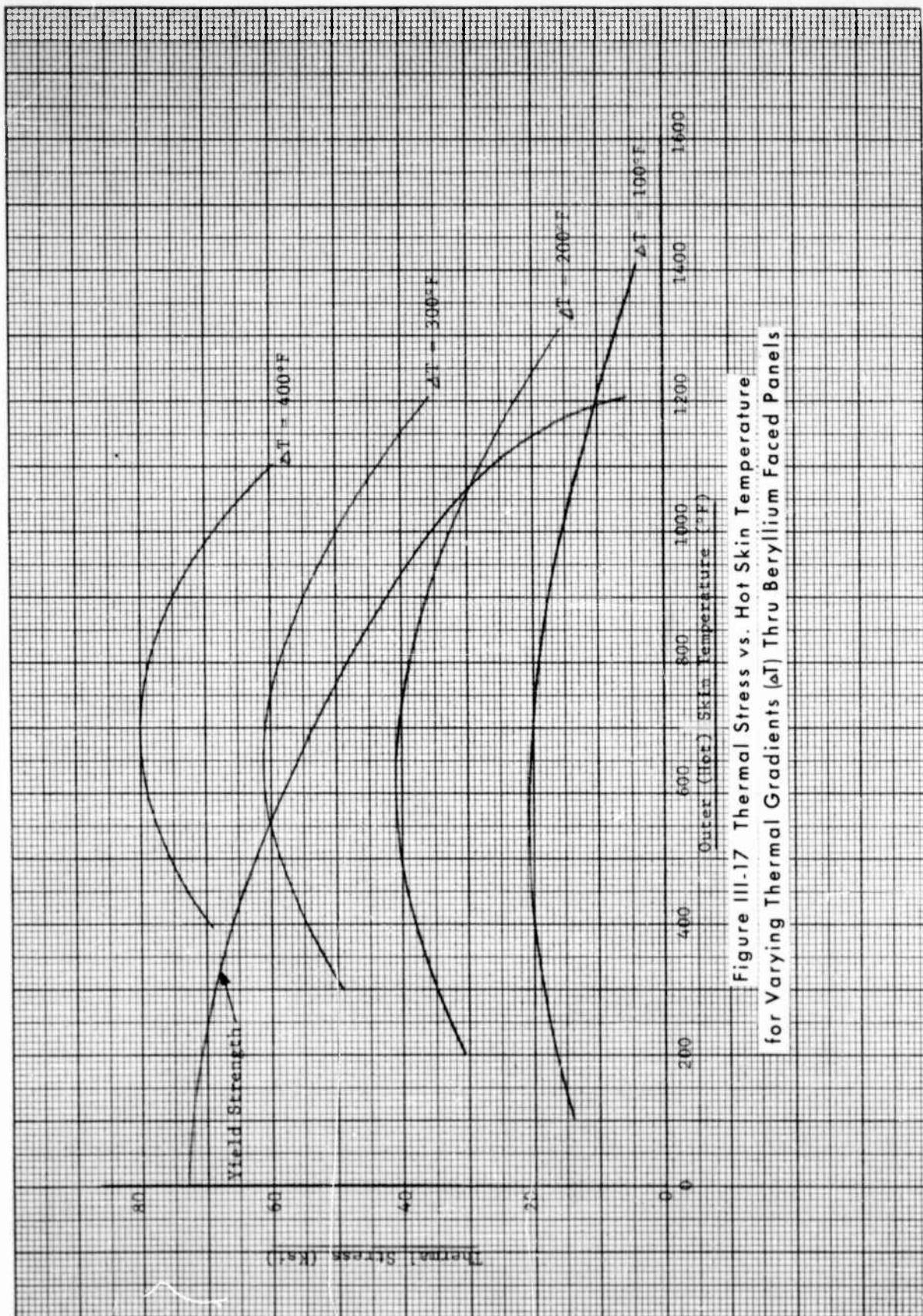


Figure III-17 Thermal Stress vs. Hot Skin Temperature for Varying Thermal Gradients ( $\Delta T$ ) Thru Beryllium Faced Panels

Superimposed on this graph is the yield strength vs temperature curve indicating the maximum thermal gradient a panel can withstand.

For Inconel X facings:

$$\sigma_2 = \frac{1.40845 E_2 (\alpha_1 \Delta T_1 - \alpha_2 \Delta T_2)}{(E_2/E_1 + 1)} = -\sigma_1$$

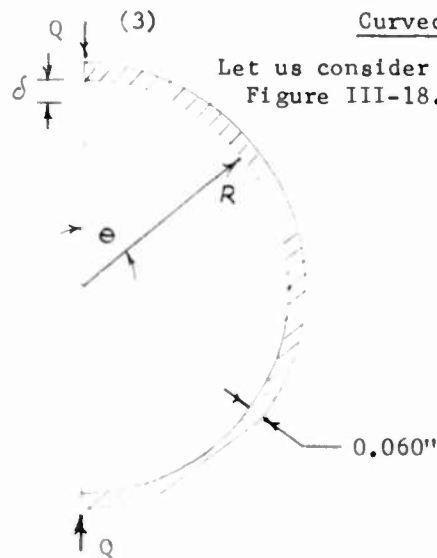
Figure III-19 indicates the same trend except the Inconel X can stand greater thermal gradients across the panel.

Finally for 0.01" Inconel X outer face and 0.020" beryllium inner face we have:

$$\sigma_2 = \frac{1.40845 E_2 (\alpha_1 \Delta T_1 - \alpha_2 \Delta T_2)}{(2 \frac{E_2}{E_1} + 1.25492)}$$

$$\text{and } \sigma_1 = \frac{-t_2}{t_1} \sigma_2$$

These two values are also plotted as the previous case and appear as Figures III-20 and III-21.



Sheet Beryllium Leading Edge  
Figure III-18

#### Curved Panel Analysis

Let us consider a typical leading edge as shown in Figure III-18.

The maximum expected temperature is 1100°F. Assuming an original temperature of 100°F the temperature rise is 1000°F.

$$\text{i.e. } \Delta t = 1000^\circ\text{F}$$

The linear expansion coefficient for beryllium is taken as  $\alpha = 9.5 \times 10^{-6}$ .

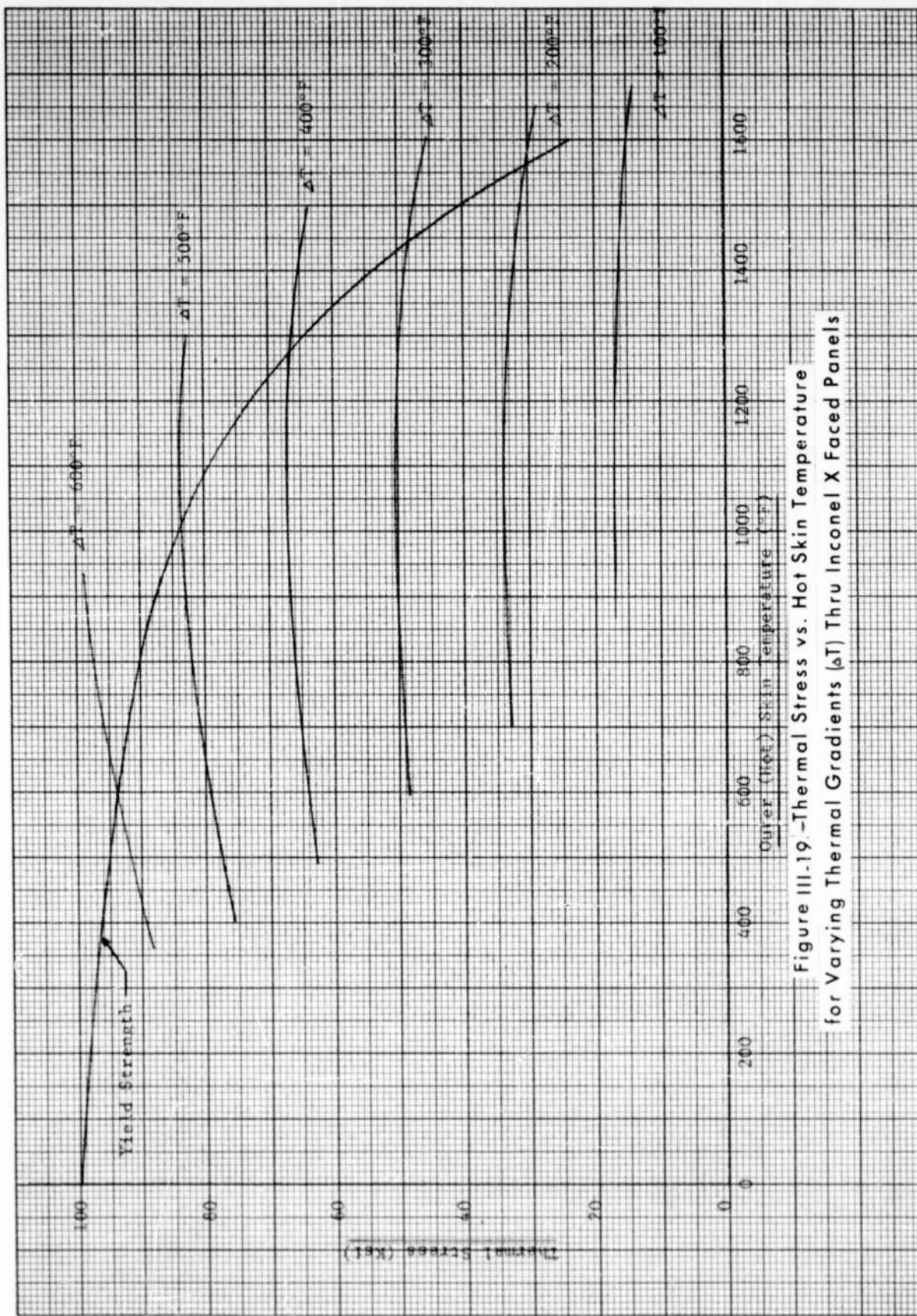


Figure III-19. Thermal Stress vs. Hot Skin Temperature  
for Varying Thermal Gradients ( $\Delta T$ ) Thru Inconel X Faced Panels

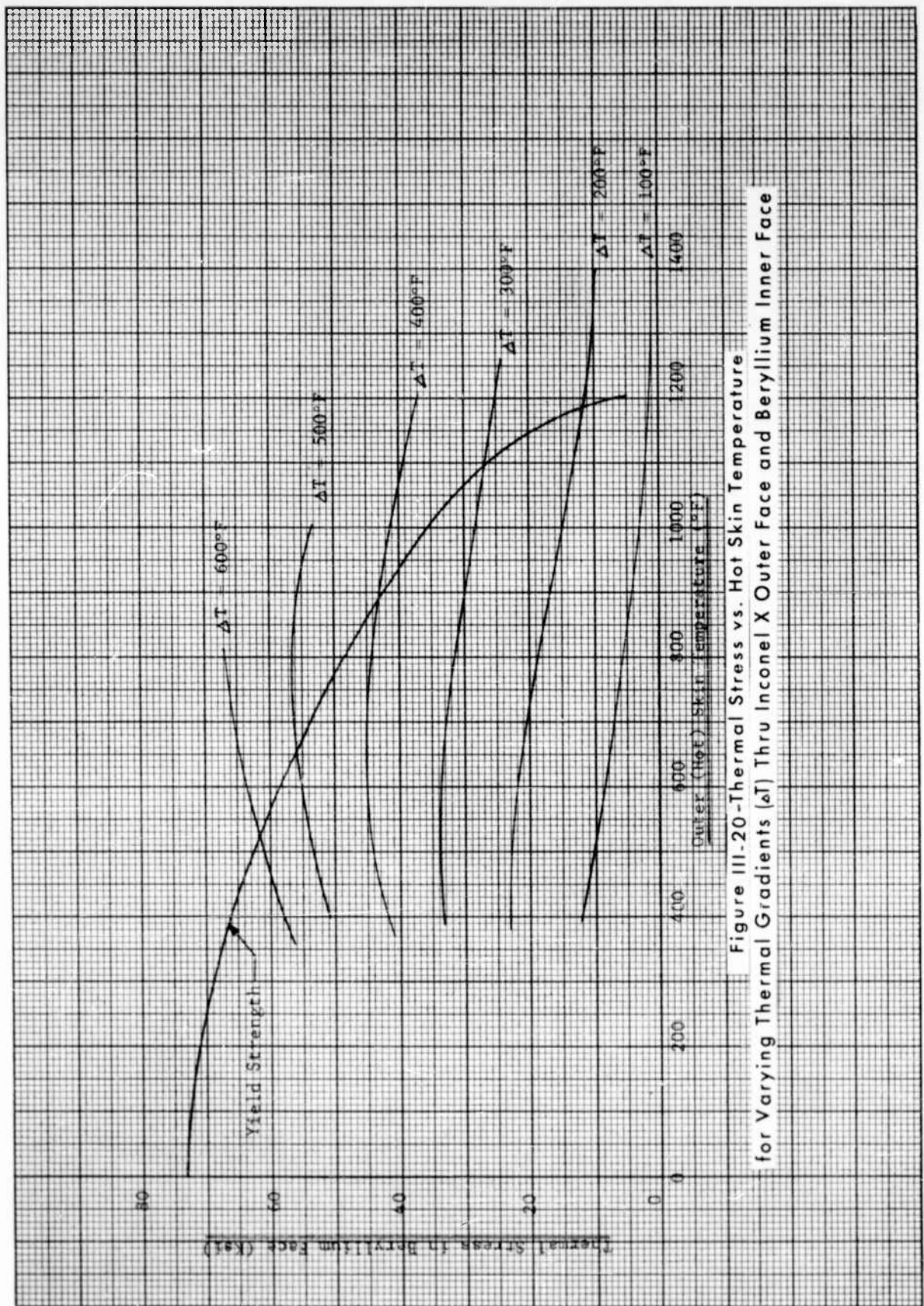


Figure III-20-Thermal Stress vs. Hot Skin Temperature  
for Varying Thermal Gradients ( $\Delta T$ ) Thru Inconel X Outer Face and Beryllium Inner Face

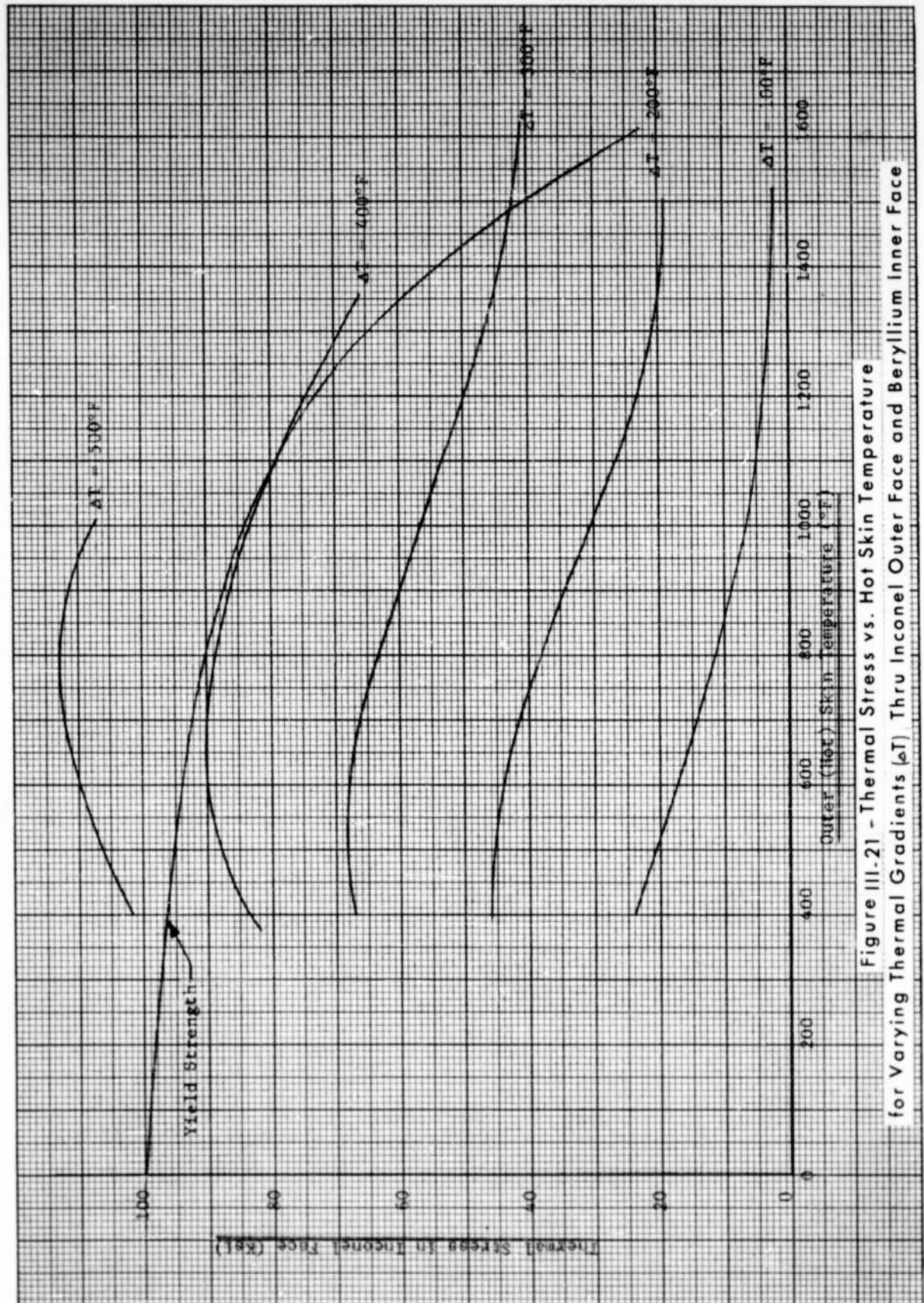


Figure III.21 - Thermal Stress vs. Hot Skin Temperature  
for Varying Thermal Gradients ( $\Delta T$ ) Thru Inconel Outer Face and Beryllium Inner Face

Therefore, the unrestrained deflection is

$$\delta = 2\alpha R \Delta t = 2 \times 9.5 \times 10^{-6} \times 3 \times 1000 = \underline{0.057} \text{ in.}$$

However, the surface is restrained at the edges and there can be no thermal deflection, thus the load necessary to bring this deflection to zero produces thermal stresses. These stresses may readily be found by energy methods.

The moment at any section is:  $M = QR \sin \theta$

$$\text{The strain energy is: } U = \int \frac{M^2 ds}{2EI} = \frac{R}{2EI} \int_0^\pi M^2 d\theta$$

The deflection in the direction of the applied load Q is:

$$\delta_Q = \frac{\partial U}{\partial Q} = \frac{R}{EI} \int_0^\pi M \frac{\partial M}{\partial Q} d\theta$$

$$\delta_Q = \frac{R}{EI} \int_0^\pi (QR \sin \theta) (R \sin \theta) d\theta = \frac{R^3 Q}{EI} \int_0^\pi \sin^2 \theta d\theta$$

$$\delta_Q = \frac{QR^3}{EI} \left[ \frac{\theta}{2} - \frac{\sin 2\theta}{4} \right]_0^\pi = \frac{\pi QR^3}{2EI}$$

$$\text{or } Q = \frac{2\delta_Q EI}{\pi R^3} = \frac{2 \times 0.057 \times 42 \times 10^6 \times 1/12 \times 0.06^3}{\pi \times 3^3}$$

$$Q = 1.01604$$

Finally the stress is:

$$\sigma = \pm K \frac{Mc}{I}$$

where K is a correction factor for curved beams:

$$\sigma = \pm 1 \times \frac{1.01604 \times 3 \times 0.03}{1/12 \times 0.06^3}$$

$$\sigma = \pm 5080.2 \text{ psi}$$

### 3. Thermoelastic Analysis

#### a. Introduction

A thermoelastic analysis for a simply supported sandwich panel with a temperature gradient and edge compression is presented. This section describes in brief form the general energy solution (as researched and developed by Chieh-Chien Chang and Ibrahim K. Ebcioğlu, see ref. 3) for a two dimensional analysis including thermal effects. The differential equation and boundary conditions from the horizontal potential energy method are presented and the matrix forms are constructed. The method is particularly suitable for computer solution and is also suitable for consideration of design parameters and comparison with test data.

A particular solution is presented for an 18" x 18" panel. The panel was under an edgewise compression load and a thermal gradient.

The analysis was performed to show the response of the panel under mechanical loads and thermal gradients, and also to establish approximate stress levels anticipated from test data. The non-dimensional curves of the results of the analysis are presented which may be used to establish structural design parameters.

A comparison of the panel analyzed with test data is not possible because the test panel contained built-in channel edge-members which are unlikely to be used in future panels.

#### b. General Analysis

##### (1) List of Symbols

A	= panel area (in. <sup>2</sup> )
$A_i^{np}, B_i^{np}, C^{np}$ $a_j$	= coefficients
D	= d/d $\eta$ , operator
D <sub>0</sub>	= $\frac{(\bar{t} + f)^2 \cdot E \cdot t}{1 + m} \frac{1}{1 - \mu^2}$ = flexural rigidity (lb-in. <sup>2</sup> /in.)
E	= Young's modulus (lb/in. <sup>2</sup> )
$e_{\alpha\beta}$	= (1/2) ( $u_{\alpha,\beta} + u_{\beta,\alpha}$ ) = strain components
f	= (t' + t'')/2 (in.)
$\bar{G}$	= core shear modulus (lb/in. <sup>2</sup> )
$\bar{g}$	= $\bar{G}_x/\bar{G}_y$ , ratio of core shear moduli
$\bar{H}$	= $\bar{t}\bar{G}$ , core shear stiffness (lb/in.)
$k_{le} = k_{je}$	= $\bar{N}_{yy}/P_e$ , edge loading parameter (positive)

b. (1) List of Symbols

$K_1$	$= 2\bar{g}R/\beta(1 + \mu)$
$K_3$	$= [(2\rho R/1 + \mu)] (1 + g) + (q/G)$
$2a, 2b$	$=$ lengths of panel in x- and y- directions (in.)
$M_0$	$= (1 + \mu) D_0 \frac{\alpha'(T' - T_n) - \alpha''(T'' - T_n)}{\bar{t} + f} =$ $R \frac{1 + m}{\bar{t} + f} D_0, \text{ moment of thermal differential (lb-in./in.)}$
$M_{\alpha\beta}$	$=$ sectional moment (lb-in./in.)
$m$	$= t'E'/t''E',$ face extension factor
$N_{\alpha\beta}$	$=$ component of edge load per unit length (lb/in.)
$n_{\alpha}$	$=$ direction cosine of unit normal in $\alpha$ direction
$P_e$	$= \frac{(\bar{t} + f)^2}{1 - \mu^2} \left( \frac{\pi^2}{2b} \right) \frac{t'E'}{1 + m} =$ Euler cylindrical buckling load (lb/in.)
$Q$	$= (q/2\bar{G}_y r_{ek_{le}} \hat{t}^2 \alpha),$ transverse load factor
$Q_{\alpha}$	$=$ transverse shear load in $\alpha$ -direction (lb/in.)
$q$	$=$ transverse load (lb/in. <sup>2</sup> )
$R$	$= \frac{\alpha'(T' - T_n) - \alpha''(T'' - T_n)}{1 + m} (1 + \mu)$
$r_e = \tau_e$	$= P_e/\hat{t}^2 \bar{t}_{ly},$ core shear stiffness parameter(positive)
$s$	$=$ length along panel edge (in.)
$t$	$=$ thickness (in.)
$\hat{t}$	$= (\bar{t} + f)/\bar{t}$
$T_n$	$=$ reference temperature at neutral surface
$U$	$=$ strain energy (lb-in.)
$U_0$	$=$ strain energy density function (lb/in. <sup>2</sup> )
$V$	$=$ potential energy (lb-in.)

b. (1) List of Symbols (Continued)

$u, v$	$= u'/b, v'/b$ , dimensionless displacements
$u', v'$	$= x$ - and $y$ -components of displacement of outer face (in.)
$w$	$= w'/b$ , dimensionless deflection
$w'$	$=$ panel deflection (in.)
$w_1$	$= w_1'/b$ , dimensionless deflection of the panel under uniaxial loading and thermal gradient
$\hat{w}_1$	$= \frac{\alpha'(T' - T_n) - \alpha''(T'' - T_n)}{2\hat{t}\alpha} (1 + \alpha) =$ dimensionless maximum thermal deflection
$\hat{w}_2$	$= 5\pi^2 q b^2 / 96 P_e$ , dimensionless maximum deflection due to transverse loading $q$
$x, y, z$	$=$ Cartesian coordinates (in.)
$\alpha$	$= \bar{t}/b$ , core thickness ratio or coefficient of thermal expansion
$\beta$	$= b/a$ , panel aspect ratio
$\delta( )$	$=$ increment of ( )
$\Delta_1^{np}, \Delta_2^{np}$ $\Delta_3^{np}, \Delta^{np}$	$\left. \begin{array}{l} \Delta_1^{np}, \Delta_2^{np} \\ \Delta_3^{np}, \Delta^{np} \end{array} \right\} =$ determinants as specified
$\xi, \eta$	$= x/a, y/b =$ nondimensional coordinates
$\lambda_s$	$=$ sth characteristic root
$\mu$	$=$ Poisson's ratio
$\rho$	$= (1/2) (1 + m)\hat{t}$
$\tau_{x\beta}$	$=$ sectional stress (lb/in. <sup>2</sup> )
$\tau_{xz}$	$=$ shear stress of core (lb/in. <sup>2</sup> )
$\Phi, \psi, \chi$	$=$ functions
<u>Superscripts</u>	
(i)	$=$ lower or upper face
-	$=$ core
'	$=$ outer face (high temperature)
''	$=$ inner face (low temperature)
np	$=$ nth and pth degrees of freedom

b. (1) List of Symbols (Continued)

Subscripts

$\alpha$ or $\beta$	= free indices each taking x or y indicating direction
$, \alpha$ or $, \beta$	= free indices taking x or y indicating derivative with respect to x or y, respectively
f	= face
i	= ith direction
$, x$ or $, y$	= derivative with respect to x or y
L	= loading
T	= temperature

Signs of Quantities

$M_{\alpha p}$ ,  $N_{\alpha p}$ ,  $Q_{\alpha}$ ,  $q$  are positive as shown in Figure III-22.

U is positive when work is done by the panel on the boundary restraint.

V, the potential, is negative when work is done by the positive external loadings on the panel.

(2) Differential Equations of the Problem:

Ref. (Figure III-22)

Assumptions imposed:

- (1) Panel is simply supported
- (2) Edge loading  $N_{xx} = N_{xy} = 0$   
 $\tilde{N}_{yy} = -N_{yy}$  ( $N_{yy}$  is in compression .. negative)  
 Then  $\tilde{N}_{yy} > 0$  when  $N_{yy}$  is in compression.
- (3) Outer face temperature ( $T'$ )  $>$  innerface temperature ( $T''$ ).
- (4) Transverse loading ( $q$ ) is constant. ( $q$  #/in.<sup>2</sup>)

A system of three differential equations which correspond to the above assumptions can be reduced to a corresponding system of nondimensional equations:

$$[1.] \begin{cases} (a) \left( \frac{4\tau_e}{\pi^2} \right) [2\beta^2 u_{,\xi\xi} + (1-\mu) u_{,\eta\eta} + \beta(1+\mu) v_{,\xi\eta}] - \\ \quad 2\bar{g}u - (\beta\bar{g}\hat{t}^2 \alpha/\rho) w_{,\xi} = 0 \\ (b) \left( \frac{4\tau_e}{\pi^2} \right) [2v_{,\eta\eta} + \beta^2(1-\mu)v_{,\xi\xi} + \beta(1+\mu)u_{,\xi\eta}] - \\ \quad 2v - (\hat{t}^2 \alpha/\rho) w_{,\eta} = 0 \\ (c) -2\rho\bar{g}\beta u_{,\xi} - 2\rho v_{,\eta} - \bar{g}\hat{t}^2 \beta \alpha w_{,\xi\xi} + \\ \quad (\tau_e k_{1e} - 1) \alpha \hat{t}^2 w_{,\eta} = q/\bar{G}_y \end{cases}$$

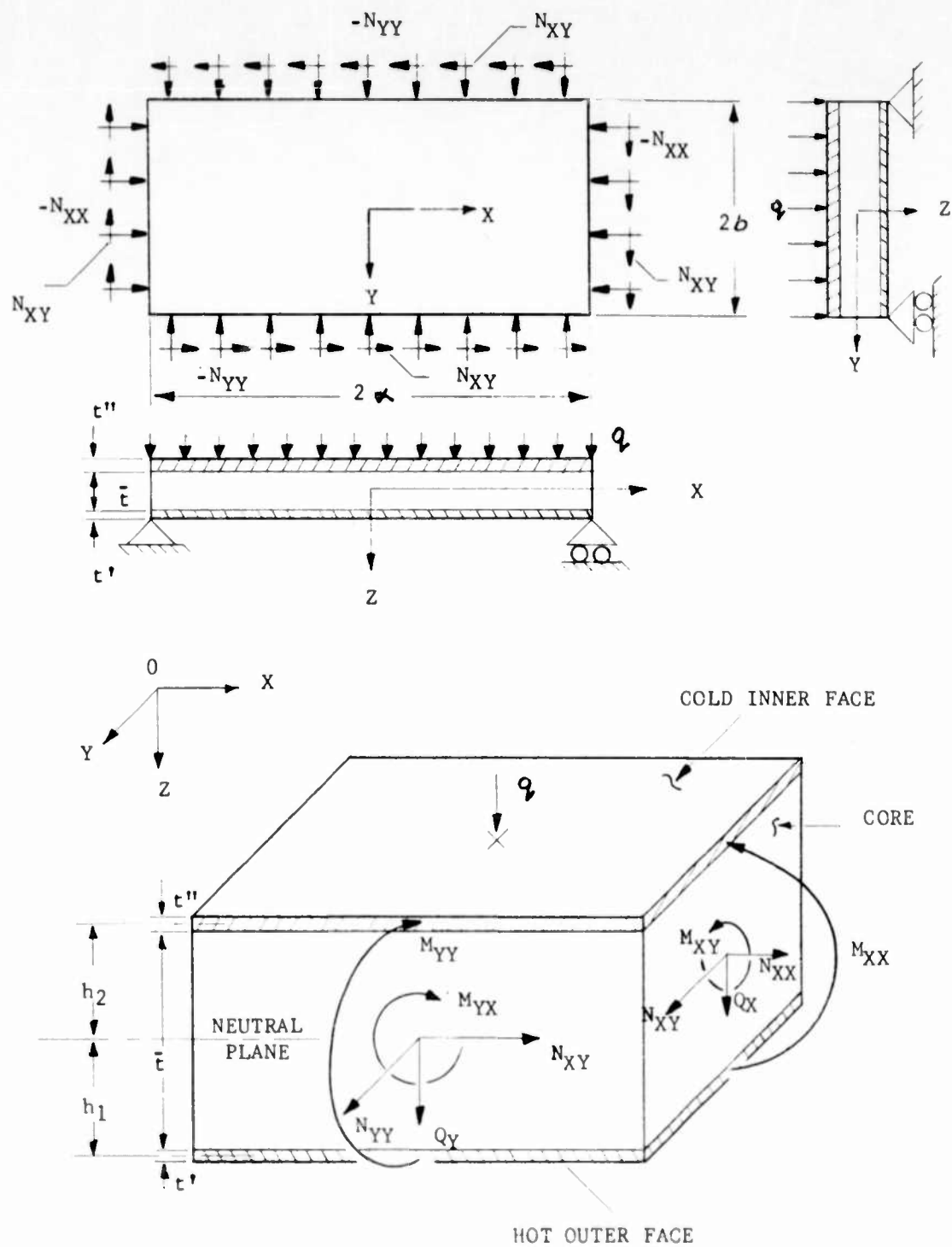


Figure III-22 Geometry for General Analysis

(2) Differential Equations of the Problem: (Continued)

where: (a)  $\bar{t} = (\hat{t} + f) / \bar{t}$ ,  $[f = (t' + t'') / 2]$

(b)  $m = t' E' / t'' E''$

(c)  $\bar{H}_x = \bar{t} \bar{G}_x$ ,  $\bar{H}_y = \bar{t} G_y$

(d)  $\xi = x/a$ ,  $\eta = y/b$

(e)  $u'/b = \eta$ ,  $v'/b = \nu$ ,  $w'/b = w$

(f)  $\alpha = \bar{t} / b$

(g)  $\beta = b/a$

(h)  $\bar{g} = \bar{G}_x / G_y$

(i)  $\rho = (1/2)$

(j)  $P_e = [(\bar{t} + f)^2 / (1 - \mu^2)] [t' E' / (1 + m)] (\pi/2b)^2$

(k)  $k_{1e} = \bar{N}_{yy} / P_e$

(l)  $r_e = P_e / \bar{t}^2 \bar{H}_y$

(3) Boundary conditions and Hoff's Modification: In the case for a simply supported panel, by rewriting the boundary condition in nondimensional form, the results are as follows:

(a)  $B_y + \mu \nu, \eta = R$   $\xi = \mp 1$

(b)  $\nu, \eta + B u, \xi = R$   $\eta = \mp 1$

(c)  $u, \eta + B \nu, \xi = 0$   $\xi = \mp 1$

(d)  $u, \eta + B \nu, \xi = 0$   $\eta = \mp 1$

(e)  $w = 0$   $\xi = \mp 1$

(f)  $w = 0$   $\eta = \mp 1$

(g)  $R = (1 + \mu) \alpha' (T' - T_h) - \alpha'' (T' - T_h) / (1 + m)$

Hoff's boundary conditions were modified for a loaded sandwich panel at room temperature by relaxing (c) and (d) above to:  
 $v = 0$ ,  $\xi = \mp 1$ ;  $u = 0$ ,  $\eta = \mp 1$ .

For thermal stresses Hoff's boundary conditions should be replaced by:

(c')  $v = (R / (1 + \mu)) \eta$  ( $\xi = \mp 1$ )

(d')  $u = (R / B (1 + \mu)) \xi$  ( $\eta = \mp 1$ )

(4) Choice of General Forms of Solutions:

$$\left\{ \begin{array}{l} \text{(a) } u(\xi, \eta) = [R / \beta (1 + \mu)] \xi + \sum_{n=1}^{\infty} \sum_{p=1}^{\infty} A_1^{np} \sin \frac{n\pi}{2} \xi \cos \frac{p\pi}{2} \eta \\ \text{(b) } v(\xi, \eta) = [R / \beta (1 + \mu)] \eta + \sum_{n=1}^{\infty} \sum_{p=1}^{\infty} A_2^{np} \cos \frac{n\pi}{2} \xi \sin \frac{p\pi}{2} \eta \\ \text{(c) } w(\xi, \eta) = \sum_{n=1}^{\infty} \sum_{p=1}^{\infty} A_3^{np} \cos \frac{n\pi}{2} \xi \sin \frac{p\pi}{2} \eta \end{array} \right.$$

Where eigenvalues or degree of freedom n and p.

b. (4) Choice of General Forms of Solutions: (Continued)

All boundary conditions are fully satisfied by the above equations provided only the odd values of the eigenvalues are used. Insight into the behavior of the dimensionless displacement ( $u, v$ ) and the dimensionless deflection ( $w$ ) indicates the choice of [2] satisfies the requirements.

By substitution of [2] into [1] we get the following:

$$[3.] \begin{cases} \sum_{n=1}^{\infty} \sum_{p=1}^{\infty} (\Phi_1 A_1^{np} + X_1 A_2^{np} + \psi_1 A_3^{np}) \sin \frac{n\pi}{2} \xi \cos \frac{p\pi}{2} \eta = K_1 \xi \\ \sum_{n=1}^{\infty} \sum_{p=1}^{\infty} (\Phi_2 A_1^{np} + X_2 A_2^{np} + \psi_2 A_3^{np}) \cos \frac{n\pi}{2} \xi \sin \frac{p\pi}{2} \eta = K_2 \eta \\ \sum_{n=1}^{\infty} \sum_{p=1}^{\infty} (\Phi_3 A_1^{np} + X_3 A_2^{np} + \psi_3 A_3^{np}) \cos \frac{n\pi}{2} \xi \cos \frac{p\pi}{2} \eta = K_3 \end{cases}$$

where:

$$(a) \Phi_1 = -\tau_e(1-\mu)p^2 - 2B^2\tau_e n^2 - 2\bar{g}$$

$$(b) X_1 = -B(1+\mu)np\tau_e$$

$$(c) \psi_1 = (B\pi\bar{g}\hat{t}^2\alpha n)/2p$$

$$(d) \Phi_2 = -B\tau_e(1+\mu)np$$

$$(e) X_2 = -2\tau_e p^2 - B\tau_e(1-\mu)n^2 - 2$$

$$(f) \psi_2 = (\hat{t}\alpha\pi p)/2\rho$$

$$(g) \Phi_3 = -B\rho\bar{g}\pi n$$

$$(h) X_3 = -\rho\pi p$$

$$(i) \psi_3 = (\alpha\hat{t}^2\pi^2/4)[B^2\bar{g}n^2 - (\tau_e k_{1e} - 1)p^2]$$

$$(j) K_1 = 2\bar{g}R/B(1+\mu)$$

$$(k) K_2 = 2R/(1+\mu)$$

$$(l) K_3 = [2\rho R/(1+\mu)](1+\bar{g}) + (q/\bar{G}_y)$$

(5) Expansion of Nonhomogeneous Terms in Eqs. [3] into Desirable Double Fourier Series:

$$[4.] \begin{cases} (a) K_1 \xi = \sum_{n=1}^{\infty} \sum_{p=1}^{\infty} B_1^{np} \sin \frac{n\pi}{2} \xi \cos \frac{p\pi}{2} \eta = 0 \\ (b) K_2 \eta = \sum_{n=1}^{\infty} \sum_{p=1}^{\infty} B_2^{np} \cos \frac{n\pi}{2} \xi \sin \frac{p\pi}{2} \eta = 0 \\ (c) K_3 = \sum_{n=1}^{\infty} \sum_{p=1}^{\infty} B^{np} \cos \frac{n\pi}{2} \xi \cos \frac{p\pi}{2} \eta = 0 \end{cases}$$

## b. (5) (Continued)

Where the Fourier coefficients are:

$$(a) B_1^{np} = (\bar{g}_p / \epsilon n) B^{np} = \begin{cases} 0 & (n, p \text{ even}) \\ (3\pi^2 K_1 / \pi^2 n^2 p) \sin(n\pi/2) \sin(p\pi/2) & (n, p \text{ odd}) \end{cases}$$

$$(b) B_2^{np} = B^{np} = \begin{cases} 0 & \text{--- } (n, p \text{ odd}) \\ (32\kappa_2/\pi^3 n p^2) \sin(n\pi/2) \sin(p\pi/2) & \text{--- } n, p \text{ even} \end{cases}$$

$$(c) B_3^{np} = C^{np} + \left(\frac{p\pi}{2}\right)(1+\bar{g}) B^{np} = \begin{cases} 0 & (16k_3/\pi = np) \sin(n\pi/2) \sin(p\pi/2) \\ - & (n, p \text{ even}) \\ - & (n, p \text{ odd}) \end{cases}$$

Provided  $q$  is held constant.  $B^{np}$  is introduced for  $B_2^{np}$  in each of the three coefficients to simplify the notation for later use.

### (6) Evaluation of Coefficients

Substituting in equation [4] in [3]

$$[5.] \begin{cases} (a) \sum_{n=1}^{\infty} \sum_{p=1}^{\infty} (\Phi_1 A_1^{np} + \chi_1 A_2^{np} + \psi_1 A_3^{np} - B_1^{np}) \sin \frac{n\pi}{2} \xi \cos \frac{p\pi}{2} \eta = 0 \\ (b) \sum_{n=1}^{\infty} \sum_{p=1}^{\infty} (\Phi_2 A_1^{np} + \chi_2 A_2^{np} + \psi_2 A_3^{np} - B_2^{np}) \cos \frac{n\pi}{2} \xi \sin \frac{p\pi}{2} \eta = 0 \\ (c) \sum_{n=1}^{\infty} \sum_{p=1}^{\infty} (\Phi_3 A_1^{np} + \chi_3 A_2^{np} + \psi_3 A_3^{np} - B_3^{np}) \cos \frac{n\pi}{2} \xi \cos \frac{p\pi}{2} \eta = 0 \end{cases}$$

All values of  $\xi$  and  $\eta$  from (-1) to (+1) are true. The terms in parenthesis must be identically equal to zero.

By a system of three simultaneous, linear, nonhomogeneous algebraic equation, that is:

$$[6.] \begin{cases} \Phi_1 A_1^{np} + \chi_1 A_2^{np} + \psi_1 A_3^{np} = B_1^{np} \\ \Phi_2 A_1^{np} + \chi_2 A_2^{np} + \psi_2 A_3^{np} = B_2^{np} \\ \Phi_3 A_1^{np} + \chi_3 A_2^{np} + \psi_3 A_3^{np} = B_3^{np} \end{cases}$$

Rewriting in matrix form equation 6

$$[7.] \begin{Bmatrix} \Phi_1 & X_1 & \psi_1 \\ \Phi_2 & X_2 & \psi_2 \\ \Phi_3 & X_3 & \psi_3 \end{Bmatrix} \begin{bmatrix} A_1^{np} \\ A_2^{np} \\ A_3^{np} \end{bmatrix} = \begin{bmatrix} B_1^{np} \\ B_2^{np} \\ B_3^{np} \end{bmatrix}$$

b. (6) Evaluation of Coefficients (Continued)

After some algebra by convention technique of matrix algebra where  $\Delta^{np}$  and  $\Delta_i^{np}$  represent determinants.

$$[8] \quad A_i = \Delta_i^{np} / \Delta^{np} \quad (i = 1, 2, 3)$$

With the coefficients of equation [8] and the differential equations [2], we have the solution to the problem.

c. Example Analytical Solution:

Let us determine the deflections and stresses in a simply-supported sandwich panel subjected to a thermal gradient and edge loading by a two dimensional analysis. The example analytical solution is based on the above mentioned general analytical method.

The values of the constants are:

Material: (face sheets) Beryllium

(core) 321 Stainless

(edge members) 321 Stainless

$$t' = t'' = .040 \text{ in.}$$

$$\mu = .1$$

$$\alpha = E/b = 1/18$$

$$a = b = 9 \text{ in.}$$

$$t = .5 \text{ in.}$$

$$T_n = 500^\circ\text{F}$$

$$R = (1 + \mu) [\alpha' (t' - T_n) - \alpha'' (T'' - T_n) / (1 + \mu)]$$

$$M = 1 = t'E'/t''E''$$

$$\beta = b/a = 1$$

$$K_{1e} = N_{yy}/P_e$$

$N_{yy}$  = Compressive edge loading in the "Y" direction.

$$E = 38 \times 10^6 \text{ @ } 500^\circ\text{F}$$

$$\bar{G}_y = 50 \text{ Ksi}$$

$$\bar{g} = \bar{G}_x / \bar{G}_y \approx 2/3 = (1/11) \text{ core ribbon}$$

$$r_e = .236$$

$$P_e = 6900 \text{ \#/in. @ } 500^\circ\text{F} = \text{Cylindrical bucking load}$$

The primary interest is the deflection at the center of the sandwich panel as a function of edge loading and temperature gradient.

At point 33 of the panel  $\mathcal{Z} = \mathcal{Y} = 0$  therefore  $w_{(0,0)} = A_3^{11} + A_3^{13} + A_3^{31} + A_3^{33}$

Note, that the deflection is calculated only up to  $N = p = 3$ . The equation of the analysis shows that the constants  $A^{12}$ ,  $A^{21}$ ,  $A^{22}$ ,  $A^{23}$ ,  $A^{32}$  are zero (0).

After some algebra, as shown in the "Analysis" and "Appendix A" of Ref. (3), the deflection ( $w$ ) as a function of ( $\Delta T$ ) and the loading parameter ( $k_{1e}$ ) was determined.

c. Example Analytical Solution: (Continued)

$$w_{\Delta T}(0,0) = \Delta T \times 10^{-5} \left[ \frac{27.3848}{2.4052 - k_{1e}} - \frac{2.1953}{3.2504 - k_{1e}} - \frac{18.1341}{22.3190 - k_{1e}} + \frac{0.7815}{6.0425 - k_{1e}} \right]$$

Presenting the results of the above equation, in the graphical form as shown in Figure III-23, the points indicated are the points calculated by the preceding equation.

$$w_1 = bw_{\Delta T} = 9 w_{\Delta T} \text{ Actual deflection of 18 inch panel}$$

Since  $T_n$  is the temperature at the neutral or reference axis of the panel, then the equations for the face sheets average temperatures ( $T'$  and  $T''$ ) are as follows:

$$T' = T_n + (\Delta T/2)$$

$$T'' = T_n - (\Delta T/2)$$

$$\text{i.e.: } T' = 500^\circ\text{F} + (500^\circ\text{F}/2) = 750^\circ\text{F}$$

$$T'' = 500^\circ\text{F} - (500^\circ\text{F}/2) = 250^\circ\text{F}$$

The next point of interest to be determined is the stress at the center of the panel. The compressive stress in the hot face is calculated by this equation per Ref. (3).

$$\tau_{yy}' = M_{yy}/(\bar{E} + f)t' + N_{yy}/t'(1+m)$$

$$\tau_{yy}' = \frac{E}{1-\mu^2} \left[ \mu B \frac{dw}{dz} + \frac{dw}{dz} - R \right] + \frac{\tilde{N}_{yy}}{t'(1+m)} \text{ (at point 33)}$$

$$\left. \frac{dw}{dz} \right|_{z=0} = \frac{R}{B(1+\mu)} + \frac{\pi}{2} A_2^{11} + \frac{\pi}{2} A_1^{13} + \frac{3\pi}{2} A_1^{31} + \frac{3\pi}{2} A_1^{33}$$

$$\left. \frac{dw}{dz} \right|_{z=0} = \frac{R}{1+\mu} + \frac{\pi}{2} A_2^{11} + \frac{3\pi}{2} A_2^{13} + \frac{\pi}{2} A_2^{31} + 3\pi A_2^{33}$$

$$\tau_{yy}' = \frac{E}{1-\mu^2} \left\{ \left( \frac{1-\mu R}{B(1+\mu)} - R + \frac{R}{1+\mu} \right) \frac{11\pi}{2} [A_1^{11} + A_1^{13} + 3A_1^{31} + 3A_1^{33}] + \frac{\pi}{2} [A_2^{11} + 3A_2^{13} + A_2^{31} + 3A_2^{33}] \right\}$$

$$\tau_{yy}' = \frac{E}{1-\mu^2} - \frac{\pi}{2} \left[ \mu (A_1^{11} + A_1^{13} + 3A_1^{31} + 3A_1^{33}) + A_2^{11} + 3A_2^{13} + A_2^{31} + 3A_2^{33} \right]$$

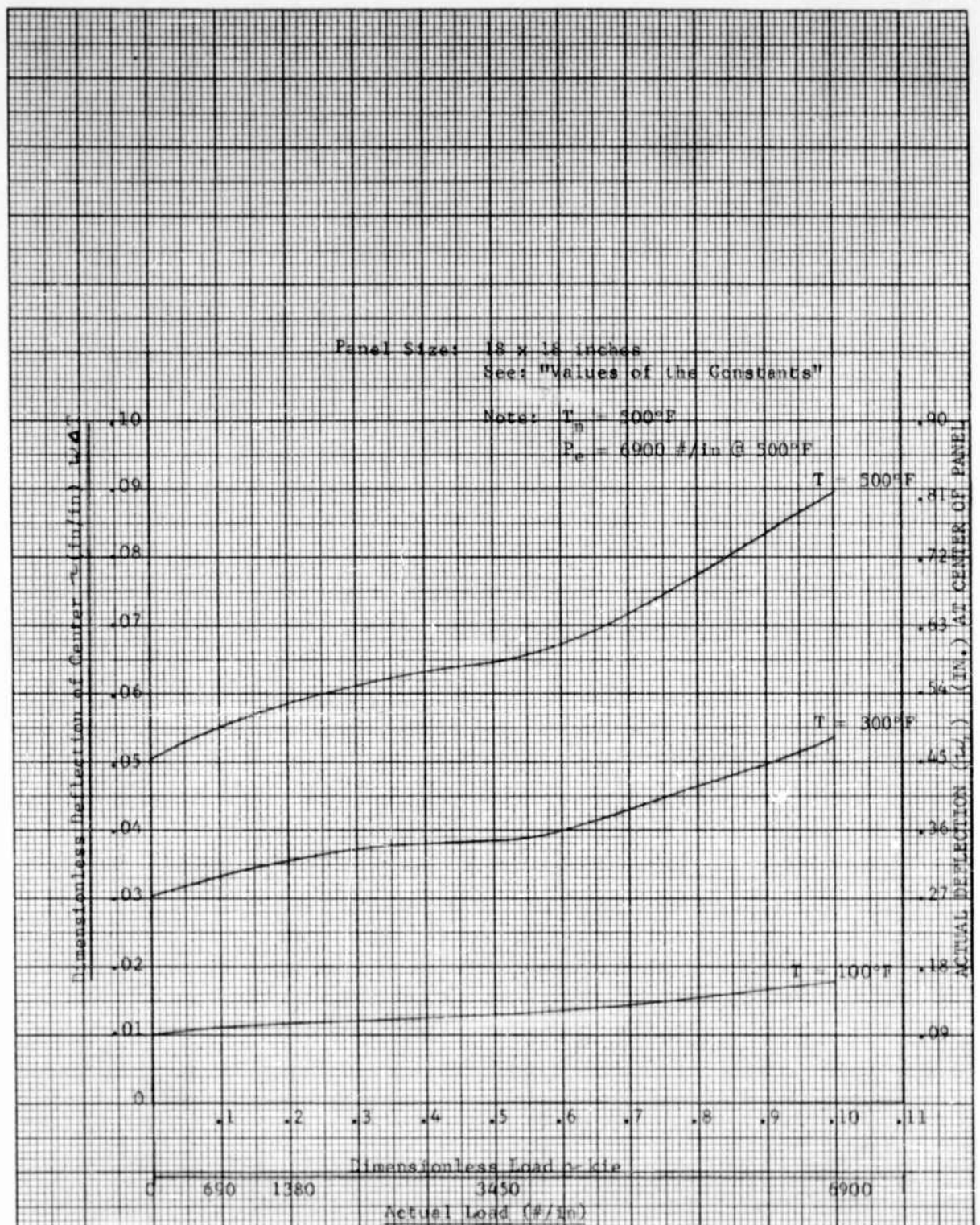


Figure III-23 Deflection vs. Edge Load for Various Temperature Gradients on a Beryllium Sandwich Panel

c. Example Analytical Solution: (Continued)

The above parameters were evaluated as shown in the Analysis and Appendix A - Ref. (3).

The solutions to the preceeding equation are graphically illustrated as stress is a faction of  $k_{ie}$  in Figure III-24.

C. COMPOSITE PANELS

1. Thermal Analysis

a. Summary

A steady state heat flow analysis of a typical thermantic individual cell was conducted to determine the pattern of heat flow and temperature distributions in an assumed heat flux field. A general method of analysis is presented and partial results as obtained from an IBM 7090 computer are shown. The method of analysis, based on Lagrangian Mechanics, was selected because of its potential for solving complex heat flow problems for large surfaces. The method offers less expensive and more accurate solutions than finite difference methods. Also the methods and procedures are compatible with structural dynamics analysis.

b. Conclusions

From the preliminary results of the study conducted herein, it is concluded that:

- (1) Accurate three dimensional microscopic analysis of the thermantic concept is practical and useful in establishing improved detailed design changes.
- (2) The metal reinforcement is cooler than the surrounding ceramic at the same level.

c. Theory

The method of analysis is based upon the use of eigen-vectors and eigen-values which are expressed as normal mode series and characteristic values. By the method of Lagrange, the normal mode series is developed into a set of differential equations which can be solved for its particular solutions. Since the functions are originally orthogonal the homogeneous solution is trivial. With the use of the operational calculus, the time dependent solutions are readily obtained for the linear problem. The non-linear problem can be handled by assuming piece-wise linearity and employing the method of successive approximations. It is to be noted that there are many problems to be solved in successfully applying the method to the non-linear case.

(1) NOTATION

q	-	generalized coordinate vector
V	-	arbitrarily defined thermal-potential function
D	-	arbitrarily defined dissipation function

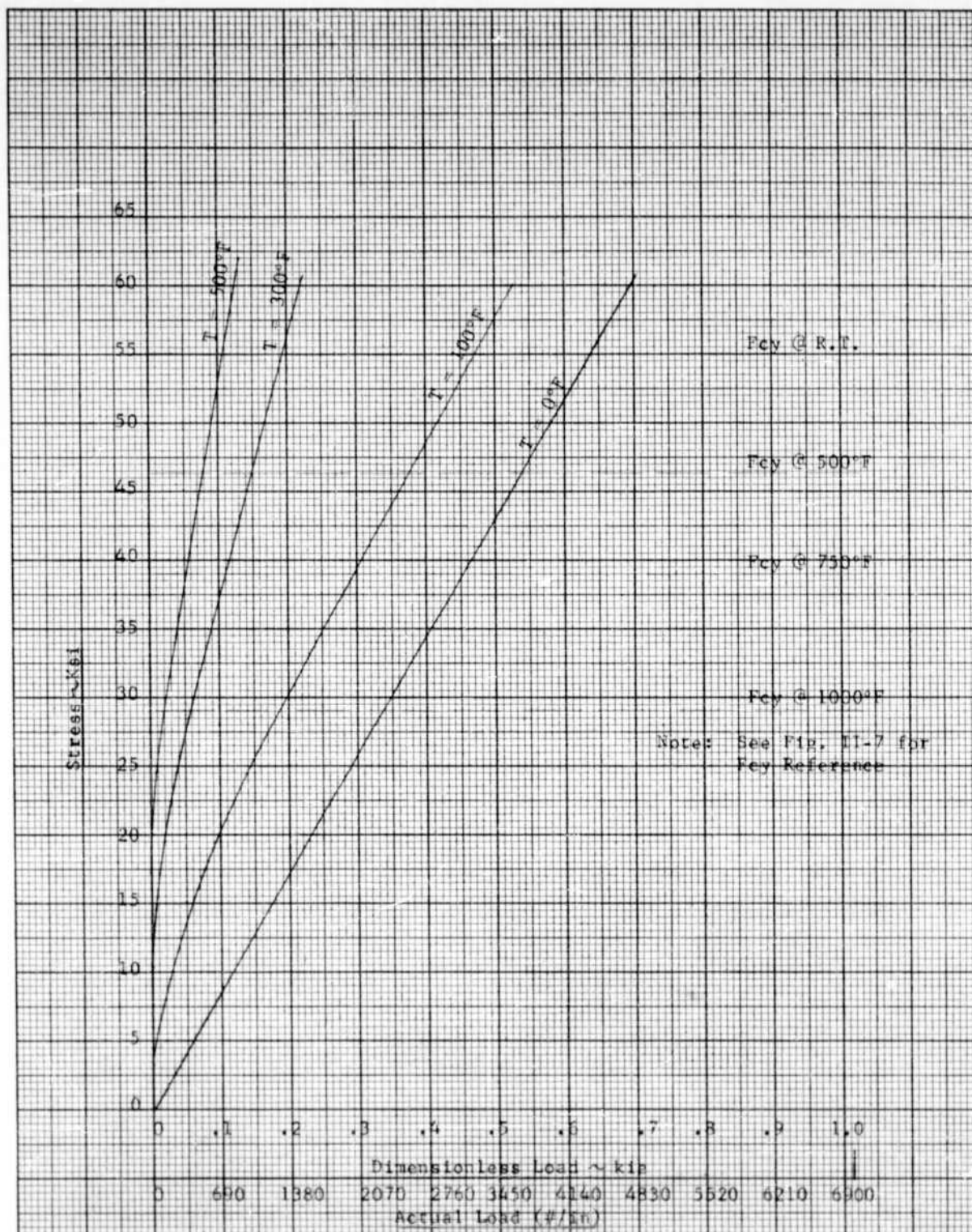


Figure III-24 Compressive Stress at Center of Hot Face of Beryllium Sandwich Panel vs. Compressive Edge Load for Various Temperature Gradient

(1) NOTATION (Continued)

A	-	conductivity matrix or generalized heat flux matrix
B	-	specific heat matrix
$\lambda$	-	relaxation time constant
$\vec{E}$	-	generalized heat input
$\xi$	-	normal coordinate
T	-	temperature
t	-	time
$\phi$	-	thermal relative mode
( $\cdot$ )	-	denotes time differential
( $)'$	-	denotes transposed matrix

Using Biot's Notation (Ref. 4)

(2) ENERGY EQUATIONS

Expressed in matrix notation are the following energy and virtual work terms:

Potential Energy (V)

$$2V = \dot{q}' A q \quad A \cdot 1$$

where  $q$  is a column vector and  $q'$  is its transpose. The conductivity matrix (A) is square and symmetric. This quantity represents the thermopotential of the system.

Dissipative Energy (D)

$$2D = \dot{q}' B \dot{q} \quad A \cdot 2$$

where  $\dot{q}$  is a column vector of the time derivative of the coordinate  $q$ . The specific heat matrix is square and positive diagonal.

Virtual Thermal Work (W)

$$\delta W = Q \delta q \quad A \cdot 3$$

where  $Q$  is the vector associated with the heat transport modes (e.g. convective, radiative or conductive).

### (3) THE HEAT FLOW EQUATIONS

With the use of the simplified Lagrangian Differential Equation

$$\frac{\partial V}{\partial q_i} + \frac{\partial D}{\partial q_i} = \frac{\delta W}{\delta q} = Q_i \quad A \cdot 4$$

The following equation of heat flow is obtained:

$$Aq + B\dot{q} = Q \quad A \cdot 5$$

This is the standard lumped parameter expression for an anisotropic medium presented in matrix notation.

### (4) GENERALIZED FORMULATION OF THE ANISOTROPIC HEAT FLOW EQUATION

Let the coordinate  $q$  be represented by a series expression of separable spacial and time varying quantities  $\phi(x, y, z)$  and  $\xi(t)$  respectively.

Hence

$$q(x, y, z, t) = \phi(x, y, z) \xi(t) \quad A \cdot 6$$

where it is understood that  $q$  and  $\xi$  are vectors and  $\phi$  is a square matrix. One possible series can be obtained from the eigen-values and function solution of equation(A · 5) if it is assumed that

$$q = \phi e^{-\lambda t} \quad A \cdot 7$$

where:  $\phi$  are the eigen-functions

$\lambda$  are the eigen-values

The eigen-functions ( $\phi$ ) are more specifically known as the normal coordinates.

With these new coordinates the transformed energy expressions are:

$$\begin{aligned} 2V &= \xi' \phi' A \phi \xi \\ 2D &= \xi' \phi' B \phi \xi \\ W &= \xi \xi' \phi' Q \end{aligned} \quad A \cdot 8$$

and upon substitution into the Lagrangian Equations yield the transformed heat conduction/transport equation

$$\phi' A \phi \xi + \phi' B \phi \dot{\xi} = \phi' Q \quad A \cdot 9$$

The steady state solution is obtained by letting  $\dot{\xi} \rightarrow 0$  in the generalized normal mode heat conduction equation resulting in

$$\xi = [\phi' A \phi]^{-1} \phi' Q$$

which must be tested for convergence, or directly from

$$T = A^{-1} Q$$

which is obtained from the standard heat conduction equation by letting

$$\dot{T} \rightarrow 0.$$

d. Discussion

A steady state heat analysis of the thermantic cell was conducted which illustrated the nature of the isotherm and adiabatic line patterns. In the ceramic portions of the cell the metal reinforcement is cooler than the ceramic at the same level. In the lower part of the cell the metal is generally hotter than the insulation at corresponding levels. Refer to Figures III-25 through III-28 and Table III-1.

An assumed net Q of 2.8 BTU/sq. ft. sec. was used which is high due to the protective coatings used on the metal. A reduction in the coating would result in increased metal temperature in the upper region, but would reduce the net Q transmitted to the structure being protected. Also the surface temperatures are for a severe environment corresponding to an off-design mission point.

THERMANTIC HEAT FLOW ANALYSIS

BASIC DATA

Thermal Conductivities

Emissivity Cap (Dense Ceramic)	$k_E = 3.5 \text{ BTU-in./ft}^2\text{-hr-}^\circ\text{F}$
Foamed Ceramic	$k_C = 2.5 \text{ BTU-in./ft}^2\text{-hr-}^\circ\text{F}$
Metal Foil (Inconel)	$k_M = 270 \text{ BTU-in./ft}^2\text{-hr-}^\circ\text{F}$
Insulation	$k_I = 0.7 \text{ BTU-in./ft}^2\text{-hr-}^\circ\text{F}$
Zirconia Coating	$k_Z = 2.3 \text{ BTU-in./ft}^2\text{-hr-}^\circ\text{F}$
NiCr Coating	$k_{NC} = 270 \text{ BTU-in./ft}^2\text{-hr-}^\circ\text{F}$

Flow Field Rates

Convected Q = 30 BTU/sec.

Assumed Net Q = 2.8 BTU/sec.

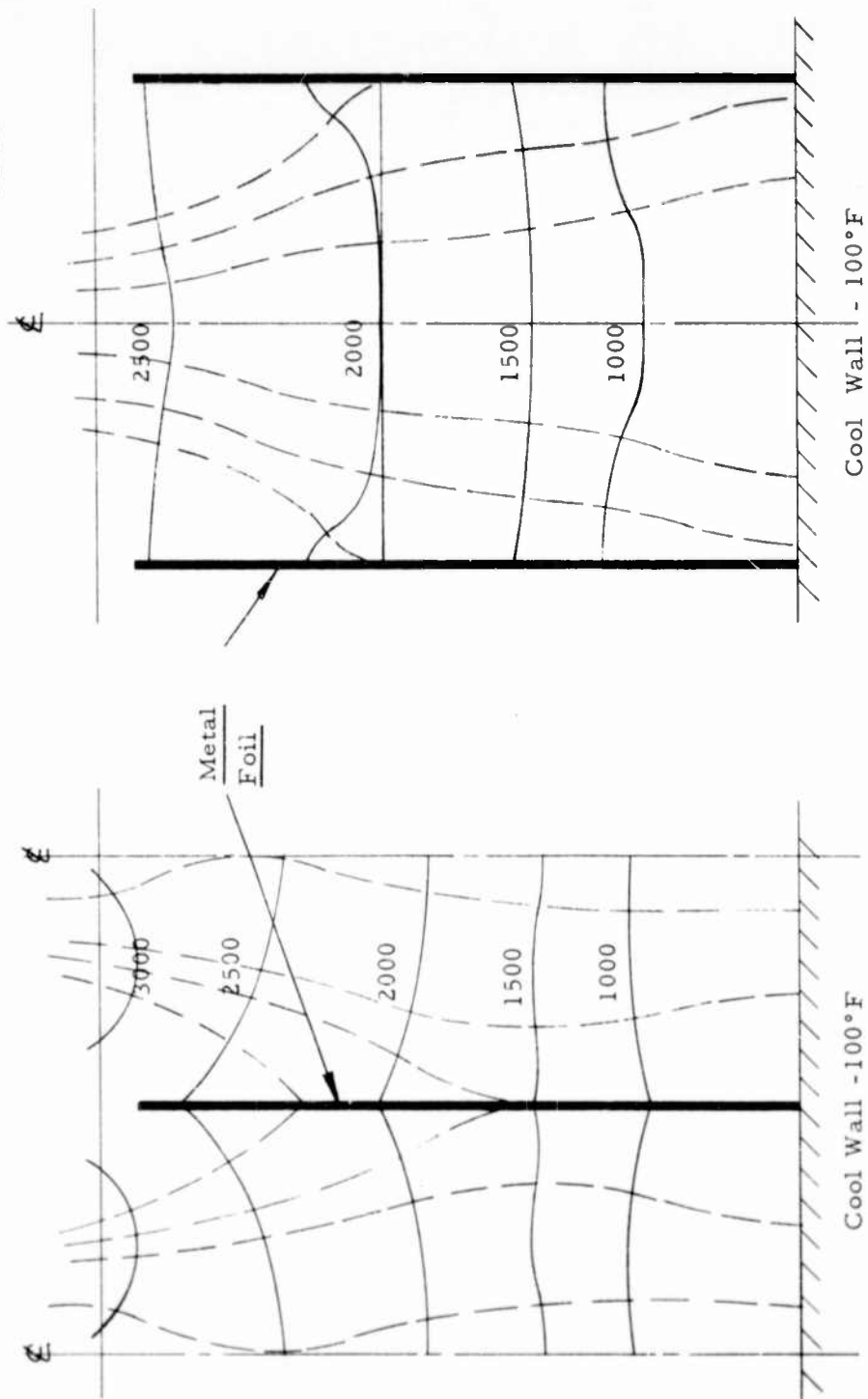
C. COMPOSITE PANELS (Continued)

2. Vibration Analysis

As part of a general environmental, reliability study a routine analytical vibration analysis was conducted.

Thermantic Heat Flow Analysis  
Three-Dimensional  
Steady-State  
Constant Net Q Distribution

Legend  
—— Isotherms  
--- Adiabatic  
Lines



Cell Mid-Section

Cell Metal Foil Plane

Figure III-25 - Isotherm and Adiabatic Line Patterns

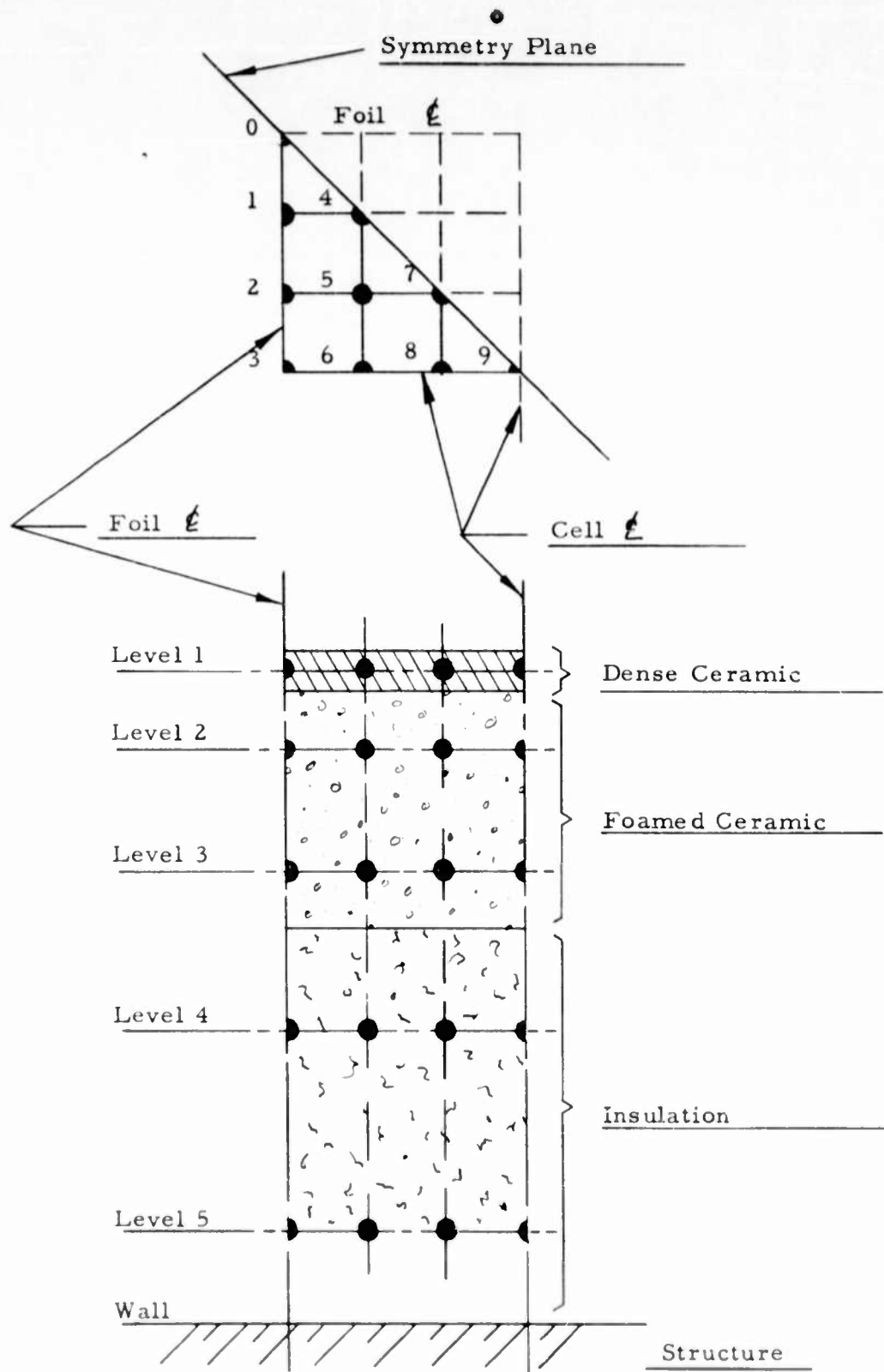


Figure III-26 Thermantic Heat Flow Analysis  
Lumped Parameter Mathematical Model

Detail - Honeycomb Cell Reinforcement  
With Protective Coatings

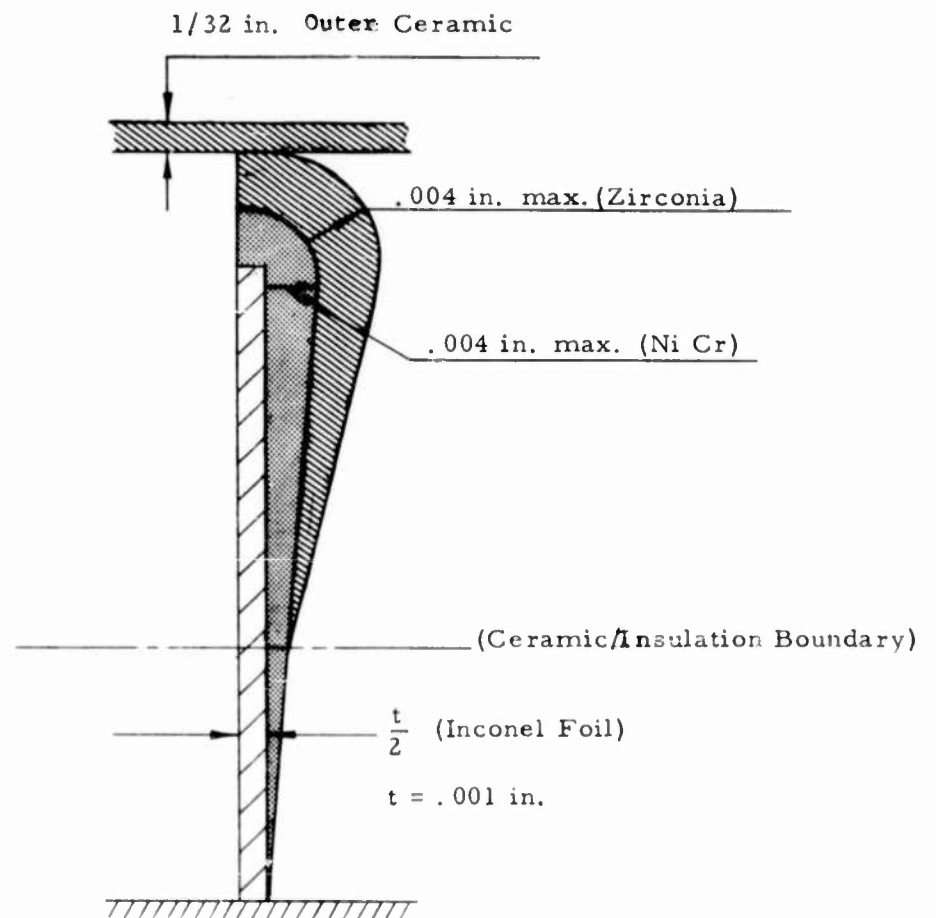


Figure III-27 Thermantic Heat Flow Analysis

**Table III-1 Results of Thermantic Heat Flow Analysis**  
**(Microscopic Study)**

Three Dimensional Steady-State  
 Constant Net Q Distribution  
 Temperature Distribution In Of

Level	LUMPED HEAT NODE NUMBER									
	0	1	2	3	4	5	6	7	8	9
1	2650	2710	2760	2780	2900	2970	3000	3070	3090	2910
2	2330	2350	2380	2400	2520	2580	2610	2690	2720	2740
3	1970	2160	2180	2185	2230	2280	2290	2340	2360	2400
4	1685	1690	1710	1710	1700	1710	1710	1715	1720	1780
5	558	705	772	790	702	710	717	695	692	682
Wall	100	100	100	100	100	100	100	100	100	100

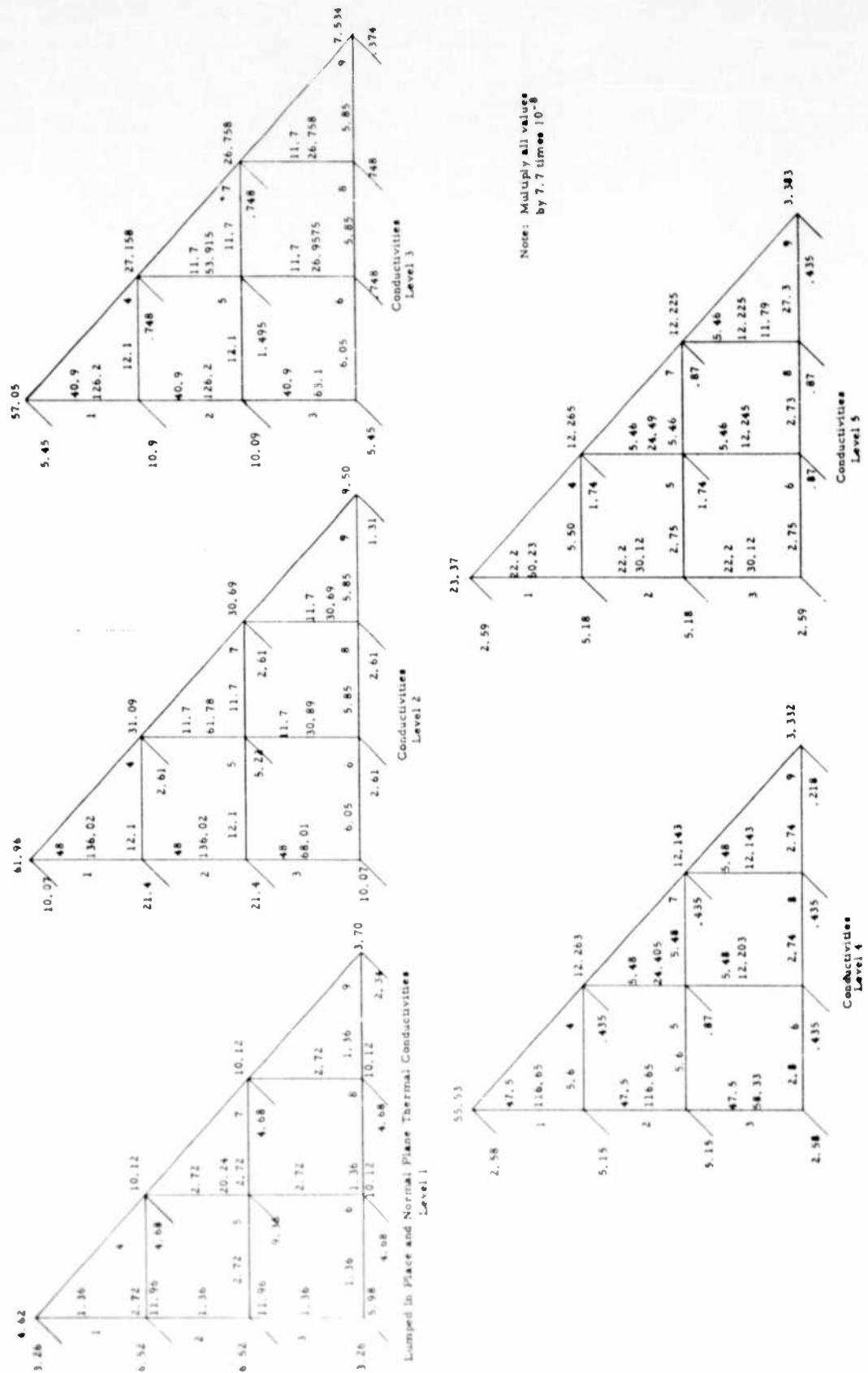


Figure III-28 Lumped Thermal Conductivities

## C. 2. Vibration Analysis (Continued)

- a. In Figure III-29 a cross-sectional, schematic view of a small section of the thermantic structure is shown. It can be seen that this represents a complicated spring-mass-damper system.

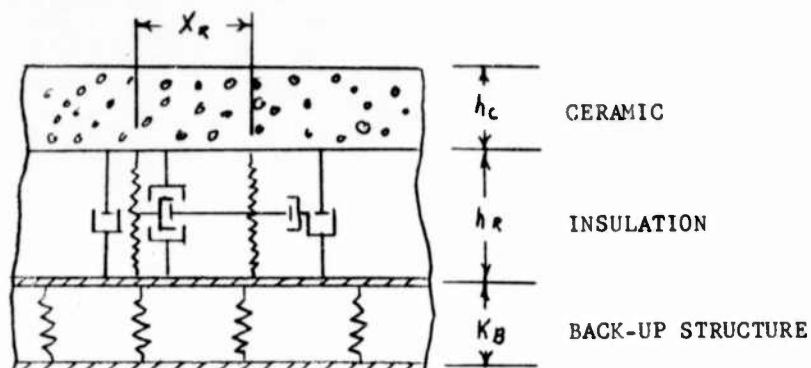


Figure III-29

Vibration - schematic view of the thermantic concept

## b. Vibration Normal to the Plane of the Specimen

Calculations based upon the following assumptions are presented below.

1. Ceramic portion of the structure is rigid.
2. Back-up structure is rigid.
3. There is no damping.
4. The vibration is linear.

Two configurations were considered:

Configuration A - 3/4" cell spacing

$h_c$	=	3/8 in.	Ceramic thickness
$h_R$	=	5/8 in.	insulation space
$W_c$	=	1.25#/ft <sup>2</sup>	density of ceramic
$K_R$	=	$AE/h_R$	stiffness of full honeycomb wall
$t$	=	.001 in.	thickness of full honeycomb wall
$x_R$	=	.75 in.	honeycomb cell size
$E$	=	$30 \times 10^6$ lb/in <sup>2</sup>	Young's Modulus

C. 2. b. (Continued)

Area of Reinforcement Cells (A)

$$A = \left(\frac{4}{3}\right)^2 \times 144 \times .001 = .256 \text{ in}^2/\text{ft}^2$$

$$K_R = \frac{.256 \times 30 \times 10^6 \times 8}{5} = 12.3 \times 10^6 \text{ \#/in/ft}^2$$

Natural frequency (ceramic vibrating relative to structure)

$$f = \frac{1}{2\pi} \sqrt{\frac{K_R g}{W_c}} = \frac{1000}{2\pi} \sqrt{\frac{12.3 \times 386.4}{1.25}} = 9,820 \text{ cps}$$

Configuration B -  $1\frac{1}{4}$  in. cell spacing

$$h_c = 3/8 \text{ in.}$$

$$h_R = 3/4 \text{ in.}$$

$$x_R = 1.25 \text{ in.}$$

$$W_c = 1.25 \text{ \#/ft}^2$$

$$t = .001$$

$$E = 30 \times 10^6 \text{ \#/in}^2$$

Area of Reinforcement Cells per sq. ft. (t)

$$A = \left(\frac{4}{5}\right)^2 \times 144 \times .001 = .092 \text{ in}^2 \text{ ft}^2$$

$$K_L = 3.68 \times 10^6 \text{ \#/in}^2/\text{ft}^2$$

$$f = 5300 \text{ cps}$$

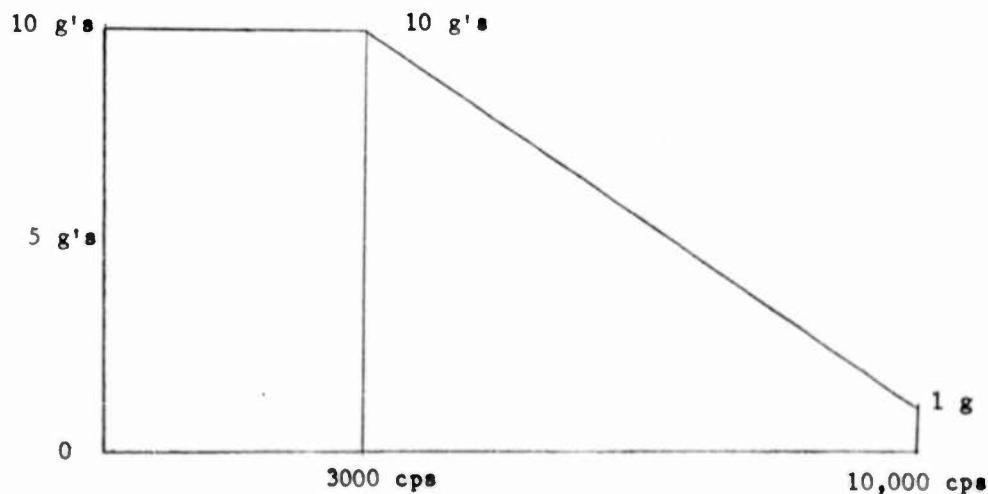


Figure III-30

Vibration Environment for 3" x 3" Test Specimen

C. 2. b. (Continued)

A 3" x 3" specimen was subjected to a vibration environment as shown in Figure III-30.

The specimen withstood the test. Some evidence of local interstructure vibration resonance as calculated was observed but did not have any apparent detrimental effect.

c. Conclusions

These calculations indicated a possible failure mode between 5,000 and 10,000 cps. More exacting calculations and a test program are required to determine the consequences of such inter-structural resonance.

d. Vibration Analysis of Thermantic Plates

In addition to the local inter-structure vibration, the effect of plate resonances or the thermantic heat shield and structural integrity was investigated. A simple calculation is made below for a typical plate.

(1) Free Plate Vibration Analysis

The assumptions are:

1. Simply supported at all edges
2. Uniform mass and stiffness properties
3. Negligible damping
4. Linear vibration

- (2) It may be easily shown that the above energy expressions result in the following rectangular plate frequency equation

$$p = \pi^2 \sqrt{\frac{D}{m_p}} \left( \frac{m^2}{a^2} + \frac{n^2}{b^2} \right);$$

and for a square plate, remembering that  $f = \frac{p}{2\pi}$ , the following equation results:

$$f = \frac{\pi n^2}{a^2} \sqrt{\frac{D}{m_p}}$$

(3) Numerical Calculations for the Simply Supported Flat Plate Steel Sandwich

$$D = 3.98 \times 10^4 \text{ lb. in for .01 in. face sheets}$$

$$t = .247'' \text{ equivalent thickness}$$

$$M_c = 1.25 \text{ \#/ft}^2 \quad \text{weight of ceramic}$$

$$M_s = 1.61 \text{ \#/ft}^2 \quad \text{weight of structure}$$

C. 2. d. (Continued)

(3) Continued

$$M_c = .8 \text{ \#/ft}^2 \quad \text{weight of coolant}$$

$$M_p = 3.66 \text{ \#/ft}^2 \quad \text{total weight of plate}$$

Beryllium-beryllium sandwich

$$D = 10.65 \times 10^4 \text{ lb. in.} \quad \text{for .01 in. face sheets}$$

$$t = .310 \text{ in. equivalent thickness}$$

$$M_s = 1.091 \text{ lb./ft}^2$$

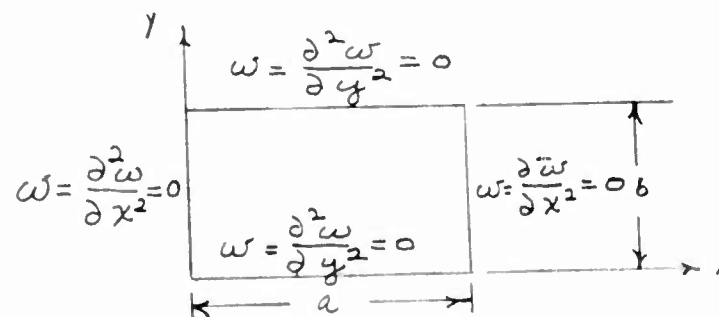
The results are shown in Figure III-31.

The kinetic energy of the plate is:

$$T = M_p \iint \dot{w}^2 \, dx dy$$

where

$$w = \sum_{m=1}^{\infty} \sum_{n=1}^{\infty} \Phi_{mn} \sin \frac{m\pi x}{a} \sin \frac{n\pi y}{b}$$



Uniform Plate Analysis

and

$$w = \frac{\partial^2 w}{\partial x^2} = \frac{\partial^2 w}{\partial y^2} = 0 \quad \text{@ } \begin{matrix} x, y = 0 \\ x = b \\ y = a \end{matrix}$$

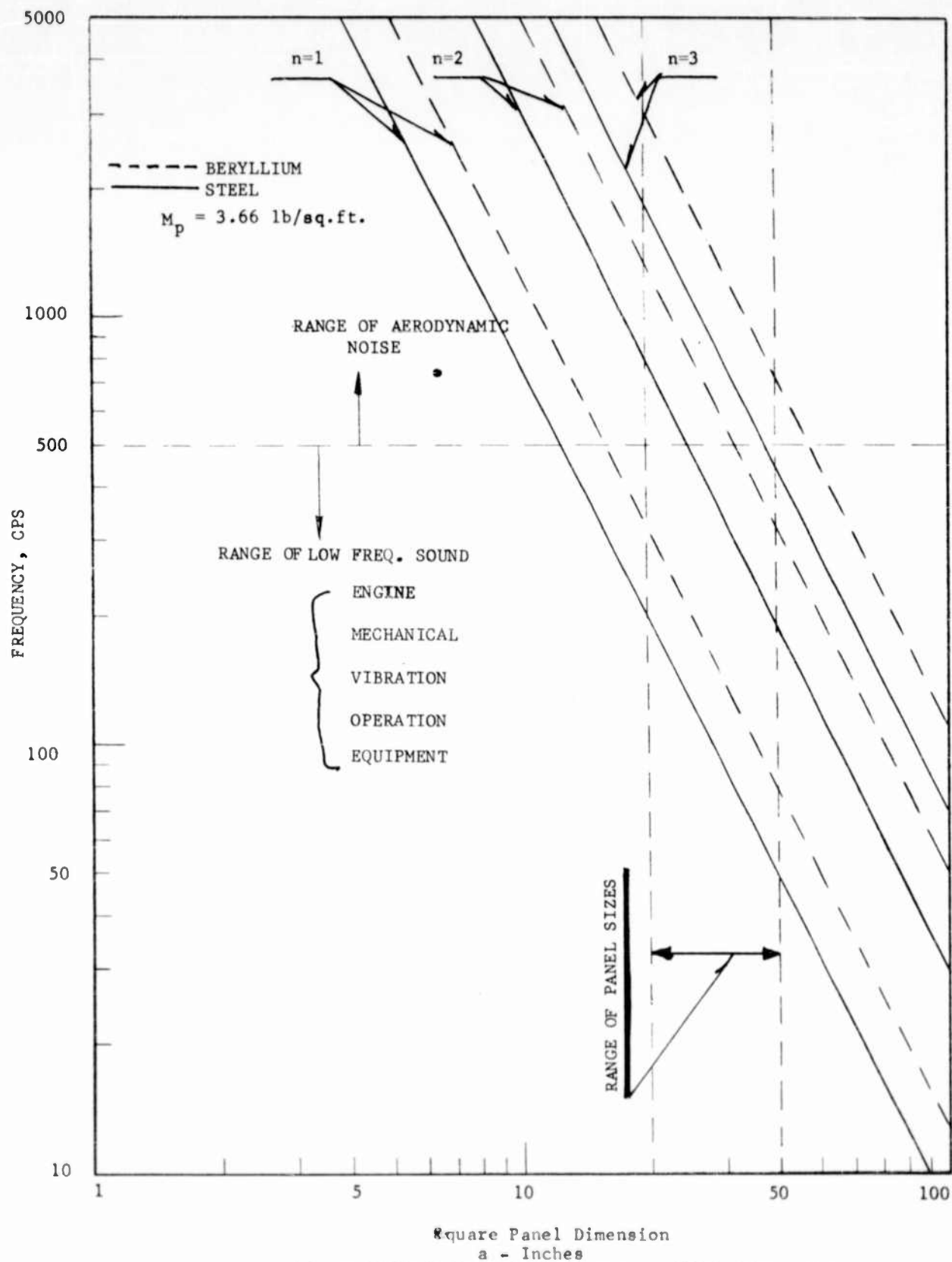


Figure III-31 Resonant Frequency vs. Plate Dimensions

C. 2. d. (3) (Continued)

Since for the assumed conditions the expression for  $w$  represents the exact solution and, hence, satisfies orthogonality relations, the expression for potential energy after integration reduces to:

Potential Energy (V)

$$V = \frac{\pi^4 a b}{8} D \sum_{M=1} \sum_{N=1} \Phi_{mn}^2 \left( \frac{m^2}{a^2} + \frac{n^2}{b^2} \right)$$

where  $a$ ,  $b$  are plate dimensions, and  $D$  is the plate rigidity constant

$$D = \frac{E I}{(1 - \nu^2)}$$

(4) Conclusions

The results of this analysis indicate that the fundamental modes of the thermantic plates can be excited at natural frequencies within the limits of engine frequency spectrum. Also indicated was the possible excitation of higher order panel resonances by the aerodynamic noise.

It is highly unlikely that flutter of the thermantic panel can occur. Estimates indicate that the possibility of flutter does exist for flat, large, unsupported panels under compressive stress. The low aspect ratio and curvature of the panels are considered sufficient to prevent flutter.

## SECTION IV

### PROPERTIES AND TEST DATA

#### A. INTRODUCTION

The tests and property evaluations conducted in this program were performed in support of the development of radiation cooled concepts utilizing beryllium and ceramics.

The test program consisted of three major phases:

Evaluation of Ceramic Materials  
Evaluation of Composite Panels  
Evaluation of beryllium sheet and beryllium  
faced sandwich structures

The test procedures were maintained relatively simple with the objectives being to provide qualitative evaluations and comparisons, as opposed to the accumulation of voluminous test results. However, it is felt that significant information relevant to design, and, in particular, preliminary design has resulted from this program. It is with this in mind that the following information is presented. (Complete test procedures are given in Volume II.)

#### B. CERAMIC PROPERTY TESTS

##### 1. Mechanical Properties

Tests were performed to obtain the physical properties of the ceramic foams developed during the program. Mechanical properties of alumina, silica, and zirconia based ceramics are summarized in Tables IV - 1 (compression test data) and Table IV - 2 (flexure data).

The average room temperature compression strength was 650-675 psi for alumina, 510-520 psi for silica and 260-270 psi for the zirconia foam. At 1000°F, the alumina exhibited a decrease in strength of approximately 10% while the silica and zirconia increased 40% and 80% respectively.

The alumina foam had an average flexure strength of 340-360 psi at room temperature while the silica and zirconia averaged 280-290 psi and 170-180 psi respectively. The alumina exhibited no appreciable change in strength at 1000°F. The flexure strength of the silica foam increased approximately 40% and the zirconia increased approximately 80% at the 1000°F test temperature.

##### 2. Thermal Conductivity

Thermal conductivity test data for the ceramic foams are listed in Table IV - 3 and are also compared to other investigator's results for dense ceramics. Table IV - 4 shows the thermal conductivity of various composite structures that were evaluated during this program.

TABLE IV - 1

RESULTS OF BLOCK COMPRESSION TESTS ON FOAMED CERAMICS

Specimen No.	Density (Lb/Ft <sup>3</sup> )	Test	Test Area (In <sup>2</sup> )	Failure Load	
		Temperature °F		LBS	PSI
ALUMINA FOAM					
1A	58	RT	1.00	660	660
2A	58	RT	1.06	760	717
3A	58	RT	1.06	720	680
9B	58	RT	1.09	590	542
10A	58	RT	1.06	795	750
8A	65	RT	1.05	1192	1140
4A	58	1000	1.00	520	520
5A	58	1000	1.00	580	580
6A	58	1000	1.03	510	496
7A	58	1000	1.06	510	480
9A	65	1000	1.06	872	823
SILICA FOAM					
1	40	RT	0.98	634	645
2	40	RT	1.07	502	469
3	40	RT	0.92	456	497
4	40	1000	0.94	826	879
5	40	1000	1.13	878	778
6	40	1000	0.85	696	820
ZIRCONIA FOAM					
1	100	RT	0.36 <sup>(1)</sup>	96	266
2	100	RT	0.36 <sup>(1)</sup>	50	139
3	100	RT	0.36 <sup>(1)</sup>	100	278
1A	100	1000	0.94	378	402
2A	100	1000	0.94	450	479

(1) These specimens were approximately 1/2" cubes; all other specimens were approximately 1" x 1" x 0.8" high.

TABLE IV - 2

RESULTS OF FLEXURE TESTS ON FOAMED CERAMICS

Specimen No.	Density (Lb/Ft <sup>3</sup> )	Test	Failure Load	
		Temperature °F	Lbs.	Psi
ALUMINA FOAM				
1B	58	RT	71	1105 <sup>(1)</sup>
2B	58	RT	83	342
3B	58	RT	94	351
4B	58	RT	97	360
5B	58	1000	117	420
6B	58	1000	67	240
SILICA FOAM				
1	40	RT	60	210
2	40	RT	99	281
3	40	RT	127	292
4	40	1000	71	302
5	40	1000	118	384
6	40	1000	187	425
ZIRCONIA FOAM				
1 <sup>(2)</sup>	100	RT	16	207
2 <sup>(2)</sup>	100	RT	13	160
3	100	RT	16	189
4	70	RT	21	85
5	70	RT	26	105
6	70	RT	15	63
1A	100	1000	79	329
2A	100	1000	113	443
3A	100	1000	81	335
5B	100	1000	90	420
7B	100	1000	76	297

(1) Tested in 3 point loading

(2) Specimens 1/2" x 1/2" x 6"

TABLE IV - 3

## THERMAL CONDUCTIVITY OF FOAMED CERAMICS

	<u>Dense (5)</u> <u>Alumina</u>	<u>Alumina</u> <u>Foam #1</u>	<u>Alumina</u> <u>Foam #2</u>	<u>Dense (6)</u> <u>Silica</u>	<u>Silica (a)</u> <u>Foam #1</u>	<u>Dense (5)</u> <u>Zirconia</u>	<u>Zirconia</u> <u>Foam #1</u>
Foam Specimen							
Type		Alumina	Alumina		Silica		Zirconia
Density	170#/ft <sup>3</sup>	58#/ft <sup>3</sup>	58#/ft <sup>3</sup>	115#/ft <sup>3</sup>	44#/ft <sup>3</sup>	250#/ft <sup>3</sup>	66#/ft <sup>3</sup>
Thickness		1"	1"		1"		1"
Weight/ft <sup>2</sup>		4.82#	4.82#		3.68#		5.52#
BTU/Hr-ft <sup>2</sup> -°F/ in. thickness	9.5	2.5	2.8	7.8	3.38	7.2	2.53

(a) This specimen contains opacifiers

Note: Numbers in parentheses indicate references

TABLE IV - 4

## THERMAL CONDUCTIVITY OF COMPOSITE STRUCTURES

	(C) ALUMINA BERYLLIUM COMPOSITE #1		
	(A) ALUMINA COMPOSITE #1	(B) ALUMINA COMPOSITE #3	(C) ALUMINA BERYLLIUM COMPOSITE #1
REINFORCEMENT CORE:			
Cell Type	Hand Cut 1/2" (1)	Hand Cut 1/2" (1)	Standard 1/2"
Foil Thickness	.0015 in.	.0015 in.	.001 in.
Alloy	Inconel "X"	Inconel "X"	Inconel
Core Height	3/4"	3/4"	3/4"
CORE COATING			
Type	Ni-Cr	Ni-Cr	Ni-Cr
Weight/ft <sup>2</sup>	1.33#	1.35#	1.28#
FOAM	ZrO <sub>2</sub>	ZrO <sub>2</sub>	ZrO <sub>2</sub>
Type	Alumina	Alumina	Alumina
Density	60#/ft <sup>3</sup>	63#/ft <sup>3</sup>	68#/ft <sup>3</sup>
Thickness	3/8"	3/8"	3/8"
INSULATION:			
Type	Fiberfrax	Fiberfrax	Fiberfrax
Weight/ft <sup>2</sup>	.378#	.378#	.357#
Thickness	3/8"	3/8"	3/8"
BACK STRUCTURE:			
	.032" 17-7PH Skin	.032" 17-7PH Skin	.032" Beryllium Faces and 1/5 Mil, 1/4" cell A-286 Honeycomb, 1/2" Cell Height
HEAT SHIELD WEIGHT #/ft <sup>2</sup> :	4.22#	3.86#	3.96#
TOTAL STRUCTURE WEIGHT #/ft <sup>2</sup>	6.00	5.14#	6.12#
CONDUCTIVITY OF HEAT SHIELD STRUCTURES (BTU-IN) (HR-FT <sup>2</sup> -OF)	7.16	5.47	3.90
CONDUCTANCE OF STRUCTURAL SANDWICH (BTU) (HR-FT <sup>2</sup> -OF)	-	-	35.88
CONDUCTANCE OF TOTAL STRUCTURE (BTU) (HR-FT <sup>2</sup> -OF)	-	-	4.39

NOTE: (1) Core originally had 1/4" cells which were hand cut to 1/2" cell size.

TABLE IV - 4 (con't)

		(D) ZIRCONIA BERYLLIUM COMPOSITE #1	(E) SILICA BERYLLIUM COMPOSITE #1	(F) ALUMINA BERYLLIUM COMPOSITE (MIN K #1)
REINFORCEMENT CORE:				
Cell Type		Standard 1/2"	Standard 1/2"	Hand Cut 1" (2)
Foil Thickness		.001"	.001"	.001"
Alloy		Inconel	Inconel	Inconel
Core Height		3/4"	3/4"	3/4"
CORE COATING				
Type		Ni-Cr	Ni-Cr	Ni-Cr
Weight/ft <sup>2</sup>		1.28#	1.28#	.124#
FOAM:				
Type		Zirconia	Silica	Alumina
Density		114#/ft <sup>3</sup>	58.5#/ft <sup>3</sup>	42#/ft <sup>3</sup>
Thickness		3/8"	3/8"	3/8"
INSULATION:				
Type		Fiberfrax	Fiberfrax	MIN K
Weight/ft <sup>2</sup>		.357#	.365#	.232#
Thickness		3/8"	3/8"	3/8"
BACK STRUCTURE				
		.032" Beryllium Faces and 1.5 Mil. 1/4" Cell A-286 Honeycomb, 1/2" Cell Height	.032" Beryllium Faces and 1/5 Mil, 1/4" Cell A-286 Honeycomb, 1/2" Cell Height	.032" Beryllium Faces and 1.5 Mil, 1/4" Cell A-286 Honeycomb, 1/2" Cell Height
HEAT SHIELD WEIGHT #/ft <sup>2</sup> :		5.35#	3.63#	1.73#
TOTAL STRUCTURE WEIGHT #/ft <sup>2</sup>		8.36#	5.38#	3.85#
CONDUCTIVITY OF HEAT SHIELD STRUCTURES		(BTU-IN) (HR-FT <sup>2</sup> -OF)	4.22	3.09
CONDUCTANCE OF STRUCTURAL SANDWICH		(BTU) (HR-FT <sup>2</sup> -OF)	42.94	29.19
CONDUCTANCE OF TOTAL STRUCTURE		(BTU) (HR-FT <sup>2</sup> -OF)	4.70	3.41
				14.50
				1.50

NOTE: (2) Core originally had 1/2" cells which were hand cut to 1" cell size.

TABLE IV - 4 (con't)

(G)		(H)	
ALUMINA BERYLLIUM COMPOSITE (MIN K #2)		ALUMINA BERYLLIUM COMPOSITE (MIN K #3)	
REINFORCEMENT CORE:		Hand Cut 1" (2)	
Cell Type	.001"	Hand Cut 1" (2)	.001"
Foil Thickness	Inconel	Inconel	3/4
Alloy	3/4		
Core Height			
CORE COATING:		Ni-Cr	
Type	ZrO <sub>2</sub>	Ni-Cr	ZrO <sub>2</sub>
Weight/ft <sup>2</sup>	.124#	.202#	.121#
FOAM			
Type	Alumina	Alumina	
Density	47#/ft <sup>3</sup>	49#/ft <sup>3</sup>	
Thickness	3/8	3/8	
INSULATION		MIN K	
Type	.286	MIN K	.262
Weight/ft <sup>2</sup>	3/8"		3/8"
Thickness			
BACK STRUCTURE:		.032 Beryllium Faces	
		and 1.5 Mil, 1/4" Cell	and 1.5 Mil, 1/4" Cell
		A-286 Honeycomb	A-286 Honeycomb
		1/2" Cell Height	1/2" Cell Height
HEAT SHIELD WEIGHT #/ft <sup>2</sup> :		2.11#	
TOTAL STRUCTURE WEIGHT #/ft <sup>2</sup>		3.55#	
CONDUCTIVITY OF HEAT (BTU-IN) SHIELD STRUCTURES (HR-FT <sup>2</sup> -OF)		1.94	
CONDUCTANCE OF (BTU) STRUCTURAL SANDWICH (HR-FT <sup>2</sup> -OF)		24.74	
CONDUCTANCE OF TOTAL (BTU) STRUCTURE (HR-FT <sup>2</sup> -OF)		2.27	

The tests of the ceramic foam were to determine the effect of porosity, stabilizers, and opacifiers on the conductivity of the basic ceramic. As can be seen in the table, the conductivity of the ceramic foam is significantly lower than that of the dense ceramic. It is believed that the reduction in the conductivity of the silica is due in part to the incorporation of opacifiers into the foam. These materials reduce the infrared transparency of silica at high temperatures.

Two alumina composites were tested to determine what effect the thickness of the protective coating on the reinforcement core had on the conductivity of the construction and the durability of the core. By comparing columns A and B of Table IV - 4, it can be seen that a thinner coating results in a lowering of the conductance as well as reducing the weight. This is due to the higher conductance of the dense coating, in comparison to that of the foamed ceramic.

Beryllium composites with silica, alumina, and zirconia foam (C, D, and E) were tested. The surface temperature of the specimens as read with an optical pyrometer, uncorrected for emissivity, was 2500°F. The actual surface temperature depending upon the emissivity of the particular foam was in the 2800-3100°F temperature range. The temperature of the rear facing sheet of the backup structure of these specimens was in the 800 to 900°F temperature range. The total conductance ranged from 3.41 to 4.70 BTU/hr-ft<sup>2</sup>-°F. Table IV - 4 lists the additional information on the construction of these composites.

A set of beryllium composites was tested utilizing larger cell size in the reinforcement core, light weight alumina foam (40 to 50 lb/ft<sup>3</sup>) and MIN K 2000 secondary insulation in place of Fiberfrax (F, G, and H). These composites, with an uncorrected surface temperature of 2700 to 2900°F possessed a total conductance in the range of 1.5 to 2.3 BTU/hr-ft<sup>2</sup>-°F. The temperature of the rear face of the back-up structure measured 500-600°F. However, these particular constructions do not possess the desired durability needed for heat shield applications; but, these tests do show the potential of the construction in regard to weight and thermal efficiency.

### 3. Emissivity

Several compositions of ceramic foam have been evaluated. Among these were compositions utilizing different coloring oxides in an attempt to raise the ceramic's emissivity to the highest possible value. As shown in Figure IV - 1, the emissivities of the plain alumina and zirconia foam were below that which was desired to take full advantage of radiation cooling during reentry. The alumina foam with a 15% addition of 80/20 NiO<sub>2</sub>-Cr<sub>2</sub>O<sub>3</sub> exhibited a 47% increase over the plain alumina. The alumina foam with a coating of oxidized Inconel X powder possessed the highest emissivity. The sample ranged from .87 at 1600°F to .82 at 2600°F. This is approximately a 140% increase over the plain alumina and 26% increase over the alumina with the NiO<sub>2</sub>-Cr<sub>2</sub>O<sub>3</sub> addition.

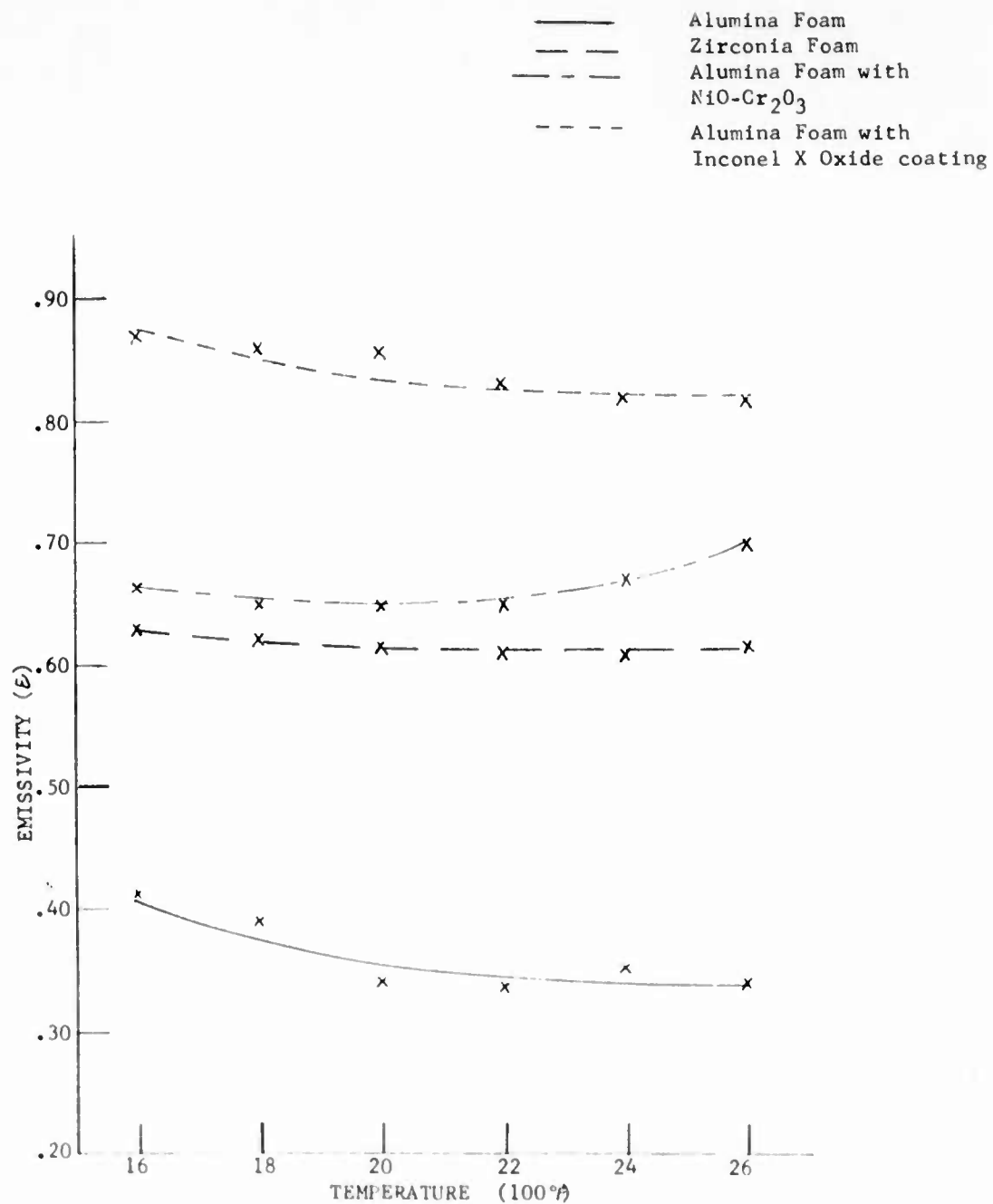


Figure IV-1 Results of Emissivity Tests of Various Oxides

The problem of providing a high emissivity and at the same time assuming high material strength and durability is recognized to be some distance from solution. The values in Figure IV - 1 represent the results of essentially initial efforts, which, however, are encouraging since relatively high values were obtained. It appears that further applied efforts along these or similar approaches should assure emissivity values of about 0.9 under operational conditions.

#### 4. Thermal Expansion

The results of the thermal expansion determinations are shown in Figures IV - 2 through IV - 4. The test data is contained in Table IV - 5. For the silica and zirconia foams, it was found that the first heating cycle produced different expansion rates than subsequent heating cycles. For the silica foam, it was felt that the sample, as received, was rather amorphous and that it undergoes further curing during the initial run. This was also indicated by the fact that the sample developed  $\frac{1}{2}$  to 1% permanent shrinkage during the first heating cycle. If this shrinkage was added to the results of the first run, a curve very similar to the second run would result. The same sample when run a second time exhibited an entirely different rate, as shown.

The zirconia foam followed the same trend as that of the silica foam with the exception that there was no apparent shrinkage during the initial run.

The alumina foam exhibited a slight shrinkage in the range of approximately 500° to 600°F. This was felt to be caused by the aluminum phosphate content in the mixture. The aluminum phosphate was formed by the reaction of the phosphoric acid with the aluminum powder and the aluminum hydroxide of the foam mix. Aluminum phosphate does have a contraction in that temperature range.

#### 5. Durability of Heat Shield Materials

Initial evaluation of the ceramic foam materials consisted of subjecting samples of the various foams to oxyacetylene torch exposures and measuring the thermal gradient across the sample. Visual examinations were conducted after exposure to determine any possible degradation of ceramic. Table IV - 6 lists typical results for constructions containing three foams; alumina, silica, and zirconia.

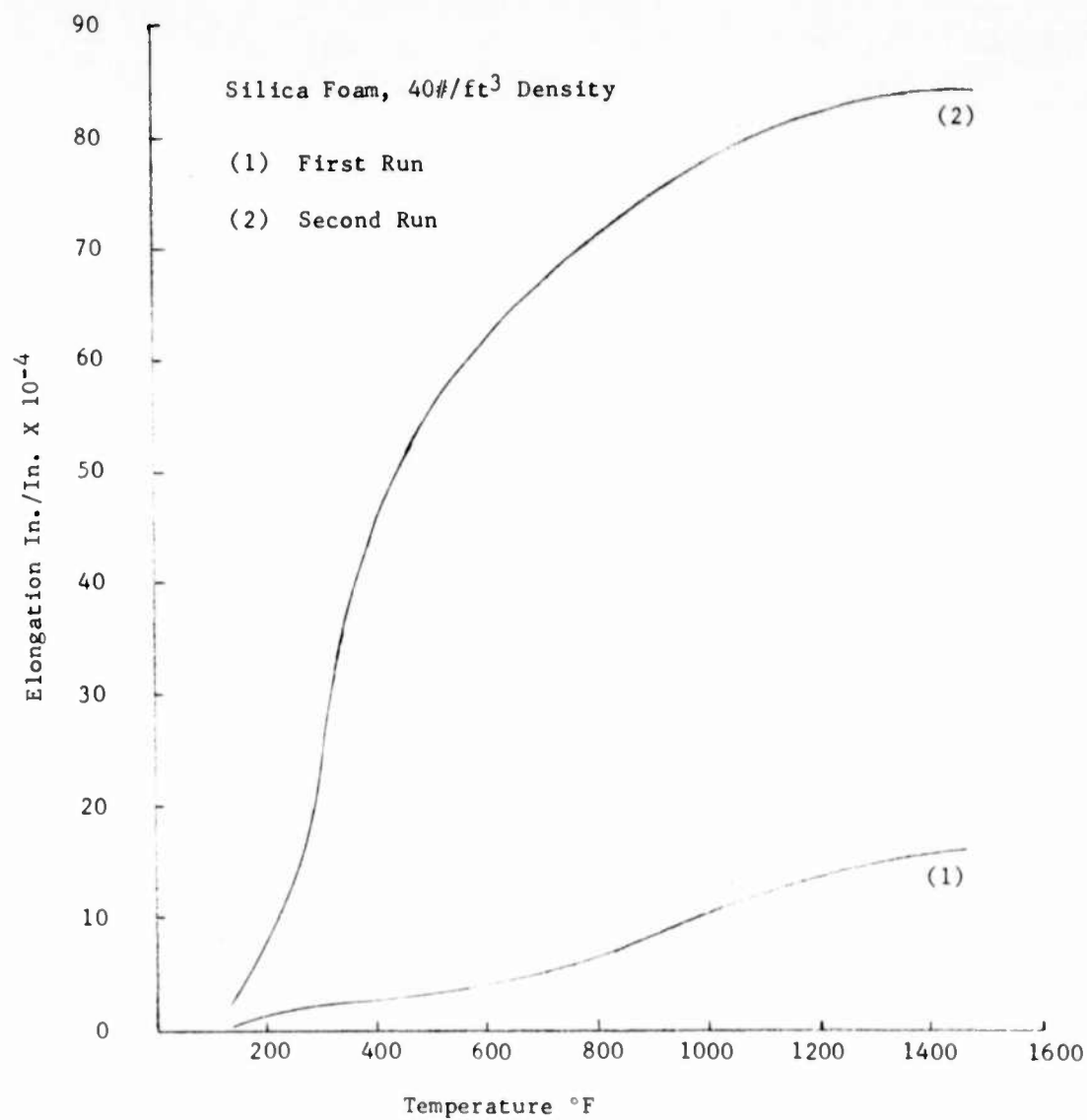


Figure IV-2 Thermal Expansion of Silica Foam

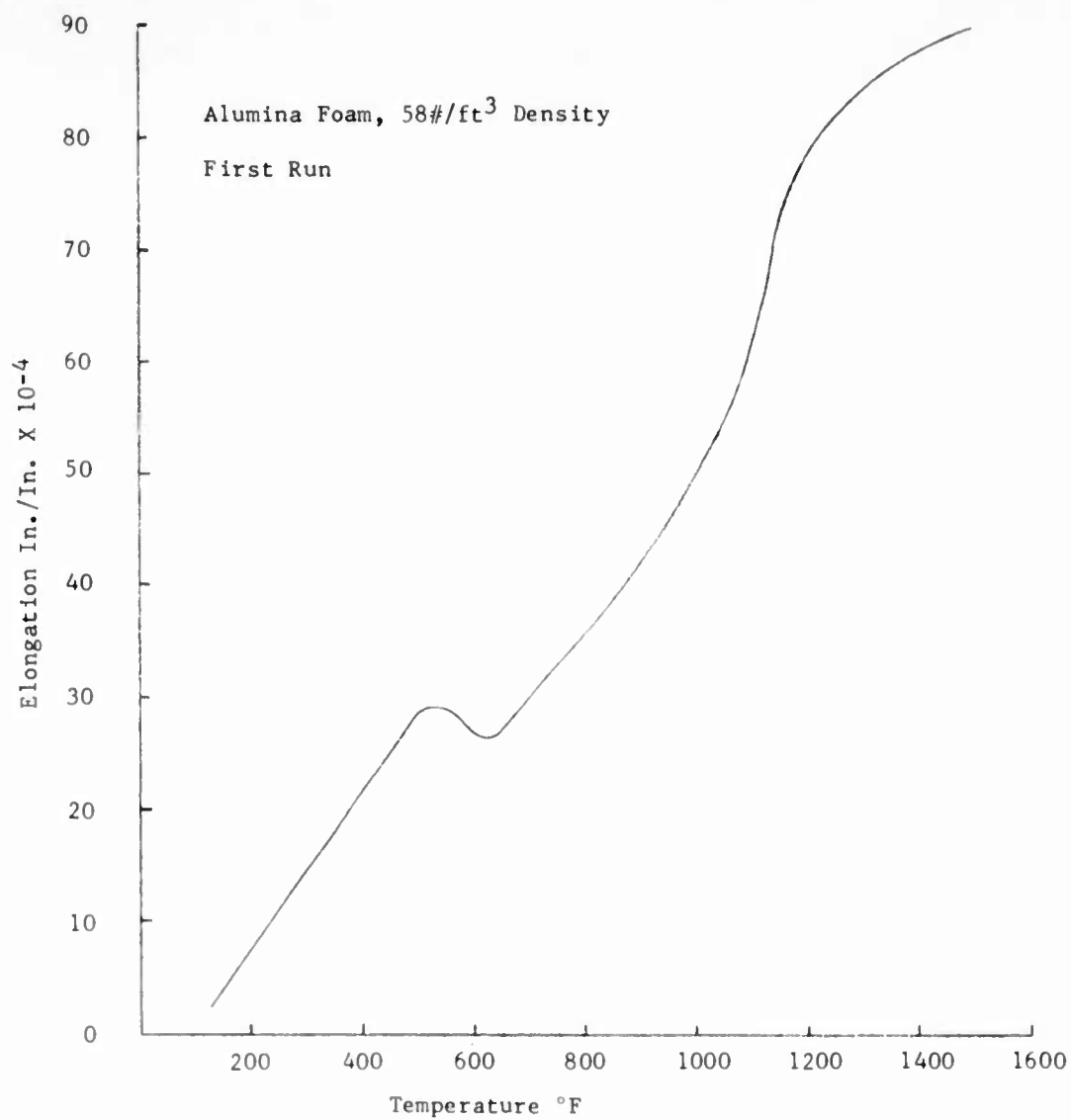


Figure IV-3 Thermal Expansion of Alumina Foam

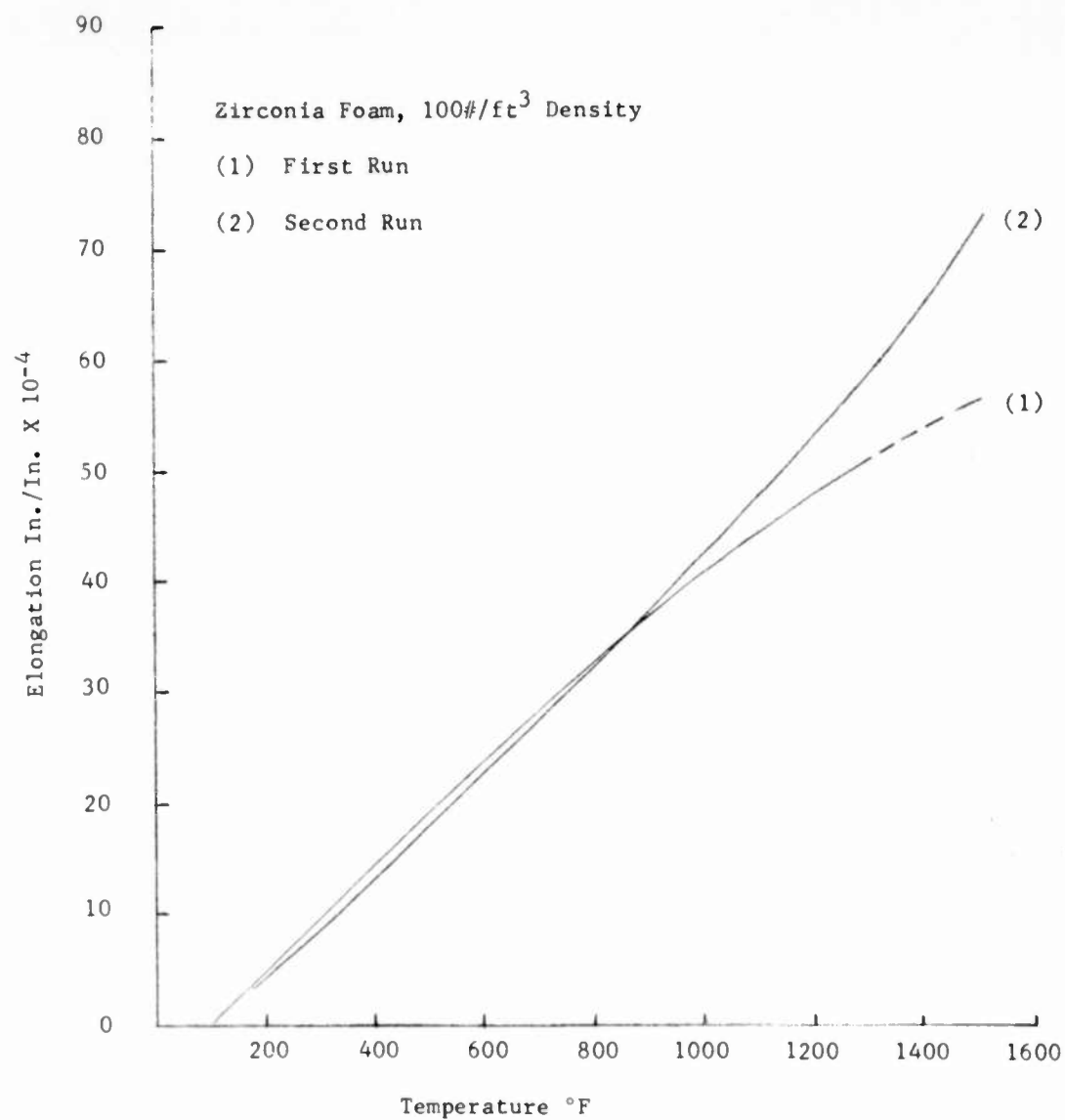


Figure IV-4 Thermal Expansion of Zirconia Foam

TABLE IV - 5

THERMAL EXPANSION RATES OF THE FOAMED CERAMICS

<u>FOAM TYPE</u>	<u>DENSITY</u> <u>(Lbs./Ft.<sup>3</sup>)</u>	<u>COEFFICIENT OF</u> <u>THERMAL EXPANSION</u> <u>(in/in °F)</u>	<u>TEMPERATURE</u> <u>(°F) RANGE</u>
Silica	44	$135 \times 10^{-7}$	200° - 600°
Silica	44	$18.6 \times 10^{-7}$	800° - 1500°
Alumina	58	$70 \times 10^{-7}$	200° - 500°
Alumina	58	$98 \times 10^{-7}$	700° - 1200°
Zirconia	100	$51.6 \times 10^{-7}$	200° - 1500°

TABLE IV - 6

THERMAL EXPOSURE TESTS

<u>Sample No.</u>	<u>Foam Type</u>	<u>Front Face Temp. (°F)</u>	<u>Back Face Temp (°F)</u>	<u>Time of Exposure (Min.)</u>
1S	Silica	2600	1490	30
2S	Silica	2600	1455	30
3S	Silica	2500	1135	15
4S	Silica	2850	1495	30
5S	Silica	2850	1245	30
6S	Silica	2850	1325	30
7S	Silica	2850	1215	30
1A	Alumina	3100	1110	20
2A	Alumina	3350	1325	20
3A	Alumina	3400	1075	20
4A	Alumina	3100	1460	20
5A	Alumina	3340	1380	20
6A	Alumina	3200	1200	20
7A	Alumina	3000	850	20
1Z	Zirconia	3100	990	20
2Z	Zirconia	3150	1250	20
3Z	Zirconia	3400	1290	20
4Z	Zirconia	3400	1120	20
5Z	Zirconia	3600	990	30
6Z	Zirconia	3800	990	30

- Note: 1. All samples consisted of 3/8" depth of ceramic foam and 3/8" depth of Fiberfrax in a 17-7PH honeycomb reinforcement.
2. All samples exposed to oxy-acetylene heat source.
3. Front face temperatures measured by optical pyrometer; back face temperatures by thermocouple.
4. Specimen dimensions: 1" x 1" x 3/4" thickness

### C. COMPOSITE PANEL TESTS

Composite panels were tested in the exhaust stream of a turbojet J75 engine with afterburner and in the supersonic exhaust of an 8" ramjet burner. In addition, mechanical and thermal loads were applied to various panels under laboratory conditions to evaluate structural properties.

#### 1. Turbojet and Ramjet Tests

These tests provided severe thermal, pressure and sonic environments, and although pressure and sonic loads were greater than expected in re-entry flight, this type of test determined basic structural durability under combined loads. The ramjet facility provided the following conditions:

Exhaust gas temperature: 3000°F to 5000°F  
Sonic level: approximately 150 db  
Dynamic pressure: 20 psi (the flat panels were inclined at an angle of 60° so that the maximum dynamic pressure component normal to the panels was approximately 10 psi).

Prior to the ramjet tests, several panels were tested in the exhaust of a J75 turbojet engine to determine the feasibility and the state of the art of this type of construction.

The first two panels listed in Table IV-7 are unimproved early designs tested during this period. They were comparatively heavy because of the high density of the foamed ceramics and the absence of fibrous insulation. It was not intended at this time to optimize the structure, but to evaluate concept feasibility. The results were sufficiently satisfactory to establish the feasibility of the construction and to encourage future work.

The next three panels (3, 4, and 5) represent the first area of the development of the thermantic structure beyond the state of the art. Fibrous insulation was added under the foamed ceramic to decrease the heat flow through the panel. The ceramic used on these panels was of comparatively high density, so that while test life was improved, the panels were considered too heavy for flight vehicles.

The next step of the development is represented by the next two panels (6 and 7, Table IV-7). On these panels, the foam density was decreased. However, because of the interest of the Dyna-Soar Phase Able Program in this construction, sufficient time was not available to give proper considerations to all the ramifications of the lower density foam. Among the factors that were not given sufficient evaluation were:

Shrinkage of ceramic during test  
Mechanical strength of the low density foam  
Oxidation protection of the honeycomb core

TABLE IV -7

TEST RESULTS FROM AFTERBURNER AND RAMJET  
EXPOSURES ON THERMANTIC CONSTRUCTIONS

Panel Type	Test No.	Engine Operating Conditions	T <sub>1</sub> = Surface (OF.) T <sub>2</sub> = Braze Line T <sub>3</sub> = Back Surface	Time to Failure (Min:Sec)	Remarks
17-7 PH Reinforcement 3/4" Alumina Foam panel on corrugated panel	(1)	80% A.B.*	Test time too short to measure	approx. 30 sec.	Panel holding fixture failed
17-7 PH Reinforcement 3/4" Alumina Foam Panel	(2)	80% A.B.	T <sub>1</sub> = 2600 T <sub>2</sub> = 1100	5:35	Failed at joint between edge and fixture
17-7 PH Reinforcement 3/8" Alumina Foam 3/8" Fiberfrax on corrugated panel	(3)	80% A.B. 80% Engine	T <sub>1</sub> = 2400 T <sub>2</sub> = Not measured T <sub>3</sub> = Not measured	10:00 (2-5 min. runs)	Failed mechanically by loss of ceramic cells in lower right corner
17-7 PH Reinforcement 3/8" Alumina Foam 3/8" Fiberfrax on corrugated panel	(4)	100% A.B. 100% Engine	T <sub>1</sub> = 2500 T <sub>2</sub> = Not measured T <sub>3</sub> = 850	7:00	Failed mechanically by loss of ceramic cells in lower right corner
17-7 PH Reinforcement 3/8" Alumina Foam 3/8" Fiberfrax on corrugated panel	(5)	80% A.B. 80% Engine	T <sub>1</sub> = 2500 T <sub>2</sub> = not measured T <sub>3</sub> = 800	7:35	Failed mechanically by loss of ceramic cells in lower right corner
Inconel "X" Reinforcement 3/8" Silica Foam Panel 3/8" Fiberfrax on corrugated panel	(6)	80% A.B. 80% Engine	T <sub>1</sub> = 2300 T <sub>2</sub> = not measured T <sub>3</sub> = not measured	1:15	Silica foam shrank from core, core oxidized, failed similar to above

\* A.B. = Afterburner

TABLE IV-7 (cont)

Panel Type	Test No.	Engine Operating Conditions	T <sub>1</sub> = Surface (°F.) T <sub>2</sub> = Braze Line T <sub>3</sub> = Back Surface	Time to Failure (Min:Sec)	Remarks
Inconel "X" Reinforcement	(7)				
3/8" Alumina Foam Panel		80% A.V.	T <sub>1</sub> = 2500		Alumina foam shrank
3/8" Fiberfrax on corrugated panel		80% Engine	T <sub>2</sub> = Not measured T <sub>3</sub> = Not measured	2:35	from core oxidized, failed similar to above
17-7 PH Reinforcement	(8)				
3/8" Zirconia Foam Panel		Ram Jet	T <sub>1</sub> = 2350	0:43	Failed by loss of cells
3/8" Fiberfrax on corrugated panel			T <sub>2</sub> = 408 T <sub>3</sub> = 134		and oxidation of core
Inconel "X" Reinforcement with nickel-chrome and NiO-ZrO <sub>2</sub> coating	(9)				
3/8" Silica foam panel		Ram Jet	T <sub>1</sub> = 2560 to 3300 (cycling)		Test halted because fixtures melted. Panel retained structural integrity
3/8" Fiberfrax on honeycomb panel			T <sub>2</sub> = 460 T <sub>3</sub> = 240	5:30	
1/16" super 3000 cement over foam					
Inconel "X" Reinforcement with nickel-chrome and NiO-ZrO <sub>2</sub> coating					
6/16" Silica foam panel (extending 1/16" over core)					Delivered to ASD - Not yet tested
3/8" fiberfrax on honeycomb panel 1 mil nickel oxide on foam for emissivity					
17-7 PH Reinforcement with nickel-chrome and NiO-ZrO <sub>2</sub> coating					
3/8" Zirconia foam panel					Delivered to ASD - Not yet tested
3/8" Fiberfrax on Honeycomb panel					

TABLE IV -7 (con't)

Panel Type	Test No.	Engine Operating Conditions	Time to Failure (Min:Sec)			Remarks
			T <sub>1</sub> = Surface (°F.)	T <sub>2</sub> = Braze Line	T <sub>3</sub> = Back Surface	
17-7 PH Reinforcement with nickel-chrome and NiO-ZrO <sub>2</sub> coating						
3/8" Alumina Foam panel						
3/8" Fiberfrax on Honeycomb panel						Delivered to ASD - Not yet tested
Inconel "X" Reinforcement with nickel-chrome and NiO-ZrO <sub>2</sub> coating						
3/8" Zirconia Foam panel						
3/8" Fiberfrax on honeycomb panel						Delivered to ASD

As a result of the hurried evaluation, the test life of the panels was very short. The failure consisted of the foam shrinking away from and exposing the honeycomb core to the hot blast. Then, failure took the form of a combination of ceramic failure, because its strength was too low to allow for the decreased reinforcement area, and degradation of the core by oxidation.

A typical panel, before testing in the exhaust stream of the turbojet engine, is shown in Figure IV-5. The same panel, after testing, as shown in Figure IV-6, illustrates the oxidation of the core followed by the loss of the ceramic foam.

The next two panels (8 and 9) were tested in the exhaust stream of an 8 inch ramjet burner at Chance Vought Aircraft, Inc. The zirconia panel was similar to the lightweight silica and alumina tested with the J75 turbojet, in that the core was not protected and the foam suffered from the same deficiencies mentioned before. Therefore, it was not expected to perform well.

The silica panel incorporated two developmental improvements: Protection of the reinforcement core and a dense ceramic layer over the ceramic foam. The core protection consisted of a layer of nickel-chromium alloy flame sprayed on the foil of the honeycomb. This was then flame sprayed with a mixture of nickel and zirconium oxides. The dense ceramic facings over the foam was 1/16 inch coating of Super 3000 cement.

A schematic of the overall test set up, Figure IV -7, shows the relative location of all the test equipment.

The silica panel was mounted on the movable sting and, after ramjet ignition, moved toward the ramjet exhaust plane at a rate of approximately one foot per second. The panel was stopped at a position 40 inches aft of the exhaust plane.

The face temperature during the test cycled from 2560°F to 3300°F due to lack of control of the ramjet. The Super 3000 coating melted and flowed from the panel surface.

A hole occurred in the test fixture water jacket prior to shutdown, and after shutdown the specimen was thoroughly sprayed with water, causing severe thermal shock.

Even though the panel lost its surface coating and suffered severe thermal shock, there was little damage to the panel and the entire panel was structurally sound.

A temperature versus time history of the temperatures in the panel are plotted in Figure IV-8. Figures IV -9 and 10 show the panel before and after testing respectively.

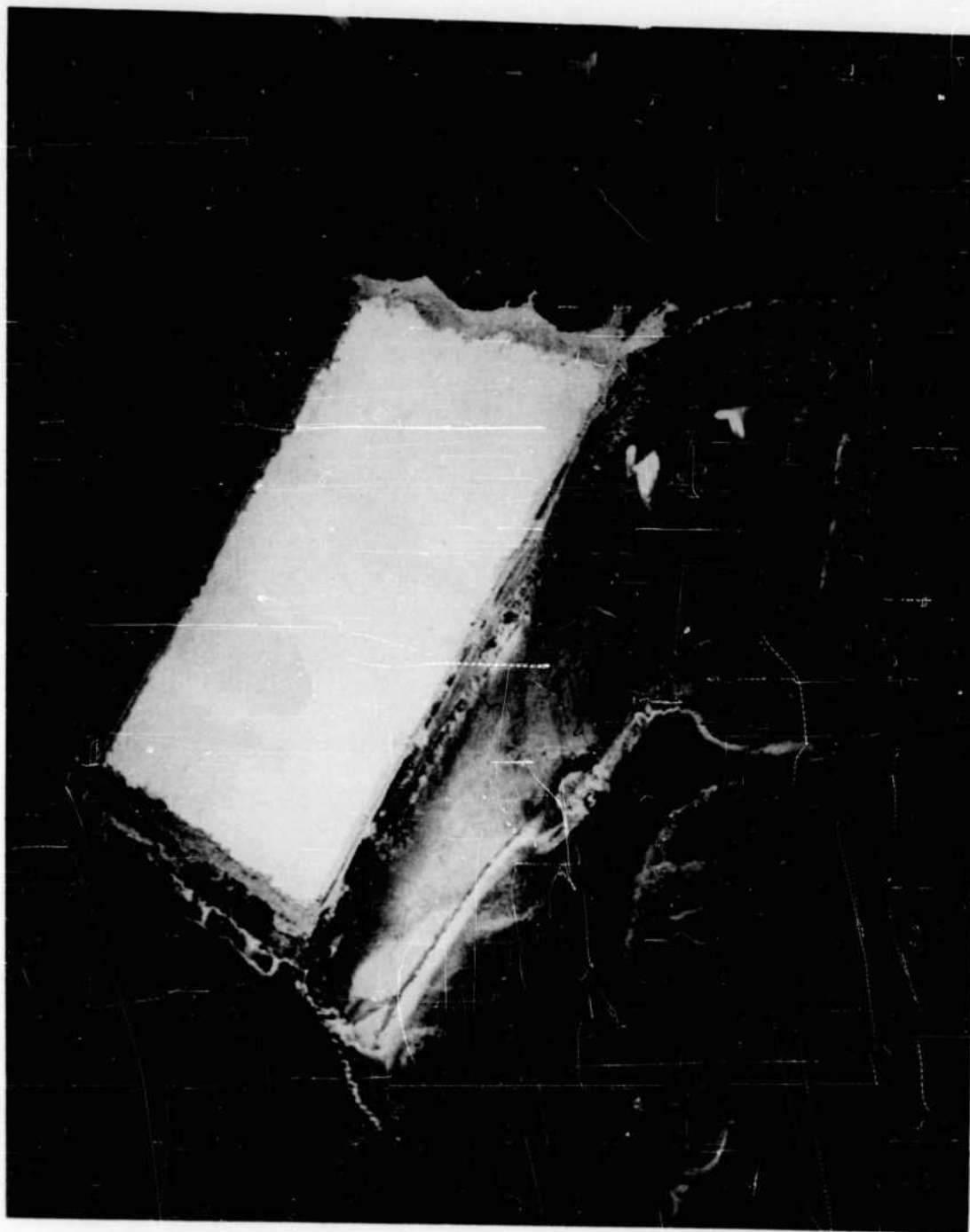


Figure IV-5 Typical Foam Ceramic Panel Before Exposure to Exhaust of J75 Turbojet

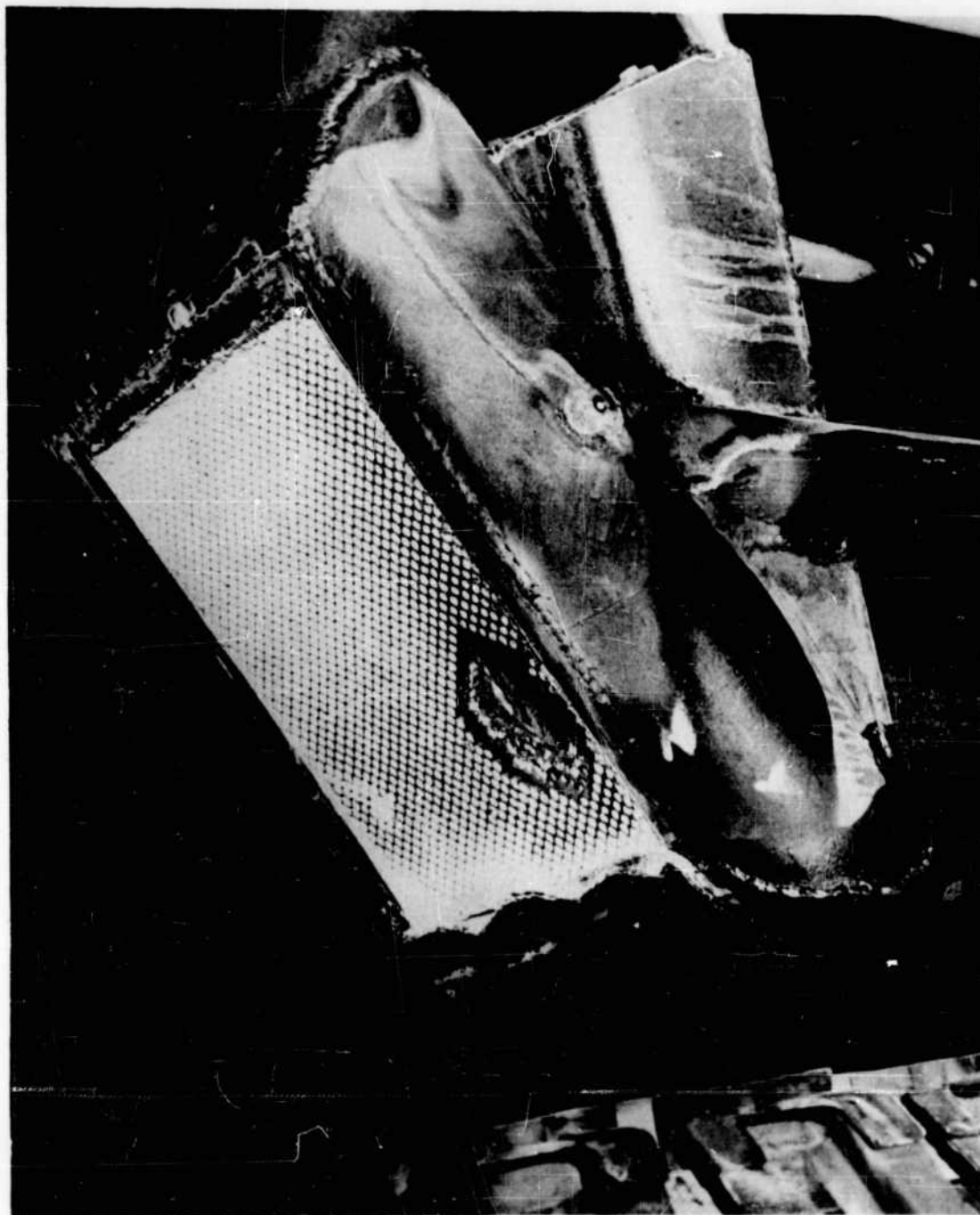


Figure IV-6 Foamed Ceramic Panel After Exposure to Exhaust of Turbojet

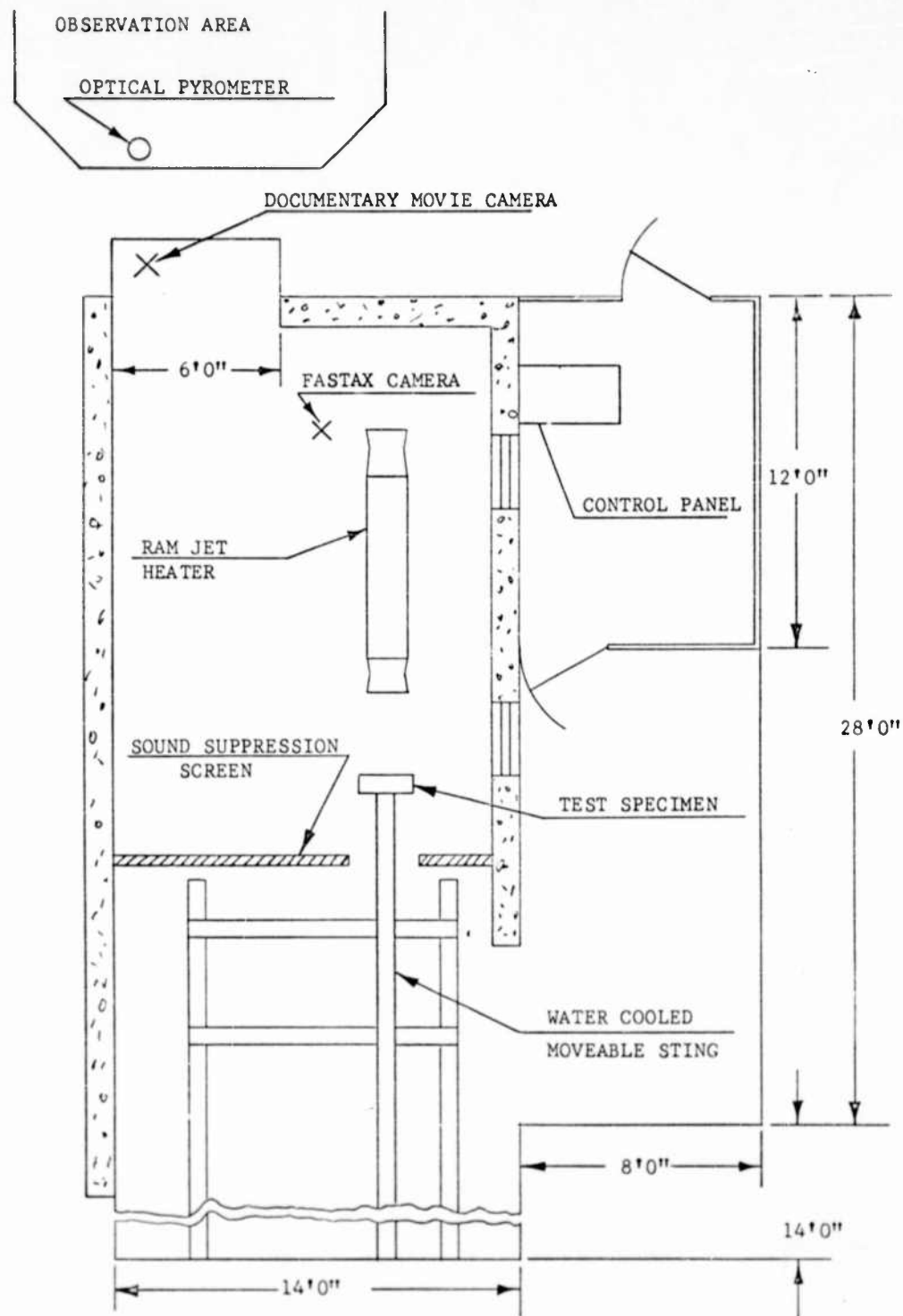


Figure IV-7 Schematic - Overall Test Setup

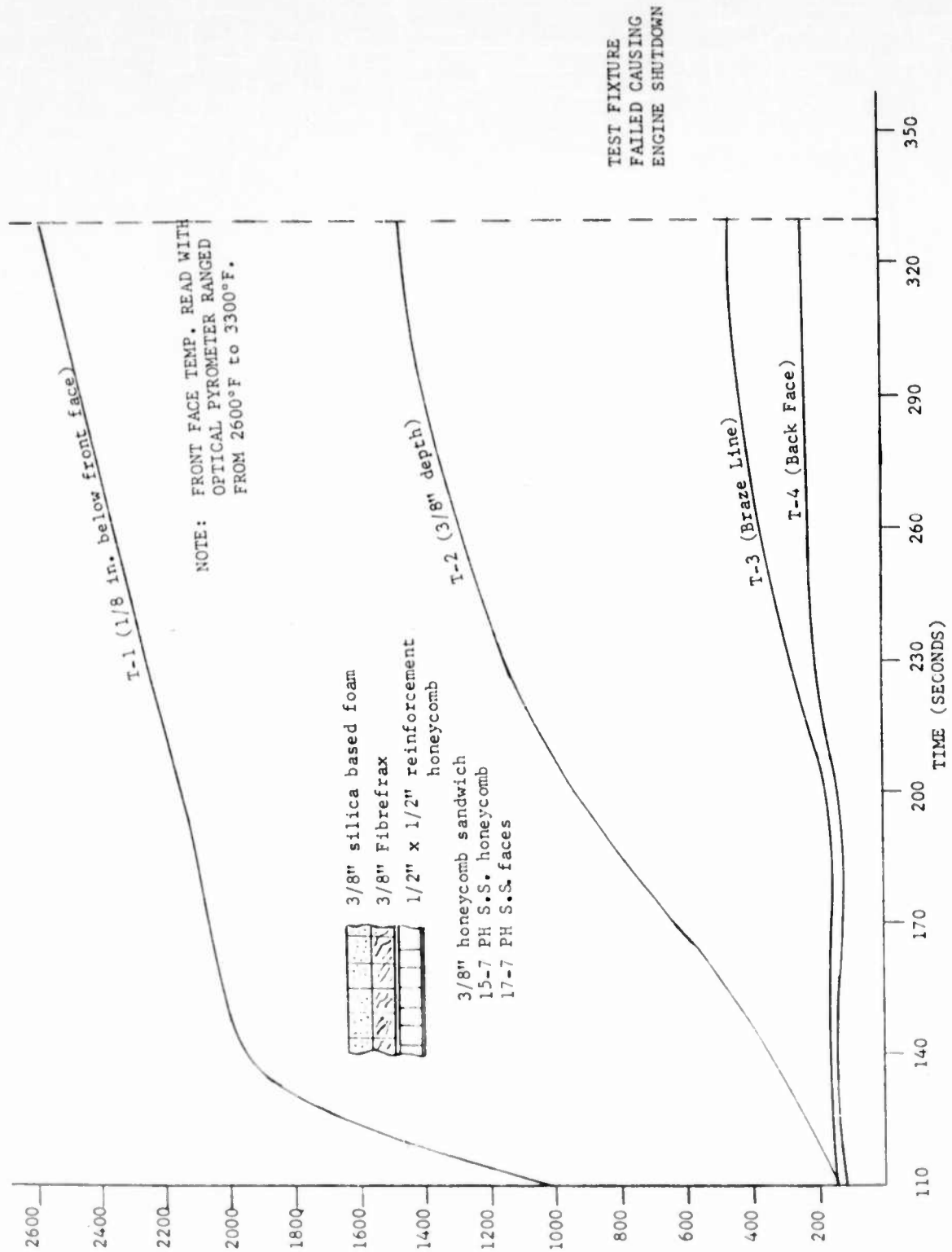


Figure IV-8 Results of Ram Jet Exposure Test

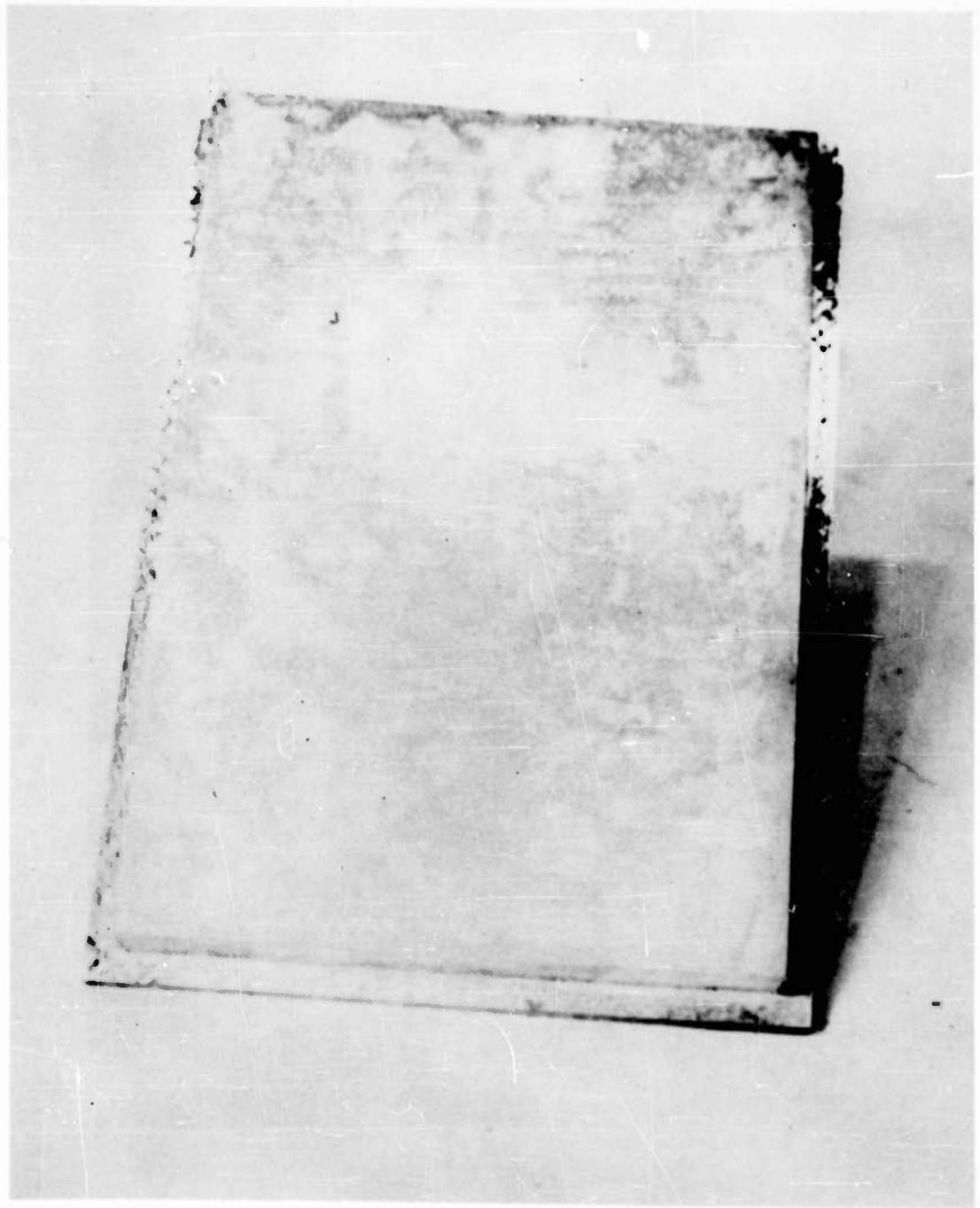


Figure IV-9 Silica Panel before Exposure to Ramjet Exhaust



Figure IV-10 Silica Panel after Exposure to Ramjet Exhaust

## 2. Mechanical and Thermal Tests

### a. Description

A beryllium sandwich panel of 18" x 18" x  $\frac{1}{2}$ " configuration was subjected to thermal and mechanical loads. The panel was composed of two beryllium sheets 18" square x .040" thickness. Sandwiched between the two beryllium sheets was a honeycomb core of 321 stainless steel and the sandwich was brazed together with silver, copper, lithium brazing alloy. The panel contained channel type edge members as shown in Figure IV-11. Method of loading is shown in Figure IV-12. An X-ray view of a portion of the panel, Figure IV-13, shows the brazing quality in the panel.

Instrumentation of the panel at selected points was performed by cementing chromel-alumel thermocouples in the axial loading plane and transverse to the axial loading plane. A total of twenty chromel-alumel thermocouples were installed on the upper and lower faces, six (6) of which correspond with three (3) dial indicator gages assembled to measure deflection on the lower face of the panel (Figure IV-14). With this location of instruments, the measurement of temperature on the upper and lower face was recorded while the deflection on the lower face was obtained at the indicated points. The deflection was monitored on the lower face of the panel only, for which a positive or negative reading could be obtained.

The heat source was one face of flat ceramic die (30" x 30"). The die was positioned to radiate heat to the upper face of the panel. Protective insulation was placed around the edges of the die to reduce edge cooling effects. The air plenum was constructed to blow air on the lower face and control its temperature and establish a uniform thermal gradient between the two faces.

Three prime categories of testing were conducted: mechanical, thermal gradient and thermal-mechanical.

#### (1) Room Temperature Compressive Test

The instrumented panel was loaded in edgewise compression when positioned in the compressive test fixture while resting on four locating legs. (Figure IV-12) The panel was subjected to loadings in increments of 1000 lbs. At each loading the deflection reading was recorded from each of the three dial indicators. One indicator was located on each plane (axial and transverse). The third indicator was located at the intersection of the two planes.

Panel deflections and behavior were observed closely to maintain maximum mechanical loads below the calculated maximum to prevent damage or failure to the panel. Total loads of 2000 to 19,000 lbs. were applied to the test panel. Panel deflections were recorded at each loading to determine the deflection characteristics with increased loading (Figure IV-15).

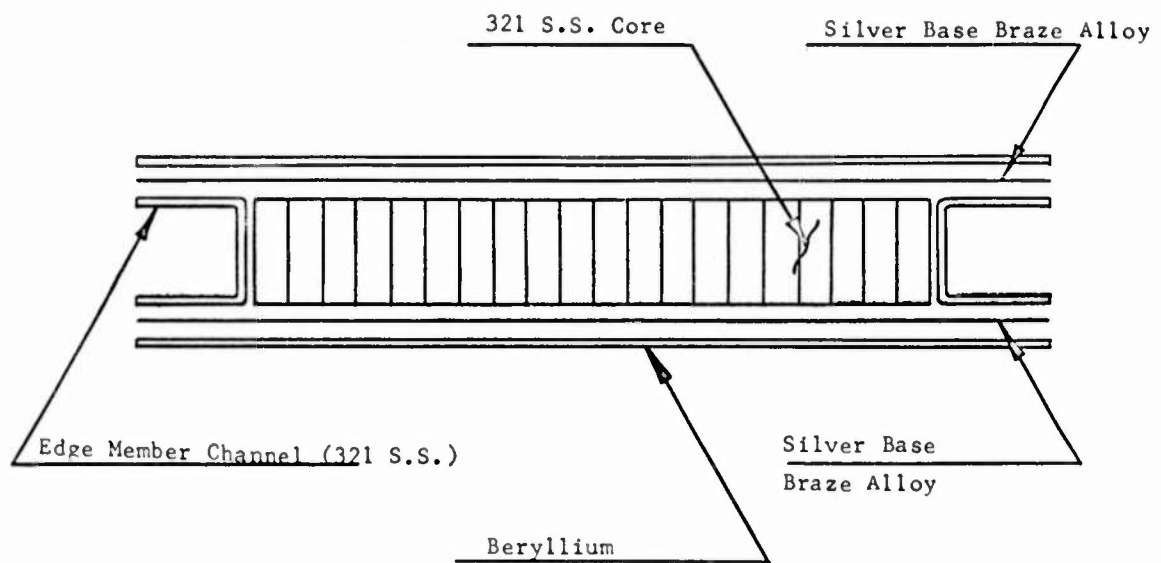


Figure IV-11 - Schematic of Panel Configuration

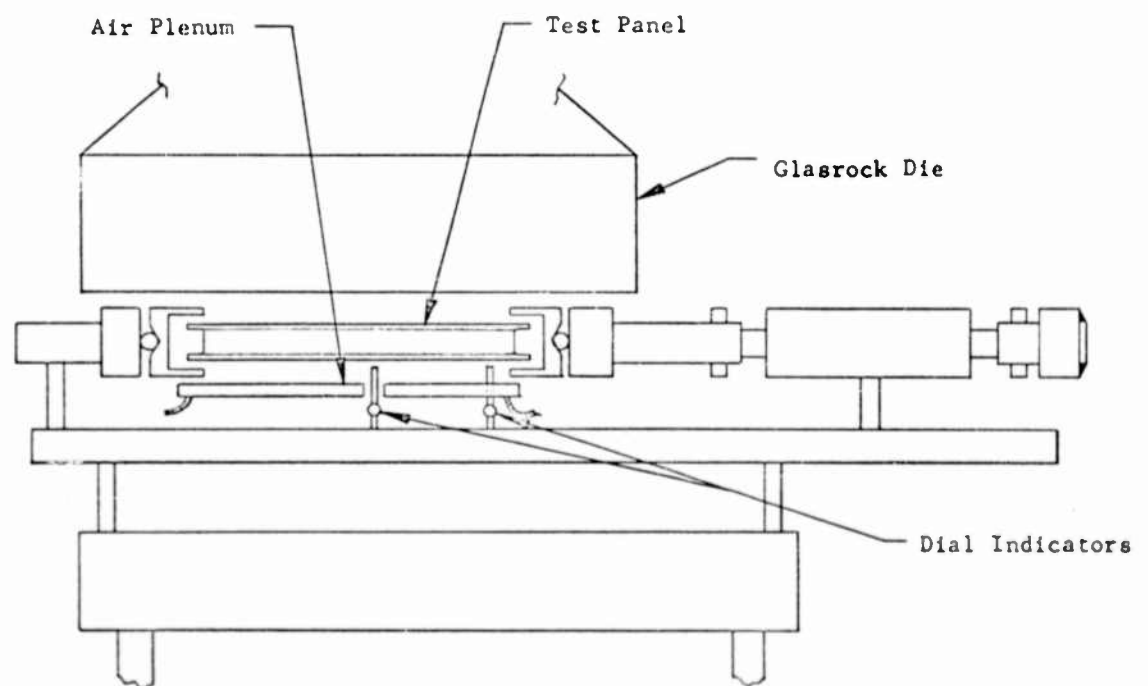
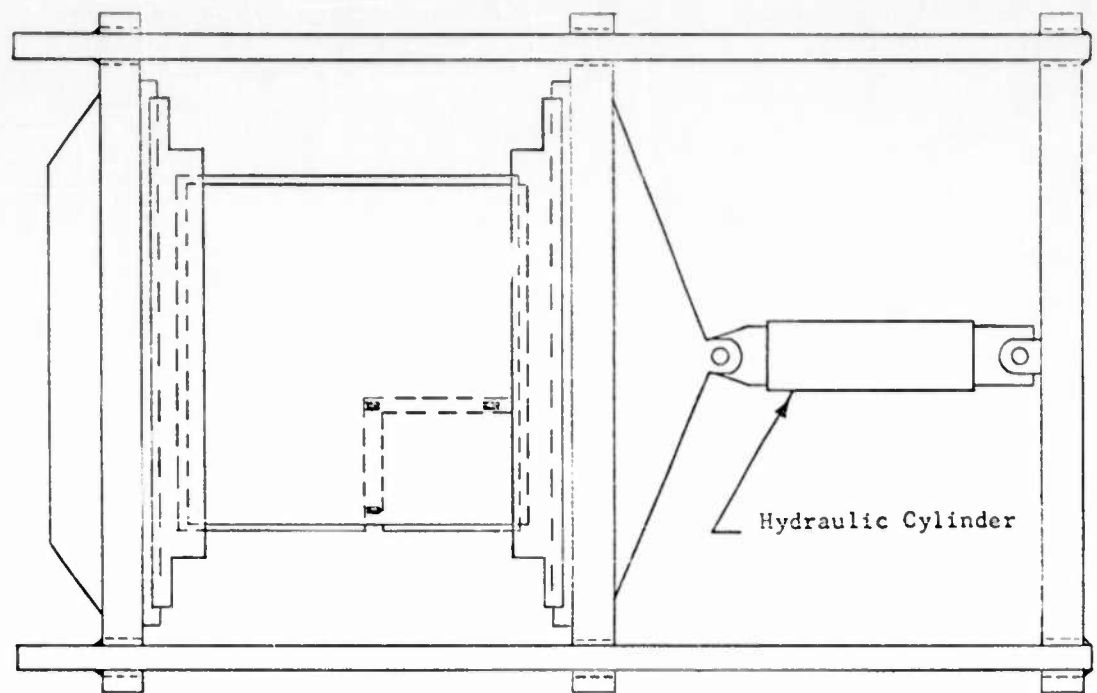


Figure IV-12- Schematic of Compréssion Test Fixture

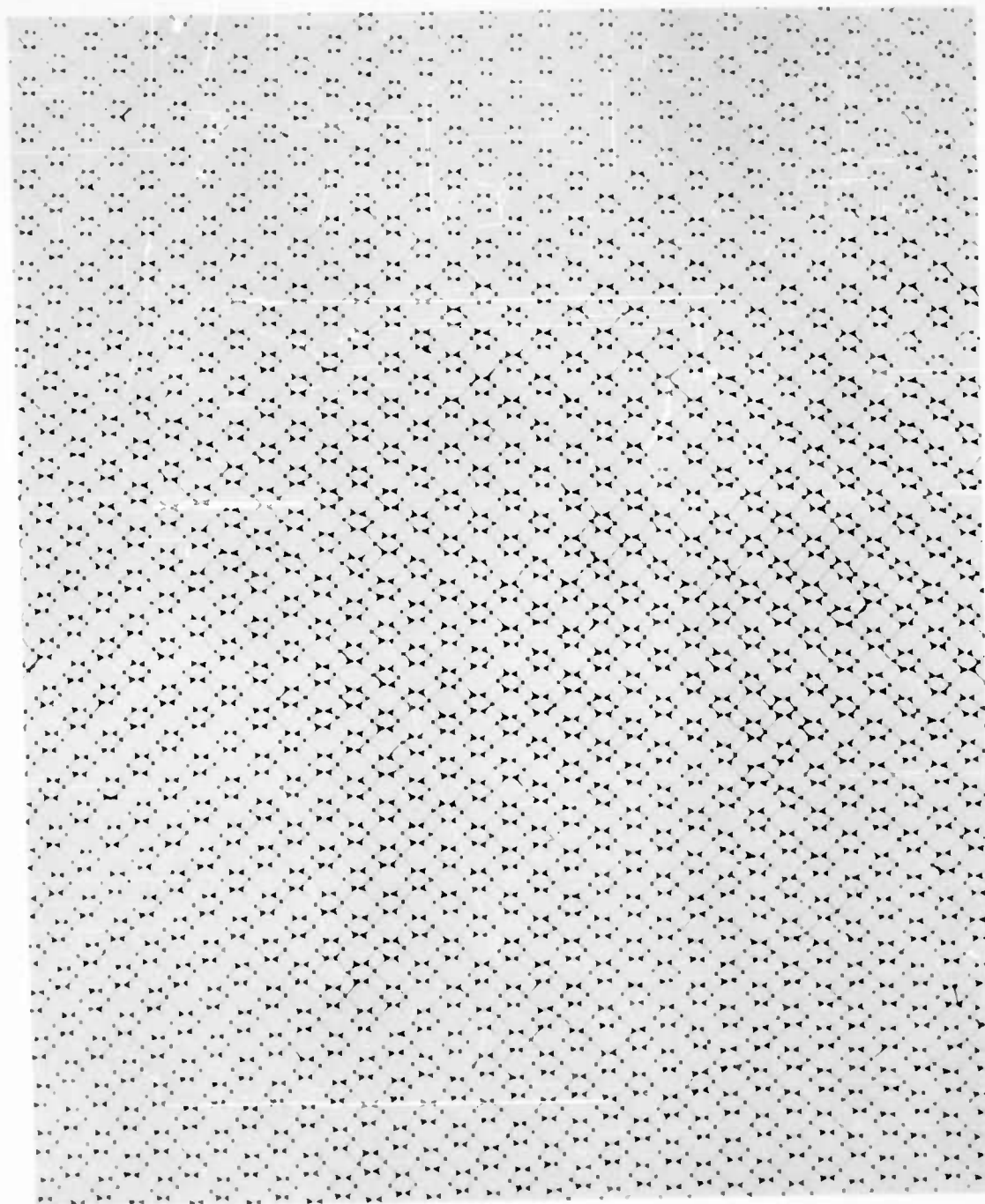
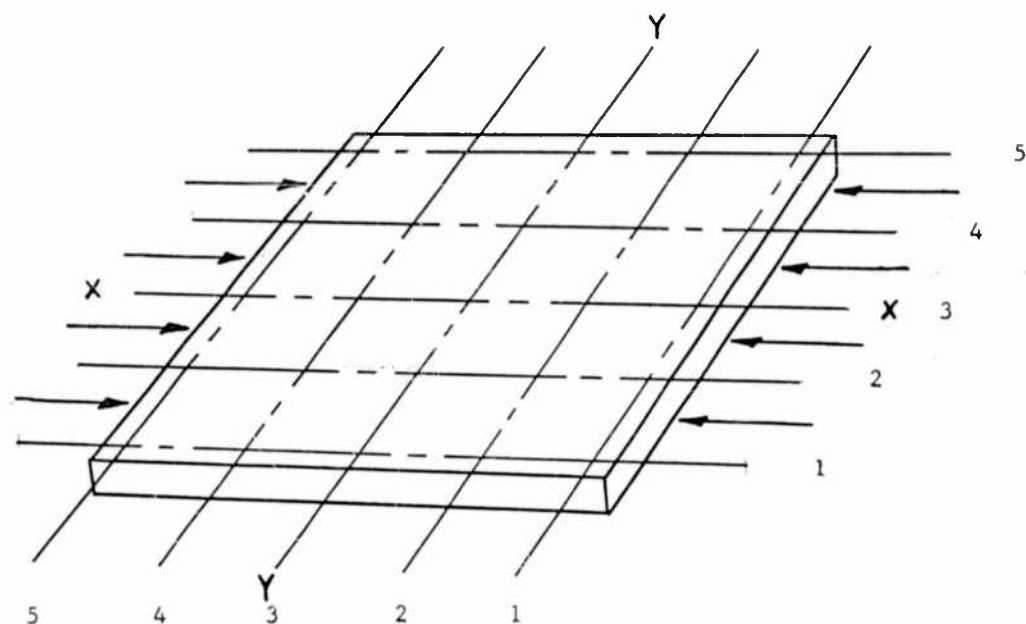


Figure IV-13 X-Ray View of a Section of the Test Panel

IV-30



#### Thermocouple Locations

##### Upper Face (Plane X-Y)

1, 1  
1, 3  
1, 5  
2, 3  
3, 1  
3, 2  
3, 3  
3, 5  
5, 1  
5, 3  
5, 5

##### Lower Face (Plane X-Y)

1, 1  
1, 3  
1, 5  
2, 3  
3, 1  
3, 2  
3, 3  
3, 5  
5, 1  
5, 2  
5, 3

#### Dial Indicator Locations

##### Lower Face (Plane X-Y)

1, 3  
3, 3  
3, 1

Fig. IV.14- SCHEMATIC OF THERMOCOUPLE AND  
DIAL INDICATOR LOCATIONS

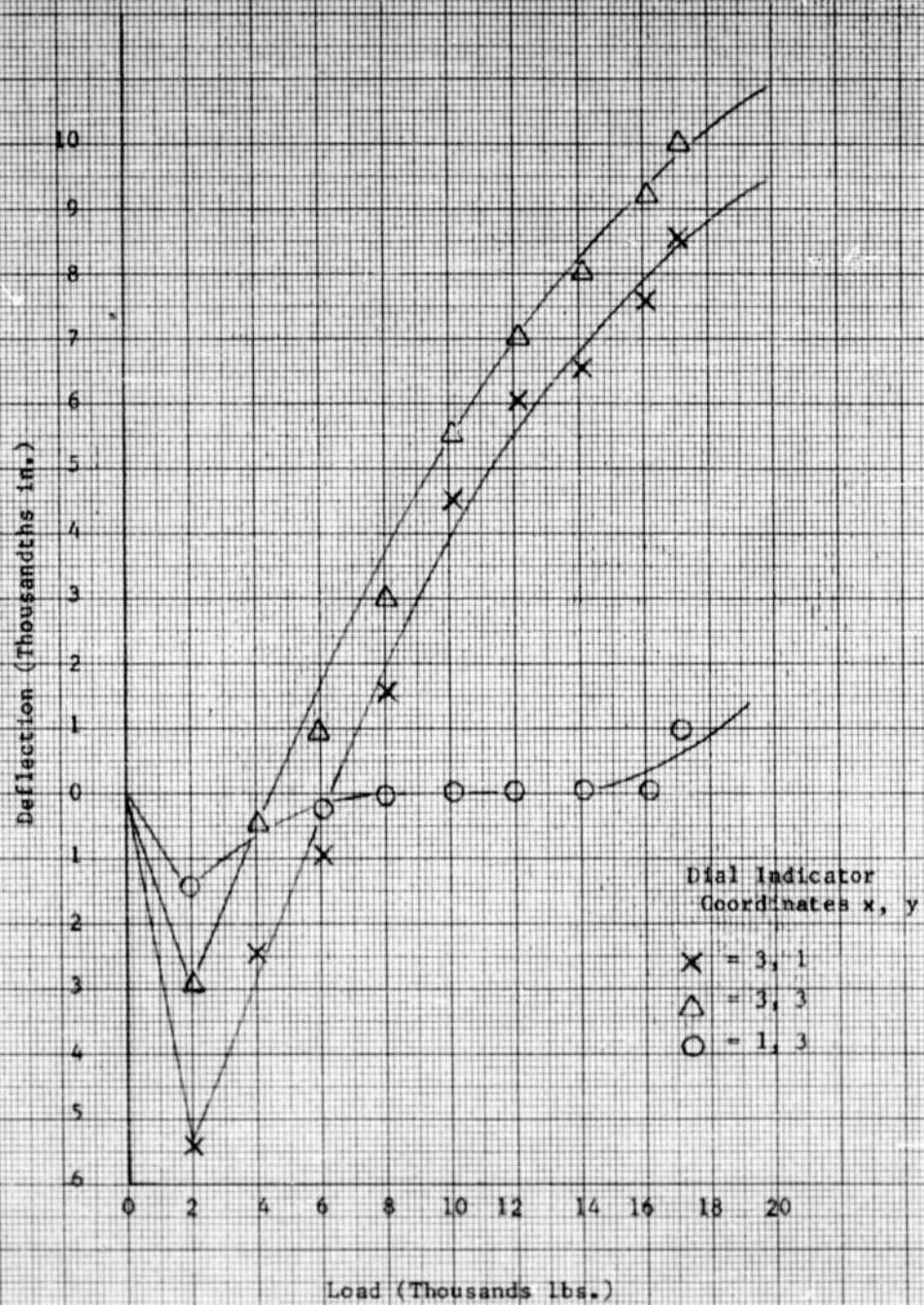


Figure IV-15 Panel Deflections - Room Temperature Compressive Test

(2) Thermal Gradient Test

During the thermal gradient test the panel was laying in a horizontal position and supported loosely on the lower face when resting on four locating legs. The panel was restrained from lateral movement during the test, but was free to deflect.

The upper face of the panel was heated to different temperature levels while the lower face was cooled to establish a different thermal gradient at each upper face temperature (Table IV-8). Deflection readings were taken on the lower face of the panel while it was at the various temperature levels (Figure IV-16).

(3) Thermal Mechanical Test

The panel was positioned in the channels of the compressive test fixture. Mechanical loading was applied during each temperature range holding a constant thermal gradient. Load limits equal to that of stress calculations were induced into the panel at different upper face temperatures and thermal gradients. The deflection through the axial loading plane and the deflection transverse to the loading plane was recorded at various face temperatures, thermal gradients and compressive loads. The panel was subjected to total loads of 2000 to 19,000 lbs. in 1000 lb. increments during these tests (Figures IV-17, 18 and 19). The test was terminated upon reaching a 20,000 lb. total load on the panel when a rupture occurred. A stress level of approximately 40,000 psi was induced into the panel at rupture.

b. Test Results

The results of the tests are shown in Figures IV-15 through IV-19. The panel survived the following loads:

- (1) Temperature gradients up to 230° F. across the faces when no mechanical loads were applied.
- (2) Edge compression loads up to approximately 1100 lbs. per in. while at room temperature.
- (3) Panel failure occurred at 1100 lbs. per in. and face temperature of 350° F. (upper face) and 150° F. (lower face). This condition created a calculated stress of approximately 40,000 psi, which indicates comparatively good structural characteristics for beryllium composite panels. Inspection of the failure, shown in Figure IV-20, revealed that the braze was weak at the failure location. This braze deficiency was not noticeable with X-ray inspection and would probably not have been detectable with other inspection methods such as ultra-sonics. The failure was a local buckling failure resulting from the separation of the core and face. For a completely sound braze, under the identical conditions, it is expected that a stress level of 55,000 psi should have been reached.

TABLE IV-8  
TEMPERATURE LEVELS MEASURED IN THE TEST PANEL  
DURING THERMAL GRADIENT TEST

<u>Upper Face Temp.</u> °F.	<u>Lower Face Temp.</u> °F.	<u>Differential Temp.</u> °F.
150	150	0
200	180	20
250	210	40
300	240	60
350	250	100
400	250	150
450	265	185
500	270	230

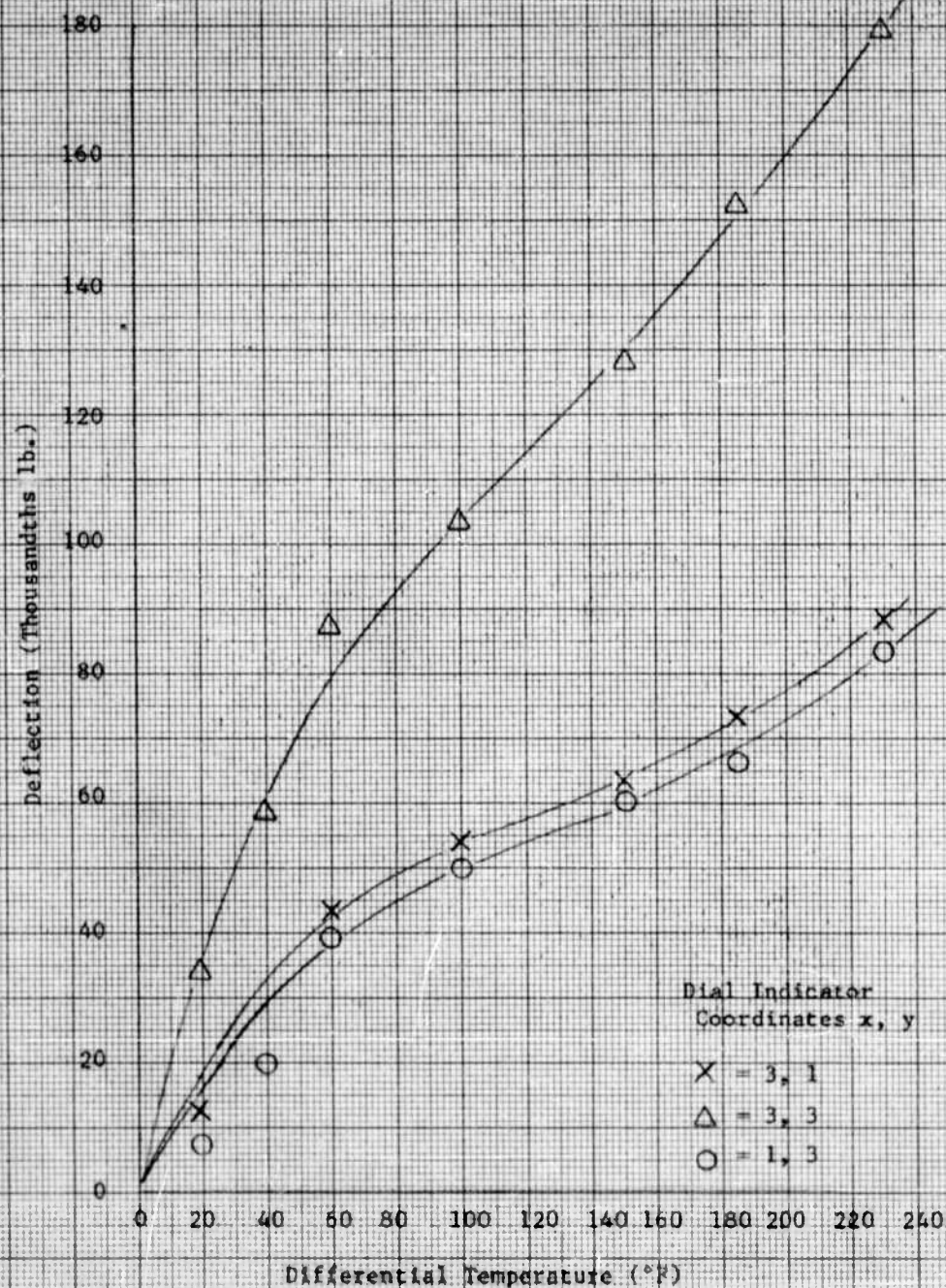


Figure IV-16 Panel Deflections - Thermal Gradient Test

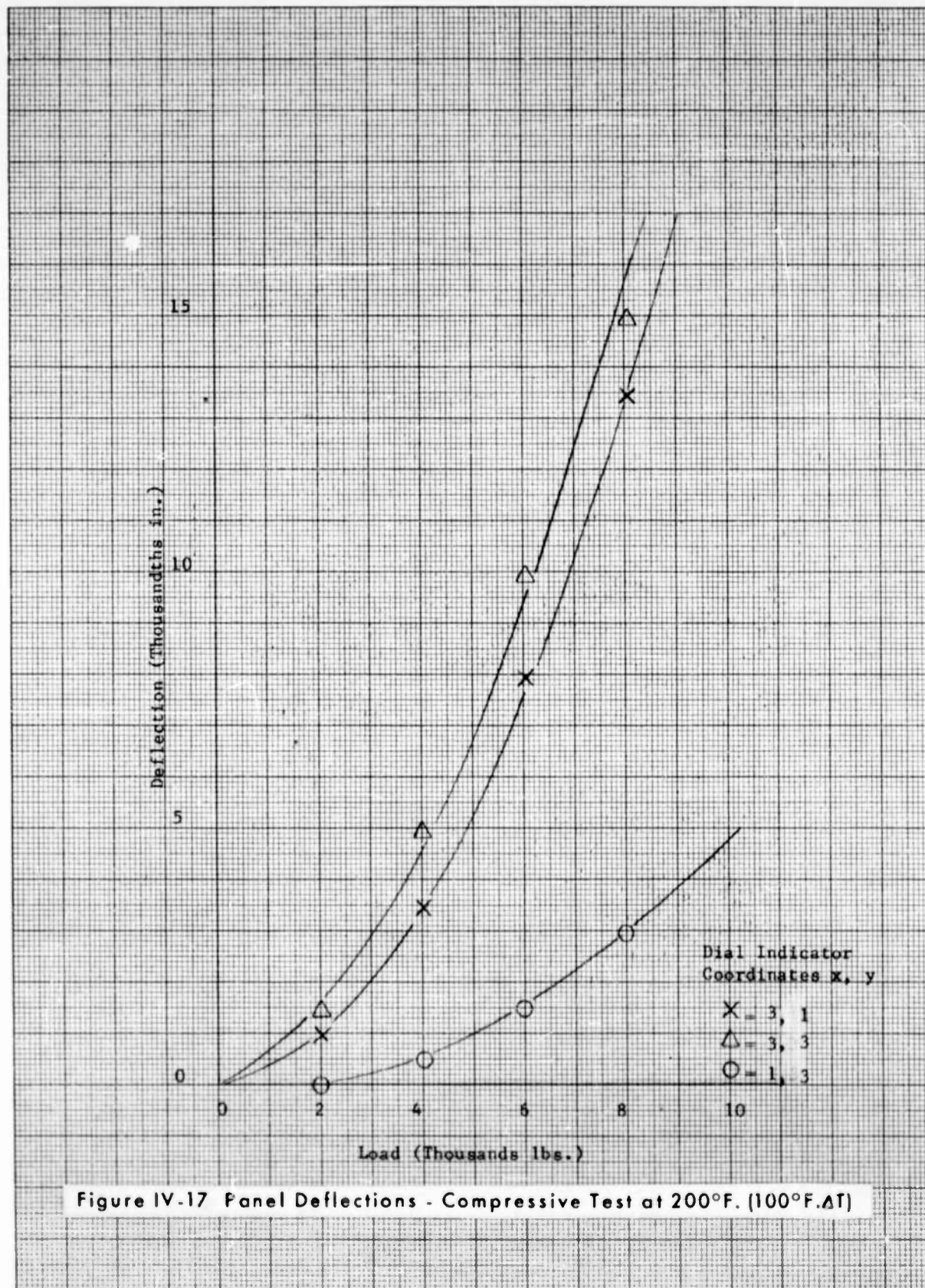


Figure IV-17 Panel Deflections - Compressive Test at 200°F. (100°F.ΔT)

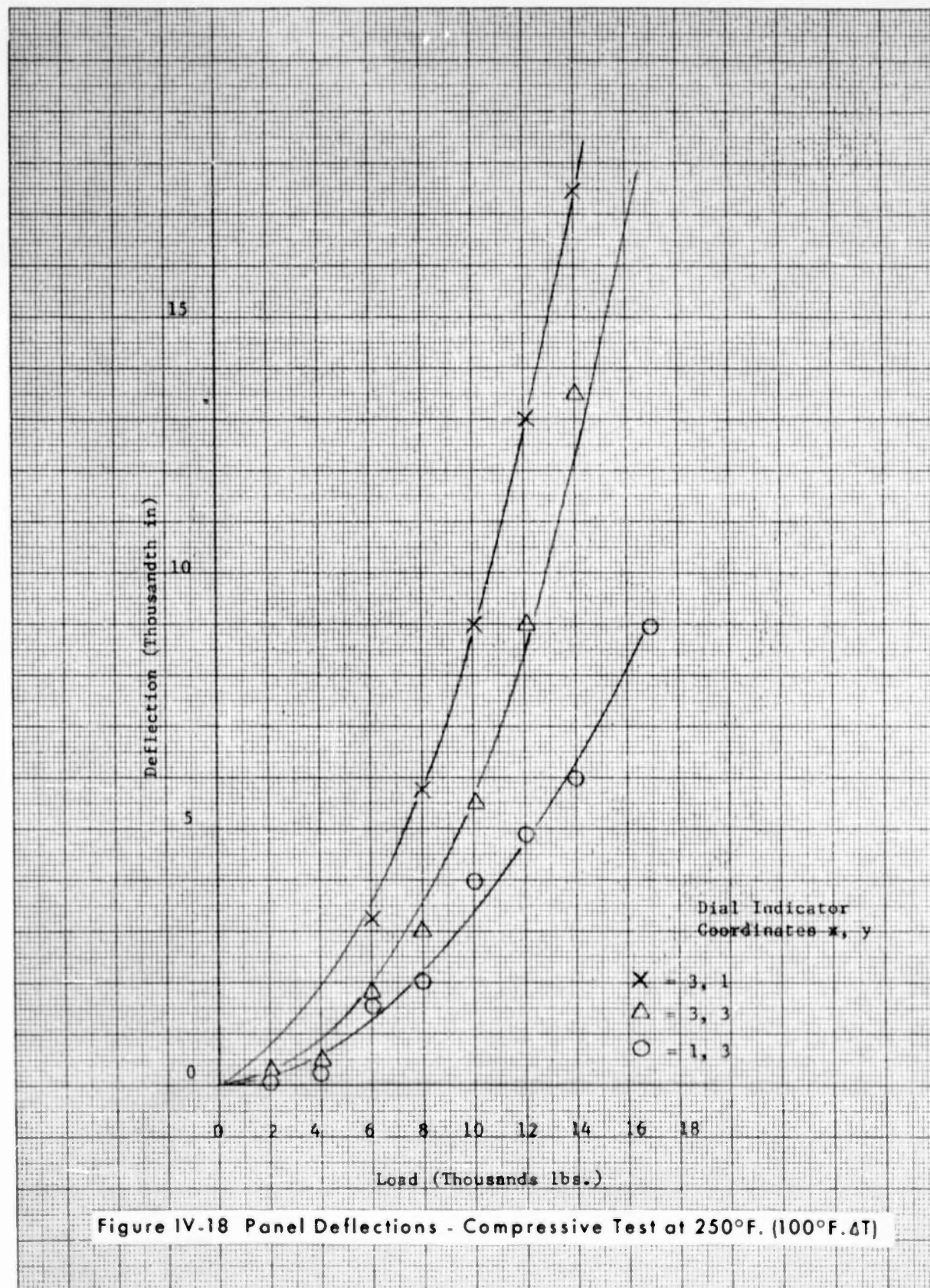


Figure IV-18 Panel Deflections - Compressive Test at 250°F. (100°F.ΔT)

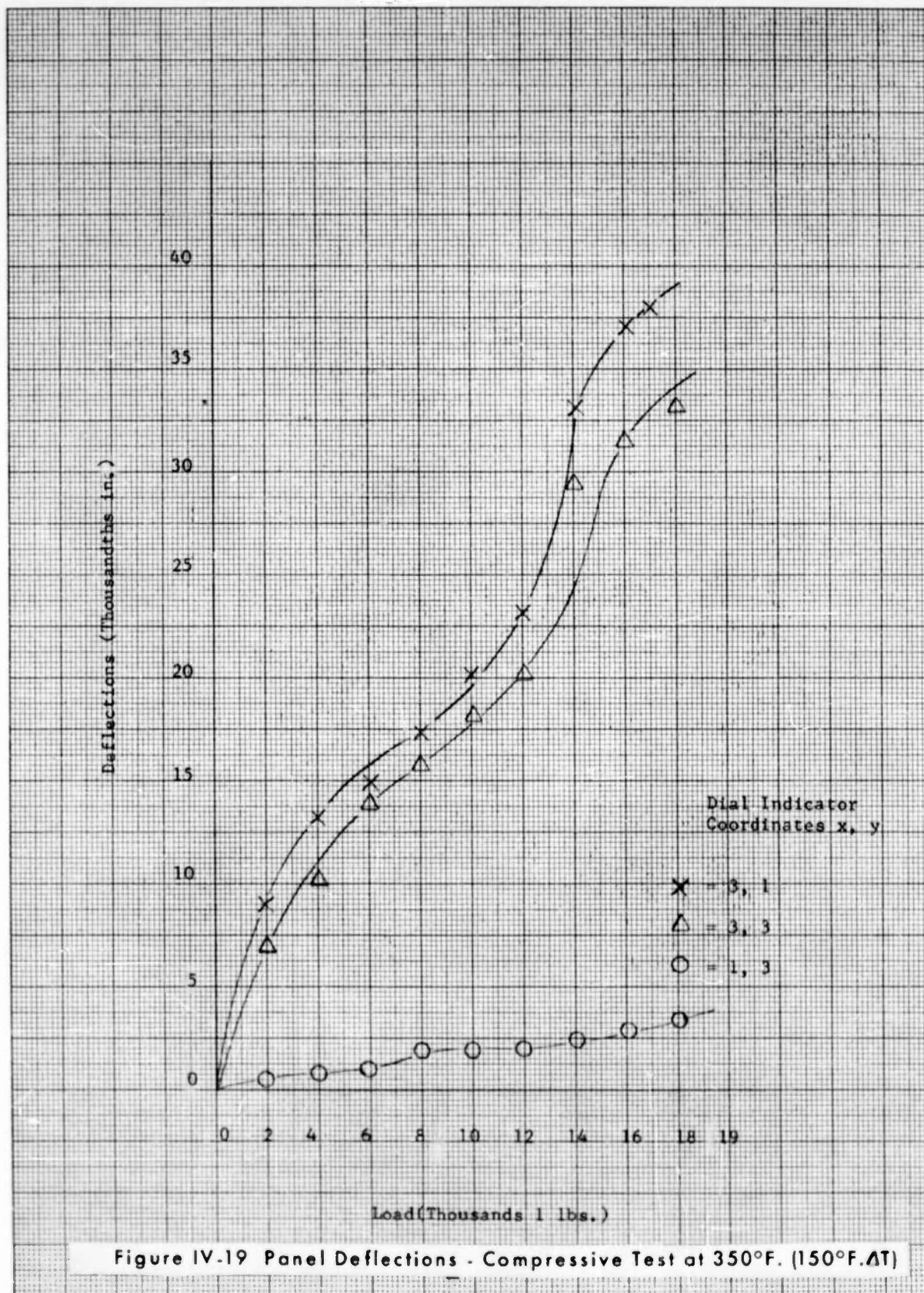


Figure IV-19 Panel Deflections - Compressive Test at 350°F. (150°F.ΔT)

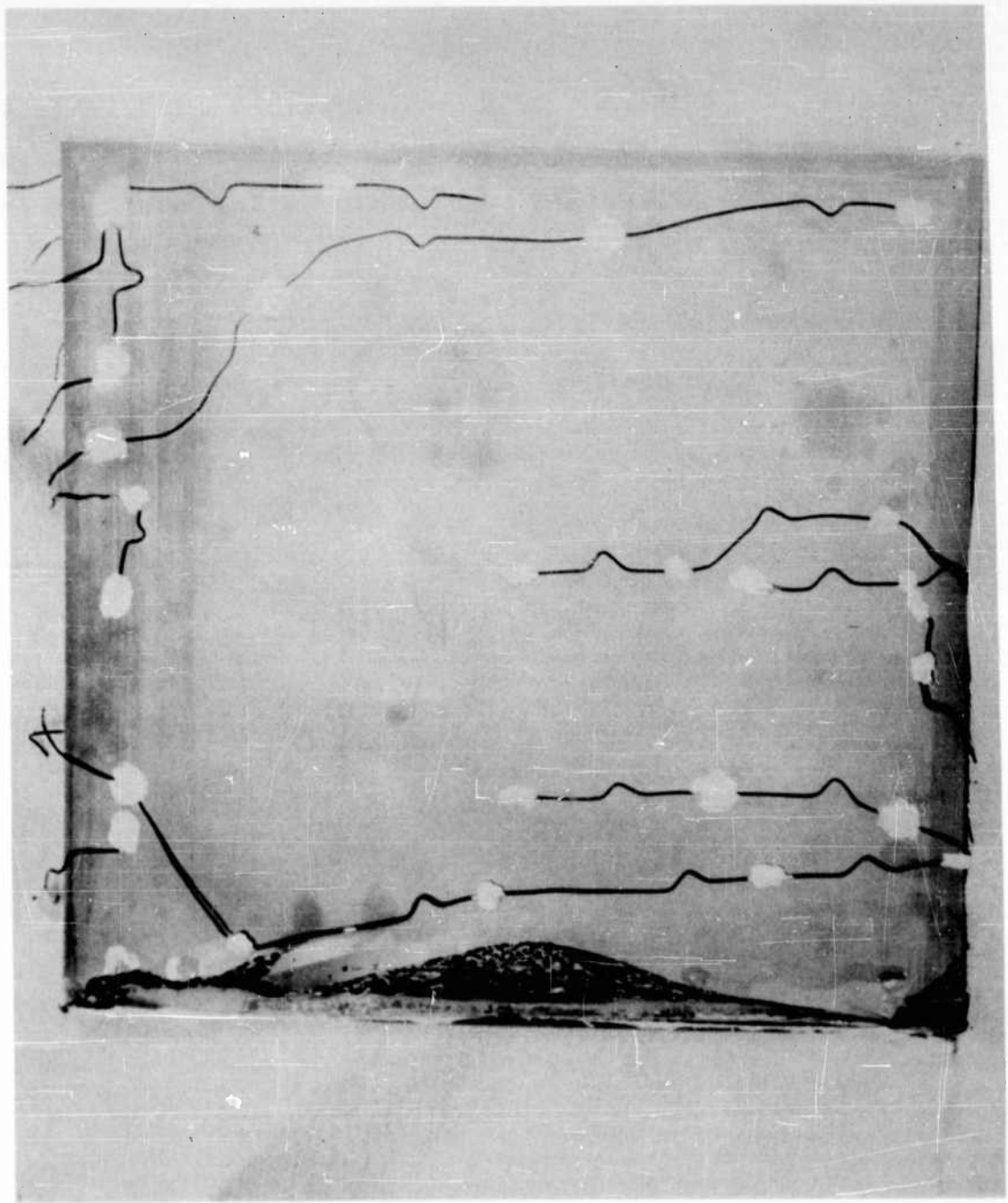


Figure IV-20 18 in. x 18 in. Flat Beryllium-Faced Honeycomb Panel  
After Testing at 350°F (150°F  $\Delta T$ )

D. BERYLLIUM TEST DATA

1. Mechanical Properties of Beryllium Sheet

a. Tensile Properties

Tests were conducted to determine the effect of edge preparation, annealing cycle and braze alloy on the tensile properties of beryllium sheet. The results of these tests are listed in Table IV-9.

The as-received properties of the beryllium, as reported by Brush Beryllium Corporation, were:

Ultimate Tensile Strength: 60,000 to 75,000 psi, 69,000 psi. avg.  
Yield Strength: 45,000 to 60,000 psi, 50,900 psi avg.

These properties represent the range for the longitudinal and long transverse direction of the sheet.

Specimens for test numbers 1, 2 and 3 with machining damage removed from the edges by hand polishing (see Section V, Volume I, on routing for details) showed an increase of approximately 7% over the average ultimate tensile strength reported by Brush.

Specimens for test numbers 4, 5 and 6, tested as machined, had an average failure 26% below the average ultimate tensile strength of the as-received sheet, indicating that the grain damage incurred during manufacture (and not removed) had a detrimental effect on the tensile properties. (It should be noted that the average ultimate strength for the group, 50,700 psi, is approximately the same as the average yield strength reported by Brush.)

For test numbers 7, 8 and 9, the specimens were taken as machined and then heated to 1750° F. for one minute in air prior to testing. The average ultimate tensile strength (59,600 psi) was approximately 13% below the as-received average but, however, greater than the average of the above group of tests, indicating partial annealing of the beryllium and relief of some of the residual stresses left by machining.

For test numbers 10, 11 and 12, the specimens were taken as machined and heated to 1400° F. for one hour in a vacuum. The average strength of this group was 55,000 psi, indicating that the anneal and stress relief was not as complete as in tests 7, 8 and 9.

For test numbers 13 and 14, the specimens were processed as above except that the atmosphere during the anneal was air rather than vacuum. The average ultimate strength (55,100 psi) is comparable to that of the vacuum annealed group, indicating that oxidation did not affect the properties. Based on these two groups of tests, it was determined that annealing would not satisfactorily remove the effects of the edge damage caused by machining.

TABLE IV -9

TENSILE TESTS OF BERYLLIUM

<u>Test No.</u>	<u>Specimen Condition</u>	<u>Y.P. psi</u>	<u>U.T.S. psi</u>
1	Hand Polish to Remove 0.006' off each edge	53,700	73,500
2	Hand Polish to Remove 0.006" off each edge	53,000	72,000
3	Hand Polish to Remove 0.006" off each edge	52,600	75,800
4	As Machined	54,100	54,100
5	As Machined	45,200	45,200
6	As Machined	41,500	55,500
7	1750° F. - 1 Minute - Air, Machined Edge	44,400	53,900
8	1750° F. - 1 Minute - Air, Machined Edge	47,100	59,400
9	1750° F. - 1 Minute - Air, Machined Edge	44,200	65,600
10	1400° F. - 1 Hour - Vacuum, Machined Edge	48,400	62,200
11	1400° F. - 1 Hour - Vacuum, Machined Edge	45,100	52,700
12	1400° F. - 1 Hour - Vacuum, Machined Edge	50,000	50,000
13	1400° F. - 1 Hour - Air, Machined Edge	43,700	68,400
14	1400° F. - 1 Hour - Air, Machined Edge	41,900	41,900
15	1700° F. - 1 Minute - Ag. Braze Alloy, Machined Edge	48,100	48,100
16	1700° F. - 1 Minute - Ag. Braze Alloy, Machined Edge	47,800	47,800
17	1700° F. - 1 Minute - Ag. Braze Alloy, Machined Edge	46,200	46,200

The last group of specimens (test numbers 15, 16 and 17) were taken as machined, and, with silver brazing foil placed on one side of the specimen, subjected to a braze cycle. The silver was allowed to melt, flow and diffuse into the beryllium in the same manner as during an actual braze cycle. The average ultimate tensile strength (47,000 psi) was 31% below the as-received average, but only slightly below the average of the as-machined specimens in tests 4, 5 and 6.

The conclusions that can be drawn from the above are:

- (1) Careful edge preparation is necessary to obtain optimum tensile properties.
- (2) Machining damage on the edge of the specimen is detrimental to the tensile properties.
- (3) Annealing does not completely remove the effect of edge damage.
- (4) Silver braze alloy decreases the tensile properties only slightly.

b. Compressive Properties

Compressive tests were run at room temperature to determine the compressive properties and compressive modulus of elasticity of beryllium sheet. A strain gage was mounted in the center of each flat side of the specimen to measure the strain in the longitudinal direction. The results are plotted as stress (psi) versus strain (micro-inch/inch) in Figures IV-21 through IV-27. From these plots were obtained the compressive modulus of elasticity and the compressive 0.02% yield strength. These values are tabulated in Table IV-10. The average modulus was  $46.6 \times 10^6$  psi which is in the range of, but slightly above, the generally accepted value. The average yield point of 46,000 psi is a little below the generally accepted value.

c. Flexural Properties

A series of cantilever bend tests were run to determine the flexural modulus of elasticity and the bend ductility of beryllium sheet.

Typical test results are plotted in Figure IV-28. The tests indicated that edge treatments of the specimens do not significantly affect the test results. This is believed to be due to the small proportion of the edge area to the total stressed area of the bend specimens. Exposure to temperature, where the treatment affected the entire width of the stressed area, resulted in slightly larger deflections for given stress levels. The flexural modulus was approximately 12% higher than the compressive modulus.

It should be noted that the stresses shown in Figure IV-28 are nominal stresses, based on the original specimen cross-section. Below the yield point, they are also true stresses but above the yield point, they do not allow for local yielding of the highly stressed surface.

ROOM TEMPERATURE    NOMINAL THICKNESS .060"

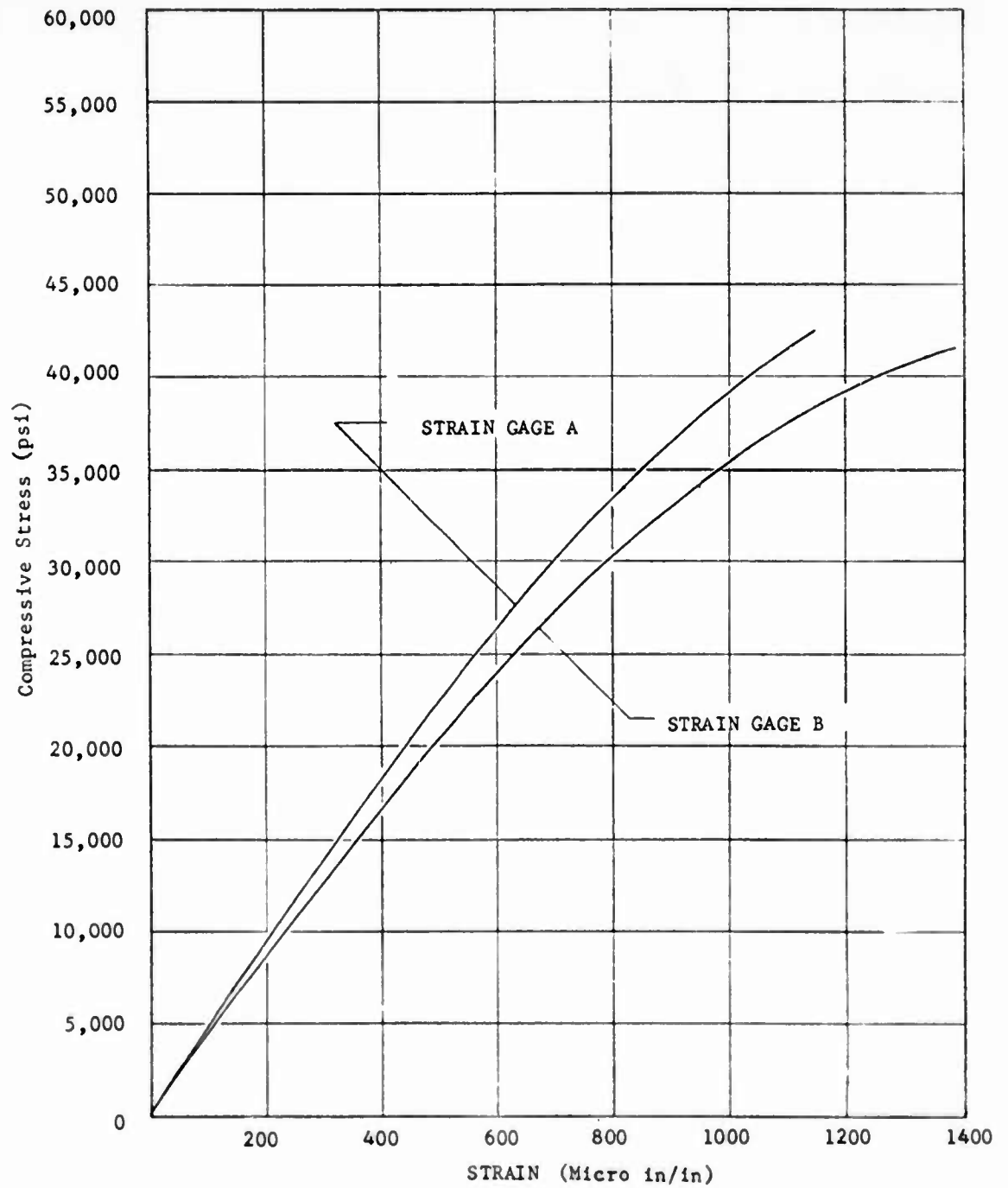


Figure IV-21 Beryllium Sheet Compression Test (Sample #1)

ROOM TEMPERATURE      NOMINAL THICKNESS .060"

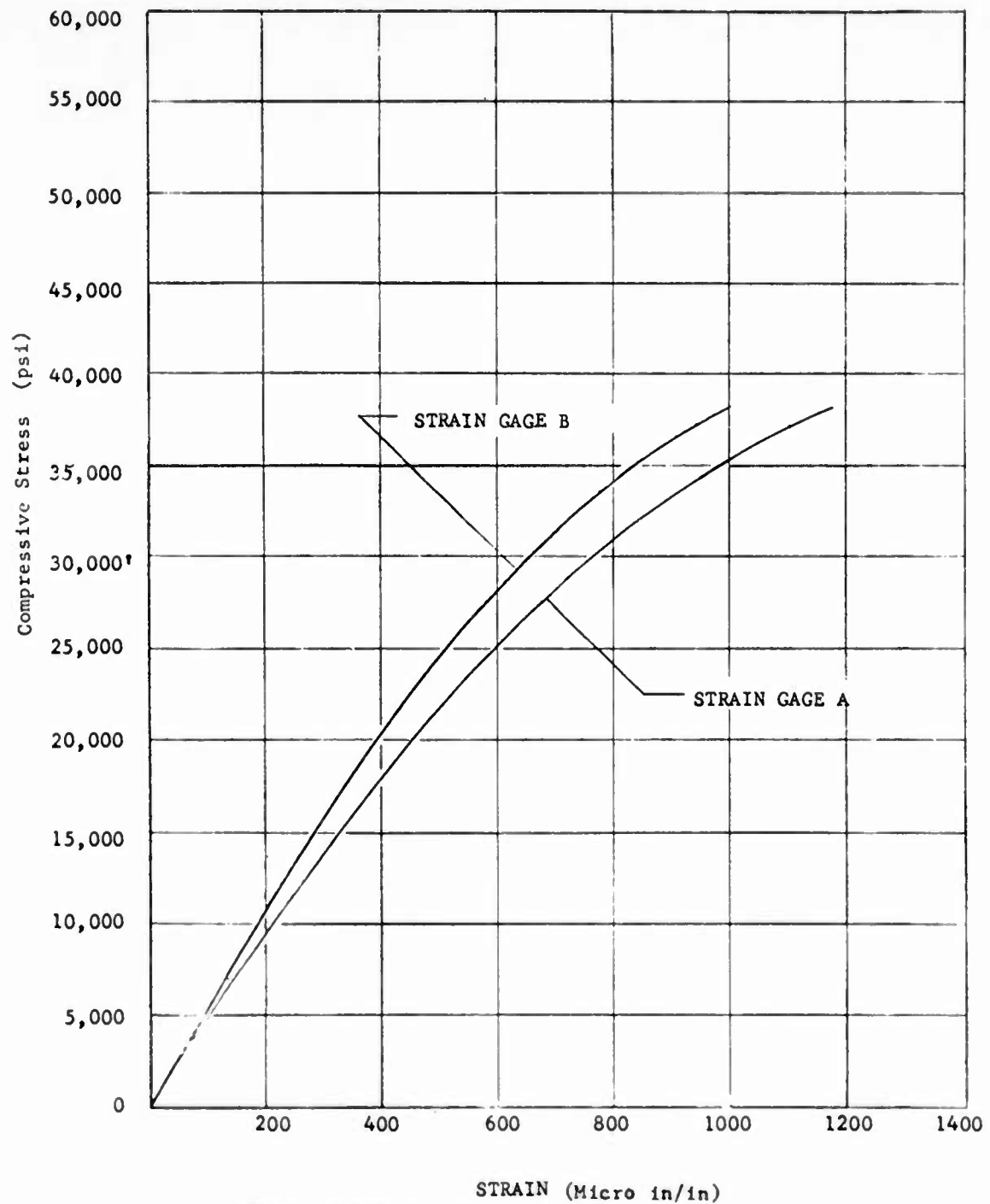


Figure IV-22 Beryllium Sheet Compression Test (Sample #2)

ROOM TEMPERATURE      NOMINAL THICKNESS .060"

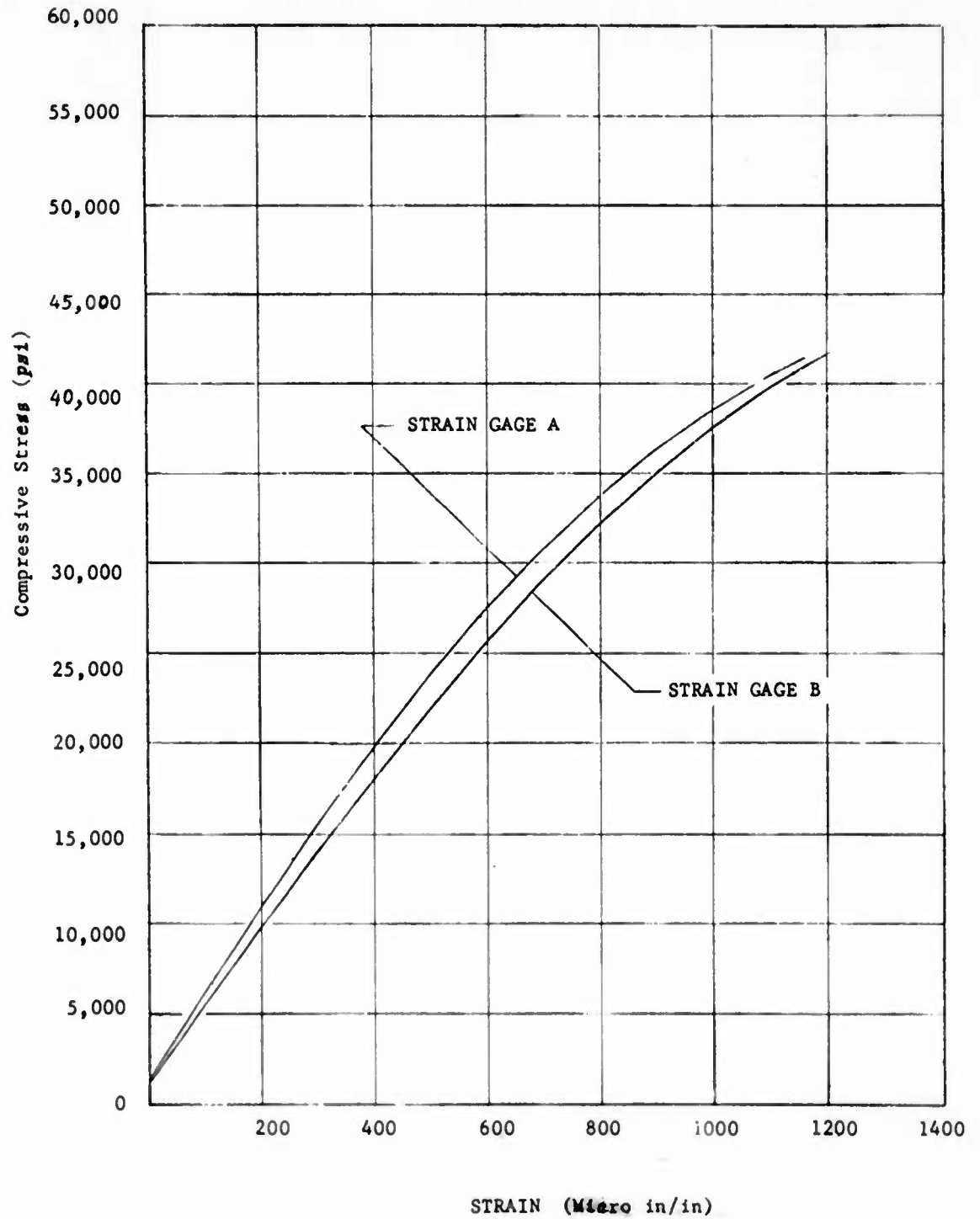


Figure IV-23 Beryllium Sheet Compression Test (Sample #6)

ROOM TEMPERATURE      NOMINAL THICKNESS .020"

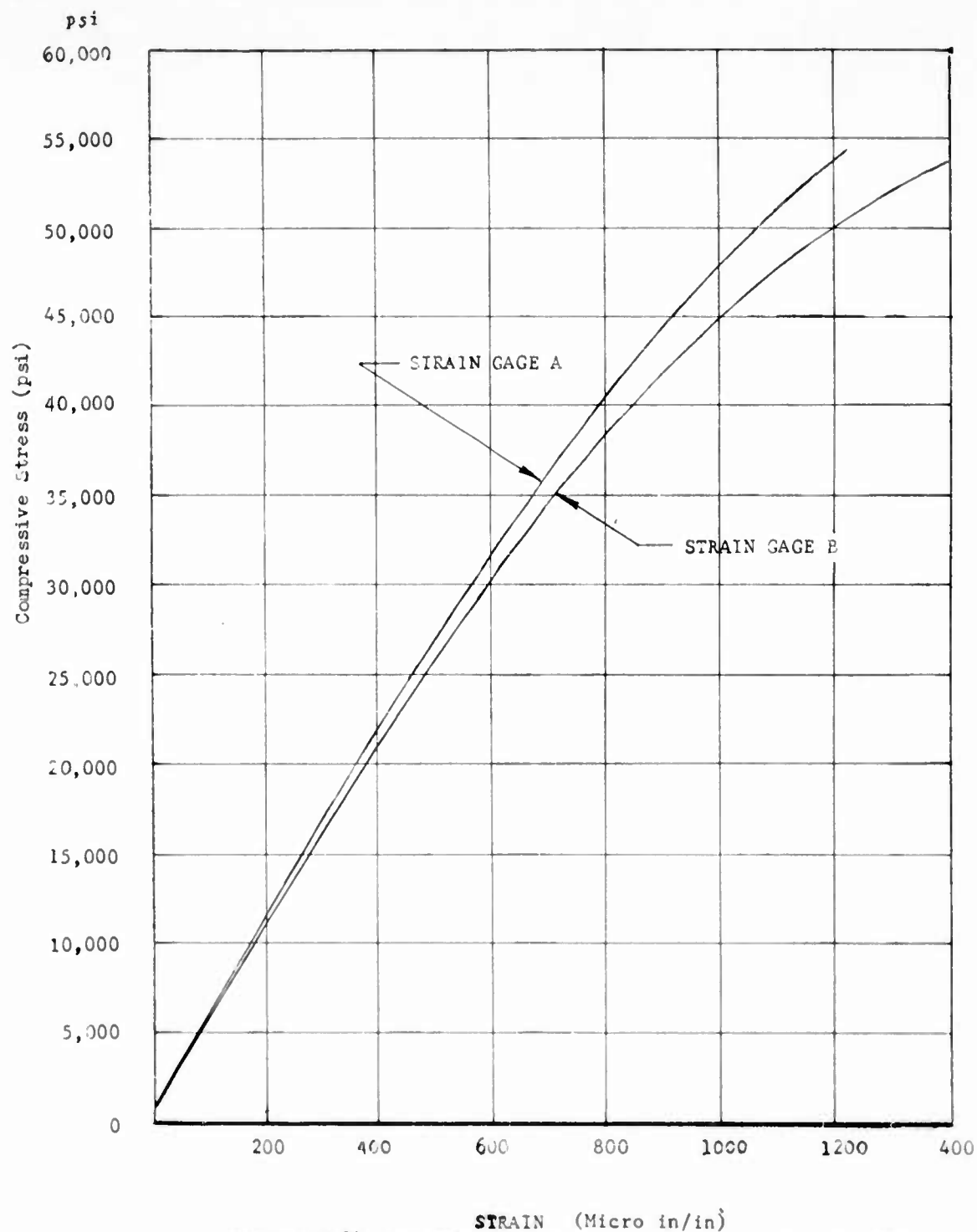


Figure IV-24 Beryllium Sheet Compression Test (Sample #7)

ROOM TEMPERATURE

NOMINAL THICKNESS .020"

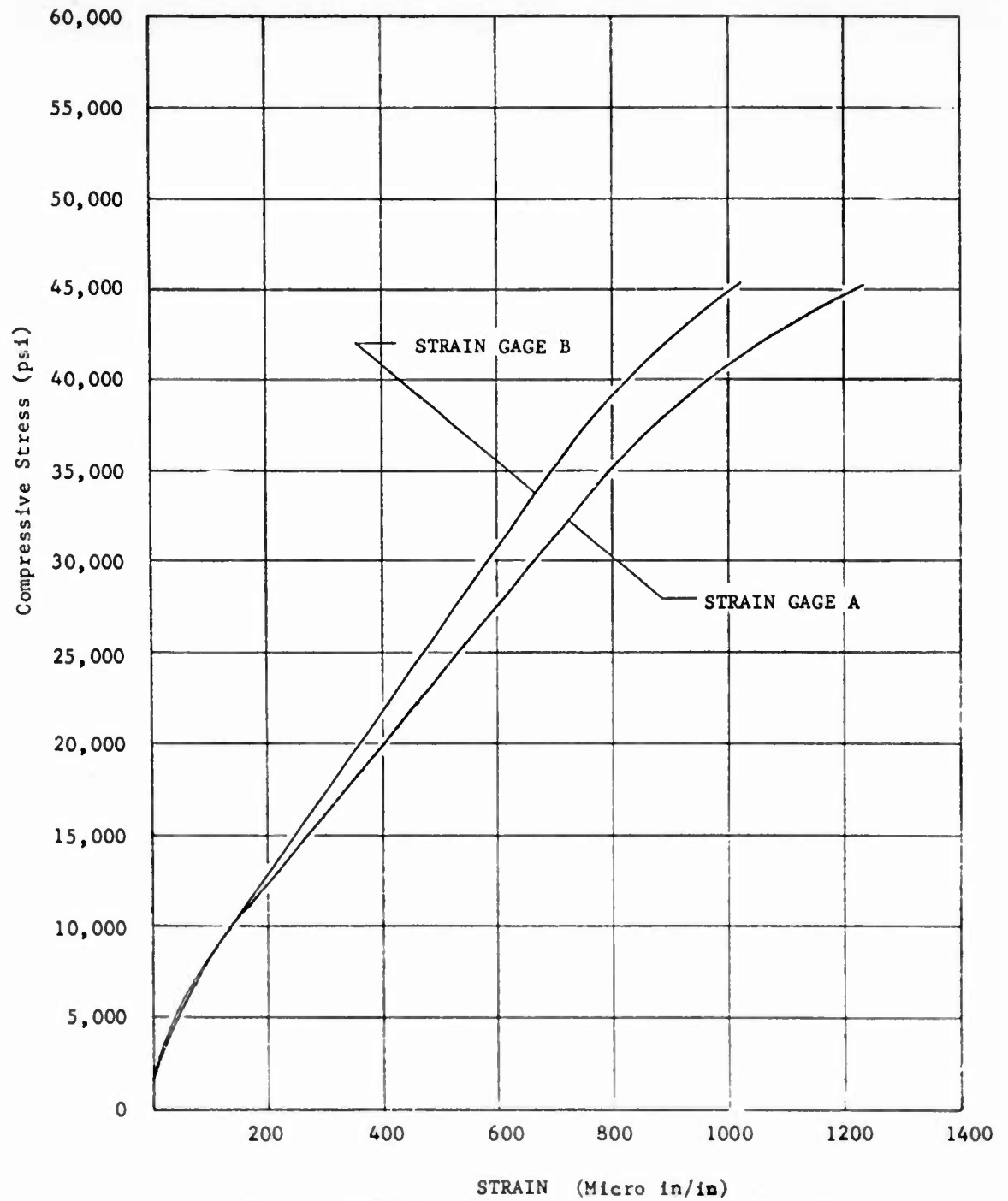


Figure IV25 Beryllium Sheet Compression Test (Sample #8)

ROOM TEMPERATURE      NOMINAL THICKNESS .040"

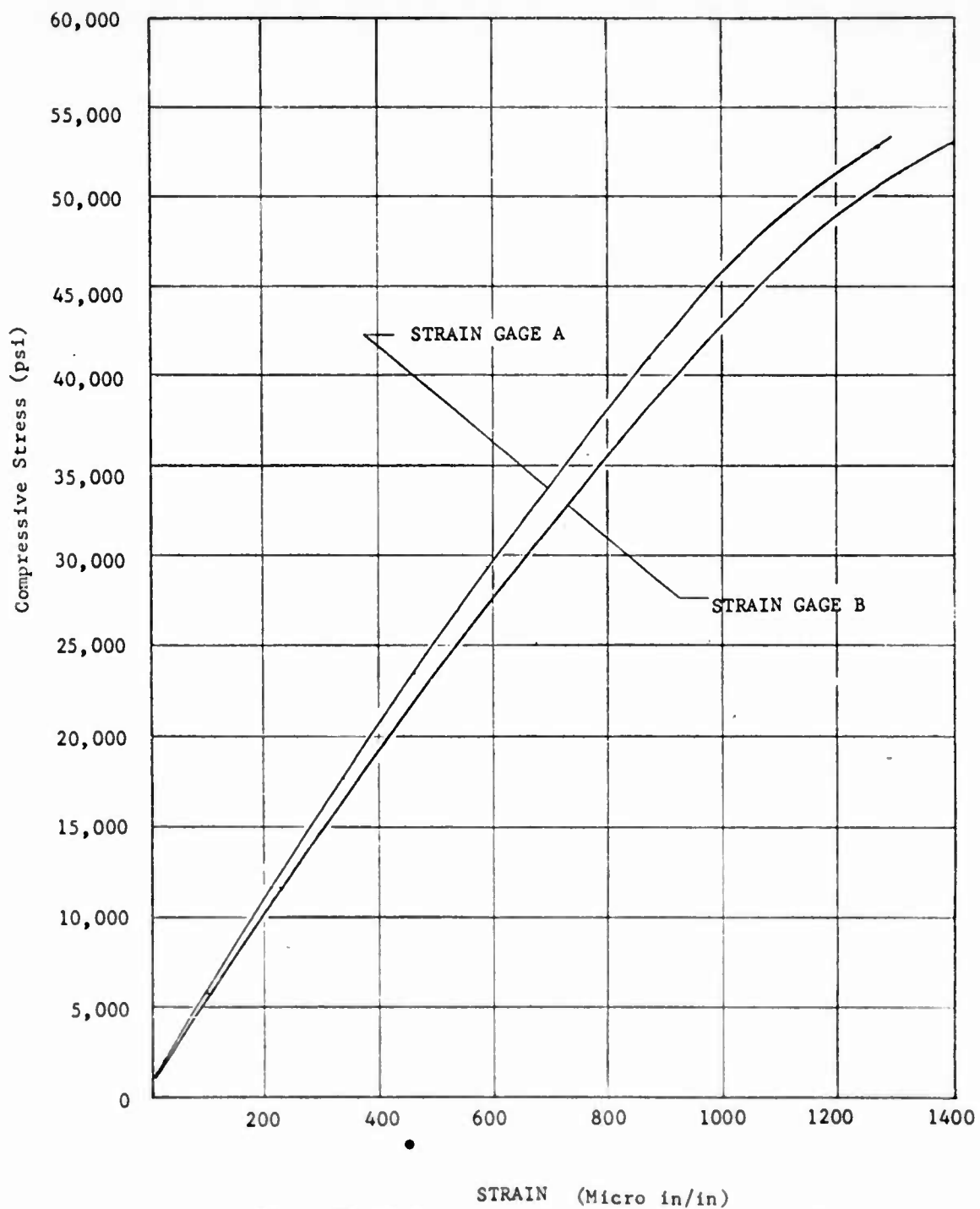


Figure IV-26 Beryllium Sheet Compression Test (Sample #9)

ROOM TEMPERATURE

NOMINAL THICKNESS .040"

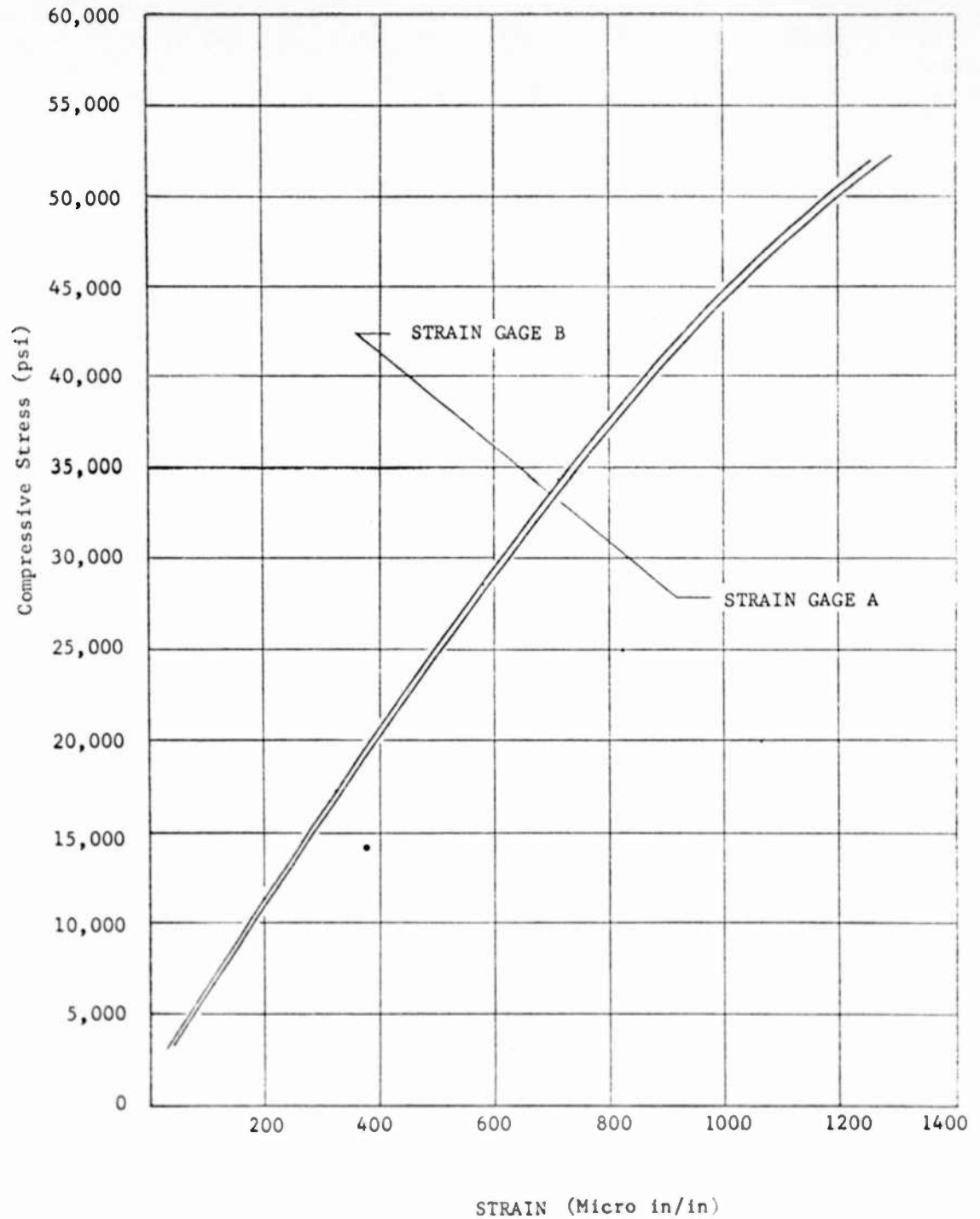
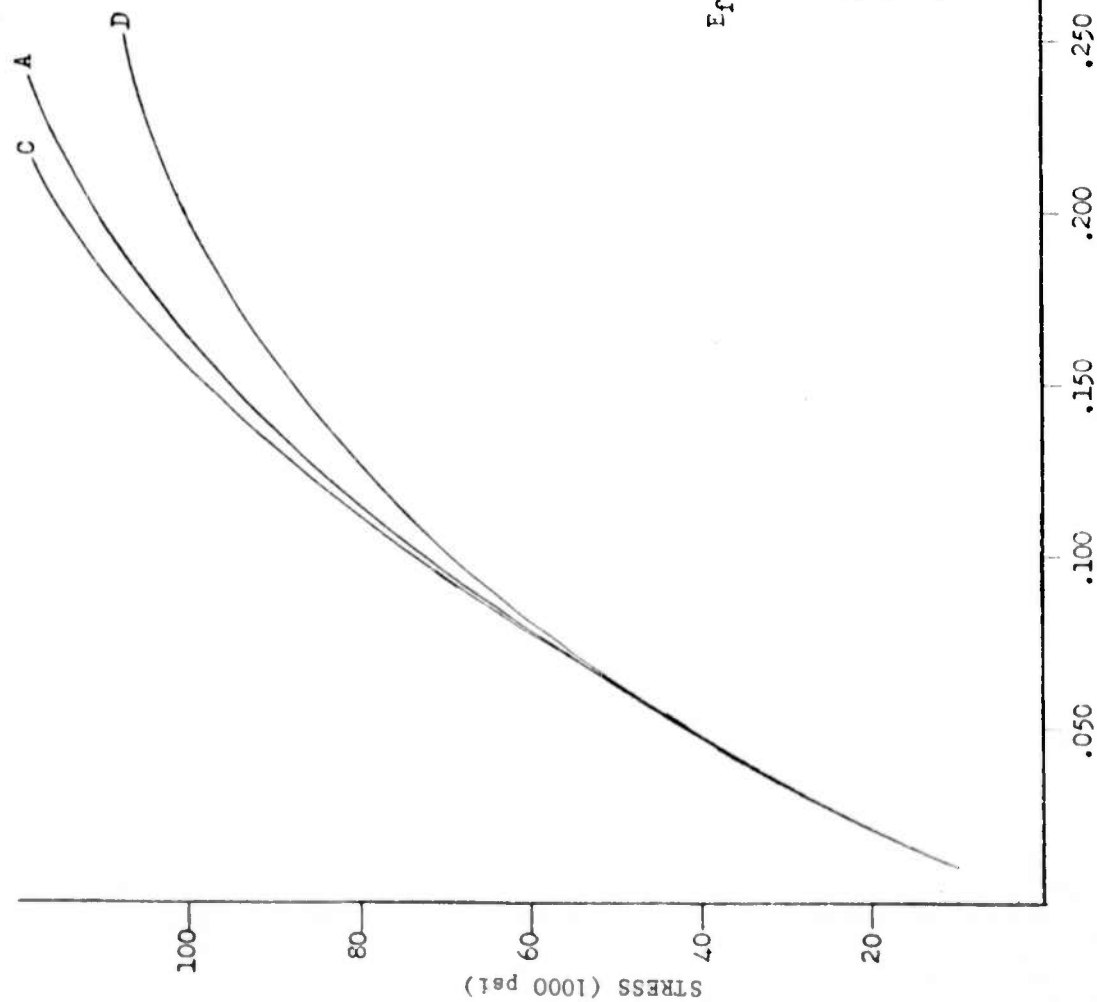


Figure IV-27 Beryllium Sheet Compression Test (Sample #10)

TABLE IV -10  
COMPRESSIVE MODULUS OF ELASTICITY AND 0.02% YIELD POINT FOR  
SHEET BERYLLIUM AT ROOM TEMPERATURE

<u>Specimen Number</u>	<u>Nominal Specimen Thickness (Inches)</u>	<u>Compressive Modulus of Elasticity (psi)</u>	<u>Compressive 0.02% Yield Point (psi)</u>
1	0.060	$41 \times 10^6$	40,000
2	0.060	$47 \times 10^6$	38,000
6	0.060	$45 \times 10^6$	39,000
7	0.020	$50 \times 10^6$	52,000
8	0.020	$50 \times 10^6$	49,000
9	0.040	$47 \times 10^6$	52,000
10	0.040	$46 \times 10^6$	52,000



A = SPECIMEN TESTED AS MACHINED

C = MACHINING DAMAGE REMOVED BY  
MECHANICALLY POLISHING

D = SPECIMEN MACHINED AND SUBJECTED  
TO SIMULATED BRAZE THERMAL  
CYCLE ( 1 MINUTE AT 1750°F. )

$$E_f = \frac{4P}{3\delta} \approx 55 \times 10^6$$

(IN ELASTIC REGION)

$$\delta = \frac{5P}{6EI}$$

$$E = \frac{5P}{6\delta I}$$

$$\delta = \frac{4P}{3EI}$$

DEFLECTION (INCHES)

Figure IV-28 Cantilever Bend Test of Beryllium Sheet

d. Lap Shear Properties

Several attempts were made to determine the lap shear properties of beryllium sheet brazed with silver-copper-lithium alloy. However, due to the strength of the minimum area of braze that could be fabricated, the total load required to shear the braze exceeded the tensile strength of the beryllium.

2. Mechanical Properties of Beryllium-faced Sandwich Structures

a. Compatibility of Materials

Various combinations of core and brazing alloys were evaluated for compatibility with beryllium sheet in the fabrication of sandwich panels. Among the core materials evaluated were:

321 Stainless Steel  
L-605  
Inconel  
A-286.

The brazing alloys evaluated included:

Silver-Copper-Lithium  
Silver - Copper (BT-Li)  
1-4-1  
1-6-1.

The brazing procedures are explained in Section V of this report. Compositions of the various braze alloys are listed in Table IV -11.

Metallographic examinations of the braze areas of the various alloys have shown that the silver-copper-lithium braze alloy is best suited for use with beryllium.

Of the other three alloys, BT-Li was rejected for lack of penetration into the beryllium and the high copper content of the alloy. The alloys 1-4-1 and 1-6-1 were discarded because their higher brazing temperatures caused recrystallization of the beryllium.

In conjunction with these examinations, it was found that three of the core materials (321 stainless steel, Inconel and A-286) developed satisfactory brazes with the silver-copper-lithium alloy. The L-605 core did not develop proper filleting and under metallographic examination did not appear to have developed an acceptable metallurgical bond. A typical satisfactory braze is shown in Figure IV-29 (321 stainless steel core and silver-copper-lithium braze alloy). The degree of silver penetration into the beryllium is acceptable and recrystallization seems to be kept to a minimum.

b. Flatwise Tensile Properties

Flatwise tensile tests were run to determine the mechanical properties of the various material combinations used in fabrication of the honeycomb panels mentioned above.

TABLE IV-11  
COMPOSITION OF BRAZING ALLOYS

<u>Brazing Alloy</u>	<u>Compositions (% by wt.)</u>	<u>Brazing Tem. (°F.)</u>
Silver-copper-lithium	Ag-92.8; Cu-7; Li-0.2	1680
Silver-copper (BT-Li)	Ag-72; Cu-27.5; Li-0.5	1500
1-4-1	Four parts fine silver cladded with one part thickness on each side of silver-copper-lithium alloy.	1720
1-6-1	Six parts fine silver cladded with one part thickness on each side of silver-copper-lithium alloy.	1750

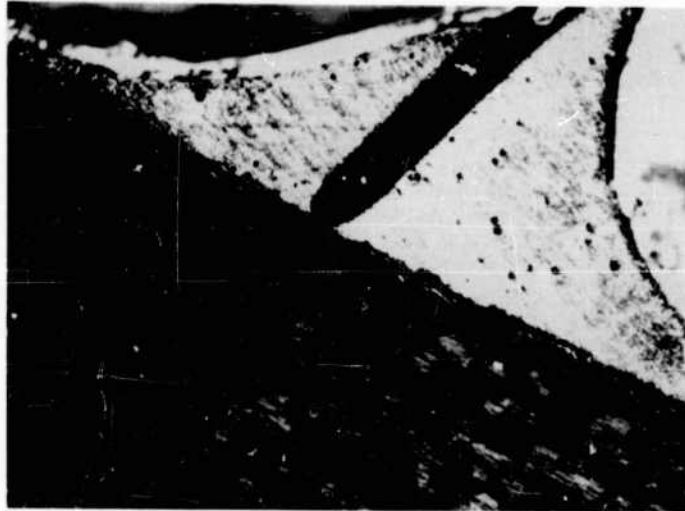


Figure IV-29 Braze Area of Honeycomb Panel -  
Beryllium Faces, 321 Stainless Steel Core and  
Silver-Copper-Lithium Braze Alloy

These tests were run at room temperature in accordance with paragraph 5.2.3 of Mil-Std.-401A (15 June, 1956).

The results are listed in Table IV-12. Specimens number 31, 32, 33 and 34 were fabricated from 17-7 PH faces and core as control specimens for a basis of comparison for the beryllium faced honeycomb structures. The strength of the beryllium faced structures with Inconel and A-286 core compare with the strength of the steel structure. Of the two, Inconel and A-286, A-286 appears slightly superior in mechanical properties when allowance is made, in interpreting the test results, for the difference of the core foil thickness. Typical failed specimens are shown in Figure IV-30.

c. Edgewise Compressive Properties

Edgewise compressive tests were run on sample panels having beryllium faces and A-286 core. The tests were conducted at room temperature, 600° F. and 1000 ° F. The test procedure was in accordance with Mil-Std.-401A, (15 June, 1956) paragraph 5.2.1.

The results are listed in Table IV-13. In five of the eighteen tests, eccentricity of loading was present and the results of these tests are not considered valid. In the remaining tests, it can be seen by the compressive stress in the faces at time of failure that the strength of the beryllium was not impaired by the braze alloy or process. The failure stresses listed agree favorably with the predicted load carrying capability of the beryllium.

d. Core Shear Properties

Core shear tests were run on honeycomb panels having beryllium faces and A-286 core of two foil thicknesses. The specimens were bonded to test fixtures and tested in accordance with paragraph 5.2.3 and 5.1.5 of Mil-Std.-401A. Figure IV-31 shows a specimen mounted in the test machine.

The test results are tabulated in Table IV-14. It should be noted that all the failures occurred in the core, indicating satisfactory brazing.

e. Sandwich Flexure Properties

Sandwich flexure tests were conducted using four point loading in accordance with paragraph 5.2.4 of Mil-Std.-401A. However, all failures occurred as core shear rather than flexural. Numerous variations of specimen configurations were tried unsuccessfully. Among these were decreasing the face thickness, decreasing the core height, increasing the core density, increasing the specimen length, and combinations of these factors. None of these variations gave a successful test. Table IV-15 contains a description of each of the test specimens and the test results.

TABLE IV-12

FLATWISE TENSILE TEST RESULTS  
HONEYCOMB STRUCTURE

(All specimens: 2" x 2" area; 1/4" core cell; 1/2" core thickness)

SPECIMEN NUMBER	BRAZE ALLOY	FACE - MAT'L.	GAGE THICK.	CORE MAT'L.	GAGE THICK.	RUPTURE LOCATION	RUPTURE LOAD, LBS.
31	AgCuLi	17-7PH	- 0.060	17-7PH	- 0.0020	Core & Braze	3500
32	B.T.	17-7PH	- 0.060	17-7PH	- 0.0020	Core & Braze	2580
33	1-6-1	17-7PH	- 0.060	17-7PH	- 0.0020	Core	4080
34	1-4-1	17-7PH	- 0.060	17-7PH	- 0.0020	Core & Braze	3610
25	AgCuLi	Be	- 0.060	321SS	- 0.0020	Braze	1530
39D	AgCuLi	Be	- 0.060	321SS	- 0.0020	Braze	2260
66B	AgCuLi	Be	- 0.018	321SS	- 0.0020	Braze	2450
2G	AgCuLi	Be	- 0.060	L-605	- 0.0020	Braze	3900
39A	AgCuLi	Be	- 0.060	L-605	- 0.0020	Braze	640
27	AgCuLi	Be	- 0.060	Inconel	- 0.0015	Braze	1680
28	AgCuLi	Be	- 0.060	Inconel	- 0.0015	Core & Braze	2400
39B	AgCuLi	Be	- 0.060	Inconel	- 0.0015	Core	2570
39C	AgCuLi	Be	- 0.060	A-286	- 0.0030	Braze	5140
65A	AgCuLi	Be	- 0.020	A-286	- 0.0030	Braze	5450
69A	AgCuLi	Be	- 0.020	A-286	- 0.0030	Braze	5250
63C	AgCuLi	Be	- 0.015	A-286	- 0.0030	Braze	4335
29	B.T.	Be	- 0.060	321SS	- 0.0020	Braze	2600
38D	1-6-1	Be	- 0.060	321SS	- 0.0020	Core & Braze	3190
41D	1-6-1	Be	- 0.060	321SS	- 0.0020	Braze	3250
41A	1-6-1	Be	- 0.060	L-605	- 0.0020	Braze	4500
38B	1-6-1	Be	- 0.060	Inconel	- 0.0015	Braze	1320
41B	1-6-1	Be	- 0.060	Inconel	- 0.0015	Core	2950
38C	1-6-1	Be	- 0.060	A-286	- 0.0030	Core & Braze	3410
41C	1-6-1	Be	- 0.060	A-286	- 0.0030	Braze	5320
35	1-4-1	Be	- 0.060	321SS	- 0.0020	Braze	2410
40D	1-4-1	Be	- 0.060	321SS	- 0.0020	Braze	3560
37	1-4-1	Be	- 0.060	L-605	- 0.0020	Braze	3200
40A	1-4-1	Be	- 0.060	L-605	- 0.0020	Braze	2280
36	1-4-1	Be	- 0.060	Inconel	- 0.0015	Core	1800
40B	1-4-1	Be	- 0.060	Inconel	- 0.0015	Core	3000
40C	1-4-1	Be	- 0.060	A-286	- 0.0030	Braze	4020

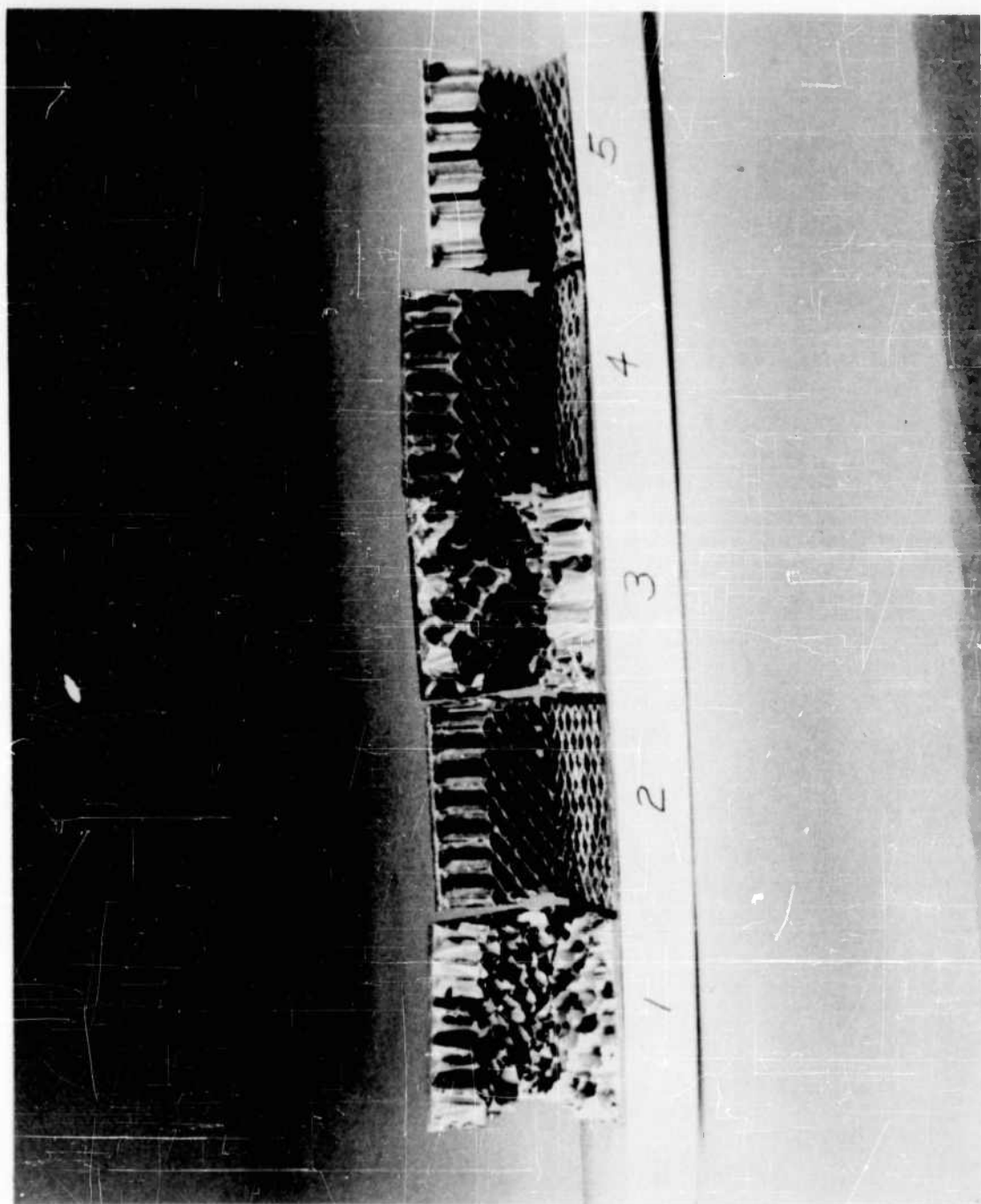


Figure IV-30 Failed Flatwise Tensile Specimens

TABLE IV-13

EDGEWISE COMPRESSIVE TESTS OF BERYLLIUM HONEYCOMB PANELS

Sample No.	Skin Thick. (in.)	Core(1)	Temp. (°F.)	Cross Section Area (Skins, In. <sup>2</sup> )	Load (lbs)	PSI
72-1	.040	A-286	RT	.162	6910	42,750 **
72-2	.040	A-286	RT	.167	12300	73,750 *
72-3	.040	A-286	RT	.165	11200	68,000 *
72-4	.040	A-286	600	.165	7100	43,050 *
72-5	.040	A-286	600	.162	4770	29,420 **
72-6	.040	A-286	600	.164	7650	46,650 *
72-7	.040	A-286	1000	.165	4860	29,430 **
72-8	.040	A-286	1000	.166	5680	34,300 *
72-9	.040	A-286	1000	.163	5000	30,700 *
73	.020	A-286	RT	.081	3500	43,150 **
73	.020	A-286	RT	.080	4730	59,100 *
68	.020	A-286	RT	.079	4750	59,950 *
73	.020	A-286	600	.079	3120	39,500 *
51	.020	A-286	600	.079	4520	57,250 *
45	.020	A-286	600	.081	2400	29,700 **
61	.020	A-286	1000	.078	2515	32,200 *
73	.020	A-286	1000	.083	2410	30,250 *
73	.020	A-286	1000	.080	2610	32,600 *

\* Both skins failed outward.

\*\* Skins failed in same direction because of specimen misalignment.

(1) Honeycomb Core 0.003 thickness,  $\frac{1}{2}$ " square cells,  $\frac{1}{2}$ " high.

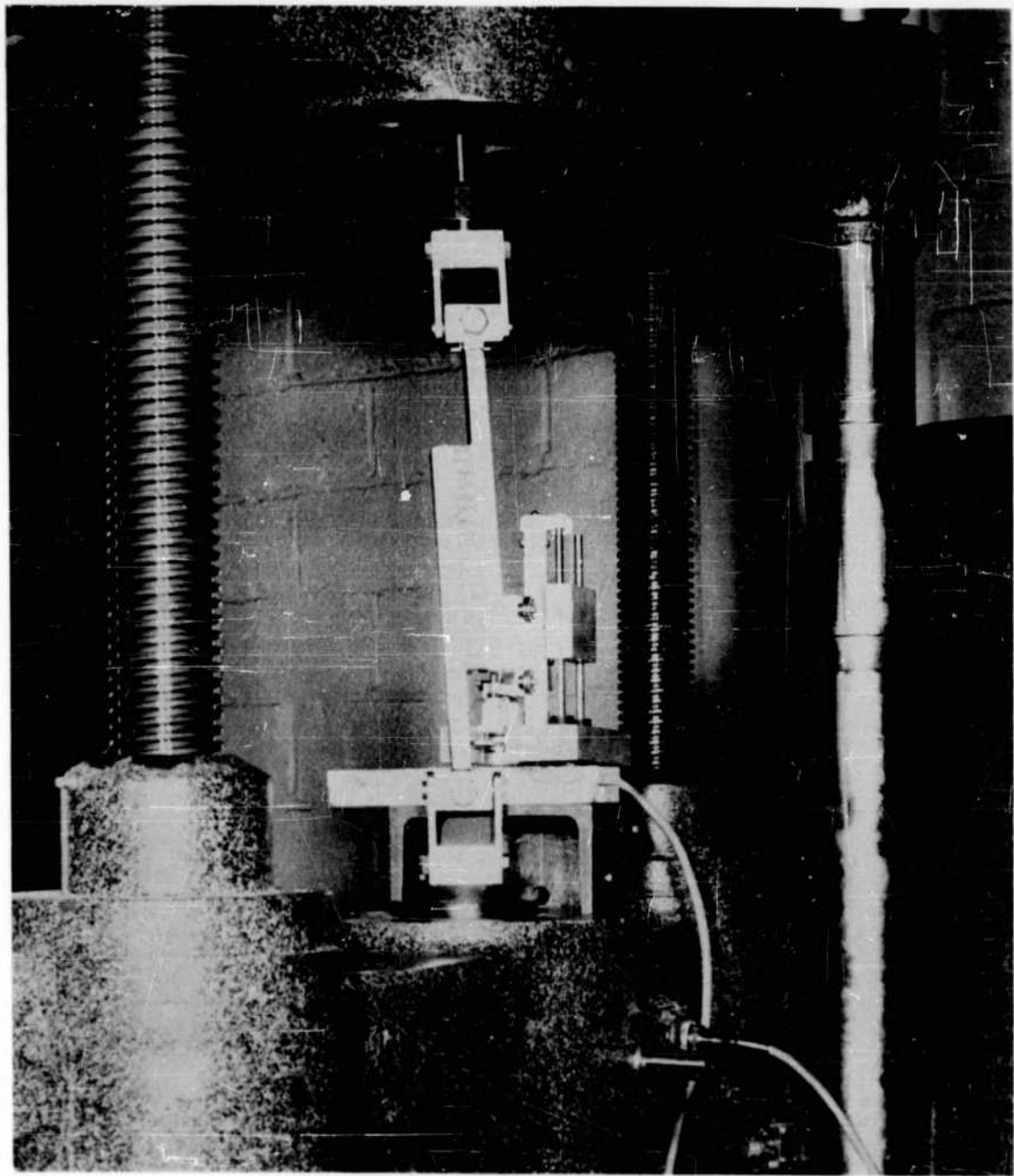


Figure IV-31 Core Shear Specimen under Test

TABLE IV-14  
CORE SHEAR TEST RESULTS

Test No.	Dimensions (in.)	Braze Alloy	Core Alloy	Honeycomb Core				Face Thickness (in.)	Face Mat'l	Face Thickness (in.)	Shear Stress (psi)	Failure Location
				Cell Size (in.)	Core Thickness (in.)	Foil Thickness (in.)						
1	6 x 1.5	Ag+Cu+Li	A-286	$\frac{1}{4}$	$\frac{1}{2}$	0.0030		0.040	Be	0.040	517	Core
2	6 x 1.5	Ag+Cu+Li	A-286	$\frac{1}{4}$	$\frac{1}{2}$	0.0030		0.040	Be	0.040	498	Core
3	6 x 1.5	Ag+Cu+Li	A-286	$\frac{1}{4}$	$\frac{1}{2}$	0.0030		0.040	Be	0.040	484	Core
4	6 x 1.5	Ag+Cu+Li	A-286	$\frac{1}{4}$	$\frac{1}{2}$	0.0015		0.032	Be	0.032	180	Core
5	6 x 1.5	Ag+Cu+Li	A-286	$\frac{1}{4}$	$\frac{1}{2}$	0.0015		0.032	Be	0.032	172	Core
6	6 x 1.5	Ag+Cu+Li	A-286	$\frac{1}{4}$	$\frac{1}{2}$	0.0015		0.032	Be	0.032	164	Core
7	6 x 1.5	Ag+Cu+Li	A-286	$\frac{1}{4}$	$\frac{1}{2}$	0.0015		0.032	Be	0.032	176	Core

TABLE IV-15

## FLEXURE TESTS OF BERYLLIUM-FACED HONEYCOMB STRUCTURES

Sample No.	Skin Thick. (in.)	Core	Core Height (in.)	Cell Size (in.)	Width (in.)	Temp. °F.	Load lbs.
75-2	.040	A-286	.5	$\frac{1}{2}$	1.5	RT	875
74-1	.040	A-286	.5	$\frac{1}{2}$	1.5	RT	655
75-1	.040	A-286	.5	$\frac{1}{2}$	1.5	600	800
74-2	.040	A-286	.5	$\frac{1}{2}$	1.5	600	862
75-3	.040	A-286	.5	$\frac{1}{2}$	1.5	1000	719
74-3	.040	A-286	.5	$\frac{1}{2}$	1.5	1000	805
80-1	.035	A-286	.5	$\frac{1}{2}$	1.5	RT	520
80-2	.035	A-286	.5	$\frac{1}{2}$	1.5	RT	520
80-3	.035	A-286	.5	$\frac{1}{2}$	1.5	600	500
80-4	.035	A-286	.5	$\frac{1}{2}$	1.5	1000	452
79-1	.032	A-286	.5	$\frac{1}{2}$	1.5	RT	400
78-1	.032	A-286	.5	$\frac{1}{2}$	1.5	RT	330
76-1	.032	A-286	.5	$\frac{1}{2}$	1.5	RT	600
76-2	.032	A-286	.5	$\frac{1}{2}$	1.5	600	480
76-3	.032	A-286	.5	$\frac{1}{2}$	1.5	600	508
76-4	.032	A-286	.5	$\frac{1}{2}$	1.5	600	444
77-1	.032	A-286	.5	$\frac{1}{2}$	1.5	1000	466
77-2	.032	A-286	.5	$\frac{1}{2}$	1.5	1000	540
79-2	.032	A-286	.5	$\frac{1}{2}$	1.5	1000	430
90	.033	A-286	.5	$\frac{1}{2}$	1.75	RT	227
91	.017	A-286	.5	$\frac{1}{2}$	1.0	RT	208
92	.030	17-7PH	.25	3/16	2.25	RT	650
97A <sub>1</sub>	.040	A-286	.5	$\frac{1}{2}$	1.30	RT	268
97A <sub>2</sub>	.040	A-286	.5	$\frac{1}{2}$	1.30	RT	320

- NOTES: 1. All specimens failed in core shear rather than flexure.
2. Core foil thickness .0015 inch except samples No. 74 and 75 which were .003 inch.
3. All tests run on four point loading on a span of 2" over 4" except samples No. 90, 91 and 92 which used a span of 3" over 6" and samples 97A<sub>1</sub> and 97A<sub>2</sub> which used a span of 8" over 16".

## SECTION V

### BERYLLIUM FABRICATION DEVELOPMENT

#### A. INTRODUCTION

As a result of this contract, substantial effort has been expended in the development of specialized beryllium fabrication techniques. This began with elemental processes such as cutting, and led to more sophisticated work such as the brazing of beryllium faced honeycomb panels. This development work has largely overcome the fabrication difficulties of the material and it is now possible to construct comparatively complex shapes.

Machining, forming and brazing of beryllium sheet have become routine operations at Aeronca. In the machining development work satisfactory methods of sawing, routing, grinding, sanding and filing were determined. Work was also successfully done in the field of chemical etching and chemical milling where efforts were concentrated in development of etchants and maskants compatible with beryllium.

In addition to machining, forming techniques were developed for angles, channels and single and double curved shapes using heated dies.

Brazed honeycomb sandwich panels with beryllium face sheets, including double curvature sections, were developed on this program. Silver-copper-lithium foil was used as the brazing alloy, and steel and nickel based high temperature alloys were used as the honeycomb cores. Three brazing methods utilizing very fast heating were developed. These were the quartz lamp method, the electric blanket method utilizing Glasrock dies, and the furnace method. All three methods were used with good results. Braze quality was found to be compatible with the fully developed strength of the core and face materials.

The above development work did much to narrow the gap between laboratory experimental samples and practical structural parts. Beryllium is now a good candidate for secondary structural applications, such as equipment mounts, brackets and special devices where stiffness and weight are prime factors, as well as for many primary structural applications.

#### B. MACHINING

Special techniques are required for the machining of beryllium because of its extreme brittleness and high notch sensitivity. Care must be exercised during machining because grain damage in the form of twinning may result. Tools must be designed to withstand the abrasive characteristic of the material. Proper safety precautions such as the use of dust masks and ventilating equipment are necessary because the metal is toxic in dust form.

## 1. Sawing

It is necessary to firmly support the edge of the beryllium sheet while sawing to prevent chipping or cracking. Clamping the sheet between heavy steel bars and sawing along one face of this clamp works satisfactorily for material .040 to .060 in. thick. Best results are obtained in gages .032 in. or less by sandwiching the beryllium sheet between sheets of aluminum before clamping and cutting the aluminum with the beryllium. The harder aluminum alloys such as 2024 and 7075 are most desirable for this purpose since the softer alloys tend to clog the saw blade. Thickness of these aluminum sheets need not exceed .020 inch. Brazed honeycomb panels with beryllium faces .032 to .060 in. thick can be cut without clamping because of the edge support given by the core. Panels with face gages of .025 in. or thinner tend to chip, however, and should be cut by routing.

The best saw blade is a 24 tooth,  $\frac{1}{8}$  inch regular blade for sawing all gages of beryllium sheet. A  $\frac{1}{8}$  inch blade is adequate for .025 inch and thinner gage material because of the relatively light pressure needed to push the work through. A blade speed of 900 feet per minute is used because it cuts most easily and still does not subject the edge of the sheet to excessive grain damage. At this speed, some metallographic samples showed no grain damage while the maximum damage was limited to .005" deep in others. The stock is fed manually at a speed of approximately 50 inches per minute. Sawing of beryllium produces a heavy burr and a fairly rough edge which should be smoothed by filing or sanding. This operation is the fastest and cheapest, where close tolerances and very smooth edges are not required, and is limited to cutting out simple shapes.

Other methods of cutting beryllium sheet such as cold shearing and scribing and breaking along the scribed line only result in cracking and shattering of the sheet. Hot shearing, on the other hand, heating the beryllium sheet with a torch, appears to be a feasible approach.

## 2. Routing

Several types and sizes of router bits were tried with standard hand router mounted in a table and it was found that a carbide rotary file gave the best results and caused slight edge damage. The cutter used was a 3/16" diameter x 5/8" long, Style 41 rotary file, made by Metal Removal Company of Chicago. This tool gives a smooth edge with no subsequent finishing being necessary. Not much success has been obtained from completely routing a part from sheet stock, since the tool tends to heat up too quickly and thereby deteriorates rapidly.

Routing is most useful for trimming an irregularly shaped part to final size, where not more material is removed than approximately half the diameter of the router bit. For example, a procedure for the making of tensile specimens is: (1) masking and sulphuric acid chemical milling the specimen oversize with approximately 1/16 to 1/8 inch trim all around, (2) rotary file finishing, (3) electropolishing for removal of grain damage caused by rotary filing, which was found to vary from zero to .010 deep. This method results in specimens with the least amount of damage to the edge and gives very satisfactory results when tested in tension. Tests of 1 x 3 in. bend specimens made by rotary filing with or without subsequent electropolishing

indicated that edge treatments of the specimens do not significantly affect these test results. Tensile test specimens, however, with as-machined edges showed a 25%-30% reduction in ultimate tensile strength over those with the edge damage removed.

### 3. Chemical Milling

Chemical milling is a process by which metal is removed by its controlled dissolution into a chemical bath. The bath, in essence, is a highly refined pickling solution, with careful attention given to the rate of metal removed and the type of surface left after processing.

Chemical milling is particularly adaptable to the fabrication of various shapes from beryllium sheet where other types of machining would be either very difficult or expensive. The type of bath to be used depends, to a large extent, upon what is desired as a final part. For example, a 10% sulfuric acid bath is satisfactory where rapid removal of metal is desired and surface condition is not critical. This could be considered the chemical milling equivalent of a blanking operation.

The chemical milling solution developed for general applications is a mixture of phosphoric, sulfuric, and chromic acids in water. Approximately 0.0005 inch of beryllium can be removed in one minute at 110° to 120° F. A finishing solution of phosphoric and sulfuric acid in a mixture of glycerol and absolute ethanol is used to smoothen and brighten the surface of the part after it has been chemical milled to within tolerances. If the part is excessively rough, the bath may be used as an electropolishing solution. It gives excellent results, but allowances must be made to accommodate the slightly increased amount of metal removed.

Protection of areas not to be chemical milled is done by masking. Any material with good adhesion and chemical stability may be used. An example of this is chem-mil pressure sensitive tape, 3M-Y-9016, made by Minnesota Mining and Manufacturing Company.

These solutions have been developed to a point where it is possible to fabricate moderately complex parts. However, all the parameters, such as the rate of undercut versus the depth of cut, have not been fully investigated and additional evaluations of the solutions are needed to remove the processes from that of an art to the status of a consistent production tool.

### 4. Other Machining Operations

#### a. Sanding and Filing

A very smooth surface can be produced by hand sanding beryllium sheet with any type or grade of sandpaper. The edge of the beryllium sheet must be sandwiched between steel for support during belt or disc sanding, however, which works very well for smoothing the surface of beryllium sheet. All edges of sheet used for making test specimens and brazed panels should be sanded to remove burrs and saw marks for appearance as well as reduction of notch sensitivity.

Hand filing is being done, with no difficulty, on beryllium and is used mostly for deburring operations.

b. Grinding

Beryllium should be ground across the edge, rather than along the edge, because the beryllium tends to overheat too rapidly. Grinding across the edge helps the beryllium to dissipate the heat before the next pass is made. To support the edge of the sheet and prevent chipping and cracking, steel back-up is clamped rigidly to the beryllium and is ground with it. Aluminum is not satisfactory for back-up because it tends to clog the abrasive wheel. Varying the type of grinding wheels does not seem to have any more effect on beryllium than on any other hard metal. Grinding produces a smooth, notch-free surface and results in negligible edge damage when light cuts are taken. This process is useful in such applications as finishing the edges of test specimens where parallel surfaces to close tolerances are required.

c. Drilling

Drilling of very thin sheet (.020 in) sandwiched between aluminum resulted in severe cracking. Sandwiching and clamping of heavier gage beryllium sheet (.040 to .060 in) between steel sheets and drilling with a very sharp carbide drill at a low speed resulted in limited damage to the drilled surface.

C. FORMING

Because of the extreme brittleness of beryllium, it is necessary to form it at elevated temperature. An optimum forming temperature must be maintained to keep from cracking the beryllium, and to keep grain growth and grain damage to a minimum. Grain growth which has a detrimental effect on structural properties occurs at temperatures above 1500° F.

The basic method of forming beryllium consists of placing the work piece between heated dies and allowing the weight of the upper die to creep form the piece as it heats up from contact with the die. Angles and channels are made in brake forming dies, one bend at a time. After preheating the dies in a furnace to approximately 1500° F. they are removed and the beryllium work piece is inserted between the upper and lower dies. The upper die is rested on the work piece and as the beryllium is heated from contact with the die to its forming temperature (1370°-1500° F.), the weight of the upper die provides the forming pressure. This works satisfactorily for .020 in. thick sheet. For .040 to .060 in. sheet it may be necessary to do the forming in the furnace, because the mass of the dies may not hold enough heat to bring the beryllium up to temperature. Good results have been obtained by preheating the beryllium work piece as well as the die. Crack-free 90 degree bends with as low as 2.25 t bend radius were formed in the temperature range of 1200° F. to 1525° F., but the scrap rate was excessive.

More consistent results with little or no scrap can be achieved by limiting the bend radius to 3 or 4 t. It is difficult to hold close tolerances in forming channels by straight bends; therefore, it is necessary to hot size the channels to final dimensions. The hot sizing is done by forming the rough

channel around a mandrel by the weight of a preheated die in a manner similar to the original forming. Several channels, .62 in. deep x .44 in. flanges x 12 in. long, were formed with an .090 in. bend radius from .040 in. material and accurately sized by the above method (Figure V-1). Sheet can also be formed to simple curvatures using contoured male and female dies in a manner similar to that for angles or channels (Figure V-2). The faces for leading edge panels (Figure V-3) were formed by a mandrel rolling across a steel plate after the entire set-up was heated in a furnace to the forming temperature.

Another method of forming is by using contoured Glasrock dies. Heating elements are imbedded in the faces of each die. The dies are preheated to approximately 1500° F., the upper die is raised, the beryllium is inserted and is formed as it heats up by the weight of the die. Double curvature pieces were formed to a 16 inch spherical radius from .020 in. thick x 5½ in. square material (Figure V-2) and to a 36 inch spherical radius from .020 and .040 in. x 18 in. square material.

Photomicrographs of specimens formed at various temperatures showed that the optimum forming range was 1370° to 1500° F. In this range, no grain growth or grain damage occurred. Grain growth occurs above 1500° F. and grain damage in the form of twinning occurs below 1370° F.

#### D. BRAZING

At high temperatures beryllium is subject to excessive grain growth which causes a loss in strength of the material. This grain growth occurs appreciably when temperatures above 1500° F. are experienced for more than 5 minutes. Brazing temperatures, depending on the brazing alloy used, ranged from 1500° F. to 1750° F. To prevent grain growth during brazing it is desirable to utilize a method of heating and cooling the sandwich panels that will limit the exposure time above 1500° F. to 5 minutes or less.

Three methods of fast heating were used on the program: the quartz-lamp, electric blanket and furnace methods. A typical sequence of operations for the manufacture of brazed honeycomb sandwich panels by any of these methods is shown by Table V-1.

##### 1. Quartz-Lamp Brazing

Banks of quartz lamps were mounted in a framework (Figure V-4) for heating a retort containing a honeycomb sandwich panel. The retort was suspended in a vertical position from a dolly which ran in a track allowing the retort to be moved between the heat source and the quenching die. After a sufficient time at the desired brazing temperature, the panel was removed from the quartz lamps and placed between the two heavy steel platens and held by pneumatic pressure. The mass of these steel dies removed heat from the panel rapidly, acting as a quench. Also, the dies served to maintain flatness of the panel. Heating time above 1500° F. to braze temperature of the retorts with the quartz lamps varied from 30 to 60 seconds, depending on the size of the panel and the braze alloy used. Soak time at braze temperature, allowing for thorough heat penetration, varied from 30 to 60 seconds depending on the thickness of the beryllium faces and the brazing alloy used. Quenching time from braze temperature to 1500° F. was in the order of 15 to 20 seconds. In all cases, the total time the beryllium was exposed to temperatures higher than 1500° F. was well under the critical 5 minutes.

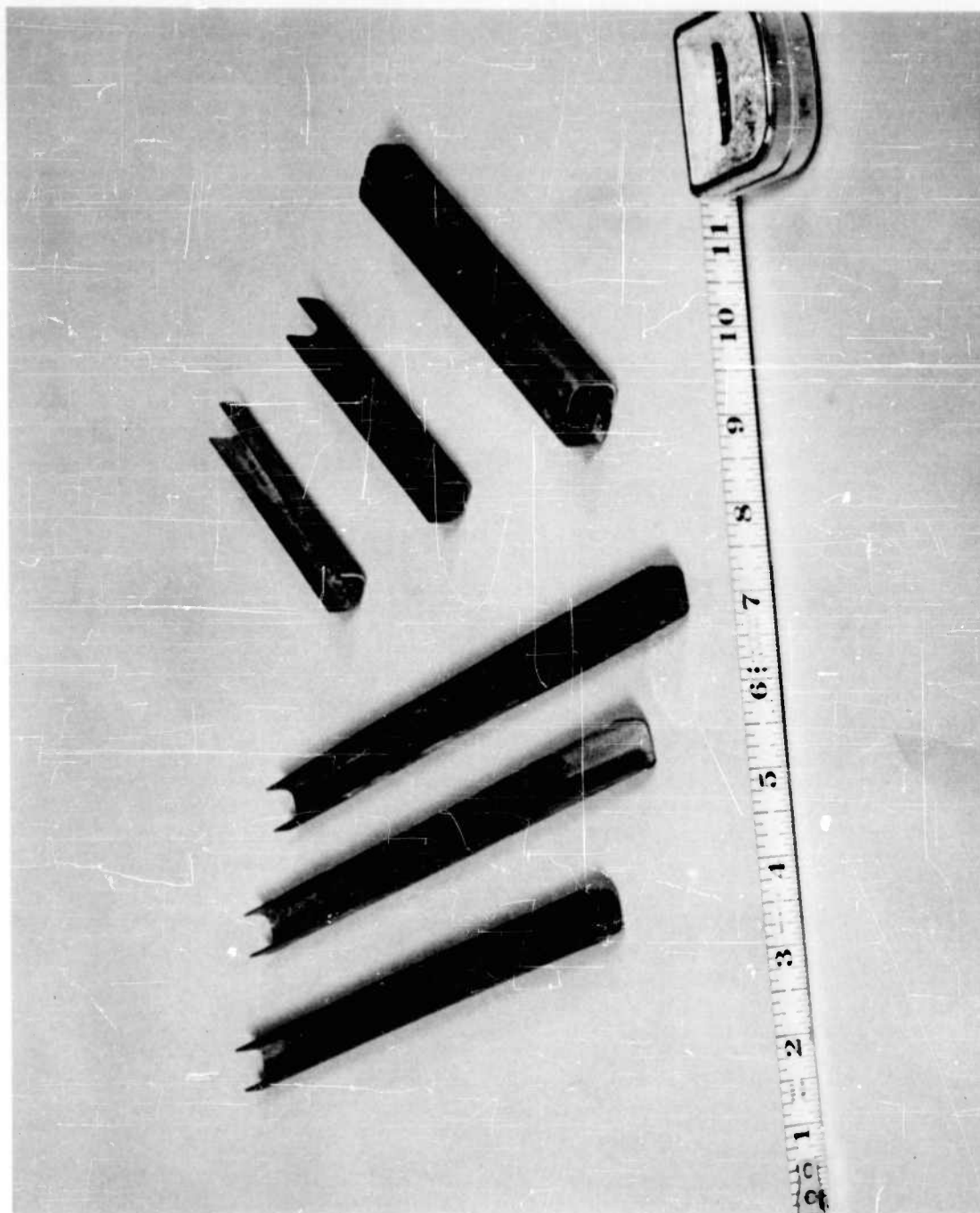


Figure V-1 Formed Beryllium Channels

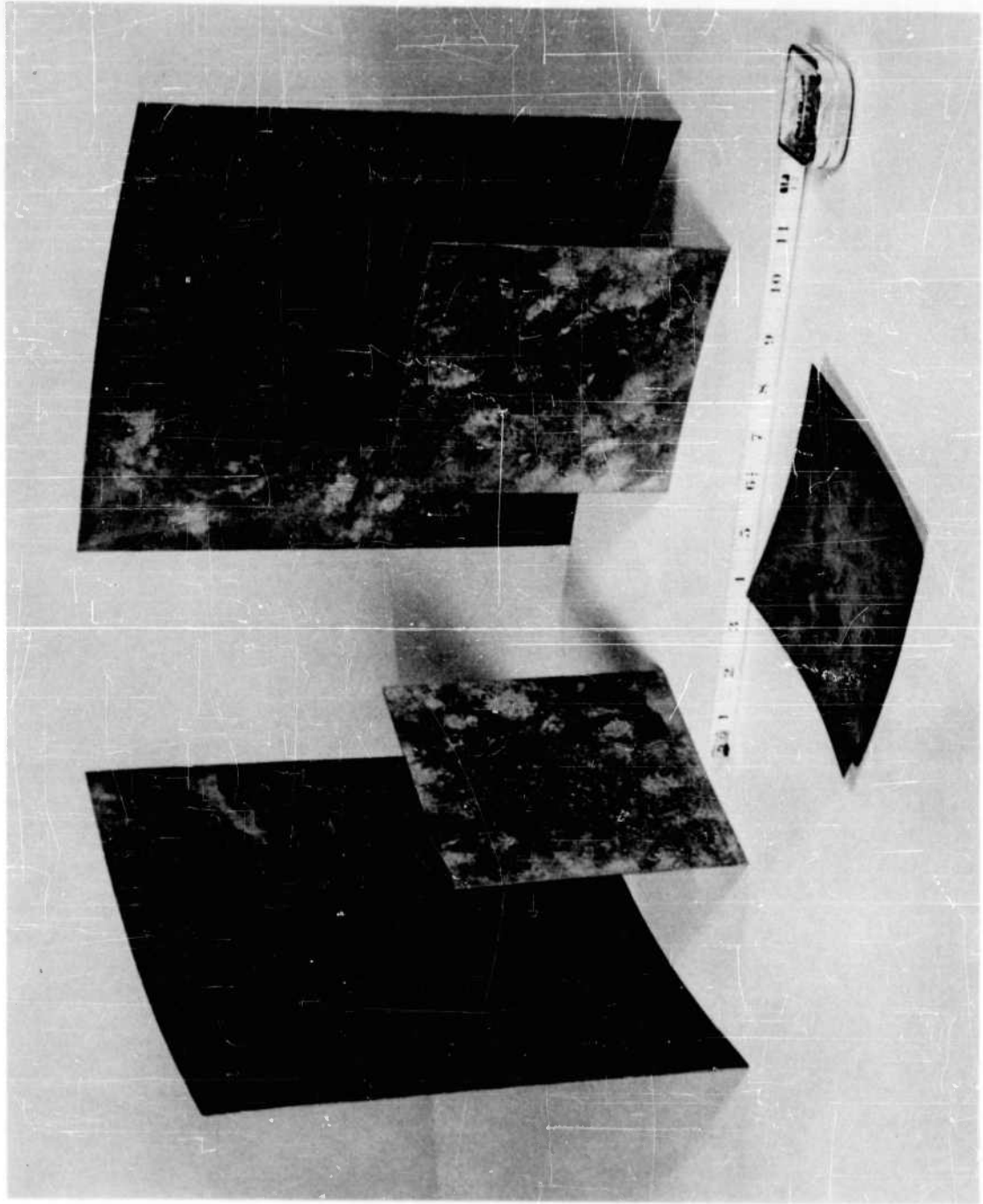


Figure V-2 Single and Double Curved Beryllium Skins

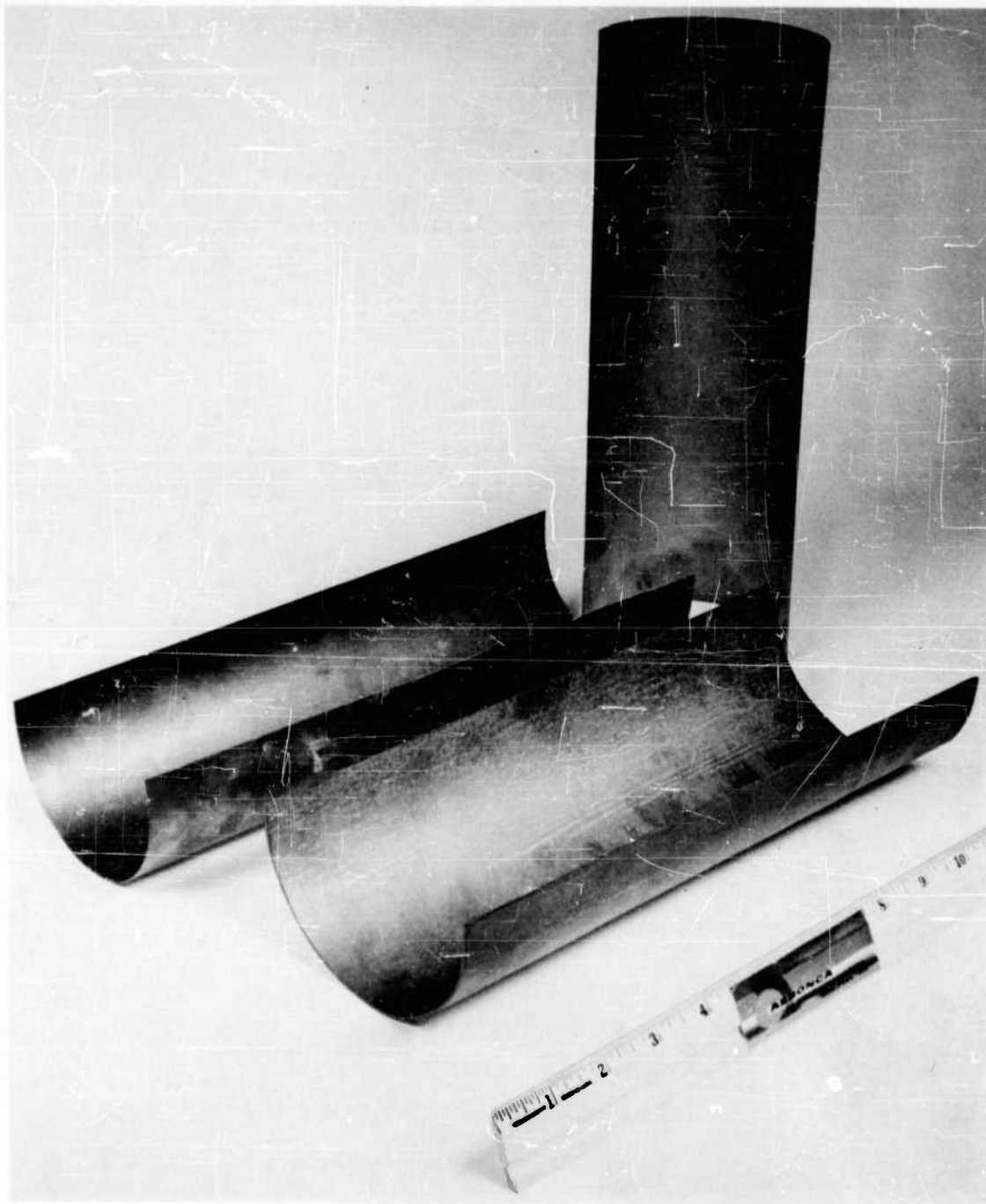


Figure V-3 Single Curved Beryllium Leading Edge Skins

Quartz Lamp - Die  
Quench Brazing  
System

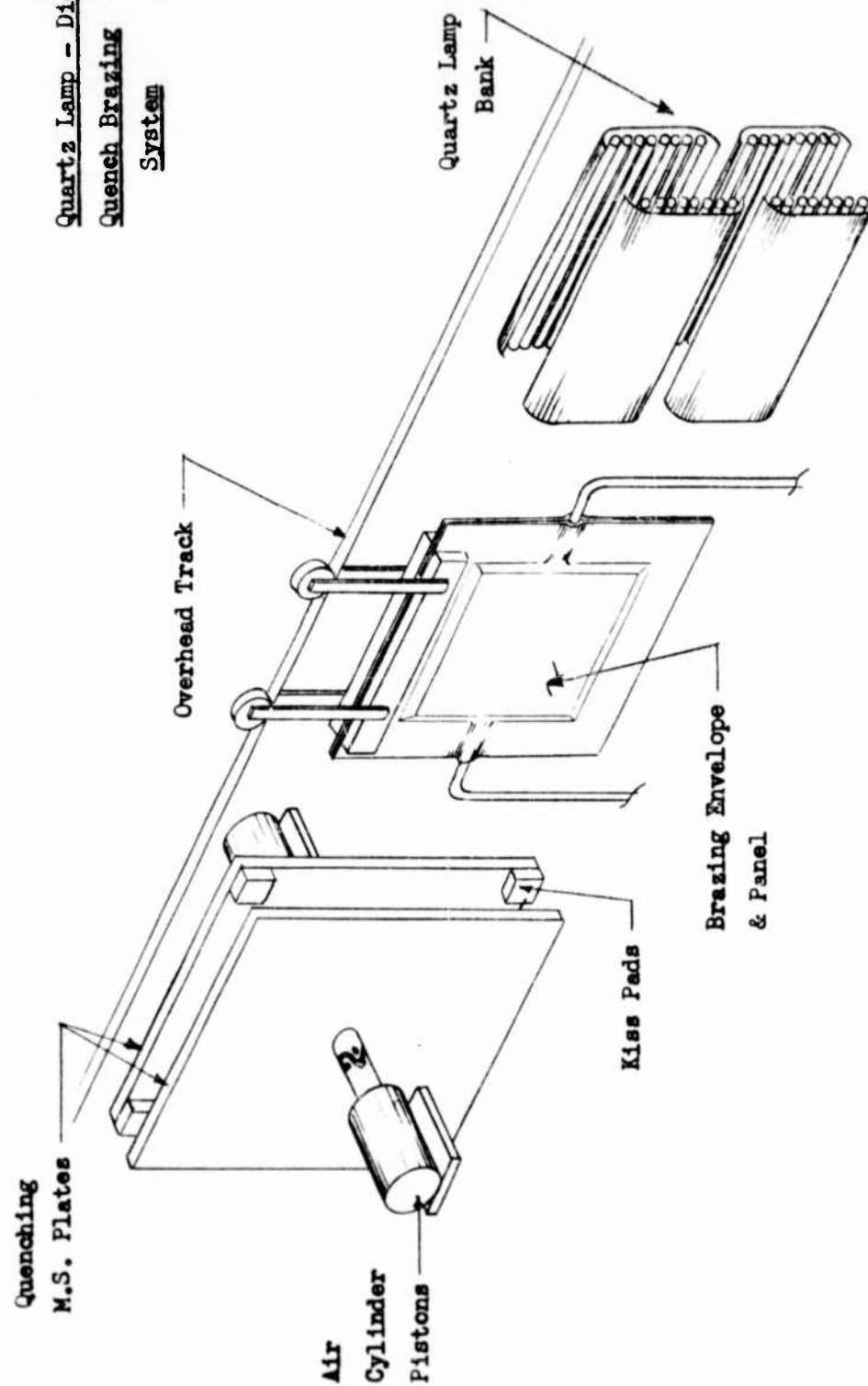


Figure V-4 Quartz Lamp Brazing System

TABLE V-1  
TYPICAL SEQUENCE OF MANUFACTURE  
OF BRAZED SANDWICH PANELS

1. Manufacture of brazing retort halves.
2. Manufacture of panel components (faces, core, brazing foil and edge members.)
3. Cleaning of retort and panel components.
4. Application of stop-off compound to inside of retort.
5. Assembly of panel components into one half of retort.
6. Closure of retort by welding and addition of thermocouples and argon and vacuum lines.
7. Checking of retort for leaks.
8. Connection of lines to argon cylinder and vacuum pump and making thermocouple connections.
9. Purging of retort and regulation of argon flow and vacuum pressure to be maintained during brazing.
10. Brazing of panel.
11. Quenching of retort.
12. Opening of retort and examination of panel after it is cooled sufficiently to handle.

Brazing of the panels took place in mild steel envelopes or retorts in an argon atmosphere at a vacuum of approximately 10 in. Hg.

Metallographic examinations of specimens that had been brazed or run through a simulated braze cycle indicated that there was no grain growth or recrystallization of the beryllium as a result of the braze time and temperature. Tensile testing of beryllium sheet that had been run through a simulated braze cycle showed a decrease of about 10% in ultimate tensile strength (to about 59,500 psi). This is believed to be caused by a partial anneal of the material rather than a metallographic change.

Panels made by this method (Figure V-5) were faced with beryllium sheet .015 to .060 in. thick. The brazing alloys used were .002 in. thick foil of the following compositions: (1) Silver-Copper-Lithium (92.8% Ag, 7.0% Cu, 0.2% Li), (2) 1-4-1 alloy (four parts fine silver clad with Ag-Cu-Li alloy), (3) 1-6-1 alloy (same as 1-4-1 except using 6 parts fine silver), (4) B.T. plus 0.5% Lithium (72.0% Ag, 28% Cu, 0.5% Li). Honeycomb core materials used were PH15-7 Mo, 17-7 PH and 321 stainless steels, and A-286, L-605, Inconel and Inconel X alloys; all showing compatibility with beryllium. The largest panels made were 7 in. square, the size being limited by the quartz-lamp facility available.

Quartz-lamp heating is particularly advantageous from the standpoint of rapid and even heating and cooling and close temperature control. The primary disadvantage is not being able to hold panel flatness within desired limits. This process is limited also to flat panels.

## 2. Electric-Blanket Brazing

Brazing by this method is very much the same as by quartz-lamps except the methods of heating and cooling. In the electric-blanket method the retort was sandwiched between heated dies until the panel reached braze temperature. Cooling was accomplished by immediately introducing compressed air into plenum chambers which fed the air through holes in the die faces, cooling the die and retort at the same time.

All of the dies used in this program were made from Glasrock, a fused-silica material. The dies were heated by Chromel A heating element wire imbedded  $\frac{1}{2}$  inch from the brazing faces. Figure IV-6 shows a typical flat panel die. Brazing of beryllium faced panels with these dies was accomplished by preheating them about 150° F. above the brazing temperature to compensate for heat lost when parting the dies before inserting the retort. Heating time above 1500° F. was approximately 3 minutes, while time to cool back down to 1500° F. was about 2 or 3 minutes. No soak time was required because the temperature rise was slow enough to allow thorough heating. The electric-blanket brazing method was found to be adequate from a rapid heating and cooling standpoint. Its primary advantage is the ability to hold precise contour during brazing.

Figures V-7 through V-10 show some of the largest panels of various configurations made to date.

The large flat panel (Figure V-7) is made up of .040 x 18 x 18 in. beryllium faces brazed to a 4-20P,  $\frac{1}{2}$  in. thick, 321 stainless steel honeycomb core. The panel has channel type edge members of .020 in. thick, 321 stainless steel. The composite panel (Figure V-8) is a honeycomb sandwich

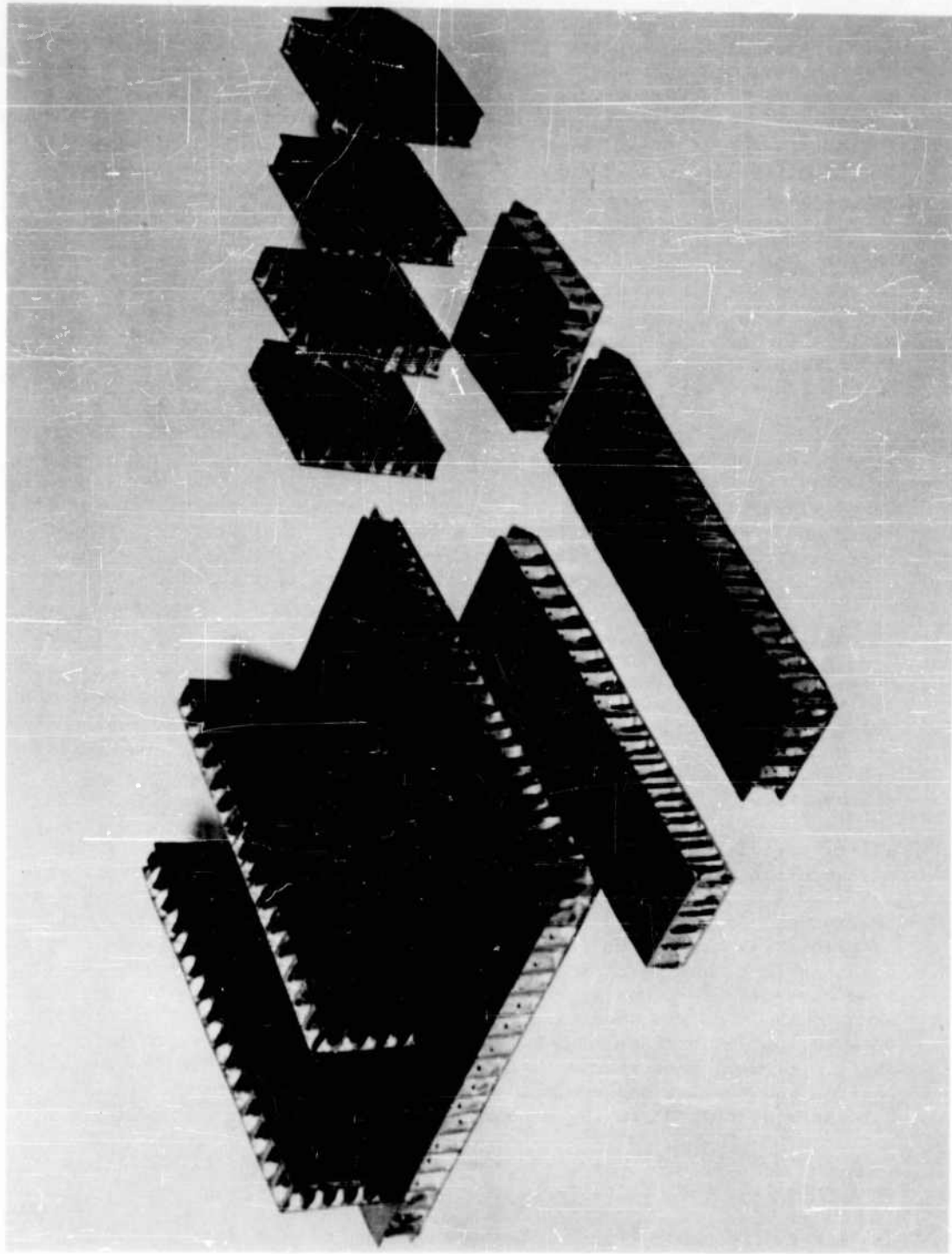


Figure V-5 Typical Beryllium-faced Brazed Honeycomb Sandwich Panels

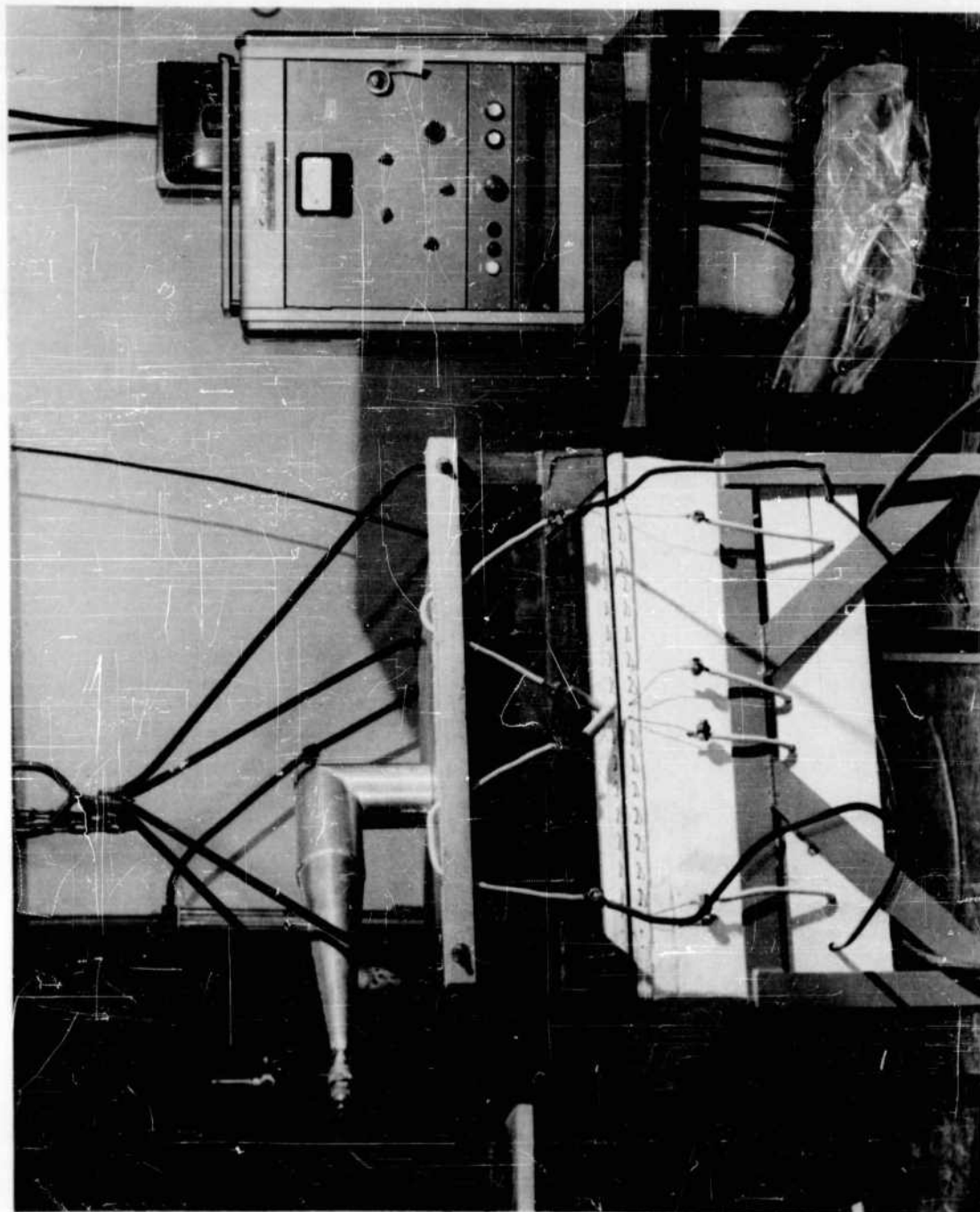


Figure V-6 Large Glasrock Die

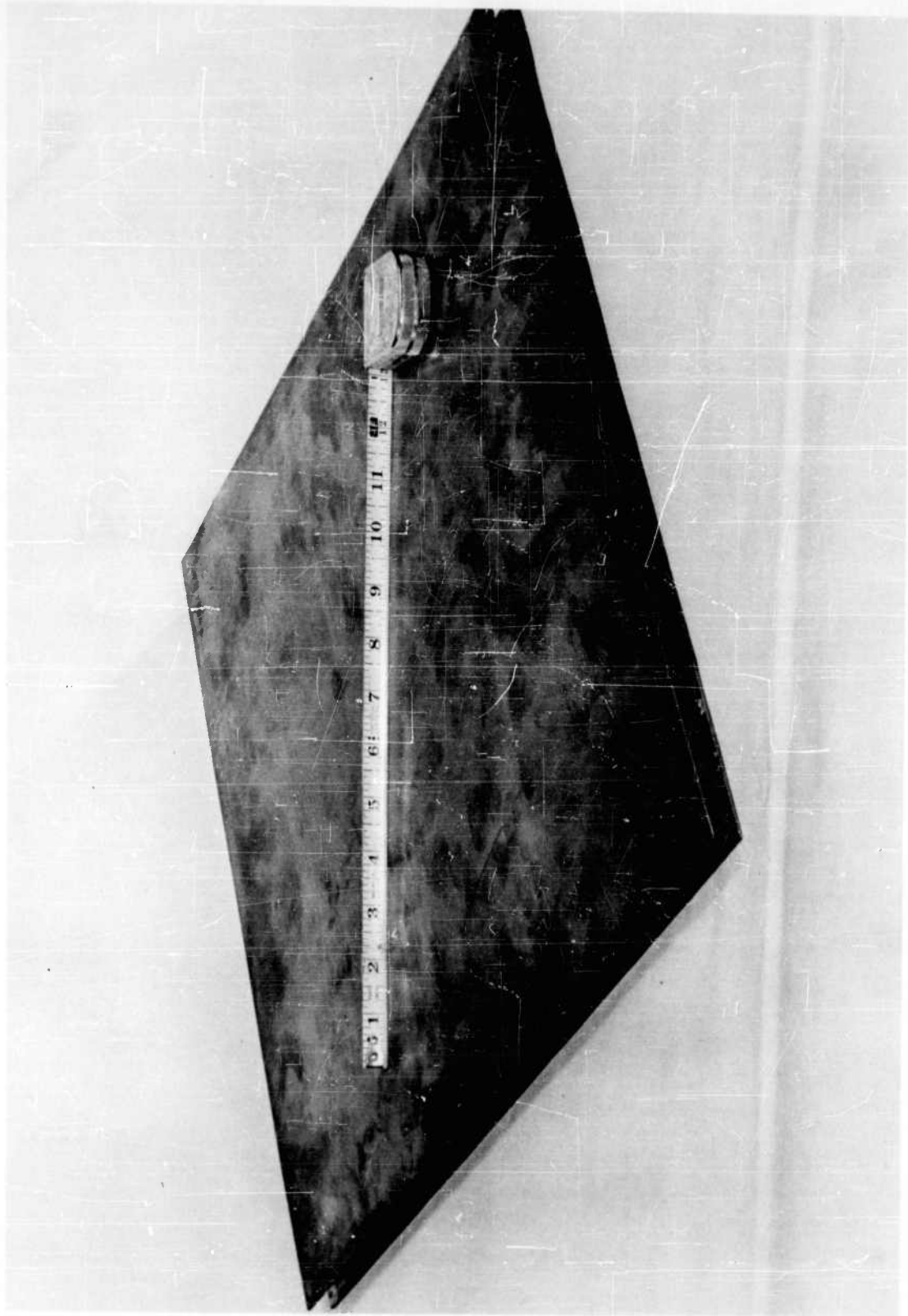


Figure V-7 18 in. x 18 in. Flat Beryllium Faced Panel

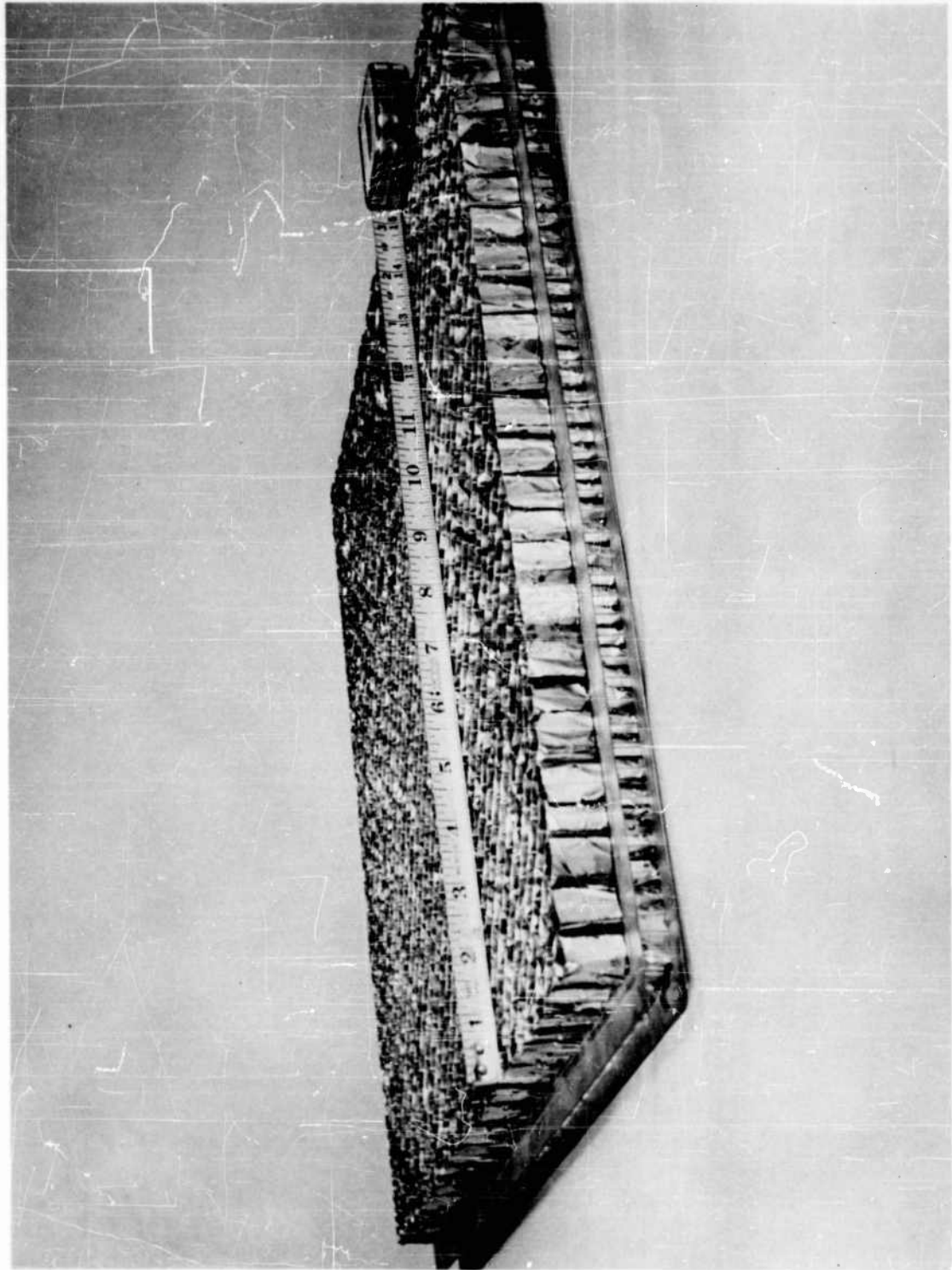


Figure V-8 18 in. x 18 in. Flat Composite Panel

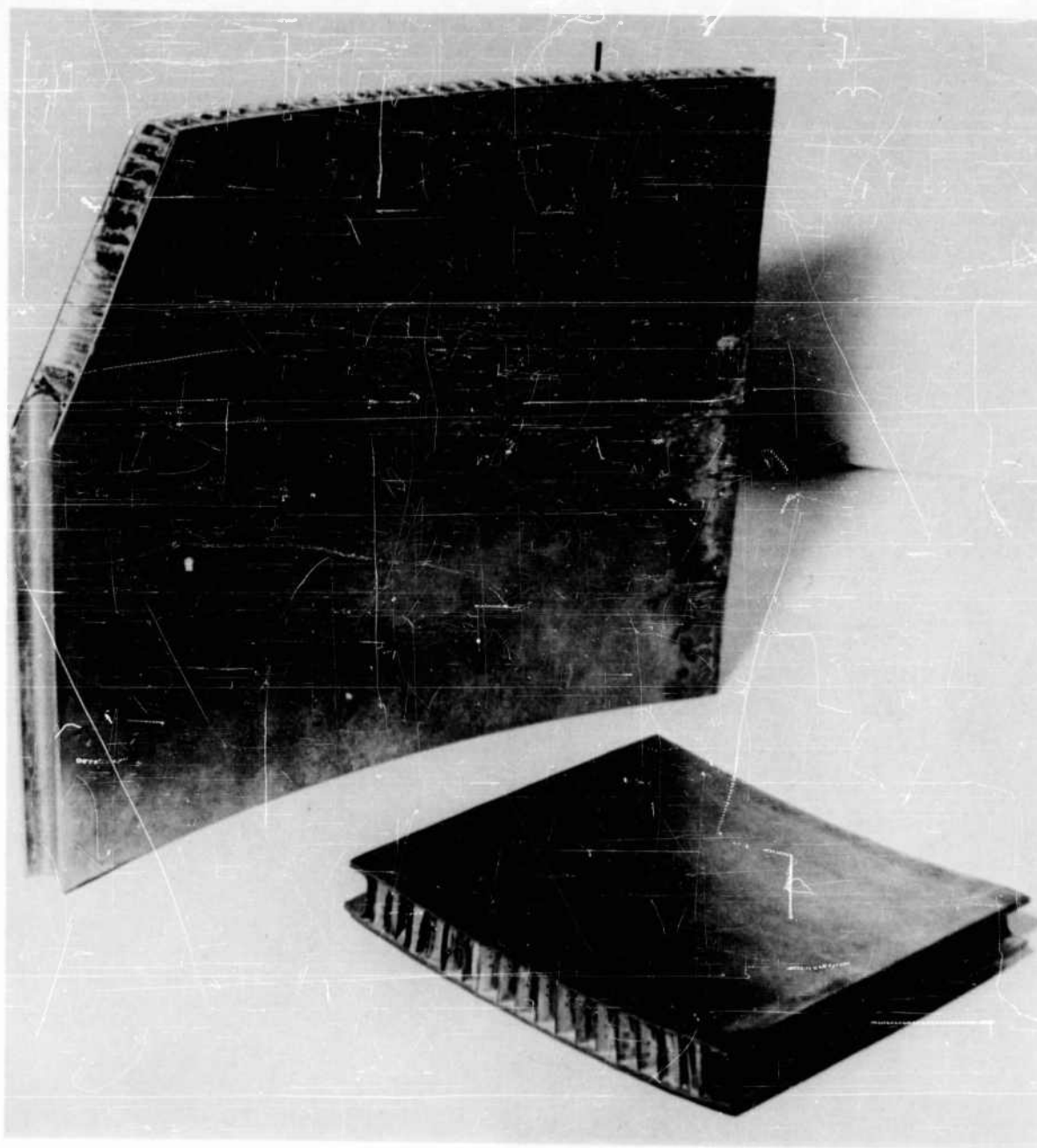


Figure V-9 Single Curvature Beryllium Faced Panels

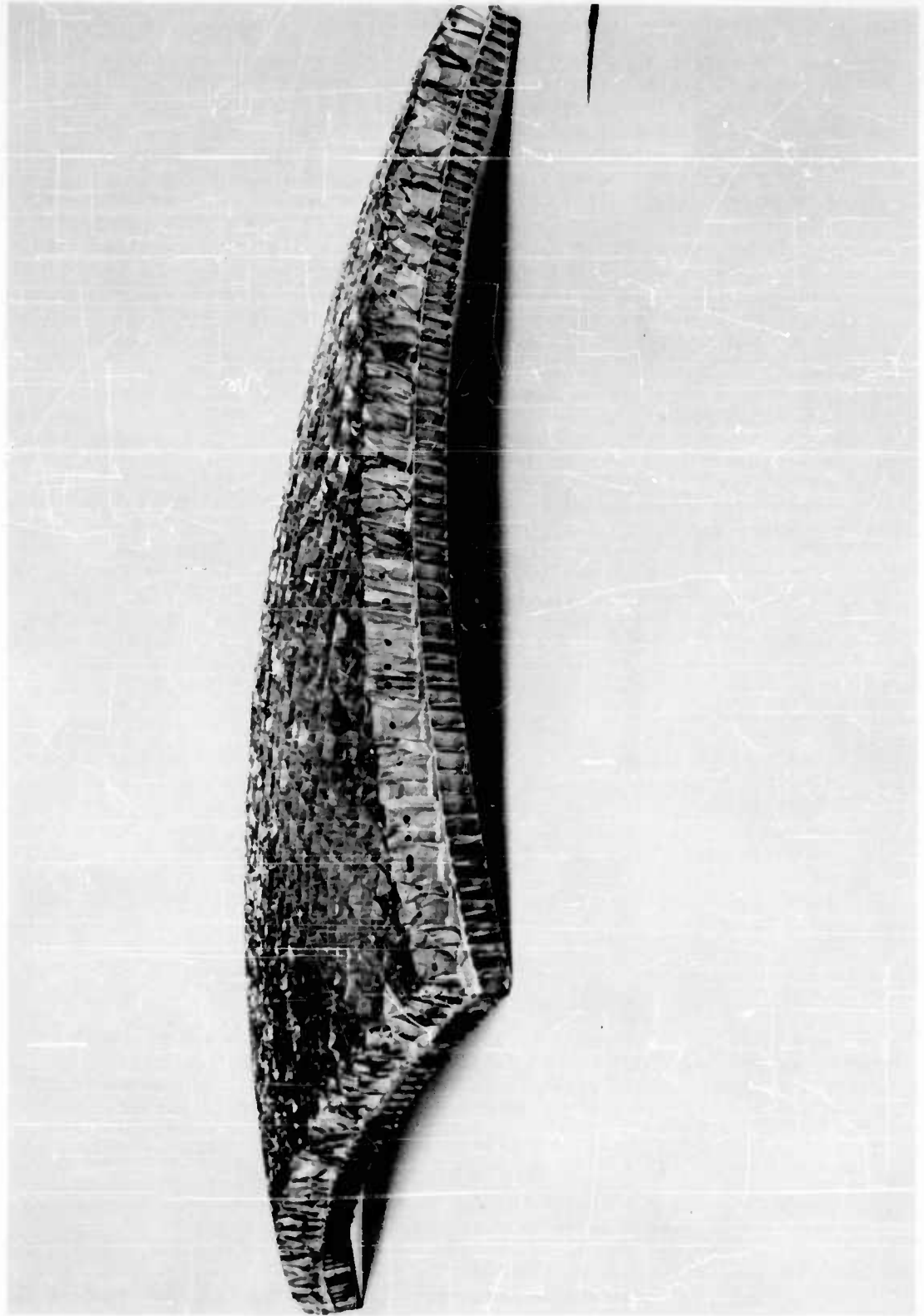


Figure V-10 18 in. x 18 in. Double Curved Composite Panel

structure with an .040 x 17 x 17 in. beryllium face, an .012 x 17 x 17 in. 321 stainless face and the 321 stainless core, to which is brazed an 8-10P, 3/4 in. thick Inconel outer core. This outer core is brazed to the stainless steel face and serves as reinforcement for the ceramic heat shield. Examples of single curved panels are shown in Figure V-9. The small panel is 6 in. square and the large one is 11 in. x 12 in. Both panels have A 286 alloy cores to which are brazed the beryllium faces (Figure V-2). The panels are curved to a 26 inch radius and have the beryllium channels described in Section V-C for edge members. Figure V-10 shows a composite panel which is contoured to a 36 in. spherical radius. The construction of this panel is similar to the flat composite panel which is described above except that the beryllium face is .020 in. thick and the other face and inner core is made from A 286 alloy material. Silver-Copper-Lithium brazing alloy was used in making all the above panels.

### 3. Furnace Brazing

While the methods described above work well with flat and slightly curved panels, they do not present the practical means of brazing more complex assemblies that furnace brazing does. Brazing by this method was accomplished by inserting the panel enclosed in its protective retort into a furnace preheated to about 150° F. above the brazing temperature. As soon as the panel reached the braze temperature it was removed from the furnace and allowed to cool in still air. The time above 1500° F. did not exceed 5 minutes. The only tooling required besides the retort itself was the core or mandrel supporting the inner wall of the retort. (Figure V-11) This mandrel was made "egg-crate" fashion to allow for rapid heating and cooling. The symmetry of the configuration allowed the brazing of two panels simultaneously.

Leading edge panels produced by this method are illustrated in Figure V-12. The larger panels are 6 in. O.D. x 12 in. long. The small panel is 3.5 in. O.D. x 6 in. long. All three have an Inconel outer core for ceramic insulation reinforcement. The backup structure for the left panel is a sandwich panel with an .020 in. beryllium inner face, an .010 in. A 286 alloy outer face and an A 286 core. The right panel has an .060 in. thick beryllium sheet for backup. The small center panel is backed up with a 17-7 PH steel sandwich panel. Silver-Copper-Lithium alloy was used for all the brazing.

## E. JOINING

One of the major problems to be solved before beryllium can be widely used structurally is the problem of joining components to be fabricated from this material. The possibilities considered were mechanical and welded joints, since little state-of-the-art information was available on either type of joint.

### 1. Welding of Beryllium

Tungsten-inert-gas fusion welding was attempted both with and without beryllium filler wire on various gages of beryllium sheet ranging from .020 to .060 in. thick. Much trouble was experienced with cracking in the welds because of the extreme notch sensitivity of the material. A few welds were eventually made without cracks but their properties were so poor that they could be easily broken by hand. Copper chill bars were tried to dissipate some of the heat generated, but without any success.

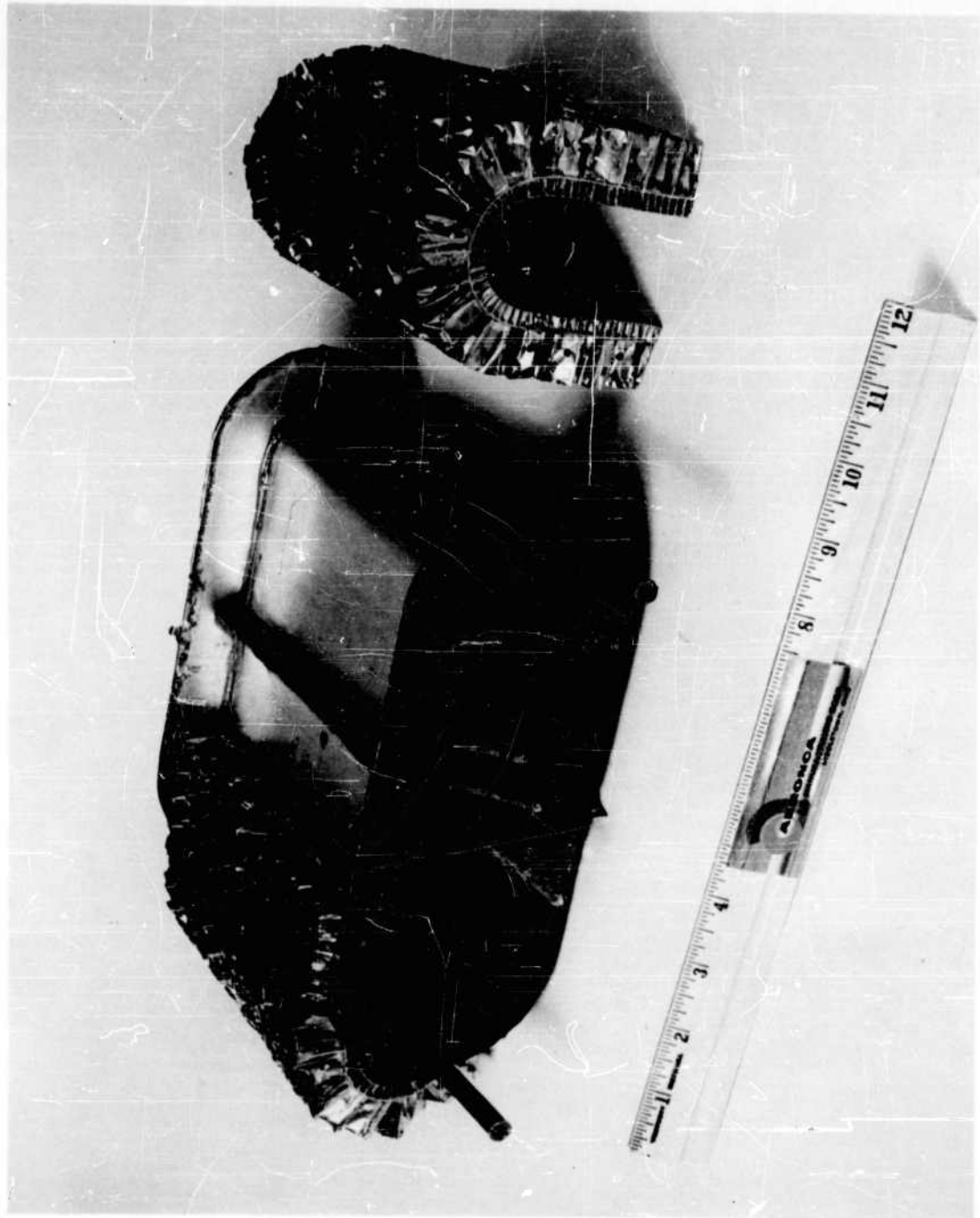


Figure V-11 Small Leading Edge Panels with Brazing Retort

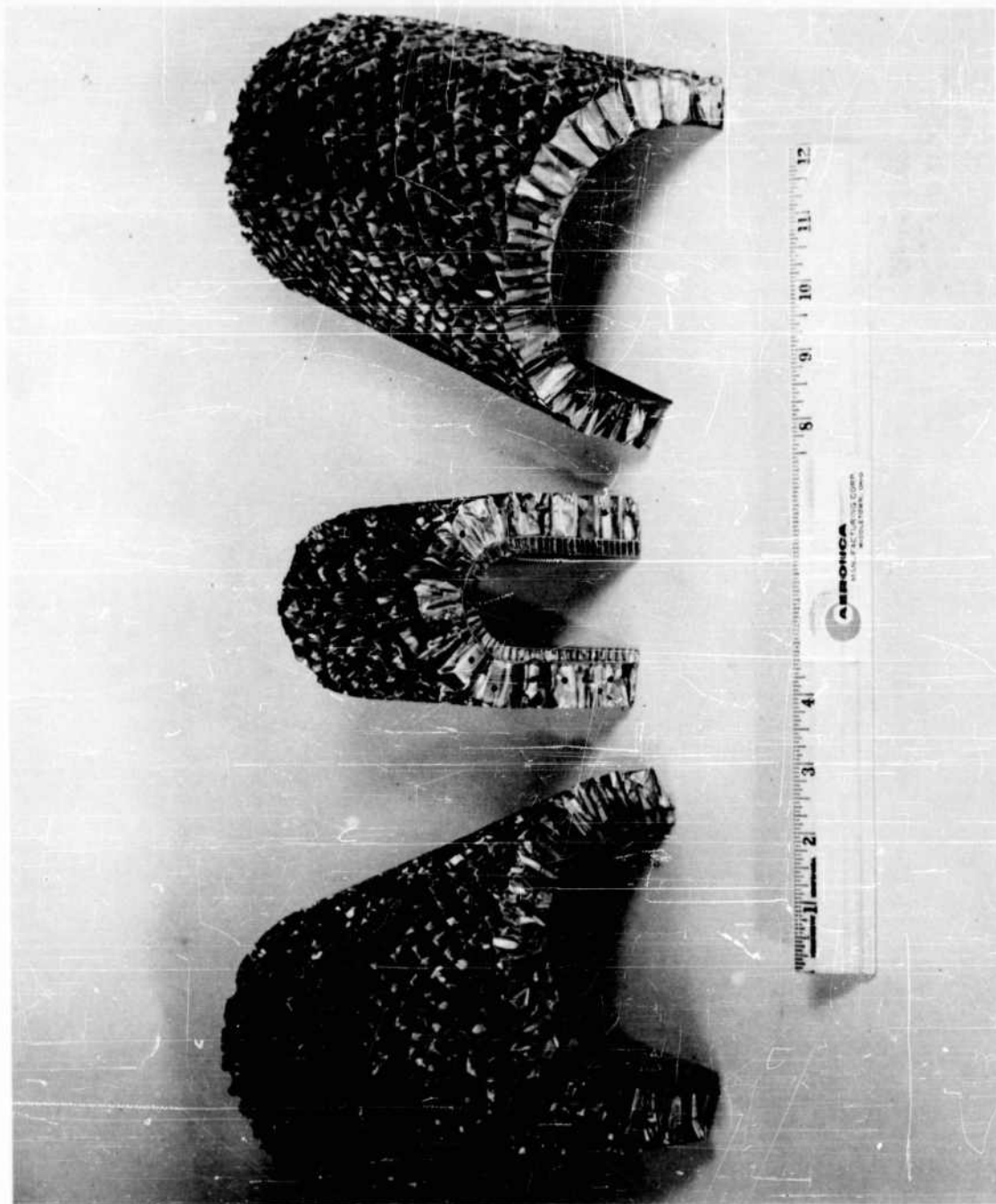


Figure V-12 Typical Leading Edge Panels

Spotwelding was also attempted by both resistance and fusion welding, again resulting in considerable cracking which was increased when a row of spots was attempted. A few spotwelds succeeded in sticking the material together but were of too low a strength to be considered structurally.

## 2. Mechanical Joining

Because of failure to produce a good weld joint in beryllium, the possibility of drilling the sheet for mechanical fasteners was explored. Some limited drilling was done (Section V.B) but it was difficult to produce crack-free holes, especially in thin material (.020 in.). Since mechanical joining is not as efficient from a weight standpoint as welding and since the reliability of fasteners in holes drilled in beryllium was questionable, this approach was abandoned.

## 3. Welding of Dissimilar Metal Edge Members

Encouraging results were obtained in brazing beryllium to various types of steel and high temperature alloys with a variety of brazing alloys (Section V.D), so it was decided to braze in edge members of a weldable material for joining panels. This approach has three significant advantages in attaining joint reliability:

- a. Demonstrated compatibility of beryllium in brazing to dissimilar metals.
- b. Capability of selection of a readily weldable material for edge members.
- c. Action of a brazed-in edge member in controlling notch effect on the edge of beryllium sheet.

Some beryllium faced honeycomb sandwich panels were made with 321 stainless steel edge members for joining studies. The edge members protruded a minimum of 3/8 inch from the edge of the beryllium sheet so they could be joined by welding without heat damage to the braze. Copper bars were needed to backup the joint during welding to dissipate the heat and prevent warpage.

### References

1. "Strength of Metal Aircraft Elements", MIL-HDBK-5, Armed Forces Supply Support Center, Washington 25, D. C., March 1959
2. "Preliminary Beryllium Data Developed for Air Force Contract AF 33(616)-6905", Lockheed Missile and Space Division, Lockheed Aircraft Corporation, Sunnyvale, California, June 14, 1960
3. Chang, Chein-Chein and Ebcioğlu, I.K. "Thermoelastic Behavior of A Simply Supported Sandwich Panel Under Large Temperature Gradient and Edge Compression", Journal of the Aerospace Sciences, Vol. 28, June, 1961
4. Biot, M. A., "New Methods in Heat Flow Analysis with Application to Flight Structures", Journal of the Aeronautical Sciences Vol. 24, December, 1957
5. Sowman, H. G., Hathaway, A. J., Comstock, G. F. "A Survey of the Properties of Refractories", Final Report Research Project R-2168, Titanium Alloy Mfg. Div., National Lead Co., Niagara Falls, N. Y., April 29, 1953
6. Glasrock Products, Inc., 1101 Glidden Street, N. W. Atlanta 18, Georgia, Glasrock Technical Data

#### BIBLIOGRAPHY

1. ASTM Design. C 109-58, C 247-52, C 396-57T, C 306-55 on Compression Testing of Cements ASTM Standards, 1958, Part 4.
2. ASTM Design. C 190-58, C 307-55, on Tensile Testing of Cements, ASTM Standards, 1958, Part 4.
3. ASTM Design, C 202-47, C 201-47, C 417-58T, C 182-47, C 236-45T on Thermal Conductivity of Refractories, ASTM Standards, 1958, Part 5.
4. ASTM Design. C 273-53, "Shear Testing Flatwise Plane of Sandwich Construction," p. 911, ASTM Standards, 1958, Part 5.
5. ASTM Design. C 297055, "Tension Test in Flatwise Plane of Sandwich Construction," p. 915, ASTM Standards, 1958, Part 5.
6. ASTM Design. C 364-57, "Compressive Strength, Edgewise of Flat Sandwich Constructions," p. 893, ASTM Standards, 1958, Part 5.
7. ASTM Design. C 393-57T, "Flexure Test, Flatwise, of Sandwich Constructions," p. 904, ASTM Standards, 1958, Part 5.
8. ASTM Design, E 8-57T, "Tension Testing of Metallic Materials (Tentative)," p. 103, ASTM Standards, 1958, Part 3.
9. Bowen, M. D., "The Measurement of Thermal Conductivity at High Temperatures," Graduate Thesis at Georgia Tech., 1959.
10. Boyd, J. E. and J. F. Richards, "An Improved Technique for Metallorgraphic Preparation of Beryllium and Beryllium Alloys," AVCO Research and Advanced Development Division, August 24, 1959.
11. Breslin, A. J. and Harris, W. B., "Health and Safety Laboratory," U. S. Atomic Energy Commission, Report HASL - 36, dated May 1, 1958.
12. Brundige, E. L., Kirby, R. S. Hanks, G. S., and Taub, J. M., "Welding of Beryllium," Welding Journal, dated October 1959, pp. 4105-4135.
13. Denke, P. J., Matrix Solution of Certain Non-Linear Problems in Structural Analysis; Journal of the Aeronautical Sciences, Vol. 23, No. 3, p. 231, March 1956.
14. DMIC Memorandum 37, Procedures for the Metallorgraphic Preparation of Beryllium, Titanium and Refractory Metals," Defense Metals Information Center, Battelle Memorial Institute, October 26, 1959.
15. Dukes, W. H., F. M. Anthony, H. A. Pearl, "Investigation of Feasibility of Utilizing Available Heat Resistant Materials for Hypersonic Leading Edge Application," Second and Third Quarterly Progress Reports, WADC Contract No. AF33(616)-6034, Task 73500, Bell Aircraft Corporation.
16. Gatewood, B. E., "Thermal Stresses," McGraw-Hill Book Company, Inc., New York, New York, 1957.

BIBLIOGRAPHY -continued-

17. Gienza, C. J., "Development and Evaluation of Structural Beryllium" WADC Technical Report 59-349, The Martin Company, dated April, 1959.
18. Greenspan, Jacob, "Ductility in Beryllium Related to Grain Orientation and Grain Size," Nuclear Metals, Inc., Report NM1-1174, dated August 9, 1957.
19. Greenspan, Jacob, Henrikson, G. A., and Kaufmann, A. R., "Beryllium Research and Development in the Area of Composite Materials," Nuclear Metals, Inc., Quarterly Progress Report NM1-9408, dated June 23, 1959.
20. Hodge, Webster, "Beryllium for Structural Applications" DMIC Report 106, Battelle Memorial Institute, dated August 15, 1958.
21. Hoff, J. N., "The Analysis of Structures," John Wiley and Sons, Inc., New York, New York, 1956.
22. Joint Conference on Lifting Manned Hyper Velocity and Re-Entry Vehicles," Vol. I, NASA - USAF, April 1960.
23. Joint Conference on Lifting Manned Hyper Velocity and Re-Entry Vehicles," Vol. II, NASA - USAF, April 1960.
24. Kingery, W. D., "Thermal Conductivity: XIV, Conductivity of Multicomponent Systems," J. Am. Ceramic Society, 42 (12) 571-658 (1959).
25. Kingery, W. D., "Property Measurements at High Temperatures," John Wiley and Sons, Inc., p. 88-148 (1959).
26. Klein, J. L., Macres, V. G., Woodward, D. H., and Greenspan, J. L., "Ductility of Beryllium as Related to Preferred Orientation and Grain Structure," ASM, The Metal Beryllium 1955, pp. 425-465.
27. Military Standard MIL-STD-401A, 15 June 1956, "Sandwich Constructions and Core Materials; General Test Methods."
28. Olafson, C. T., "Machining of Beryllium," Battelle Memorial Institute, DMIC Memorandum 21, dated June 5, 1959.
29. O'Sullivan, Jr., W. J. and W. R. Wade, "Theory and Apparatus for Measurement of Emissivity for Radiative Cooling of Hypersonic Aircraft with Data for Inconel and Inconel X, NACATN-4121, 1957.
30. Passmore, E. M., "Beryllium Joining, WADC Sponsored Program" Summary Technical Report 59-695, Research and Advanced Development Division, AVCO Corporation, dated 18 February 1960.
31. Peery, D. J., "Aircraft Structures," McGraw-Hill Book Company, Inc., New York, New York, 1950.
32. Roark, R. J., "Formulas for Stress and Strain," McGraw-Hill Book Co., Inc., New York, New York, Third Edition, 1954.

BIBLIOGRAPHY -continued-

33. Timoshenko, S. and Woinowsky-Krieger, S.; Theory of Plates and Shells; McGraw-Hill Book Company, 1959.
34. Udy, M. C., G. K. Manning and L. W. Eastwood, "Metallographic Examination of Beryllium Alloys," Metals Transactions, Vol. 185, October 1949, p. 779.
35. Warren, W. P. and N. S. Diaconis, "The Performance of Ablation Materials as Heat Protection for re-entering Satellites," LAS Paper 60-49, Institute of the Aeronautical Services, 1960.
36. Weare, N. E., and Monroe, R. E., "Joining of Beryllium," Battelle Memorial Institute DMIC Memorandum 13, dated March 30, 1959.
37. Yans, F. M., "Third Dimensional Ductility and Crack Propagation in Beryllium Sheet," Nuclear Metals, Inc., Report NM1-1212, dated March 18, 1959.
38. Yans, F. M., "Investigation of Fabrication and Formability Processes for Structural Beryllium Sheet," Nuclear Metals, Inc., Report NM1-5006, dated April 30, 1959.

Aeronautical Systems Division, Dir/Aeromechanics, Flight Dynamics Lab, Wright-Patterson AFB, Ohio.

Rpt Nr ASD-TR-61-706, Vol I. BERYLLIUM COMPOSITE STRUCTURES: Design and Application. Final report, May 62, 169p. incl illus., tables, 44 refs.

Unclassified Report

Design information is presented for beryllium and ceramic composite structures for re-entry vehicle applications. The Volume includes a summary of materials and process developments for beryllium panels and heat shield ceramics,

( over )

analytical evaluations, and discussion of application of insulated structural concepts to re-entry vehicle systems. Also, included are the results of panel tests in the severe environments of turbojet and ramjet exhausts. Data suitable for preliminary design considerations are presented for three reinforced heat shield ceramic foams: alumina, silica and zirconia. Beryllium sandwich panels constructed in the course of the program are described with regard to fabrication potential and performance features in aerospace structures.

1. Design - Beryllium structures
2. Design - Ceramics composites
3. Application - Insulated structural concepts
4. Re-entry heat shields ramjet tests

- I. AFSC Project 1368, Task 136806
- II. Contract AF33(616)-7050
- III. Aeronca Mfg. Corp., Middletown, Ohio
- IV. J. N. Krusos, et al

- V. Secondary rpt Nr Aeronca ER-532
- VI. Avail fr OTS
- VII. In ASTIA collection

Aeronautical Systems Division, Dir/Aeromechanics, Flight Dynamics Lab, Wright-Patterson AFB, Ohio.

Rpt Nr ASD-TR-61-706, Vol I. BERYLLIUM COMPOSITE STRUCTURES: Design and Application. Final report, May 62, 169p. incl illus., tables, 44 refs.

Unclassified Report

Design information is presented for beryllium and ceramic composite structures for re-entry vehicle applications. The Volume includes a summary of materials and process developments for beryllium panels and heat shield ceramics,

( over )

analytical evaluations, and discussion of application of insulated structural concepts to re-entry vehicle systems. Also, included are the results of panel tests in the severe environments of turbojet and ramjet exhausts. Data suitable for preliminary design considerations are presented for three reinforced heat shield ceramic foams: alumina, silica and zirconia. Beryllium sandwich panels constructed in the course of the program are described with regard to fabrication potential and performance features in aerospace structures.

1. Design - Beryllium structures
2. Design - Ceramics composites
3. Application - Insulated structural concepts
4. Re-entry heat shields ramjet tests
  - I. AFSC Project 1368, Task 136806
  - II. Contract AF33(616)-7050
  - III. Aeronea Mfg. Corp., Middletown, Ohio
  - IV. J. N. Krusos, et al

- V. Secondary rpt Nr Aeronea ER-532
- VI. Avail fr OTS
- VII. In ASTIA collection

Aeronautical Systems Division, Dir/Aeromechanics, Flight Dynamics Lab, Wright-Patterson AFB, Ohio.

Rpt Nr ASD-TR-61-706, Vol I. BERYLLIUM COMPOSITE STRUCTURES: Design and Application. Final report, May 62, 169p. incl illus., tables, 44 refs.

Unclassified Report

Design information is presented for beryllium and ceramic composite structures for re-entry vehicle applications. The Volume includes a summary of materials and process developments for beryllium panels and heat shield ceramics,

( over )

analytical evaluations, and discussion of application of insulated structural concepts to re-entry vehicle systems. Also, included are the results of panel tests in the severe environments of turbojet and ramjet exhausts. Data suitable for preliminary design considerations are presented for three reinforced heat shield ceramic foams: alumina, silica and zirconia. Beryllium sandwich panels constructed in the course of the program are described with regard to fabrication potential and performance features in aerospace structures.

1. Design - Beryllium structures
2. Design - Ceramics composites
3. Application - Insulated structural concepts
4. Re-entry heat shields ramjet tests
- I. AFSC Project 1368, Task 136806
- II. Contract AF33(616)-7050
- III. Aeronca Mfg. Corp., Middletown, Ohio
- IV. J. N. Krusos, et al

- V. Secondary rpt Nr Aeronca ER-532
- VI. Avail fr OTS
- VII. In ASTIA collection

Aeronautical Systems Division, Dir/Aeromechanics, Flight Dynamics Lab, Wright-Patterson AFB, Ohio.

Rpt Nr ASD-TR-61-706, Vol I. BERYLLIUM COMPOSITE STRUCTURES: Design and Application. Final report, May 62, 169p. incl illus., tables, 44 refs.

Unclassified Report

Design information is presented for beryllium and ceramic composite structures for re-entry vehicle applications. The Volume includes a summary of materials and process developments for beryllium panels and heat shield ceramics,

( over )

analytical evaluations, and discussion of application of insulated structural concepts to re-entry vehicle systems. Also, included are the results of panel tests in the severe environments of turbojet and ramjet exhausts. Data suitable for preliminary design considerations are presented for three reinforced heat shield ceramic foams: alumina, silica and zirconia. Beryllium sandwich panels constructed in the course of the program are described with regard to fabrication potential and performance features in aerospace structures.

1. Design - Beryllium structures
2. Design - Ceramics composites
3. Application - Insulated structural concepts
4. Re-entry heat shields ramjet tests

- I. AFSC Project 1368, Task 136806
- II. Contract AF33(616)-7050
- III. Aeronca Mfg. Corp., Middletown, Ohio
- IV. J. N. Krusos, et al

- V. Secondary rpt Nr Aeronca ER-532
- VI. Aval fr OTS
- VII. In ASTIA collection